Aus dem Institut für Tumorimmunologie,

Direktorin: Prof. Dr. Elke Pogge von Strandmann

des Fachbereichs Medizin der Philipps-Universität Marburg

The role of the tumor suppressor p53 in the biogenesis and function of extracellular vesicles

Inaugural-Dissertation

zur Erlangung des Doktorgrades der Naturwissenschaften

dem Fachbereich Medizin der Philipps-Universität Marburg

vorgelegt von

Manuel Linder

aus Stuttgart

Marburg, 2024

Angenommen vom Fachbereich Medizin der Philipps-Universität Marburg

am: **19.02.2024**

Gedruckt mit Genehmigung des Fachbereichs Medizin.

Dekanin: Prof. Dr. Denise Hilfiker-Kleiner

Referentin: Prof. Dr. Elke Pogge von Strandmann

Korreferentin: Dr. Silke Reinartz

Table of Contents

Abstract

The progression and metastasis of ovarian cancer (OC) relies on the intricate interplay between cancer cells and their surrounding tumor microenvironment (TME). Within this complex ecosystem, various cell types, particularly fibroblasts, play a significant role in facilitating OC invasion and metastasis. The TME also encompasses diverse soluble components, including cytokines or extracellular matrix (ECM) and, notably, extracellular vesicles (EVs). EVs have emerged as critical mediators of cellular communication by transporting and presenting their cargo, including proteins, lipids, and nucleic acids. The complex biogenesis of EVs involves different mechanisms and factors, with recent attention focusing on the tumor protein p53. In the majority of ovarian cancer cases, p53 is mutated, but its potential role as a facilitator of EV biogenesis remains elusive. Therefore, this study aims to further unravel the role of p53 in EV biogenesis and its impact on the TME, with a specific focus on cancer-associated fibroblasts (CAFs).

To address this, I genetically engineered ovarian cancer cell lines (OVCAR8) with a defined p53 status, including lines with a p53 knockout (KO), a p53 wildtype (WT), and two specific hot spot mutations (mutp53; R175H or R273H). The characterization of the secreted EVs revealed no significant differences in particle size and EV marker expression between knockout and mutated cells. Of note, transcriptomic analysis demonstrated higher expression of genes involved in exosome biogenesis, such as ESCRT components, in p53 WT cells, which also released elevated amounts of EVs. Moreover, EVs preferentially transferred WTp53 compared to mutp53 to recipient cells, although it was lower expressed in the respective cells. Treatment of human fibroblast with EVs from p53 wildtype cells and, to a remarkably lesser extent, from p53KO/mutp53 cells induced an inflammatory phenotype. This was shown to be at least partially mediated by NFκB and STAT3 activity. Secretome analysis further confirmed the inflammatory phenotype of wildtype EV-treated fibroblast with the secretion of cytokines and chemokines, such as IL6, CXCL1, and CXCL8. In contrast, EVs from p53KO cells induced a phenotype associated with ECM remodeling, including secretion of COMP, POSTN, and TGFB1. Notably, EV from mutp53 cells did not cause a specific phenotype in fibroblasts.

In conclusion, our findings indicate that EVs from OC cells expressing p53 wildtype influence the phenotype of human fibroblasts, indicating that p53 directs specific EV cargo loading. These findings provide the basis to further investigate p53 as an essential

mediator of EV biogenesis and potentially develop innovative strategies to educate the TME and, specifically, fibroblasts to an anti-tumorigenic phenotype by utilizing p53 wildtype-derived EVs.

Zusammenfassung

Die Progression und Metastasierung von Eierstockkrebs werden maßgeblich durch das komplexe Zusammenspiel von Krebszellen mit ihrer umgebenden Tumormikroumgebung beeinflusst. Innerhalb dieses hochkomplexen Ökosystems spielen verschiedene Zelltypen, insbesondere Fibroblasten, eine entscheidende Rolle. Die Tumormikroumgebung setzt sich außerdem aus verschiedenen löslichen Bestandteilen zusammen, darunter Zytokine, extrazelluläre Matrix (ECM) und extrazelluläre Vesikel (EVs). EVs die als innovative Vermittler der zellulären Kommunikation hervorstechen, haben die einzigartige Fähigkeit, eine breite Palette von Molekülen, darunter Proteine, Lipide und Nukleinsäuren, zu transportieren und zu präsentieren. Die Biogenese von EVs ist komplex und involviert verschiedene Mechanismen und Faktoren. In den letzten Jahren hat sich das Tumorprotein p53, welches in fast allen Fällen von Eierstockkrebs mutiert ist, als potentiell wichtiger Faktor in der Biogenese von EVs herauskristallisiert. Allerdings ist die genaue Rolle von p53 nach wie vor unklar, weshalb diese Studie das Ziel hat, diese Funktionen und dessen Auswirkungen auf die Tumormikroumgebung, insbesondere im Zusammenhang mit krebsassoziierten Fibroblasten weiter zu erforschen.

Um dies zu untersuchen, haben wir Eierstockkrebszelllinien (OVCAR8) mit einem bestimmten p53-Status genetisch erzeugt, sodass sie entweder, einen p53-Knockout (KO), ein p53-Wildtyp (WT) oder eine von zwei spezifischen Hotspot-Mutationen (mutp53, R175H oder R273H) exprimieren. Bei der Charakterisierung der sekretierten EVs wurden keine signifikanten Unterschiede in Partikelgröße und EV Marker Expression zwischen Knockout- und mutierten Zellen beobachtet. Die transkriptomische Analyse zeigte jedoch eine höhere Expression von Genen in p53WT-Zellen, die an der Exosom-Biogenese, wie z.B. verschiedene ESCRT-Komponenten, beteiligt sind. Außerdem sekretierten diese Zellen erhöhte Mengen an EVs. Es konnte weiterhin gezeigt werden, dass WTp53 bevorzugt in EVs geladen wird, und diese von Zielzellen, wie z.B. Krebszellen oder Fibroblasten, aufgenommen werden können. Die Behandlung von humanen Fibroblasten mit EVs von p53WT Zellen resultierte in einen entzündlichen Phänotyp, welcher zumindest teilweise durch NFκB und STAT3 Aktivität vermittelt wird. Eine Sekretome-Analyse zeigte außerdem eine erhöhte Ausschüttung von Zytokinen und Chemokinen wie z.B. IL6, CXCL1 und CXCL8 durch die mit WT-EVs behandelten Fibroblasten was somit die Ergebnisse in den Transkriptomanalysen bestärken. Im Gegensatz dazu zeigten p53KO EV-behandelte Fibroblasten einen Phänotyp der mit der

Modellierung der extrazellulären Matrix assoziiert ist, wie zum Beispiel durch Sekretion von COMP, POSTN oder TGFB1. Interessanterweise, zeigten Fibroblasten die mit EVs von mutierten p53 Zellen behandelt wurden keinen gesonderten Phänotyp.

Zusammenfassend zeigen unsere Ergebnisse, dass EVs von Eierstockkrebszellen, die WTp53 exprimieren, den Phänotyp von humanen Fibroblasten beeinflussen, was darauf hindeutet, dass p53 an einer spezifische EV Biogenese beteiligt ist. Diese Erkenntnisse bilden eine Grundlage für weitere Untersuchungen von p53 als einen wichtigen Vermittler der EV-Biogenese.

Abbreviations

ABB	Annexin binding buffer
ALIX	ALG-2 interacting protein X
ApoBD	Apoptotic bodies
ApoExo	Apoptotic exosome-like vesicles
ApoMV	Apoptotic microvesicles
BAG	Bcl2-associated athanogene
BCA	Bicinchoninic Acid Assays
BSA	Bovine Serum Albumin
CAF	Cancer-associated fibroblast
Cas9	CRISPR-associated 9
CAV1	Caveolin-1
CDKN1A	Cyclin-dependent kinase inhibitor 1A (p21)
cDNA	Complementary DNA
CM	Conditioned medium (Secretome)
CRISPR	Clustered Regularly Interspaced Short Palindromic Repeats
DBD	DNA-binding domain
DMSO	Dimethylsulfoxide
DNA	Deoxyribonucleic acid
DNA-SCARS	DNA segment with chromatin alterations reinforcing senescence
dsDNA	double-stranded DNA
dUC	differential Ultracentrifugation
ECM	Extracellular matrix
EMT	Epithelial-to-mesenchymal transition
EOC	Epithelial ovarian carcinoma
ESCRT	Endosomal sorting complexes required for the transport
ESE	Early sorting endosome
EVs	Extracellular vesicles
Exo	Exosomes
FAP	Fibroblast-activating protein
FC	Fold change
FSP1	Fibroblast-specific protein

GO:BP	Gene Ontology Biological processes
GO:CC	Gene Ontology Cellular Component
GOF	Gain of function
GOI	Gene of interest
HDFn	Human dermal fibroblast cell line
HGSOC	High-grade serous ovarian carcinoma
HRP	Horse-radish peroxidase
HSP90	Heat-shock-protein-90
iCAF	inflammatory CAF
IL	Interleukin
ILVs	Intraluminal vesicles
IκBα	inhibitor of NFκB
KEGG	Kyoto Encyclopedia of Genes and Genomes
LFQ	Label-free quantitation
LOD	Limit of detection
LOF	Loss of function
MDM2	Mouse double minute 2 homolog
MDSC	Myeloid-derived suppressor cells
MMP	Matrix metalloprotease
MMT	Mesothelial-to-mesenchymal transition
mutp53	mutant p53
MV	Microvesicles
MVB	Multivesicular bodies
myCAF	myofibroblastic CAF
NFκB	Nuclear factor kappa-light-chain-enhancer of activated B cells
NPX	Normalized Protein expression
nSMase2	Neutral sphingomyelinase 2
OC	Ovarian Cancer
p53KO	p53 knockout
p53RE	p53 response elements
PAGE	Polyacrylamide gel electrophoresis
PBS	Phosphate Buffered Saline

PCA	Principal component analysis
PI	Propidium iodide
POSTN	Periostatin
PRD	Proline-rich domain
qPCR	quantitative polymerase chain reaction
RD	regulatory domain
RNA	Ribonucleic acid
RNAseq	RNA sequencing
RT-qPCR	reverse transcription quantitative PCR
rtTA	reverse tetracycline-controlled transactivator
SASP	Senescence-associated secretory phenotype
SB	Sleeping beauty
SDS	Sodium dodecyl sulfate
STIC	Serous tubal intraepithelial carcinoma
TAD	Transactivation domain
TD	Tetramerization domain
TME	Tumor microenvironment
TP53	Tumor protein 53
TPM	Transcript per million
TRRUST	Transcriptional regulatory relationships unraveled by sentence-based text-mining analysis
VEGF	Vascular endothelial growth factor
WTp53	Wildtype p53
αSMA	alpha-smooth muscle actin

1. Introduction

1.1 The role of extracellular vesicles in cancer

Extracellular vesicles (EVs) are a heterogeneous group of membranous vesicles ubiquitously secreted by virtually all cell types (van Niel, D'Angelo, and Raposo 2018). Although many names have been used to categorize these vesicles based on their distinct characteristics, they can be broadly classified into three major subtypes: exosomes, microvesicles (ectosomes), and apoptotic bodies (ApoBD) (van Niel, D'Angelo, and Raposo 2018; Doyle and Wang 2019). Exosomes originate from the endosomal compartment and are usually between 40 and 150 nm in size, while microvesicles arise from blebbing of the cellular membrane and generally range from 50 to 1000 nm (van Niel, D'Angelo, and Raposo 2018). Apoptotic bodies are secreted by apoptotic cells and vary in size but can reach up to 10 µm (Santavanond et al. 2021). However, separation of the subgroups by specific markers or distinct functions is still difficult, which is why we will use the general term EV throughout the thesis.

Initially, EVs have been described as the "garbage bags" of cells by merely releasing unwanted cargo as part of a clearance process or quality control mechanism (Vidal 2019). However, emerging evidence established key functions of EVs in intercellular communication through their ability to transfer many molecules, including proteins, lipids, and nucleic acids (van Niel, D'Angelo, and Raposo 2018; Kalluri and LeBleu 2020). Specifically, in cancer, EVs have been shown to impact the function of cancer cells and their surrounding tumor microenvironment (TME) and, therefore, mediate the initiation, progression, and metastasis of cancer (Kalluri, n.d.). Early genetic drivers were shown to influence EV biogenesis and cargo loading during the initiation of cancer. For instance, the tumor suppressor protein p53, which is regularly mutated in cancer, can enhance EV secretion and modulate the composition of EVs (Kalluri, n.d.; Pavlakis, Neumann, and Stiewe 2020). Consistent and dynamic communication of cancer cells with the TME by EVs further determines the progression of the disease. For example, the transfer of cancer-derived TGFβ, miRNAs, or mutated p53 (mutp53) can activate cancer-associated fibroblasts (CAF), providing an immune suppressive and tumor-promoting environment, eventually contributing to cancer metastasis. In contrast, EVs can also mediate anti-tumorigenic functions such as the recruitment of immune cells for tumor cell killing or direct inhibition of cancer growth (Kalluri, n.d.). EVs, therefore, play a significant role in

cancer progression, emphasizing the need to understand the mechanisms that drive the communication in either direction.

1.1.1 Biogenesis of EVs

Cargo heterogeneity is a major characteristic of EVs, which typically reflects the physiological or pathological state of the cell (van Niel, D'Angelo, and Raposo 2018). Many distinct mechanisms are involved in the formation of EVs that can be further influenced by environmental factors, such as hypoxia or acidic pH (Ribovski et al. 2023). Both are hallmarks of cancer, reinforcing the role of the cellular state in EV biogenesis (Ribovski et al. 2023). It has been observed that hypoxic conditions and acidic pH can increase or decrease vesicle secretion, respectively, and that both can alter the composition of the cargo (Pachane et al. 2022; Nakase et al. 2021; Parolini et al. 2009).

Exosomes

Exosomes originate from the endosomal compartment by double invagination of the plasma membrane (Teng and Fussenegger 2021). The first invagination occurs by endocytosis of molecular cargo, including cell surface and soluble proteins, eventually generating early sorting endosomes. At this stage, cargo can be altered in exchange with the Golgi apparatus and endoplasmic reticulum. A second invagination of the membrane then leads to the formation of multivesicular bodies (MVB), which contain intraluminal vesicles (ILVs). In the following, MVBs can either fuse with lysosomes or autophagosomes for degradation or with the plasma membrane, where ILVs are released as exosomes into the extracellular lumen (van Niel, D'Angelo, and Raposo 2018; Kalluri and LeBleu 2020; Teng and Fussenegger 2021).

Several pathways and many different factors are described to be involved in the formation and release of exosomes. One central machinery is the endosomal sorting complexes required for transport (ESCRT) system, which encompasses four complexes (ESCRT-0, I, II, III) and additional accessory proteins. By variations in the interplay of the ESCRT complexes with other proteins, different pathways (canonical and non-canonical), as well as ESCRT-independent pathways, are described (Teng and Fussenegger 2021).

In the canonical pathway, the formation of MVBs depends on the consecutive recruitment of all four ESCRT complexes. At first, ESCRT-0, consisting of HRS and STAM, is recruited to the membrane of early sorting endosomes by phosphatidylinositol-3-phosphate (PtdIns3P) (Teng and Fussenegger 2021). After further mobilization of

clathrin by HRS, ESCRT-I is recruited through direct interaction with TSG101 (Raiborg et al. 2001; Lu et al. 2003). Next, ESCRT-II is recruited, which induces the invagination of endosomal membranes (Gill et al. 2007; Wollert and Hurley 2010). Finally, the scission of ILVs into the MVB lumen is conciliated by the assembly of the ESCRT-III complex (Babst et al. 2002; Teo et al. 2004; Teis, Saksena, and Emr 2008).

Alternatively, syndecan recruits syntenin on the endosomal membrane, which subsequently interacts with the ALG-2 interacting protein X (ALIX) (Baietti et al. 2012). ALIX further mobilizes the ESCRT-III complex for MVB formation (Baietti et al. 2012; Dores et al. 2012). This non-canonical pathway is independent of ESCRT 0, I, and II but still depends on the scission of ILVs by the ESCRT-III complex (Baietti et al. 2012).

Moreover, MVB formation can also occur without any involvement of the ESCRT machinery (Horbay et al. 2022). For instance, neutral sphingomyelinase 2 (nSMase2) can produce ceramide from sphingomyelin, which leads to the spontaneous formation of ILVs due to the cone-shaped structure (Horbay et al. 2022; Trajkovic et al. 2008). Other ESCRT-independent pathways are also described, which involve tetraspanins (e.g., CD63), the RAB protein RAB31, or Flotillin (van Niel et al. 2011; Wei et al. 2021).

During ILV formation, cell-specific cargo can be loaded depending on the physiological or pathological state of the cell (van Niel, D'Angelo, and Raposo 2018; Teng and Fussenegger 2021). For instance, proteins of the ESCRT complexes 0, I, and II (e.g., STAM, HRS, TSG101, EAP45) contain ubiquitin-binding domains and were shown to drive cargo sorting in EVs (Sundquist et al. 2004; Slagsvold et al. 2005; Bilodeau et al. 2002; C et al. 2002). Moreover, ALIX can participate in cargo sorting in a ubiquitin-dependent and independent manner (Baietti et al. 2012; Dores et al. 2012). This also includes the tetraspanins, CD9, CD63, or CD81 (Larios et al. 2020). Other ways are also described, including ceramide or tetraspanin-mediated cargo loading into ILVs (Teng and Fussenegger 2021). Besides proteins, RNA is also found in EVs and can be sorted by RNA-binding proteins, such as hnRNPA2B1 or SYNCRIP (Santangelo et al. 2016; Villarroya-Beltri et al. 2013).

After MVB formation, the common endosomal pathway would lead to the fusion with lysosomes and subsequent degradation. However, during vesicle secretion, this pathway is somehow altered, whereas the exact mechanisms are still largely unknown. One study showed that conjugation of TSG101 with the interferon-stimulated gene 15 (ISG15) on EVs, also known as ISGylation, determined its fate to fuse with lysosomes (Villarroya-Beltri et al. 2016). Subsequently, the transportation of MVBs to the plasma

membrane is mediated by microtubules and is mainly driven by RAB GTPases (Stenmark 2009). These molecular switches can recruit many effector proteins, including kinases, sorting adaptors, phosphatases, or motors (Stenmark 2009). At the plasma membrane, fusion and vesicle release are regulated by soluble NSF attachment protein receptor (SNARE) complexes and are dependent on the rearrangement of phospholipids and associated cytoskeleton in the plasma membrane (Jahn and Scheller 2006).

Microvesicles

Microvesicles are formed by outward budding and fission of the plasma membrane. One mechanism involves aminophospholipid translocases, scramblases, and calpain, which drive the physical bending of the plasma membrane by rearranging phospholipids. Moreover, ESCRT proteins, including ALIX, TSG101, VPS22, VPS4, or CHMP1/3, are also involved in ectosome formation. Microvesicle secretion is further regulated by RHO GTPase, RHO-associated protein kinase (ROCK), and the ADP-ribosylation factor 6 (ARF6) (van Niel, D'Angelo, and Raposo 2018; Teng and Fussenegger 2021; Tricarico, Clancy, and D'Souza-Schorey 2017). The formation of EVs is summarized in Figure 1.

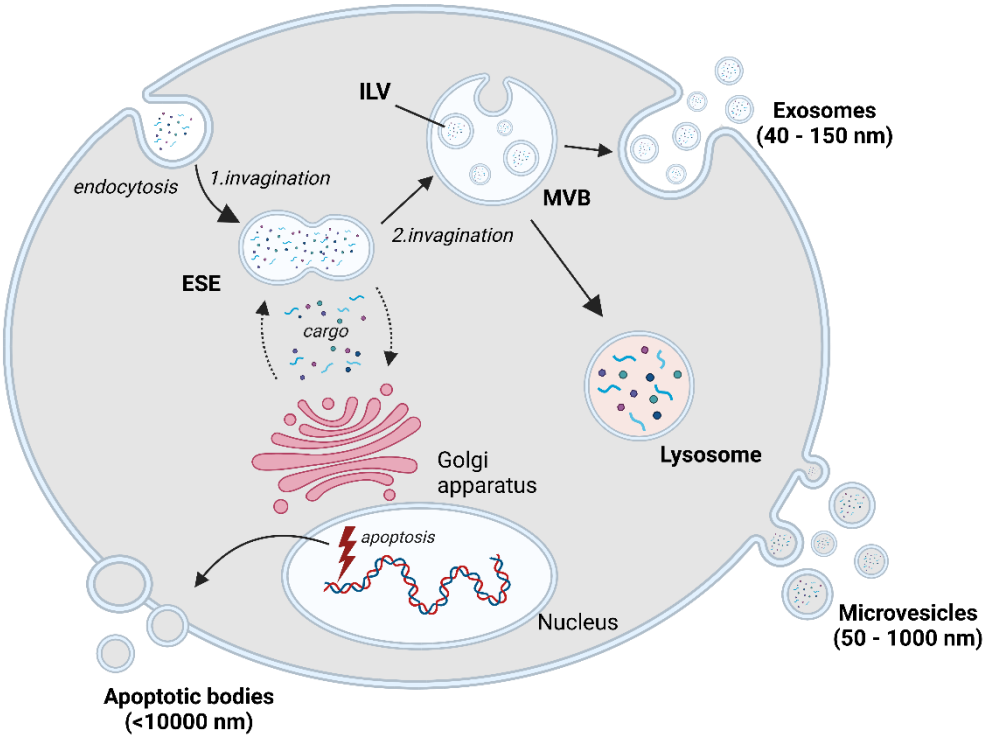

Figure 1: Schematic representation of EV biogenesis.
For further information, please refer to the introductory text. ESE: Early sorting endosome. MVBs: Multivesicular bodies. ILV: Intraluminal vesicle. Created with BioRender.com

1.1.2 EV uptake

To participate in intercellular communication, EVs need to bind and be taken up by recipient cells (Mulcahy, Pink, and Carter 2014; O'Brien et al. 2022). Many EV-associated proteins, including tetraspanins, integrins, proteoglycans, and lectins, can directly bind to cell receptors and, therefore, mediate functional effects or the subsequent uptake of the vesicle. The most common route is endocytosis into endosomal compartments, which can either be cell-specific or spontaneous, hence unspecific (Mulcahy, Pink, and Carter 2014; O'Brien et al. 2022). Besides classical clathrin-mediated endocytosis, EV uptake can also occur via caveolin-dependent endocytosis, micropinocytosis, phagocytosis, or lipid raft-mediated endocytosis (Mulcahy, Pink, and Carter 2014; O'Brien et al. 2022). After the uptake, the cargo must escape into the cytoplasm to mediate its function. Otherwise, the vesicles will either be recycled, degraded by lysosomes, or directly secreted. The "endosomal escape" of EV cargo is still not fully understood (Ribovski et al. 2023; Mulcahy, Pink, and Carter 2014). One potential mechanism is the fusion with endosomes. It is described that acidification of EVs by endosomes leads to fusion with the endosomal membrane ("back fusion") and subsequent cargo release (Bonsergent et al. 2021). This process has an efficiency of approximately 25-30 % (Bonsergent et al. 2021; Joshi et al. 2020). Besides endocytosis, direct fusion of EVs with the plasma membrane and release of its contents can also trigger functional effects. Here, direct fusion can be mediated by the interaction of transmembrane proteins or directly by both membranes (Ribovski et al. 2023). Similar to EV biogenesis, uptake can be influenced by environmental factors (Ribovski et al. 2023; Nakase et al. 2021). For instance, EVs secreted at a lower pH (pH=5) increased internalization in serum-free conditions. In contrast, in serum, an opposite effect was shown (Nakase et al. 2021). Moreover, hypoxic conditions can also influence the uptake of EVs, potentially by increasing proteoglycan-dependent endocytosis (M et al. 2021). In summary, the uptake and avoidance of rapid degradation are key requirements of EVs to mediate their function in recipient cells.

1.2 Tumor suppressor protein p53

The protein p53 is a regulatory factor encoded by the tumor suppressor gene *TP53* and is known as the "guardian of the cell," exerting significant roles in DNA damage repair, cellular senescence, or apoptosis (Hernández Borrero and El-Deiry 2021; Foroutan 2023). It was first described in 1979 and soon classified as an oncogene due to its high expression in many cancers (Foroutan 2023; Kress et al. 1979). However, after more

and more studies contradicted this theory, *TP53* was proposed as a tumor suppressor gene (Baker et al. 1989).

The canonical human p53 protein has a length of 393 amino acids (aa), which, depending on nomenclature, comprises five domains: a transactivation domain (TAD), a proline-rich domain (PRD), a DNA-binding domain (DBD), a tetramerization domain (TD) and a regulatory domain (RD). The N-terminal TAD is essential for co-factor binding, subsequently regulating the tumor-suppressive transcriptional activity of the protein (Hernández Borrero and El-Deiry 2021; Foroutan 2023). It is also the binding site of MDM2, the most common negative regulator of p53 (J. Lin et al. 1994). The PRD is essential for the stability and nuclear localization of the protein, while the DBD is critical for the recognition and binding of specific DNA sequences, known as p53 response elements (p53RE). The TD enables the oligomerization of p53 into tetramers, which is necessary for DNA recognition and binding. Finally, the C-terminal RD can regulate p53 activity by altering its DNA-binding capacity, which is mainly mediated by post-translational modifications, such as phosphorylation or acetylation (Hernández Borrero and El-Deiry 2021; Foroutan 2023).

The canonical functions of p53 are predominantly mediated by its activity to transactivate the translation of many target genes. After cellular stress, such as DNA damage, p53 can activate or alter multiple mechanisms, including DNA repair by inducing DNA damage response genes (e.g., *DDB2, XPC*), cell cycle, and growth arrest (e.g., *CDKN1A* (p21), *GADD45A)*, apoptosis (e.g., *BBC3, BAX*) or metabolism (e.g., *TIGAR, ALDH1A3*). It further regulates its expression and activity by inducing *MDM2*, which can ubiquitinate p53 at its TAD, eventually leading to protein degradation (Hernández Borrero and El-Deiry 2021; Foroutan 2023).

1.2.1 Role of WTp53 in the EV biogenesis of viable cells

Next to regulating cellular functions, p53 can induce many secreted factors and, therefore, extend its tumor-suppressor effects in a non-cell-autonomous way (Hernández Borrero and El-Deiry 2021). For instance, secretion of thrombospondin or PAI-2 leads to growth arrest of adjacent cells, also known as the “bystander effect” (Komarova et al. 1998). Another way p53 can influence intercellular communication is by regulating the production and secretion of EVs. For example, tumor suppressor-activated pathway 6 (TSAP6/STEAP3), a direct p53-target, is important for exosome secretion (Yu, Harris, and Levine 2006). Similarly, p53 can induce CHMP4, a subunit of the ESCRT-III

complex, which is essential in MVB formation by scission of ILVs into the MVB lumen (Vietri, Radulovic, and Stenmark 2020; Yu, Riley, and Levine 2009). It further has a critical role in the non-canonical ESCRT pathway in bridging cargos by interaction with ALIX (Baietti et al. 2012). Besides ESCRT-III, p53 was shown to regulate HRS, a subunit of the ESCRT-0 complex, that can mediate endosome formation by recruiting clathrin and the ESCRT-I complex and also drives cargo sorting by its ubiquitin-binding site (Teng and Fussenegger 2021; Raiborg et al. 2001; Lu et al. 2003; Y. Sun et al. 2016). The ESCRT-independent pathway, which is based on ceramide production by nSMase2, can also be influenced by WTp53. It was shown that nSMase activity was upregulated by ATR, Chk1, and p53 (Shamseddine et al. 2015). Caveolin-1 (CAV1), another factor directly upregulated by WTp53, can drive exosome biogenesis and cargo loading by controlling the cholesterol content in the endosomal compartment. It was shown that fibroblasts harboring CAV1 knockout failed to deposit extracellular matrix (ECM) by exosomal secretion, which led to increased tumor invasion *in vivo* (Albacete-Albacete et al. 2020). Furthermore, in melanoma cells, p53 and BAG6 were necessary for the secretion of anti-metastatic EVs. Specifically, BAG6 in complex with CBP/p300 acetylated p53 leads to recruitment of the ESCRT system, eventually producing EVs containing IL10 or CXCL13. This leads to patrolling monocytes being recruited with anti-tumorigenic functions (Schuldner et al. 2019). Finally, p53WT was shown to inhibit the transfer of several exosomal microRNAs to fibroblasts, which blocked the activation of the cells by altering p53 activity (Yoshii et al. 2019).

In summary, by orchestrating EV biogenesis, p53 can extend its functions to the environment in a non-cell-autonomous manner (Fig. 2).

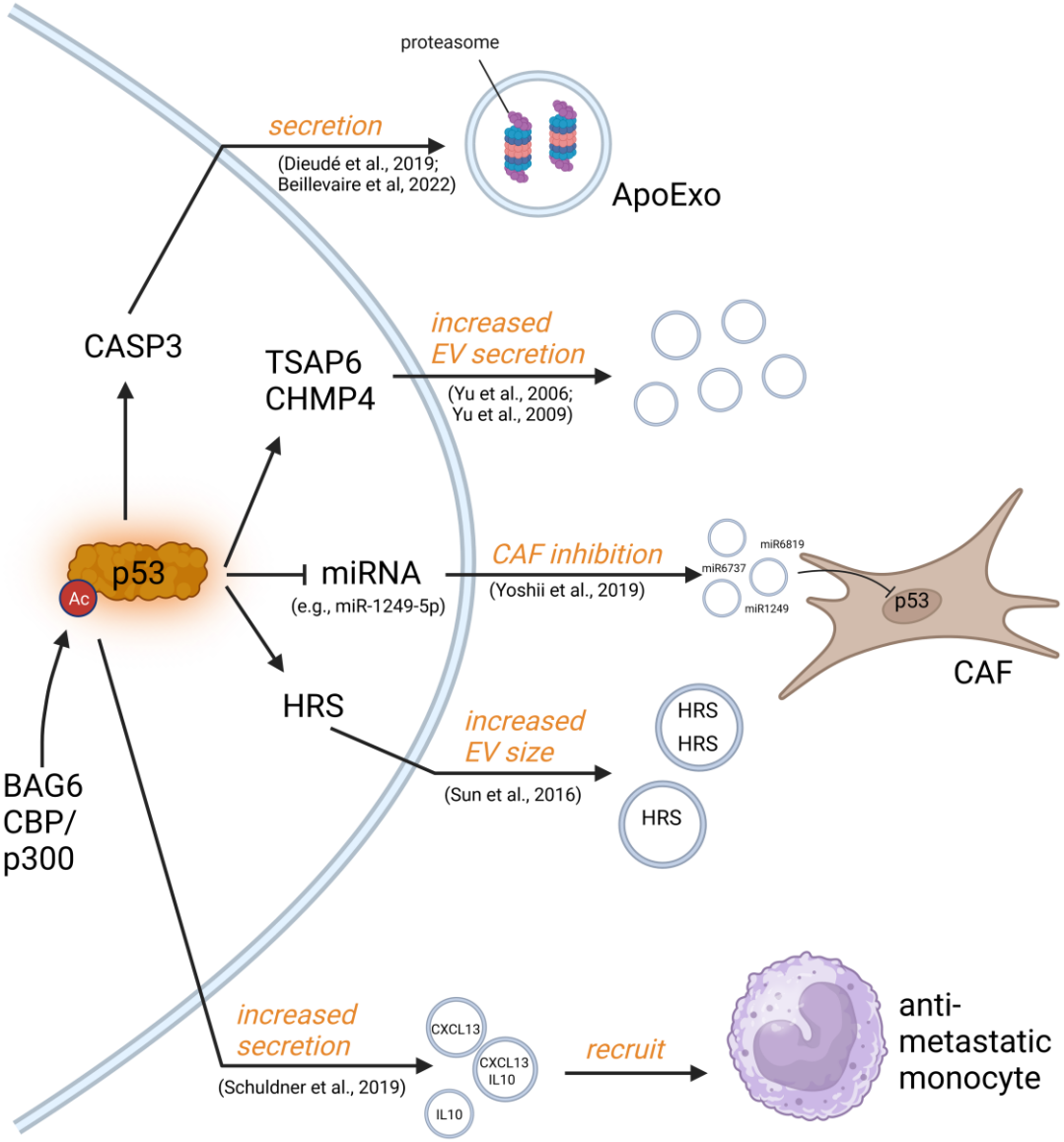

Figure 2: Role of p53 in the EV biogenesis.
P53 can influence the formation of EVs from viable cells and ApoExo by regulating different factors (Dieudé et al. 2015; Beillevaire et al. 2022; Yu, Harris, and Levine 2006; Yu, Riley, and Levine 2009; Y. Sun et al. 2016; Schuldner et al. 2019; Yoshii et al. 2019). For further information, please refer to the introductory text. ApoExo: apoptotic exosome-like vesicles, CAF: Cancer-associated fibroblast, miRNA: micro RNA, CASP3: caspase-3, HRS: hepatocyte growth factor. Created with BioRender.com

1.2.2 Role of WTp53 in apoptosis and secretion of small apoptotic EVs

Apoptosis is programmed cell death, which is a highly regulated and controlled mechanism that plays an essential role in the development or prevention of cancer by removing damaged cells. It can be triggered by intrinsic (e.g., cellular stress) or extrinsic factors, leading to corresponding pathways all regulated by p53 (Aubrey et al. 2018).

In the intrinsic pathway, p53 induces the upregulation of pro-apoptotic BCL2 family proteins (e.g., NOXA, PUMA), which can either directly or indirectly activate effector

proteins BAX/BAK by inhibition of pro-survival factors (e.g., BCL2, MCL). BAX/BAK permeabilizes the outer mitochondrial membrane, releasing cytochrome C and consequently activating a cascade of caspases. The caspase can then proteolytically dismantle the cell.

In the extrinsic pathway, apoptosis is mediated by cell death receptors (e.g., FAS, TNFR), which recruit and activate caspase-8. This triggers another cascade of caspases (e.g., caspase-3/caspase-7) and subsequent apoptosis. The extrinsic pathway can also be influenced by p53, such as upregulation of the FAS receptor (Hernández Borrero and El-Deiry 2021; Aubrey et al. 2018; Feroz and Sheikh 2020).

During apoptosis, cells are fragmentized, and molecules, including whole organelles, can be secreted by large apoptotic bodies (ApoBD, ⌀ 1-5 µm). Subsequently, apoptotic cells and ApoBD can be cleared by immune cells via phagocytosis (Santavanond et al. 2021). Secretion of smaller apoptotic EVs (ApoEV), including apoptotic microvesicles (ApoMV, ⌀ 100-1000 nm) and apoptotic exosomes (ApoExo, ⌀ <150 nm), was also observed recently (Dieudé et al. 2015; Poon et al. 2019; S. J. Park et al. 2018). Although less studied, ApoMV and ApoExo are believed to form similarly to their counterparts in healthy cells. While ApoMVs are created by blebbing from the plasma membrane, ApoExo forms intracellularly (S. J. Park et al. 2018; Zou et al. 2023; Gregory and Rimmer 2023). However, the formation of ApoExo is potentially independent of the ESCRT machinery and partly relies on the Sphingosine-1-phosphate (S1P)-S1P-receptor (S1PR) signaling pathway (S. J. Park et al. 2018; Sirois et al. 2011). During early apoptosis, sphingosines at the cell membrane are phosphorylated by sphingosine kinases (SPHK). The resulting S1Ps are transferred outside and subsequently bind and activate S1PR. Downstream signaling then modulates the actin cytoskeleton and forms endosomes. Maturation to MVB and fusion with the plasma membrane finally leads to the secretion of ApoExo, containing S1P and S1PRs, but also typical exosome markers, such as CD63 or TSG101 (S. J. Park et al. 2018). Notably, caspase-3, a direct p53 target, was shown to be necessary for the release of ApoExo by regulating the fusion with the cell membrane (Fig. 2) (Dieudé et al. 2015; Beillevaire et al. 2022).

Although apoptosis is generally considered a non-immunogenic process, ApoExo can function as a damage-associated molecular pattern (DAMP). Specifically, S1P, with S1PR and its associated G-coupled receptor proteins, can activate NFκB and induce cytokine expression, including IL1β (S. J. Park et al. 2018; Brodeur et al. 2023). In cancer, the exact functions of ApoExo remain elusive. However, it is proposed that they

play a major role in the onco-regenerative niche (ORN), a complex milieu of cells and soluble factors, which contributes to tissue repair and regeneration, subsequently mediating tumor progression (Gregory and Dransfield 2018). In summary, p53, as the central mediator of apoptosis, plays a role in the biogenesis of ApoEVs, which can have specific effects on recipient cells and potentially influence cancer progression.

1.2.3 Mutation of p53 and its functional implications in EV biogenesis

TP53 is a vital tumor suppressor gene and is often mutated or altered in cancer. While approximately 50 % of all cancers possess a mutation in the *TP53* gene, others show abnormal expression of the negative regulator *MDM2* (Freed-Pastor and Prives 2012; Mantovani, Collavin, and Del Sal 2019). Most mutations are single nucleotide variations (missense mutations) in the DNA-binding domain (~90 %), predominantly leading to loss of the anti-tumorigenic effects of the protein. However, mutp53 can also form tetramers with WTp53, altering its functions by exerting a dominant negative effect (Freed-Pastor and Prives 2012; Mantovani, Collavin, and Del Sal 2019). Here, the severity of the dominant negative effect depends on the ratio of mutated and wild-type proteins (Willis et al. 2004). In addition, some p53 mutants show gain-of-function (GOF) activities by promoting proliferation, metastasis, or therapy resistance. Therefore, cancer cells favor specific gain-of-function mutations or “hot-spot” mutations, which provide a survival advantage for the cell (Freed-Pastor and Prives 2012; Mantovani, Collavin, and Del Sal 2019; Hainaut and Pfeifer 2016). This includes two classes of mutations: conformational or contact mutants. The first includes R175H or Y220C, resulting in an altered, unfolded protein structure due to lower thermodynamic stability. In contrast, contact mutants retain their structure but are impaired in their ability to bind the p53RE. This includes mutants such as R248Q, R248W or R273H (Hainaut and Pfeifer 2016)

One specific characteristic of mutp53 is its increased stability. While WTp53 is highly regulated and primarily degraded in unstressed cells, mutp53 is overexpressed in many cancer cells. This is due to the altered negative feedback loop with MDM2 (Lukashchuk and Vousden 2007). Although MDM2 can potentially bind, ubiquitinate, and degrade some forms of mutp53, the efficiency is lower due to missing transactivation by WTp53 (Lukashchuk and Vousden 2007). Moreover, mutp53 can attach to the heat-shock-protein-90 (HSP90), which represses MDM2 regulatory functions (Y. Peng et al. 2001). Therefore, mutp53 is stabilized in cancer cells and can exert its oncogenic activity, for instance, by altering the transcriptome of the cells. Although the ability of GOF mutp53 to bind to the p53RE is compromised, it was shown to bind to novel DNA-binding sites

and regulate gene transcription (Göhler et al. 2005; E. Kim and Deppert 2007). It can further bind and influence other transcription factors, including p63, p73, SMAD, or NFκB (M. P. Kim and Lozano 2018). Besides the transcriptional level, mutp53 was shown to promote tumor proliferation and metastasis in many ways (Mantovani, Collavin, and Del Sal 2019; Muller et al. 2009). A particular mechanism is its influence on the endosomal pathway, leading to the recycling of cell surface receptors and integrins. By interacting with the Rab-coupling protein RCP, mutp53 increases the translocation of EGFR and α5β1 integrin, leading to increased tumor invasion (Muller et al. 2009).

Alteration in the endosomal pathway further plays an essential role in the secretome, including the secretion of EVs. It was shown that mutp53 can influence the composition of EVs (Pavlakis, Neumann, and Stiewe 2020; Pavlakis and Stiewe 2020; Novo et al. 2018). For instance, the transcription and sorting of podocalyxin (PODXL) into EVs were repressed, which was shown to drive receptor recycling and migration in recipient cells (Novo et al. 2018). In addition, HSP90 is preferentially sorted into EVs by mutp53, associated with tumor malignancy, motility, and metastasis (S. Zhang et al. 2020; Wong and Jay 2016). Vice versa, it was recently shown that HSP90 is vital for mutp53 sorting into the EVs, promoting fibroblast conversion into a pro-tumorigenic phenotype (S. Ma et al. 2021). Besides specific protein sorting, altered miRNA composition in EVs can further influence tumor progression. SUMOylation of the RNA-binding protein hnRNPa2b1 leads to enrichment of miR-1246 in EVs, eventually reprogramming macrophages into the tumor-promoting M2-phenotype (Villarroya-Beltri et al. 2013; Cooks et al. 2018). Other miRNAs, predominantly transferred by mutp53-derived exosomes, were shown to activate fibroblasts and increase tumor metastasis (Ju et al. 2019).

In summary, a mutation in the *TP53* gene leads to loss of tumor suppressor function and can also lead to neomorphic GOF. This includes transcriptional changes as well as changes in secretome and EV cargo composition, ultimately promoting tumor progression.

1.2.4 Role of WTp53 in senescence and SASP – crosstalk with NFκB

Cellular senescence is a hallmark of aging characterized by a stable cell cycle arrest but continuous metabolic activity. This includes the secretion of proinflammatory cytokines or chemokines (e.g., IL6, CXCL1, CXCL8), growth factors, and proteases, altogether forming the senescence-associated secretory phenotype (SASP). Senescence is a

major mechanism to prevent carcinogenesis and is implicated in development and tissue repair (Coppé et al. 2010; W. Huang et al. 2022). Besides aging, it can be induced by external and internal stimuli, such as oxidative stress, abnormal cell growth, or radiation (W. Huang et al. 2022). Initiation of senescence was shown to be dependent on p53 and Rb pathways (W. Huang et al. 2022; Mijit et al. 2020). For instance, DNA damage can induce phosphoinositide 3-kinase-like kinase (PIKKs, e.g., ATM/ATR), which phosphorylate p53 and MDM2, subsequently stabilizing the transcription factor. In turn, p53 induces CDKN1A, an inhibitor of cyclin-dependent kinases (CDK), eventually halting the cell cycle for DNA damage repair. Moreover, p53 and PIKKs regulate the assembly of DNA damage foci, which are local accumulations or modifications of DNA damage response proteins to the site of a double-strand break (DSB) (W. Huang et al. 2022; Mijit et al. 2020). DNA damage foci are typically transient and resolve after the DSB is repaired. However, in case of irreparable damage, the foci persist and become “DNA segments with chromatin alterations reinforcing senescence” (DNA-SCARS), which were shown to be essential for SASP formation (Rodier et al. 2009; 2011). Initially believed to represent senescence markers, SASP is now considered an active contributor. For instance, IL6 and CXCL8, two key components, can have autocrine or paracrine effects to reinforce or induce senescence in recipient cells (Kortlever, Higgins, and Bernards 2006; Takasugi et al. 2023; Xue et al. 2007). Moreover, both can recruit immune cells for clearing senescent cells, therefore mediating an anti-tumorigenic function (Xue et al. 2007). However, SASP is a double-edged sword, and prolonged senescence can lead to pro-tumorigenic effects, including enhanced tumor proliferation and invasion (Coppé et al. 2010; Takasugi et al. 2023). Regulation of the SASP formation was shown to be primarily mediated by the nuclear factor kappa-light-chain-enhancer of activated B cells (NFκB) transcription factor family (Chien et al. 2011).

The mammalian NFκB family comprises five structurally related proteins, including NFκB1 (p50), NFκB2 (p52), RelA (p65), RelB, and c-Rel (Taniguchi and Karin 2018). To exert its functions as a transcription factor, NFκB forms homo- or heterodimers (predominantly as p50/RelA or p50/c-Rel for canonical or p52/RelB for non-canonical pathway) and translocates into the nucleus. In the canonical pathway, NFκB proteins are retained in the cytoplasm and, therefore, inactivated by the IκB protein family. Upon activation, a complex of IκB kinase, consisting of the catalytic subunits IKKα, IKKβ, and the regulatory IKKγ (NEMO), phosphorylates the inhibitor of NFκB (IκBα), which leads to dissociation of the NFκB complex and proteasomal degradation of IκBα. The dimer can eventually translocate into the nucleus and induce transcription of many target genes.

The non-canonical pathway involves the activation of the NFκB-inducing kinase (NIK) and subsequent phosphorylation of IKKα, which further triggers the processing of the NFκB2 precursor in its active form – p52. Together with RelB, the NFκB dimer can translocate into the nucleus and activate transcription (Taniguchi and Karin 2018).

During senescence, NFκB can be activated in several ways, including DNA damage response, which is mediated by p53 (Rodier et al. 2009; Lopes-Paciencia et al. 2019). Specifically, the cytosolic DNA sensor cGMP-AMP synthase (cGAS) detects DNA damage and produces the second-messenger cGMP, activating the adapter protein STING. STING then recruits TANK-binding kinase 1 (TBK1) and IκB kinase to activate NFκB (H. Yang et al. 2017). Alternatively, STING can be activated in a non-canonical pathway by ATM and the DNA-binding protein IFI16, forming a complex together with p53 and TRAF6, eventually inducing NFκB (Dunphy et al. 2018). Therefore, DNA damage can lead to cellular senescence and SASP via crosstalk of p53 and NFκB. However, p53 is also considered a negative regulator of the SASP by suppressing p38MAPK activity, which is an essential inducer of NFκB (Freund et al. 2012). This was proposed to inhibit a prolonged SASP, which is associated with a malignant phenotype in cancer (Lopes-Paciencia et al. 2019; Coppé et al. 2008).

1.3 Ovarian Cancer

Ovarian Cancer (OC) is the leading cause of death in women with gynecological diseases (Matulonis et al. 2016). It is not a single disease but a hypernym of various tumors affecting the ovaries. It can be divided into histological subtypes, with epithelial ovarian carcinoma (EOC) representing ~90 % of all cases. EOC is further divided into class I and class II type tumors. While class I represents mainly low-grade tumors, which are characterized by slower growth and better patient outcomes, class II represents high-grade tumors, including the most common form of EOC, high-grade serous ovarian carcinoma (HGSOC) (Matulonis et al. 2016).

1.3.1 High-Grade Serous Ovarian Carcinoma (HGSOC)

The origin of HGSOC was initially believed to be in the ovaries; however, emerging research suggests that it predominantly starts in the epithelium of the fallopian tube (Matulonis et al. 2016; Labidi-Galy et al. 2017). In almost all cases, epithelial cells acquire p53 mutations (~96 %), leading to non-proliferative precursor cells, also called “p53 signature”. This further progresses to a serous tubal intraepithelial carcinoma (STIC) lesion often characterized by BRCA gene mutations (~40 %), nuclear polymorphism, and

loss of polarity. By acquiring more mutations, cells become invasive and can invade the ovaries, where they become HGSOC. However, only 60-80 % of HGSOC cases are associated with a STIC lesion, indicating other possible ways of disease induction (Matulonis et al. 2016; Punzón-Jiménez et al. 2022).

The primary treatment of HGSOC involves cytoreductive surgery with subsequent platinum-based chemotherapy, including carboplatin and paclitaxel. Some targeted therapies, such as the VEGF-targeting antibody bevacizumab or PARP inhibitors, are also used in the clinic. Although primary treatment is initially successful in about 70 % of cases, most patients will relapse at some stage (>80 %). In addition, recurrent tumors are often resistant to platinum-based therapy, complicating the treatment of these patients (Matulonis et al. 2016; Punzón-Jiménez et al. 2022; Bowtell et al. 2015).

One hallmark of HGSOC is its unusual dissemination at an early stage of the disease (Matulonis et al. 2016; Punzón-Jiménez et al. 2022). Compared to other tumors, HGSOC does not require blood vessels or lymph nodes for metastasis and, therefore, does not need to undergo a massive cellular transformation before its dissemination. It mainly spreads within the peritoneal cavity by detaching from the primary tumor and disseminating by the passive physiological flow of the peritoneal fluid. In most cases, HGSOC metastasizes to the omentum, a structure of adipose and connective tissue (Matulonis et al. 2016; Pogge von Strandmann et al. 2017; Nieman et al. 2011). Specifically, tumor cells predominantly invade “milky spots” in the omentum, comprising immune cells and adipocytes (Nieman et al. 2011). The early dissemination, together with low and nonspecific symptoms, is a major factor in the late detection of the disease, which typically occurs at advanced stages (Matulonis et al. 2016; Pogge von Strandmann et al. 2017).

Another hallmark of HGSOC is an abnormal accumulation of peritoneal fluid, called ascites, which indicates OC dissemination. Mechanistically, the accumulation occurs through lymphatic obstruction, increased fluid production, and enhanced vascular permeability, partly driven by the vascular endothelial growth factor (VEGF) (Nunes and Ricardo 2022; Rickard et al. 2021). Malignant ascites contain various cells and molecular factors, forming a unique TME, which promotes cancer proliferation, survival, and therapy resistance (Nunes and Ricardo 2022; Worzfeld et al. 2017).

1.3.2 Role of the tumor microenvironment in HGSOC

The unique TME OC comprises molecular factors, including cytokines, lipids, integrins, matrix metalloproteases (MMPs) or nutrients, and stromal cells, including cancer cells, fibroblasts, macrophages, adipocytes, T cells, or NK cells. It is essential in tumor progression, promoting proliferation, invasion, metastasis, and therapy resistance (Worzfeld et al. 2017; Mei et al. 2023). For instance, tumor cells can form a pre-metastatic niche by controlling the phenotype of cancer-associated fibroblasts (CAFs) via TGFβ expression or inducing mesothelial-to-mesenchymal transition in mesenchymal cells (Cai et al. 2012; Mei et al. 2023). Tumor-derived TGFβ can further activate neutrophils to form a premetastatic niche in the milky spots of the omentum, eventually facilitating metastasis (Lee et al. 2020). Moreover, adipocytes can provide nutrition for tumor cells by upregulating the fatty-acid receptor CD36 in OC cells. (Ladanyi et al. 2018). Other important cells of the TME, such as macrophages, T cells, or NK cells, can also enhance metastasis, proliferation, angiogenesis, or therapy resistance, thereby promoting cancer progression (Worzfeld et al. 2017; Mei et al. 2023).

1.3.3 Role of EVs in HGSOC

Besides direct and indirect interaction through soluble factors, OC cells and their unique TME can communicate via EVs. It was shown that EVs can participate in immune evasion, tumor invasion, and drug resistance (Worzfeld et al. 2017; Strandmann and Müller 2016). For instance, EVs isolated from OC ascites express FAS ligand (FAS-L), which impairs the cytotoxicity of lymphocytes by inducing apoptosis (Abrahams et al. 2003). Moreover, transported phosphatidylserine (PS) can arrest T cell signaling cascades, further impairing the anti-tumorigenic functions of T-cells (Kelleher et al. 2015). Immune evasion is also promoted by EV-associated HSP70, which activates myeloid-derived suppressor cells (MDSCs) via its Toll-like receptor-2 (TLR2). Subsequently, MDSCs suppress T cell and NK cell activity, further promoting tumor progression (Gobbo et al. 2016). Furthermore, EVs can carry many proteins or micro RNAs implicated in invasion, angiogenesis, and metastasis of OC (W. Tian et al. 2022). The glycoprotein Basigin (CD147) on OC-EVs induces angiogenetic activity in endothelial cells (Millimaggi et al. 2007). The cell adhesion molecule CD44 was shown to be transferred by EVs to peritoneal mesothelial cells, subsequently promoting invasion (Nakamura et al. 2017). Notably, mutp53 was shown to be transferred by EVs and activate CAFs, enhancing tumor growth (S. Ma et al. 2021).

Chemoresistance is a major problem of HGSOC and can be strongly influenced by EVs (W. Tian et al. 2022). Interestingly, EV secretion is correlated to OC aggressiveness, and therapy-resistant cancers were shown to secrete more EVs (Sharma et al. 2018). Paracrine transfer of EVs containing miR-21-3p was shown to confer therapy resistance in the recipient cells (Pink et al. 2015). Similarly, sensitive OC cells treated with cisplatin triggered EV secretion which induce therapy resistance and invasiveness in bystander cells (Samuel et al. 2018). However, EV-mediated drug resistance can also be achieved by altering the TME. EV-carried plasmas gelsolin (pGSN) can induce $CD8^+$ T cell apoptosis, which conferred cisplatin resistance of OC cells by increasing glutathione (GSH) (Asare-Werehene et al. 2020).

In summary, EVs in the TME of OC can vigorously promote tumor progression by reciprocal interaction between tumor cells and adjacent stromal or immune cells. However, the role of p53 in this interaction remains elusive.

1.4 Cancer-associated fibroblasts (CAFs)

1.4.1 Fibroblasts and Cancer-associated Fibroblasts

Fibroblasts, a heterogeneous population of mesenchymal cells, play pivotal roles in synthesizing complex extracellular matrices and establishing signaling microenvironments. Through the secretion of biophysical and biochemical cues, fibroblasts contribute to the dynamic regulation of cellular activities and the overall tissue microenvironment (Plikus et al. 2021). Moreover, they can serve as progenitor cells for other specialized mesenchymal cells, such as chondrocytes or adipocytes, and can transdifferentiate into epithelial or endothelial cells. Less than 20 % of fibroblast-enriched genes overlap between organs, underscoring the cells' substantial heterogeneity (Muhl et al. 2020). In consequence, unique and specific fibroblast markers are missing. However, they can be characterized depending on their location and state by their typical spindle or stellate form and a combination of markers, such as vimentin (Vim), platelet-derived growth factor receptor alpha (PDGFRα), fibroblast-specific protein (FSP1/S100A4), fibroblast-activating protein (FAP) or alpha-smooth muscle actin (αSMA) (Plikus et al. 2021).

An essential function of fibroblasts in adult organs is the regulation of wound healing (Plikus et al. 2021). Upon tissue damage, quiescent fibroblasts, characterized by low proliferation and minor extracellular matrix (ECM) secretion, can be activated

predominantly via the TGFβ-SMAD2/SMAD3 pathway. The resulting myofibroblast expresses contractile proteins, such as αSMA, and orchestrates ECM remodeling. In addition, immune cells are recruited by cytokine and chemokine release, further contributing to tissue repair (Plikus et al. 2021; Van Linthout, Miteva, and Tschöpe 2014). Usually, activation of quiescent fibroblasts is a reversible process; however, continuous or aberrant activation of myofibroblasts can lead to excessive secretion of ECM, and sustained inflammation can promote several diseases, including cancer (Plikus et al. 2021).

Notably, cancer is referred to as a wound that does not heal, explaining aberrant activation of fibroblasts in the TME (Dvorak 1986). These CAFs are predominantly described as tumor-promoting, for instance, by establishing an immune-suppressive TME, conferring therapy resistance, or encouraging tumor proliferation, invasion, and metastasis (Sahai et al. 2020; Biffi and Tuveson 2020). However, anti-tumorigenic functions are also described, which is explained by the vast heterogeneity of CAFs. Although many subtypes of CAFs are identified in different cancers, two main groups are regularly reported: myofibroblastic CAFs (myCAFs) and inflammatory CAFs (iCAFs) (Sahai et al. 2020; Biffi and Tuveson 2020).

MyCAFs are usually located close to the tumor and characterized by a high αSMA expression and aberrant ECM deposition, which can act as a barrier and confer therapy resistance or provide nutrients to cancer cells. In contrast, iCAFs are located distally from the tumor and primarily secrete inflammatory markers as well as growth factors, including CXCL12, IL6, or CXCL1, which can promote tumor growth and establish immunosuppression (Sahai et al. 2020; Biffi and Tuveson 2020). CAFs can be activated by several mechanisms, including hypoxia, oxidative stress, ECM remodeling, or tumor-derived cytokines. The main regulatory switches of CAF activation are TGFβ/TGFBR, IL1/IL1R1, CXCL12/CXCR4, and CXCL1/CXCR2 with their associated pathways NFκB, JAK/STAT, PI3K/AKT, or MAPK pathway (Sahai et al. 2020; Biffi and Tuveson 2020; Fang et al. 2022).

1.4.2 CAFs in ovarian cancer progression

Activated CAFs play a pivotal role in the disease progression of OC by promoting tumor growth, metastasis, and therapy resistance. In line, high CAF expression in the TME of HGSOC is associated with poor patient survival (M. Zhang et al. 2022). Four major subtypes (CAF-S1, -S2, -S3, -S4) were identified in HGSOC based on their expression

of αSMA, CD29 (ITGB1) and FAP, with CAF-S1 (FAP^{high} $CD29^{med\text{-}high}$ αSMA^{high}) and CAF-S4 (FAP^{-} $CD29^{high}$ αSMA^{high}) representing activated CAFs (M. Zhang et al. 2022; Givel et al. 2018). In a single-cell analysis, CAF-S1 expression was further divided into a myCAF (αSMA^{high}) and iCAF (αSMA^{low}) phenotype (M. Zhang et al. 2022; Givel et al. 2018; Hornburg et al. 2021).

CAFs can promote OC progression by the direct communication with cancer cells, mediated by soluble factors or extracellular vesicles. For instance, secretion of periostatin (POSTN) by TGFβ-activated CAFs can induce EMT and subsequent OC invasion by triggering the PI3K/Akt pathway via interaction with the integrin αvβ3 (Yue et al. 2021). VCAN, another TGFβ-induced factor in CAFs, was also shown to mediate tumor invasion by stimulating NFκB signaling in OC cells, subsequently upregulating MMP9 and CD44 (Yeung et al. 2013a). CAFs can further form heterotypic spheroids with ascites-derived cancer cells, critically contributing to their metastatic potential (Gao et al. 2019). This was shown to be induced by the reciprocal communication of cancer cells and CAFs. Cancer-derived TGFβ enhanced EGF secretion in CAFs, which upregulated ITGA5 in OC cells. ITGA5 then recruits CAFs to form pro-metastatic spheroids (Gao et al. 2019).

Besides direct function on cancer cells, CAFs can shape the TME and influence the innate and adaptive immune system (M. Zhang et al. 2022; C. Zhang et al. 2023). For instance, by excessive deposition of ECM, tumor infiltration of $CD8^{+}$ T-cells is reduced, which prevents T-cell contact-dependent tumor cell killing (Bougherara et al. 2015). Furthermore, the secretion of cytokines and chemokines, including TGFβ, CXCL1, CXCL12, IL6, or IL8, can create a tumor-suppressive and pro-tumorigenic environment by recruitment of regulatory cells (e.g., MDSC, T regs) or by altering immune cell functions (M. Zhang et al. 2022; C. Zhang et al. 2023). However, IL6 was also shown to transform T cells into highly cytotoxic T cells, presenting an anti-tumor function of CAFs (Szulc-Kielbik et al. 2021).

By shaping the TME, CAFs also contribute to chemotherapy resistance. ECM secretion can lead to physical barriers for immune cells and therapeutic drugs, both associated with therapy resistance (Kieffer et al. 2020; W. Wang et al. 2016). Other ways CAFs induce therapy resistance in OC cells include triggering autophagy-related genes or inhibiting apoptosis. EV-mediated transfer of miR-21, for example, induced paclitaxel resistance by suppressing pro-apoptotic APAF1 (Au Yeung et al. 2016). Moreover, increased reactive oxygen species produced by CAFs induced the expression of

autophagy genes YAP or CTGF, which mediated cisplatin resistance (M. Zhang et al. 2022).

In summary, CAFs can influence HGSOC progression by directly altering cancer cell behavior or indirectly shaping the TME.

1.4.3 Role of p53 in the activation of CAFs

In almost all cancers, p53 is either mutated or altered in its activity (Mantovani, Collavin, and Del Sal 2019). Although mutations in CAFs are rare, altered p53 activity was demonstrated and associated with activation and tumorgenicity of CAFs (Fang et al. 2022; Hosein et al. 2010). Specifically, suppressing p53 in normal fibroblasts (NFs) increases the expression of αSMA, indicating an active CAF state (Procopio et al. 2015; Hayashi et al. 2016). Increased signaling of STAT3 was shown to activate CAFs, further leading to increased collagen contractions and secretion of CXCL12, which is associated with enhanced tumor invasion (Q. Liu et al. 2020; Addadi et al. 2010). In addition, loss of p53 functionality induced TSPAN12 expression, which is critical for contact-mediated invasion of tumor cells. In contrast, it was shown that overexpression of p53 induces a resting state, resulting in reduced tumor growth (Saison-Ridinger et al. 2017; Schmid et al. 2012). Therefore, altering the p53 activity in CAFs is a valid mechanism for tumor progression and can directly be influenced by cancer-derived EVs (J Bar et al. 2009; Yoshii et al. 2019). Mechanistically alerted p53 activity can induce CAFs by transcriptional-dependent or independent mechanisms (Arandkar et al. 2018).

1.4.4 Role of EVs in the crosstalk of cancer cells and CAFs

Activation of CAFs can be achieved by the crosstalk with cancer cells, which can be mediated by EVs (X. Yang et al. 2019). For instance, EV-delivered TGFβ can induce NFs transition to myofibroblast in various tumors, including ovarian cancer (Ringuette Goulet et al. 2018; Mazumdar et al. 2020; Giusti et al. 2018). Interestingly, EV-associated TGFβ was demonstrated to account for over 50 % of total TGFβ in the cell supernatant and exclusively activated the SMAD pathway (Ringuette Goulet et al. 2018). Moreover, micro RNAs transported by EVs can also induce CAF activation (X. Yang et al. 2019). Besides NFs, EVs were also shown to mediate the transdifferentiating of mesenchymal stem cells to CAFs. In OC, EVs induced the differentiation of mesenchymal stem cells (MSC) into a pro-tumorigenic myofibroblast subtype by triggering SMAD or Akt-dependent signaling (Cho et al. 2011). Mechanistically, the transition could depend on TGFβ, tetraspanins, or miRNA signaling (X. Yang et al. 2019; He et al. 2021).

Activated CAFs can secrete EV-containing microRNAs, lipids, or proteins, influencing cancer proliferation, metastasis, metabolism, and therapy resistance (Z. Peng et al. 2023). For instance, EV-mediated transfer of the metallopeptidase domain 10 (ADAM10) enhanced cell motility in breast cancer cells by activating RhoA signaling (Shimoda et al. 2014). Moreover, CD81-positive EVs induced Wnt-signaling in breast cancer, while CD9-enriched EVs induced MMP2-signaling in gastric cancer, both resulting in enhanced tumor invasion and motility (Z. Peng et al. 2023).

1.5 Aim of the thesis

EVs are pivotal in orchestrating OC progression by mediating communication between tumor cells and the surrounding TME, including CAFs. Previous research from our group has revealed the significant impact of p53 on EV biogenesis and cargo loading by interaction with BAG6 and CBP/p300, resulting in the secretion of antitumorigenic vesicles (Schuldner et al. 2019). Therefore, this project aimed to enhance our comprehension of the role of p53 in shaping EVs within the context of OC and its surrounding TME.

To this end, OC cell lines with defined p53 status were generated, and the following questions were investigated:

- How does the p53 status influence the gene expression and secretome in the generated cell lines?
    - Does the p53 status influence the expression of EV biogenesis-related genes?
    - Is there any gene expression or secretome differences between mutp53 and knockout cell lines?
- What is the composition/cargo loading of EVs isolated from the different cell lines?
- Are the EVs transferred and taken up by recipient cells, such as tumor cells and fibroblasts?
    - Are WTp53 or mutp53 transferred by EVs?
- What is the impact of the distinct EVs on the phenotype of fibroblasts?
    - What is the impact on the transcriptomic landscape?
    - How do the EVs influence the secretome of fibroblasts?
- What pathways are involved in the phenotypic changes of EV-treated fibroblast?

2. Material

2.1 Equipment

Equipment	Name	Manufacturer
Blotting system	Mini Trans-Blot® Cell	Bio-Rad Laboratories GmbH
Centrifuge	Heraeus MEGAFUGE 40R	Thermo Fischer Scientific
Confocal microscope (AG Jacob)	LEICA Stellaris	Leica Microsystems GmbH
Counting Chamber	Neubauer improved	Paul Marienfeld GmbH & Co. KG
Flow cytometer	FACS Canto II	Becton Dickinson
Flow cytometer for sorting	FACS Aria™ III	Becton Dickinson
Fluorescence microscope	Leica DM3000B with DFC300 FX camera	Leica Microsystems GmbH
Freezer (-80°C)	HERAfreeze™ HFU T	Thermo Fischer Scientific
Fridge (4°C) / Freezer (-20°C)	LIEBHERR MEDLINE	Liebherr
Gel documentation	Gel ix20 imager	Intas Science Imaging Instruments GmbH
Gel-Imager	ChemiDoc™ XRS	Bio-Rad Laboratories GmbH, München
Gel-imager (Fluorescence)	ChemiDoc MP Imaging System	Bio-Rad Laboratories GmbH, München
Heater	UniTHERMIX2	Lab Logistics Group GmbH
Incubator	HERAcell 240i	Thermo Fischer Scientific
Incubator (Hypoxia)	CB 210	BINDER GmbH
Incubator (Primary cells)	HERAcell 240	Thermo Fischer Scientific
Microplate Reader	SPECTRA MAX 340	Molecular Devices GmbH
Microscope	Leica DM IL LED	Leica Microsystems GmbH
Microscope for life cell imaging (AG Jacob)	LEICA DMI 8	Leica Microsystems GmbH
Milli-Q water system	GenPure Pro UV	Thermo Fisher Scientific
Nano-Flow Cytometry	Flow Nanoanalyzer	NanoFCM Co., Ltd
PCR cycler	Thermal Cycler T100™	Bio-Rad Laboratories, Inc.
Pipetboy	Acu 2	Integra Biosciences AG
qPCR System	Mx3000P	Agilent Technologies
Roller shaker	RS-TR05	Phoenix instrument GmbH
Rotor (for 10,000 xg)	TX-1000 Fiberlite F15-6x 100y	Thermo Fisher Scientific

Rotor (for UC big)	SW 32 TI	Beckman Coulter
Rotor (for UC small)	SW 41 Ti	Beckman Coulter
Shaker	SHAKER DRS-12	neoLab Migge GmbH
Spectrophotometer	NanoDrop2000	Thermo Fisher Scientific
Table centrifuge	Heraeus PICO 17	Thermo Fisher Scientific
Table centrifuge (refrigerated)	Heraeus FRESCO 17	Thermo Fisher Scientific
Ultracentrifuge (large)	Optima™ XPN-80 ultracentrifuge	Beckman Coulter
Ultracentrifuge (small)	Optima™ MAX-XP	Beckman Coulter
Vacuum pump	BVC control	VACUUBRAND GMBH + CO KG
Water bath	W6	GK Sondermaschienenbau GmbH
Workbench	MSC-ADVANTAGE	Thermo Fischer Scientific
Mass spectrometry	timsTOF Pro 2	Bruker Daltonics GmbH & Co
nanoflow liquid chromatography	nanoElute® 2	Bruker Daltonics GmbH & Co

2.2 Consumables

Pipette tips, cell culture flasks, falcon tubes, and plastic pipettes were acquired from different companies, including Sarstedt Inc, Lohmann & Rauscher, Carl Roth GmbH + Co. KG, Sigma-Aldrich or Thermo Fisher Scientific.

Consumable	**Manufacturer**
Syringe filters, Millex® (0.22 µm; PES)	Merck Millipore
Amersham™ Protran® 0.2 nitrocellulose Western blotting membranes	Cytiva
Microfuge tubes 1.5 ml	Beckman Coulter
Whatman filter paper	GE Healthcare Life Sciences
Syringe filters, Acrodisc®, Supor® membrane 0.1 µm	Cytiva
Amicon Ultra-15 Centrifugal Filter Unit with Ultracel-100 membrane, 3 kDa, 15 ml	Merck Millipore
Ibidi µ-slide 8 Well ibiTreat	Ibidi GmbH
Ibidi Culture-Inserts 2 Well for self-insertion 25 per case	Ibidi GmbH
Adhesive sealing foils for qPCR plates	Thermo Fisher Scientific
PCR plate without skirt, 96 well, white, High Profile, 200 µl, PCR Performance Tested, PP	Sarstedt AG
Circular cover slips, 18 mm	Menzel

2.3 Chemicals

Chemicals	Manufacturer
7-AAD Viability Staining Solution	BioLegend
Absolute qPCR SYBR Green Mix	Thermo Fisher Scientific
Ammonium persulfate	Carl Roth GmbH + Co. KG
Bovine Serum Albumin (BSA)	Carl Roth GmbH + Co. KG
Bromphenol blue	Thermo Fisher Scientific
CD 293 Medium (1X)	Thermo Fisher Scientific
Chloroform / Trichlormethan 99 % p.a.	Carl Roth GmbH + Co. KG
CL-2B sepharose matrix	GE Healthcare Life Sciences
Cleaning solution	NanoFCM Co., Ltd
Dimethylsulfoxid (DMSO)	Carl Roth GmbH + Co. KG
Doxycycline hydrochloride	MP Biomedicals
Dulbecco's Phosphate Buffered Saline (DPBS)	Gibco by Thermo Fisher Scientific
Ethanol 99,8 % p.a.	Carl Roth GmbH + Co. KG
FACS Clean solution	Becton Dickinson
FACS Flow	Becton Dickinson
FACS Rinse solution	Becton Dickinson
FACS Shutdown solution	Becton Dickinson
FastDigest Buffer, 10x	Thermo Fisher Scientific
Fetal bovine serum	Thermo Fisher Scientific
Formaldehyde 10 % ultrapure methanol-free	Polysciences, Inc
Geneticin (G418)	Capricorn Scientific GmbH
Glycerin	GERBU Biotechnik GmbH
Glycin	Carl Roth GmbH + Co. KG
HEPES solution	Sigma-Aldrich
Isopropanol	Carl Roth GmbH + Co. KG
Kanamycin sulfate	Sigma-Aldrich
L-Glutamine 200 mM (100x)	Thermo Fisher Scientific
Lipofectamine® 2000	Thermo Fisher Scientific
Methanol 99 %	Carl Roth GmbH + Co. KG
Milk powder	Carl Roth GmbH + Co. KG
Mowiol mounting media	Carl Roth GmbH + Co. KG
NaCl	Carl Roth GmbH + Co. KG
Opti-MEM	Thermo Fisher Scientific
Page Ruler™ pre-stained protein ladder, 10 to 180 kDa	Thermo Fisher Scientific
Penicillin + Streptomycin (100x)	Sigma Aldrich
Peptone ex casein	Carl Roth GmbH + Co. KG
Phosphatase Inhibitor Cocktail 3, DMSO solution	Sigma-Aldrich
Protease Inhibitor Cocktail	Sigma-Aldrich
ROTIPHORESE®Gel 30 (37,5:1)	Carl Roth GmbH + Co. KG

Saponin	Carl Roth GmbH + Co. KG
Sodium deoxycholate	Sigma-Aldrich
Sodium dodecyl sulfate (SDS) Pellets	Carl Roth GmbH + Co. KG
ß-Mercaptoethanol	Sigma-Aldrich
TEMED	Carl Roth GmbH + Co. KG
Thiazolblau (MTT)	Carl Roth GmbH & Co.KG
TRIS-HCl	Carl Roth GmbH + Co. KG
TRITON X-100	Sigma-Aldrich
TRIzol™ Reagent	Thermo Fisher Scientific
Trypan Blue Solution, 0.4 %	Gibco by Thermo Fisher Scientific
Trypsin-EDTA solution (10x)	Sigma-Aldrich
Tween 20	AppliChem GmbH
Vectashield with DAPI	Vector Labs
Water, nuclease-free (DEPC treated)	Carl Roth GmbH + Co. KG
Western HRP substrate, Immobilon® Forte	Merck Millipore
Yeast extract	Carl Roth GmbH + Co. KG

2.4 Buffers and Solutions

SDS-PAGE and Western Blot	
10x Ripa Buffer (pH 8.0)	500 mM TRIS Base (pH 8) 1.5 M NaCl 1 % SDS 5 % Triton X-100 5 % DOC (Deoxycholic acid)
Separating gel 20 % (200 ml) (pH 8.9)	133 ml Rotiphorese Gel30 AA/BA 50 ml 1.5 M Tris/HCl 10 % SDS 15 ml ddH_2O
Collecting gel 4 % (200 ml) (pH 6.8)	26.5 ml Rotiphorese Gel 30 AA/BA 25 ml 1.5 M Tris/HCl 10 % SDS 146.5 ml ddH_20
Tris/SDS Buffer (200 ml) (pH 8.9)	50 ml 1.5 M Tris/HCl 10 % SDS 148 ml ddH_20
10x TBST (pH 7.5)	60.5 g/l TRIS 87.6 g/l NaCl

	1 % Tween20
10x Running buffer (pH 8.3)	0.25 M TRIS 1.92 M Glycin 1 % SDS
10x Blotting buffer (Stock)	0.25 M TRIS 1.92 M Glycin
1x Blotting buffer	100 ml 10x Blotting buffer 700 ml ddH_20 200 ml Methanol
6x Laemmli Buffer	375 mM TRIS/HCL (pH 6.8) 50 % Glycerin 9 % SDS 9 % ß-Mercaptoethanol 0.03 % Bromphenol blue
10 % APS	1 g ammonium persulfate in 10 ml ddH_20
Cell death and viability	
10x Annexin-Binding-Buffer (pH 7.4)	1.4 M NaCl 100 mM HEPES 25 mM $CaCl_2$ 1 % BSA
Solubilization (MTT)	80 % Isopropanol 10 % Triton-X100 10 % 1 M HCl
Cloning	
LB Medium	1 % Peptone 1 % NaCl 0.5 % Yeast extract
Immunofluorescence	
Fixation buffer	4 % PFA in PBS
Permeabilization buffer	0.5 % Triton X-100 in PBS
Permeabilization buffer (AG Jacob)	0.1 % Triton X-100 in PBS

2.5 Cells

Name	Origin	Cultivation
OVCAR8	Human High-Grade Serous Ovarian Carcinoma Cell line	RPMI Glutamax + 10 % FCS + 1 % Penicillin/Streptomycin
Human Dermal Fibroblast neonatal (HDFn)	neonatal foreskin	DMEM + 10 % FCS + 1 % Penicillin/Streptomycin

2.6 Antibodies

Western Blot

Primary Antibody	**Host**	**Dilution**	**Company**	**Order No.**
β-Actin	mouse (monocl.)	1:2500	Sigma-Aldrich	A1978
ALIX (1A12)	mouse (monocl.)	1:1000	Santa Cruz Biotechnology	sc-53540
Anti-STAT3	rabbit (polycl.)	1:1000	Sigma-Aldrich	06-596
BAG6	Rabbit	1:1000	Selfmade in a hybridoma system	
GAPDH	rabbit (polycl.)	1:10000	Sigma-Aldrich	G9545
HSP70/72 (C92F3A-5)	mouse (monocl.)	1:1000	Enzo Life Sciences	ADI-SPA-810
IκBα (L35A5)	mouse (monocl.)	1:1000	Cell Signaling Technology	4814P
p53	rabbit (polycl.)	1:1000	Cell Signaling Technology	9282
p53 (DO-1)	mouse (monocl.)	1:1000	Santa Cruz Biotechnology	sc-126
p65 (D14E12)	rabbit (monocl.)	1:1000	Cell Signaling Technology	8242S
PARP	mouse (monocl.)	1:1000	BD Transduction Laboratories	611038
Phospho-IkBa (Ser32) (14D4)	rabbit (monocl.)	1:1000	Cell Signaling Technology	2859P
phospho-p65 (Ser536) (93H1)	rabbit (monocl.)	1:1000	Cell Signaling Technology	3033S
Phospho-STAT3 (Tyr705)	mouse (monocl.)	1:1000	Thermo Fisher Scientific	MA5-15193
Secondary Antibody	**Host**	**Dilution**	**Company**	**Order No.**
rabbit IgG-HRP	goat	1:10000	Cell Signaling Technology	7074

mouse IgG-HRP	horse	1:10000	Cell Signaling Technology	7076
Goat Anti-Rabbit IgG IRDye® 800CW	goat (polycl.)	1:10000	LI-COR Biosciences	926-32211
Goat Anti-Mouse IgG IRDye® 680RD	goat (polycl.)	1:10000	LI-COR Biosciences	926-68070

Immunofluorescence

Primary Antibody	**Host**	**Dilution**	**Company**	**Order No.**
p53 (DO-1)	mouse (monocl.)	1:400	Santa Cruz Biotechnology	sc-126
NFκB p65	rabbit (polycl.)	1:100	Thermo Fisher Scientific	510500
α-tubulin	mouse (monocl.)	1:100	Sigma Aldrich	T9026
Secondary Antibody	**Host**	**Dilution**	**Company**	**Order No.**
Anti-Mouse IgG Alexa Fluor 633	goat	1:400	Thermo Fisher Scientific	A-21050
Anti-Mouse IgG Alexa Fluor 533	goat	1:200	Thermo Fisher Scientific	A28180
Anti-Rabbit IgG Alexa Fluor 647	goat	1:200	Thermo Fisher Scientific	A-21244

Nano-flow cytometry

Antibody	**Host**	**Conc. / sample**	**Company**	**Order No.**
PE anti-human CD9	mouse (IgG1, κ)	100 ng	Biolegend	312106
FITC anti-human CD63	mouse (IgG1, κ)	100 ng	Biolegend	353005
FITC anti-human CD81 (TAPA-1)	mouse (IgG1, κ)	100 ng	Biolegend	349504
PE anti-human CD29 [TS2/16]	mouse (IgG1, κ)	100 ng	Biolegend	303003

2.7 Cytokines and enzymes

Cytokine/Inhibitor	**Stock**	**Manufacturer**
TGFβ1	20 µg/ml	R&D Systems (#240-B)
SfiI	(10 U/µL)	Fisher Scientific (#ER1821)
Shrimp Alkaline Phosphatase (SAP)		Fisher Scientific (#15533687)
Phusion high-fidelity polymerase 100U	(2 U/µl)	Fisher Scientific (#10024537)

2.8 Primers (RT-qPCR/Sequencing)

All oligonucleotides are designed for human and ordered from Sigma-Aldrich. Primers were reconstituted to 100 µM in ddH2O and tested for efficiency.

RT-qPCR

Target	Sequence 5'→3'	Amplification Efficiency (%)	R^2
ACTA2_fw *ACTA2_rev*	TGCCTTGGTGTGTGACAATG TCACCCACGTAGCTGTCTTT	99	1.00
BRCA2_fw *BRCA2_rev*	GAAGAATGCAGCAGACCCAG CAGCAGATTCCATGGCCTTC	101	1.00
CD9_fw *CD9_rev*	AAATTCCACATCATCGGCGC CGGATAGCACAGCACAAGAT	98	1.00
CDKN1A_fw *CDKN1A_rev*	TGGAGACTCTCAGGGTCGAAA CCGGCGTTTGGAGTGGTA	107	0.99
COL1A1_fw *COL1A1_rev*	ATGTGCCACTCTGACTGGAA ACCAGTCTCCATGTTGCAGA	99	0.99
CXCL1_fw *CXCL1_rev*	ACCCCAAGAACATCCAAAGTG TTTCCGCCCATTCTTGAGTG	97	0.99
CXCL8_fw *CXCL8_rev*	TACTCCAAACCTTTCCACCC CCAGTTTTCCTTGGGGTCCA	98	0.96
GAPDH_fw *GAPDH_rev*	GGAAGGTGAAGGTCGGAGTC TGAAGGGGTCATTGATGGCA	103	0.97
IL1A_fw *IL1A_rev*	ACTGCCCAAGATGAAGACCA TTAGTGCCGTGAGTTTCCCA	88	0.90
IL1B_fw *IL1B_rev*	TGAAAGCTCTCCACCTCCAG TTCAACACGCAGGACAGGTA	81	0.93
IL-6_fw *IL-6_rev*	AGACAGCCACTCACCTCTTC AGTGCCTCTTTGCTGCTTTC	111	0.98
L27_fw *L27_rev*	AAAGCTGTCATCGTGAAGAAC GCTGTCACTTTGCGGGGGTAG	90	0.99
LIF_fw *LIF_rev*	ACCGCATAGTCGTGTACCTT CGTTGAGCTTGCTGTGGAG	100	1.00
MDM2_fw *MDM2_rev*	AGTGAATCTACAGGGACGCC GTATCACTCTCCCCTGCCTG	100	0.99
MMP11_fw *MMP11_rev*	CCTGGACTATCGGGGATGAC AAAGGTGTAGAAGGCGGACA	99	0.90
RELB_fw *RELB_rev*	ATGGATCCTGTGCTTTCCGA GGCCCGCTTTCCTTGTTAAT	99	1.00
TGFB2_fw *TGFB2_rev*	GACCCCACATCTCCTGCTAA TAAAGTGGACGTAGGCAGCA	109	0.99

TP53_fw *TP53_rev*	CTCTCCCCAGCCAAAGAAGA GTTCCAAGGCCTCATTCAGC	98	0.99
U6_fw *U6_rev*	CTCGCTTCGGCAGCACATA GCTTCACGAATTTGCGTGTCA	103	1.00

Sequencing

Name	Sequence 5'→3'	Description
p53 cloning Sfi1	Fw: GGCCTCTGAGGCCACCATGGAGGAGCCGCAGTCAGA Rev: TAGGCCTGACAGGCCTCAGTCTGAGTCAGGCC	Primer for cloning p53 into vector
pSBtet sequencing	Fw: TACGGTGGGCGCCTATAAAA Rev: AAAACCTCCCACATCTCCCC	Sequencing primer

2.9 Vectors

Vector	Function
px330-TP53-1 (Addgene, #121917)	Encodes sgRNA (ACCATTGTTCAATATCGTCC) targeting exon 4 of *TP53*. Used to create p53 knockout cells
px330-TP53-2 (Addgene, #121918)	Encodes sgRNA (GGAGAGGAGCTGGTGTTGT) targeting exon 9 of *TP53*. Used to create p53 knockout cells
pCMV(CAT)T7-SB100 (Addgene, #34879)	Contains SB100X transposase and was used to insert GOI located on a transposon vector
pSBtet-GN (Addgene, #60501)	Sleeping Beauty (SB)-transposon with inducible SfiI cloning site for GOI and constitutive expression of GFP, a reverse tetracycline-controlled transactivator (rtTA) and neomycin resistance gene
pSBbi-GN (Addgene, #60517)	SB-transposon with a constitutive bi-directional promoter, one side: SfiI cloning site for GOI, other side: GFP and neomycin resistance gene
p53-GFP (Addgene, #11770)	Contains 72R variant of p53 tagged with GFP
GFP-p53 (Addgene, #12091)	Contains 72R variant of p53 tagged with GFP

2.10 Kits

Name	Manufacturer
iScript™ cDNA Synthesis Kit	Bio-Rad Laboratories, Inc.
NucleoBond Xtra Midi (DNA Prep)	MACHEREY-NAGEL
NucleoSpin RNA Kit	MACHEREY-NAGEL
PierceTM BCA protein assay Kit	Thermo Fisher Scientific
Pierce™ NE-PER® Nuclear and Cytoplasmic Extraction Reagent Kit	Thermo Fisher Scientific

Proteome Profiler Human XL Cytokine Array Kit	R&D Systems

2.11 Software and online tools

Software/Tool	Developer/Website
BD FACS DIVA	BD Bioscience
BioRender	https://www.biorender.com/
EnrichR	Ma'ayan Laboratory, Computational Systems Biology (https://maayanlab.cloud/Enrichr/)
Fiji: ImageJ	https://fiji.sc/
FlowJo v10.9	BD Bioscience
Grammarly (v6.8.261)	Grammarly, Inc.
GraphPad Prism 10	GraphPad Software
Image Lab Software	Bio-Rad
Inkscape v1.3	The Inkscape Project (https://inkscape.org/de/)
InteractiVenn	http://www.interactivenn.net/
Microsoft Office	Microsoft
MxPro qPCR Software	Agilent Technologies
National Center for Biotechnology Information (NCBI)	https://www.ncbi.nlm.nih.gov/
Primer3web v4.1	https://primer3.ut.ee/
SnapGene Viewer v4.2	SnapGene
Softmax PRO	Molecular Devices, LLC
Zotero v6	Corporation for Digital Scholarship

3. Methods

3.1. Cell culture

The ovarian carcinoma cell line OVCAR8 was cultured in Roswell Park Memorial Institute (RPMI) 1640 GlutaMAX® media, supplemented with 10 % fetal calf serum (FCS) and 1 % Penicillin/Streptomycin (P/S). The primary human dermal fibroblast cell line (HDFn), initially derived from the neonatal foreskin, was cultured in Dulbeccos Modified Eagle Medium (DMEM) medium supplemented with 10 % FCS and 1 % P/S. Before experiments, the HDFn cells were cultured in "starvation medium" (DMEM + 0.5 % FCS and 1 % P/S). In the following method sections, the RPMI and DMEM, containing 10 % FCS, are named "standard growth medium."

Cells were split every 2-3 days after washing with 1xPBS, detaching with 1xTrypsin/EDTA for 5-10 min at 37°C (see Table 1), and resuspending in standard media in at least a 3:1 ratio to trypsin. Following centrifugation at 300 xg for 5 min, cells were seeded in an appropriate volume of fresh media, dependent on the size of the flask or dish (Table 1). Standard growth conditions were 37°C and 5 % CO_2 in normoxia. To maintain the consistency in cell phenotype among experiments, OVCAR8 was used in passages 2-6, while HDFn cells were restricted to passages 2-4. Thawing cells is considered as passage 0.

Table 1: Flask/Dish size and used volumes of medium and trypsin.

Flask/dish	Media volume	Trypsin volume
T175	20-30 ml	3 ml
T75	15-20 ml	1 ml
T25	6-10 ml	1 ml
10 cm	10 ml	2 ml
6 well	2 ml	500 µl
12 well	1 ml	300 µl
24 well	500 µl	200 µl
48 well	300 µl	100 µl
96 well	100 µl	100 µl

Freezing and thawing of cells

Cells were frozen at -80°C freezer for short-term storage and at liquid nitrogen (~-180°C) for long-term storage. Each cryotube contains 2-3 million cells aliquoted and resuspended in 1 ml of freezing medium (standard medium supplemented with 20 % FCS and 10 % DMSO). Freezing boxes containing either isopropanol or a metal ring were used to ensure a slow and gradual freezing process.

For thawing cells, aliquots were quickly warmed for 10 seconds (s) in a 37°C water bath, resuspended in 10 ml of warm medium, and centrifugated at 300 xg for 5 min. Cells were resuspended in 1 ml of standard medium and transferred into a T75 flask in 20 ml of fresh medium.

Cell counting

To count, the cell suspension was usually diluted between 1:4 and 1:10 in PBS, and 10 µl were loaded into a Neubauer counting chamber. Four large quadrants were counted, and the concentration was calculated by the following formula:

$$Concentration/ml = \frac{cell\ count\ in\ all\ quadrants}{dilution\ factor}\ x\ 10^4$$

3.2 Generation of OVCAR8 cells with defined p53 status

OVCAR8 cells contain a homozygous splice site mutation (c.376-1G>A), leading to a loss of function variant of p53 (Leroy et al. 2014). Therefore, to generate a cell line with a defined p53 status, knockouts were created by CRISPR/Cas9 before reintroducing either p53WT or a mutant p53 (R175H or R273H) by an inducible sleeping beauty system.

3.2.1 Cloning of plasmids

While the plasmids for the p53KO generation were directly acquired from Addgene (#121917 and #121918), the sleeping beauty plasmids containing WT or mutant p53 had to be cloned. Cloning was done by our technical laboratory assistant, Kathrin Stelter. Sequence templates of the p53 variants were taken from older existing plasmids in the lab and amplified by Phusion-*Taq* PCR (1,200 bp/35 cycles) with specific primers (see section 2.8). Afterward, the PCR product was separated on a 1 % agarose gel, and bands at 1.2 kb were cut out and purified with the Gel Extraction Kit (Thermo Fisher

Scientific). Digestion with SfiI for three hours at 50°C was done before the agarose gel and the extraction was repeated.

Similarly, the target plasmids (pSBtet-GN, #60501 and pSBbi-GN, #60517) were digested with SfiI for three hours at 50°C, cleaned up via agarose gel and treated with shrimp alkaline phosphatase (Thermo Fisher) as recommended by the manufacturer to dephosphorylate the 5'-termini to prohibit self-ligation. The enzyme was inactivated at 65°C for 15 min before precipitation with ethanol and sodium acetate. The concentration was measured at the Nanodrop2000.

Ligation was done in a 10 µl volume overnight at 16°C with 100 ng of vector in a 1:5 ratio to the template sequence. The transformation was done in *E. coli* (XL-1 blue) on LB-ampicillin plates. Colonies were picked and checked by PCR for the insert and correct orientation of the sequence.

Miniprep of correct plasmids was done with the GeneJET plasmid-miniprep kit (Thermo Fisher) according to the manufacturer protocol; then, the samples were sent for sanger sequencing by LGC genomics. After successful sequencing, Maxipreparations were conducted with the Nucleobond XtraMaxi kit (Macherey-Nagel), and the concentrations were measured spectrophotometrically using the Nanodrop2000. All generated plasmids were stored at -20°C.

3.2.2 Transfection, Selection and Sorting

Stable transfection of knockouts and inducible p53-expressing cells

OVCAR8 (parental or p53KO) were seeded at 300,000 cells per well in a 6-well plate one day before transfection. The next day, cells were washed, and 1.7 ml of fresh medium was added to the cells (RPMI + 10 % FCS, no P/S). Two 1.5 ml Eppendorf tubes were prepared, one with 5 µl of Lipofectamine2000 and the other with 4 µg of DNA, each in 150 µl Opti-MEM medium. The tubes were incubated for 5 min at room temperature (RT) before the lipofectamine was slowly added to the DNA. To enable the formation of DNA-lipofectamine complexes, the tube was incubated for 25 min at RT before slowly adding the mixture to the cells dropwise while continuously shaking the plate. Cells were incubated for six hours at 37°C before a medium change.

Depending on the stress of the cells (morphology checked by microscopy), cells were split 24 or 48 hours after transfection and seeded into a new 6-well plate. For antibiotic selection, 1,000 µg/ml of G-418 was added, and medium + antibiotic was changed every

2-3 days. After the cells recovered, GFP-positive/successful transfected cells were sorted with a BD FACS Aria III into a 24-well plate. Sorting was done by Dr. Hartmann Reifer of the FACS core facility at Marburg University. Finally, after cells were expanded, flow cytometry (FACS Canto II) was used to validate the percentage of GFP-positive cells/transfection efficiency. All stable transfected cells listed in this thesis are summarized in Table 2.

Table 2: Generated cell lines

Generated cell	Original cell	Plasmids used	Description
OVCAR8 p53KO C19	OVCAR8	px330-TP53-1 px330-TP53-2	p53 KO cell line (clone 19, 28 and 39)
OVCAR8 p53KO C28			
OVCAR8 p53KO C39			
OVCAR8 C39 p53WT-SBI	OVCAR8 p53KO C39	pCMV(CAT)T7-SB100 pSBtet-GN (WT, R175H or R273H)	Cell lines expressing inducible p53
OVCAR8 C39 p53R175H-SBI			
OVCAR8 C39 p53R273H-SBI			
OVCAR8 C39 p53-GFP	OVCAR8 p53KO C39	p53-GFP	Express p53 linked to GFP
OVCAR8 C39 GFP-p53		GFP-p53	

Transient transfection of constitutive p53-expressing cells

To validate the results of the inducible system, transient transfection of cells with a constitutive sleeping beauty system was conducted. One million cells were seeded into a 10 cm dish one day before transfection. The transfection was done as described in section 3.2.2 of the Methods; however, 15 µl of Lipofectamine2000 and 10 µg of DNA were used per dish.

3.2.3 Induction of p53

The inducible sleeping beauty system contains a reverse tetracycline-controlled transactivator (rtTA); therefore, doxycycline can induce gene expression. To induce p53 expression, the cells were treated with 0.5 µg/ml of doxycycline for 24 hours before an experiment. The stock concentration of the doxycycline hydrochloride was 1 mg/ml in DMSO.

3.3 MTT Assay

MTT is a commonly employed yellow tetrazolium salt for assessing cell viability, proliferation, and cytotoxicity (Ghasemi et al. 2021). In living and proliferating cells, MTT is reduced within the mitochondria by succinate dehydrogenase, producing purple formazan crystals. This represents the fundamental principle of the assay and can be measured in a spectrophotometer by its maximum absorbance at 570 nm. The measurement corresponds to the number of viable cells (Ghasemi et al. 2021).

Proliferation of p53KO cells

To assess the proliferation of different p53KO clones compared to the parental cell line, cells were seeded in 100 µl standard growth medium at a density of 2,500 cells per well in a 96-well plate (5x plates total). Cells were allowed to adhere overnight before the first MTT assay was done. Eleven microliters of MTT (5 mg/ml) were added to obtain a final concentration of 0.5 µg/ml. After incubation of 3.5 hours at 37°C (dark), the supernatant was carefully removed, and purple formazan was resuspended in solubilization solution (80 % isopropanol, 10 % Triton-X100, 10 % 1 M HCl) for 15 min at 37°C. Absorbance was measured at 570 nm at the SPECTRA MAX 340 microplate reader. MTT assays were repeated 48, 72, 96, and 168 hours after seeding. Absorbance (nm) was plotted with time (hours), and growth curves were generated.

Cell viability after treatment with doxycycline

Different p53-expressing OVCAR8 cell lines were seeded at a density of 5,000 cells per well in a 96-well plate to investigate cell viability after doxycycline treatment. After adherence overnight, control MTT (t=0) was done as described above. Cells were treated with different concentrations of doxycycline (0, 0.2, 0.4, 0.6, 0.8, and 1 µg/ml) for 48 hours. Another MTT assay was done, and the percentage of cell viability was calculated by comparing both assays.

3.4 EV isolation

To isolate EVs, cells were seeded at 7 million cells per T175 flask in standard growth media containing 10 % FCS and 1 % P/S. The day after, 0.5 µg/ml of doxycycline was added to induce p53 expression. Cells were incubated for another 24 hours under normoxic conditions at 37°C and 5 % CO_2. The supernatant was removed, cells were washed with PBS, and 20 ml of CD293 media was added to each flask. Afterwards, the cells were incubated at hypoxic conditions (O_2 = 1 %) at 37°C for 24 hours.

EVs were isolated by differential ultracentrifugation (dUC), a method utilizing consecutive centrifugation steps with increasing speed to eventually obtain EVs. Specifically, the supernatant was collected in 50 ml falcon tubes and centrifuged for 5 min at 300 xg (4°C) to remove dead cells. After transferring the supernatant to a fresh tube, samples were centrifuged at 2,000 xg for 10 min (4°C) to remove cell debris. Next, the supernatant was centrifuged at 10,000 xg for 60 min to separate large vesicles such as apoptotic bodies. The supernatant containing the small EVs was then transferred into 30 ml ultracentrifugation tubes and centrifuged at 100,000 xg for 2 hours with an Optima™ XPN-80 ultracentrifuge. After the supernatant was discarded, the pellet was resuspended in ~1 ml of 0.2 µm filtered PBS and transferred to a 1.5 ml polypropylene tube with a Snap-on Cap. The small vesicles were purified and concentrated by another ultracentrifugation step for 2 hours at 100,000 xg with the Optima™ MAX-XP centrifuge. The resulting pellets were resuspended in 25 µl of filtered PBS per used T175 flask. Usually, the EV-containing pellets of three T175 flasks were combined before the last UC step and resuspended in 75 µl of PBS. EVs were stored at -80°C.

3.5 Electron microscopy

Electron microscopy pictures of EVs were taken by Dr. Frederik Helmprobst from the electron microscopy core facility of Marburg University. For each sample, $5x10^8$ EVs were used. Sample preparation and image acquisition were done as described in Verel-Yilmaz et al. 2021 (Verel-Yilmaz et al. 2021). The EVs were fixed with 4 % PFA before loading onto a Formvar/carbon-coated 200 mesh electron microscopy grid. Subsequently, after the vesicles adhered to the grid, the grids were rinsed with sterile filtered PBS and fixed with 1 % glutaraldehyde for 5 min. A total of 8 two-minute washes with sterile filtered water were followed by treatment with 1 % uranyl acetate for 5 min. An additional incubation was done on ice with a mixture of 2 % methylcellulose and 4 % uranyl acetate in a 9:1 ratio. The excess liquid was removed using filter paper, and the grids were allowed to air dry for about 10 min. Imaging of the EVs was carried out using a Zeiss EM 900 operating at 80 kV.

3.6 Flow cytometry

3.6.1 Cell Death Measurement by Annexin/PI Assay

To assess the influence of doxycycline on the cell viability of the different OVCAR8 p53-expressing cells, an AnnexinV/propidium iodide (PI) Assay was carried out. Cells were

seeded in 6-well plates at 200,000 cells per well and incubated at 37°C. The next day, cells were treated either with 0.5 or 1 µg/ml of doxycycline for 6, 12, or 24 hours before cells were washed and the medium was changed to standard growth media. Forty-eight hours after the treatment started, cells were trypsinized and resuspended in fresh medium. Half of the cells were transferred into a FACS tube and washed once with PBS and once with Annexin binding buffer (1xABB). After the second washing step, cells were resuspended in 100 µl of 1xABB, and 2.5 µl of Annexin V-APC was added. Cells were incubated for 30 min on ice (dark). Subsequently, the cells were washed and centrifugated at 300 xg for 5 min with 1 ml of 1xABB. The supernatant was removed, leaving approximately 200 µl of volume in the FACS tube. Afterward, two microliters of PI (1:20 in H_2O) were added, and samples were measured at the FACS CANTO II.

3.6.2 Nano-flow cytometry

To measure size, concentration, and marker expression of EVs, conventional flow cytometry is not sufficient due to the small size of the particles. Therefore, we used the NanoFCM, which can detect particles down to 40 nm in size. This high-sensitivity flow cytometry (HSFCM) consists of three single-photon-counting avalanche photodiode (APD) detectors, of which one detects side scattering (SSC) and the other two detect fluorescence. By utilizing a hydrodynamically focused, narrow sheath flow (e.g., 1-2 µm), particles pass slowly and individually past the laser beam, enabling the detection of different properties of the nanoparticles (S. Wang et al. 2017; Y. Tian et al. 2018). Two lasers, Blue (488 nm) and Red (640 nm), allow the detection of different fluorochromes, such as FITC, PE, or APC.

Size & Concentration

To detect the size & concentration of isolated particles, a pre-dilution was done in a 0.2 ml tube in a 1:50 ratio with filtered PBS. Depending on the expected concentration, further dilutions were made before measuring. Optimal dilution led to event counts between 2,500-12,000, ensuring quantitative and individual measurement of the single particles. The size distribution of the particles is examined by comparing them to a mixture of silica nanoparticles (SiNPs) with a defined size, which is used to calibrate the device at the start. Concentration is measured over time since the sheath flow is constant.

Antibody staining – Marker expression

To investigate the expression of typical EV surface markers, such as the tetraspanins (e.g., CD9, C63, or CD81), $1x10^9$ particles were stained with the respective antibody. Specifically, particles were diluted in 60 µl PBS, and 20 µl of antibody master mix was added. The master mix contained 100-200 ng of antibody, either alone or as double staining (e.g., CD9-PE + CD63-FITC). EVs were stained overnight at 4°C on a shaker before washing with 1 ml of PBS and subsequent ultracentrifugation at 100.000 xg for 45 min (4°C). The pellet was resuspended by 50 µl of filtered PBS and measured in a nano analyzer. The percentage of positive events was compared between samples.

3.7 Western Blot

Immunoblot or Western Blot is a technique to detect specific proteins in lysates (e.g., Cell or EV) by transferring them to a carrier membrane and targeting them with specific antibodies, subsequently detecting proteins by chemiluminescence or fluorescence.

3.7.1 General procedure

Cell and EV lysis

Extracting protein from lysing cells or EVs without damaging the proteins is critical for successful detection in Western Blot. Here, Radioimmunoprecipitation Assay (RIPA) buffer was used, which contains TRIS (pH=8), NaCl, SDS, Triton-X100, and DOC (see section 2.4). The correct pH and buffer system are essential to avoid protein precipitation and ensure their stability. The buffer's ionic salts help disrupt the cell membrane without damaging the proteins. Moreover, adding chaotropic agents, such as SDS, DOC (both ionic), and Triton-X100 (non-ionic), is crucial for the solubilization of the proteins. Depending on the specific experiment, protease (1:1,000) and phosphatase inhibitor (1:100) were added freshly before every use, which protects proteins from digestion by proteases and preserves the protein's phosphorylation status.

To generate cell lysates, cells were either trypsinized, centrifuged, and resuspended with 1xRIPA buffer, or the cells were directly scraped in 1xRIPA buffer from the plate. To protect the proteins, the extraction proceeded on ice. After cells were resuspended in RIPA, samples were incubated on ice for at least 10 min before centrifugation at 17,000 xg for 30 min 4°C. The supernatant was transferred into a fresh 1.5 ml Eppendorf tube, and lysates were stored at -20°C.

EV lysates were generated by adding 10xRIPA buffer to the EVs (e.g., 50 µl of EVs in PBS + 5.5 µl of 10xRIPA). Lysates were then incubated for 30 min at RT before transferring to ice. All lysates were stored at -20°C if not used directly.

BCA Assay and sample preparation

To determine protein concentration, Bicinchoninic Acid Assays (BCA) was done. BCA is a colorimetric assay based on the biuret reaction, where the sodium salt of bicinchoninic acid reacts with copper ions and results in a deep blue color, which can be quantified with a spectrophotometer at 562 nm. Here, Pierce™ BCA Protein Assay Kit (Thermo Fisher Scientific) was used after the manufacture protocol. Each sample was tested in duplicates and compared to a standard curve of albumin (BSA) with defined concentrations. The standard curve is generated by blotting BSA concentrations vs absorbance, and the trendline equation is used to calculate protein concentration.

For sample preparation, 15 µg of cell lysates or 5 µg / $1x10^9$ particles of EV lysates were used. To reduce the proteins and disrupt disulfide bonds, 6xLaemmlie buffer was used, which contains the reducing agent β-mercaptoethanol. After 5 min at 95°C, samples were shortly centrifuged and put back on ice until loading. Total volumes per lane were dependent on well size. For 10-well gels (1.5 mm), between 20-40 µl, and for 15-well (1.5 mm), 20-30 µl was used.

SDS-PAGE

To separate proteins depending on their molecular size, a Sodium dodecyl sulfate-polyacrylamide gel electrophoresis (SDS-PAGE) was done. SDS-PAGE is based on a gel from polyacrylamide and SDS, which binds the proteins and results in a constant negative charge. By applying an electric field, proteins run through the gel, whereas bigger proteins are slower, leading to a separation after molecular size.

Here, 10 % gels were used as described in the Material section. Proteins were loaded (20-40 µl) together with a Prestained Protein Ladder (Thermo Fisher Scientific). Per gel, a constant current strength of 20 mA was applied for the first 30 min before increasing it to 25 mA for approximately 2-2.5 hours.

Immunoblot

Immunoblotting was done with nitrocellulose membrane in a tank blot system. The membrane was put on the anode side of the gel between two Whatman papers each.

Flanked by sponges, the cast was put into the tank, and the blot was run at 300 V and 350 mA for 1.45 hours at 4°C.

Protein detection

Afterward, the blot was blocked with 5 % skimmed milk in TBST for one hour at RT to prevent unspecific binding of the antibody. Subsequently, the membrane was incubated overnight at 4°C with primary antibody (more details on the dilution of antibodies are provided in the Material section 2.6). On the next day, the membrane was washed 3x10 min with TBST and incubated for 2 hours at RT with a secondary antibody coupled with horse-reddish peroxidase (HRP). After another 3x10 min washing, proteins were detected with Immobilon Forte Western HRP substrate in ChemiDoc™ MP Imaging System.

3.7.2 Activation and translocation of NFκB

Activation of NFκB and its translocation into the nucleus of EV-treated HDFn cells was examined in Western Blot. Here, 300.000 HDFn cells were seeded into a 6-well plate in standard growth medium and grown overnight at 37°C. The medium was changed to starvation medium, and cells were incubated for another 24 hours at 37°C. On day three, cells were treated with 50 µl of EVs (WT- or KO-EVs) for 0, 6, or 24 hours.

Fractionation of proteins was done with the Pierce™ NE-PER® Nuclear and Cytoplasmic Extraction Reagent Kit (Thermo Fisher) after following the manufacturer protocol. Here, cells from two wells were pooled to obtain enough cells for the fractionation. Afterward, BCA was done to determine the protein concentration, and 15 µg was prepared and loaded onto a 10 % SDS-PAGE as described above. Membranes were blocked in 5 % milk in TBST, and primary antibodies were used overnight at 4°C, while HRP-linked secondary antibodies were used for two hours at RT. All antibodies were prepared in blocking solution.

- β-Actin (#A1978) – 1:2,500
- IκBα (#4814P) – 1:1,000
- phospho-IκBα (#2859P) – 1:1,000
- p65 (8242S) – 1:1,000
- phospho-p65 (#3033S) – 1:1,000
- PARP (#611038) – 1:1,000
- Anti-mouse HRP (#7076) – 1:10,000
- Anti-rabbit HRP (#7074) – 1:10,000

3.7.3 STAT3 phosphorylation

To analyze if STAT3 is a potential upstream regulator in the phenotype of both OVCAR8 cells or EV-treated HDFn cells, STAT3 phosphorylation was investigated in Western Blot.

OVCAR8 cells

OVCAR8 p53KO or p53WT cells were seeded into a 6-well plate in standard growth medium. The next day, 0.5 µg/ml of doxycycline was added for 24 hours before cells were lysed in RIPA buffer. Fifteen micrograms were loaded onto a 10 % SDS-PAGE, blotted, blocked in 5 % milk in TBST, and primary antibodies against phospho-STAT3, STAT3 (both 1:1,000), and GAPDH (1:10,000) were used at 4°C overnight. HRP-linked secondary antibodies were used at 1:10,000 dilution, and the detection was done at ChemiDoc™ MP Imaging System.

HDFn cells

Fibroblasts (HDFn) were seeded at 100,000 cells into a 12-well plate in standard growth media and incubated at 37°C overnight. The medium was changed to starvation medium for 24 hours, followed by treatment with 25 µl of EVs from KO or WT cells. STAT3, pSTAT3, and GAPDH were detected as described in 3.7.1.

3.8 RNA isolation, cDNA synthesis, and RT-qPCR

3.8.1 General procedure

This work used reverse transcription quantitative PCR (RT-qPCR) to investigate transcriptional changes in the different OVCAR8 cells and EV-treated fibroblast.

RNA Isolation

Depending on the experiment, cells were grown in 24- or 6-well plates. For RNA Isolation, the supernatant was discarded, and 500 µl of TRIzol Reagent was directly added to the plate to lyse the cells. TRIzol is an acidic reagent based on guanidium salts and phenol, and it can separate DNA and RNA while maintaining RNA integrity. The lysates were subsequently transferred to a 1.5 ml tube, and chloroform was added in a 1:5 ratio (100 µL). After vortexing for 5-10 s, tubes were incubated for 2 min at RT before centrifuging at 17,000 xg for 15 min (4°C). This led to the separation into 3 phases, where RNA is located in the top, aqueous phase. After carefully transferring the aqueous phase into a new tube, cold ethanol (100 %) was added in a 1:1 ratio, and everything was

loaded onto an RNA column from the Nucleospin RNA Kit (Macherey-Nagel). The remaining steps of RNA isolation were performed according to the manufacturer's instructions. Finally, RNA was resuspended in nuclease-free water, and the concentration and purity (A260/280 and A260/230) were measured with the Nanodrop2000. RNA was stored at -80°C if not used directly.

cDNA synthesis

Complementary DNA (cDNA) does not occur naturally in humans and is synthesized from RNA using the enzyme reverse transcriptase. In this dissertation, iScript™ cDNA Synthesis Kit (Bio-Rad) was used according to the manufacturer protocol. Besides the enzyme, the kit contains a mix of oligo(dT) and random hexamer primers. Between 100 and 500 ng of RNA was used for the synthesis. Afterward, cDNA was diluted 1:4 for every 100 ng of used RNA (e.g., 500 ng = 1:20) and stored at -20°C.

qPCR

Quantitative PCR (qPCR) is a technique where cDNA is amplified by a DNA polymerase with specific primers against a gene of interest. Here, quantitation is done together with the fluorescent dye SYBR Green, which can intercalate into double-stranded DNA (dsDNA) and, therefore, directly proportional to the exponential growth of the PCR product.

First, a master mix was prepared with 5 µl of 2xSYBR Green mix, containing the DNA-polymerase and 4 µl of diluted cDNA per well. Nine microliters of the master mix were then pipetted into each well of a 96-well qPCR plate before adding 1 µl of primer mix (forward and reverse). In general, samples were run in technical duplicates. All primers were designed and tested as described in 3.8.2. The plate was sealed with adhesive film, shortly spun down, and run in Agilent Stratagene Mx3000P qPCR system with the following program:

1. Warm Up and initial denaturation – 1 cycle
    a. 15 min at 95°C
2. Denaturation, hybridization, and polymerization – **40 cycles**
    a. 15 s at 95°C (denaturation)
    b. 20 s at 60°C (annealing)
    c. 15 s at 72°C (elongation)
3. Dissociation/Melting curve – 1 cycle
    a. 60 s at 95°C

b. 20 s at 72°C
c. 30 s at 95°C (gradually increased)

At least two housekeeping genes (e.g., GAPDH, U6, L27) were used in every experiment. This step was crucial to normalize the data. First, the mean of all replicates was formed, and primer efficiency corrected ΔCT was calculated after Pfaffl, 2001 (Pfaffl 2001)

$$\Delta CT = primer\ efficiency^{(CTControl - CTSample)}$$

Finally, ΔΔCT was calculated by dividing ΔCT of the GOI with the combined ΔCT of the housekeeping genes. For better graphical output, the $\log_2$ of ΔΔCT was used.

3.8.2 Primer efficiency

Gene-specific primers were designed on the primer3 website with the following main settings:

- Primer size: between 18 – 23 nucleotides, with 20 being optimal
- Primer Tm: between 57 and 62°C, with 59°C being optimal
- Primer GC %: between 30 and 70, with 50 % being optimal
- Product size: between 80 and 150 bp
- Species: homo sapiens
- Checked for mispriming with the provided library for humans

Exon-spanning primers were preferred if possible, and selected primers were double-checked for correct binding on the NCBI website. Oligos were ordered at Sigma-Aldrich and resuspended in nuclease-free water to a concentration of 100 µM as listed by the company. Next, forward and reverse primers were diluted in water to 10 µM each and mixed to produce a 5 µM primer mix.

To test primer amplification and its efficiency, undiluted cDNA (generated from 500 ng of RNA) was diluted in a series of 5 steps: 1:2, 1:4, 1:8, 1:16, and 1:32 in nuclease-free water. Moreover, minus reverse transcriptase-cDNA (therefore RNA) was diluted 1:5 and used as a control. Template master mix was done with 5 µl 2xSYBR Green mix, 1 µl of cDNA, and 3 µl of water per sample. The remaining steps of the qPCR were done as described above.

The primer amplification efficiency was calculated by plotting the CT value with $\log_{10}$ of the dilution factor and calculating the slope. Finally, the following equation was used (Pfaffl 2001):

$$Amplification\ efficiancy\ E = 10^{(\frac{-1}{slope})}$$

Primers with an amplification efficiency between 1.8 and 2.1 (80-120 %) were accepted for use.

3.8.3 Gene expression in OVCAR8 cell lines

Validation of transcriptomic data in constitutive p53-expressing cells

At first, transcriptomic data was validated with the same cells used for RNA sequencing. Therefore, differentially expressed genes were chosen (e.g., *CXCL8, IL6, TGFB1, RELB*) and tested in qPCR as described in 3.8.1. Moreover, cells were transiently transfected with a constitutive sleeping beauty system (for WT, R175H, and R273H) and tested for gene expression 48 hours after transfection (see also section 3.2.2).

Rescue experiment

This experiment assessed if the distinct phenotype of p53WT cells could be rescued in p53KO cells by EVs from WT cells. OVCAR8 cells (KO, WT) were seeded into a 24-well plate at a density of 50.000 cells per well in standard growth medium. The next day, 25 µl of either WT or KO-originated EVs were added to the knockout cells (in 400 µl volume). Additionally, 0.5 µg/ml doxycycline was also added to all cells. After 30 hours, RNA was isolated, and qPCR was done as described above (Section 3.8).

3.8.4 Fibroblast Assay

An RT-qPCR was carried out to assess and verify the transcriptomic changes of HDFn cells after the treatment of EVs. At first, HDFn cells were seeded at a density of 50,000 cells into a 24-well plate in standard growth media. The next day, the medium was changed to 400 µl of starvation media, and cells were incubated for 24 hours. Based on the experimental setting, either $5x10^9$ particles/ml or a volume of 25 µl of EVs (isolated from 7 million initially seeded cells) were used. After another 48 hours, RNA, DNA, and qPCR were done as described in 3.8.1. Many genes were tested, including *αSMA (ACTA2), COL1A1, MMP11, CXCL1, IL6 and CXCL8*. The *GAPDH, U6, L27, and β-Actin* genes were used as housekeeping genes.

3.9 Immunofluorescence

3.9.1 Transfer and uptake of p53

The transfer and uptake of p53 were studied by treating KO cells with p53-containing EVs from WT cells and utilizing immunofluorescence staining of p53. At first, 75,000 p53KO cells were seeded onto 18 mm cover slips in a 12-well plate. After growing for 24 hours at 37°C, 25 µl of WT-EVs were added into 500 µl of media for 6 hours. Cells were washed twice with 1 ml of PBS before fixing with 500 µl of 4 % formaldehyde (PFA) in PBS for 10 min at RT. Fixation is done to preserve cell morphology while keeping antigenicity. Next, cells were rewashed once with PBS before permeabilizing the cell membrane with 0.5 % Triton-X100 in PBS (RT). Another washing step was done, and unspecific binding of antibodies was prevented by blocking the cells for 1 hour in 10 % FCS in PBS. During incubation, the primary antibodies were prepared in 100 µl volume per sample. P53 (DO-1) was used 1:400, together with 10 % goat serum (in which the secondary antibody was raised) and 0.1 % of Saponin (from 10 % Stock in PBS). Drops of 100 µl were pipetted into a wet chamber, and coverslips were placed on top and incubated overnight at 4°C. The next day, the secondary antibody, goat anti-mouse Alexa-Fluor 633 (1:400), was prepared similarly to the primary antibody. Coverslips were washed by dipping them ~16 times in PBS-filled boxes before transferring them again into a wet chamber on 100 µl of secondary antibody. Incubation was done at RT (dark) for 2 hours. Furthermore, cells were washed as before and shortly rinsed with ddH_2O before mounting the coverslips onto microscopy slides with mounting media containing DAPI (Vectashield). Slides were stored in the dark at 4°C until pictures were taken with a LEICA Stellaris together with Prof. Dr. Ralf Jacob.

3.9.2 Co-culture of HDFn and OVCAR8 cells

To further investigate the transfer and uptake of p53-containing EVs, a fibroblasts co-culture with OVCAR8 cells containing GFP-linked p53 was done. This experiment was done in the group of Prof. Dr Ralf Jacob.

OVCAR8 p53-GFP and HDFn cells were seeded in a 3:1 ratio, and live cell imaging over 60 min was done with a LEICA DMI8 microscope at 37°C and 5 % CO_2.

3.9.3 Translocation of NFκB

Here, 50,000 HDFn cells were seeded into a 24-well plate in standard growth medium for 24 hours before the medium was changed to starvation medium. On day 3, cells were

treated with ~2x10^9 WT-EVs for either 6 or 24 hours. After treatment, cells were directly put on ice, washed 3x with ice-cold PBS, and fixed for 20 min at RT with 4 % PFA in PBS. After washing again 3x with PBS, cells were permeabilized with 0.1 % TritonX100 in PBS for 15 min (RT). Rewashed twice and blocked in 1 % BSA in PBS for 1 hour at RT. Primary antibodies p65 (1:100, rabbit) and α-tubulin (1:100, mouse) were used in 1 % BSA in PBS for 2 hours at RT. After three washing steps with PBS, cells were incubated with secondary antibodies goat anti-mouse Alexa Fluor 555 and goat anti-rabbit Alexa Fluor 647 (both 1:200 in 1 % BSA in PBS) for one hour at RT. Finally, after another washing step, Hoechst33342 was added in 1:200 dilution in PBS for 10 min. After washing twice with PBS and once with ddH_2O, cells were mounted in a Mowiol mounting medium.

Pictures were taken on LEICA Stellaris, whereas the pixel intensity ratio of p65 staining was compared between the nucleus and cytoplasm to obtain the percentage of nuclear NFκB. Altogether, 50 different nuclei were evaluated.

3.10 Cytokine Array

A cytokine array was done to evaluate differences in the inflammatory secretome of EV-treated fibroblast. To generate the needed conditioned medium (CM), HDFn cells were seeded in a 24-well plate in standard growth media overnight. Starvation with 0.5 % FCS in DMEM was done the following 24 hours before treatment with 25 µl of PBS or EVs (from KO, WT, or R273H). After 24 hours, the medium was changed to 500 µl fresh starvation medium and incubated for another two days. CM was collected and centrifuged twice (300 xg 5 min, 2000 xg 15 min) to eliminate dead cells and cell debris. The CM was stored at -80°C before use. The Proteome Profiler Human XL Cytokine Array Kit (R&D Systems) was performed according to the manufacturer protocol, and pixel density was compared between the groups. Samples were done in duplicates.

3.11 OMICS and Olink

3.11.1 Transcriptomics

To evaluate both the transcriptomic phenotype of the different OVCAR8 p53 cell lines and the phenotype of the EV-treated fibroblasts, RNA sequencing was done in cooperation with the Cologne Center for Genomics (Cologne University).

For the p53-expressing cell lines, 300,000 cells were seeded into a 6-well plate, adhered overnight, and treated with or without 0.5 µg/ml of doxycycline for 24 hours. HDFn, cell seeding, and treatment were done as described in 3.8.4. RNA isolation for both was done as described in section 3.8.

In general, 2 µg of total RNA was needed with a concentration between 50 and 200 ng/µl. The OD260/280 was between 1.8 and 2.1 for all samples, whereas OD260/230 was above 1.5. All RNA showed no degradation (RIN >7), which was measured by an Agilent Tape Station system by the Center for Genomics. Illumina sequencing was done with paired-end, 2x100 bp, and 15 million reads per sample. In total, five different cell lines (parental, KO, WT, R175H, and R273H), two treatment options (Doxy/No Doxy), and all in triplicates were sequenced (30 samples) For the fibroblasts, 18 samples were sequenced, including untreated (PBS-treated) HDFn, and EV-treated HDFn cells (EVs from parental, KO, R175H and R273H) (all n=3).

FASTA files were delivered by the Center for Genomics and processed by our bioinformatician, Dr. Florian Finkernagel. Raw sequencing reads were aligned by STAR (2.7.10a) against Ensemble Homo Sapiens (v106) and quantified by Python Scripts. The resulting list was filtered for protein-coding and lncRNA and normalized to transcripts per million. Differential analysis was done by edgeR (unpaired) with a threshold of FDR ≤ 0.05 and $\log_2$(FC) ≥ 1. Genes with less than ten reads in at least one condition were excluded.

Genes between two groups were considered differential expressed when $\log_2$(FC) ≥ 1 and FDR ≤ 0.05. Functional and pathway enrichment analyses were performed using the web-based software EnrichR (E. Y. Chen et al. 2013).

3.11.2 Proteomics

Proteomic data was collected from isolated EVs of the different cell lines. EVs were isolated by dUC from induced (+ doxycycline) and non-induced cells (no doxy) as triplicates, and $5x10^8$ EVs in 50 µl PBS were sent to the Institute of Translational Proteomics of Prof. Dr. Johannes Graumann (Marburg University). Preparation and measurement of the samples were done as described in de Pedro et al. 2023 (de Pedro et al. 2023). In general, samples were prepared for mass spectrometry by denaturation to reduce proteins into peptides, reduction, and alkylation to prevent re-oxidation, digestion by endopeptidases to shorten the peptides, and desalting to clean and desalt the molecules. Subsequently, liquid chromatography-tandem mass spectrometry was

carried out on a Bruker Daltonics timsTOF Pro instrument connected to a Bruker Daltonics nanoElute instrument, which is characterized by a combination of two measurements, MS1, which measures the mass of an intact ion of the ionized peptides and MS2 which measures the spectra of fragmentized individual ions selected by data-dependent acquisition. To finally identify proteins in the samples, peptide spectrum matching with the UniProt-SwissProt canonical database as reference was done. Moreover, Label-free quantitation (LFQ) was done to normalize protein intensities across samples. The initial bioinformatical analysis was done by Dr. Witold Szymanski, where statistical differences between groups were calculated using Limma's moderated t-test. Furthermore, the data was imputed to account for missing values. Only proteins with a medium number of four peptide fragments were considered for analysis. Proteins with a $\log_2(FC) \geq 1$ and $FDR \leq 0.05$ between two groups were considered differential expressed. Functional and pathway enrichment analyses were performed using the web-based software EnrichR (E. Y. Chen et al. 2013).

3.11.3 Olink Explore

Olink Explore represents a cutting-edge biomarker discovery system, integrating proximity extension assay (PEA) technology with Next Generation Sequencing (NGS) as its readout. PEA fuses an antibody-based immunoassay with PCR, whereas a pair of antibodies, each tagged with distinctive DNA markers, simultaneously attach to a target protein in the solution. This enables the DNA nucleotides to merge, further serving as a template for the PCR. This consequently generates a double-stranded DNA "barcode", in which quantity is directly proportional to the initial concentration of the target protein (Wen Zhong et al. 2021). Here, an Olink Explore 3072 assay was done by the Institute of Translational Proteomics (Marburg University), which enables the analysis of 2926 unique proteins, including secreted proteins, inflammatory markers, or other biomarkers.

In this dissertation, Olink was done from the OVCAR8 cell lines (KO, WT, R175H, R273H), EVs (from KO or WT cells), and PBS or EV-treated HDFn (KO or WT-EVs) cells. All samples were run as biological duplicates.

Data was normalized by including three internal and external controls in the assay. The final readout is Normalized Protein expression (NPX) values (in $\log_2$ scale), which are calculated by normalizing the NGS counts on the internal control (extension control) before standardizing them on the external control (plate control). While the extension control is a known standard, plate control is a standard plasma pool.

To simplify the analysis between samples, all missing values and values below the limit of detection (LOD) were replaced by the value of the LOD. While looking for differences between groups and samples, an NPX difference of 1, so doubling of the protein concentration, was considered. Functional and pathway enrichment analyses were performed using the web-based software EnrichR.

3.12 Statistical Analysis

Statistical analysis was performed using Graph Pad Prism software 10 to interpret the data. All data are shown as mean with standard deviation (SD). The predetermined significance level α was set to 0.05. If not specified otherwise, the actual significance level p was calculated either by a two-tailed unpaired t-test when comparing two groups or by an Ordinary One-Way ANOVA with Tukey's multiple comparisons test if comparing more than two groups. When p is ≤ 0.05 (*), ≤ 0.01 (**), ≤ 0.001 (***), or ≤ 0.0001 (****), the data is categorized as significant. In all graphical representations, significance is denoted by the corresponding number of asterisks (*, **, ***, ****).

4. Results

4.1 Increased EV secretion in chemically-defined CD293 medium

Intercellular communication by EVs is gaining more and more interest as an essential field of study. However, researchers face many challenges, especially regarding the isolation and characterization of the vesicles. Besides different isolation methods, the culture medium can also play a key role (Szatanek et al. 2015). Cells are often grown in media containing FCS, which also includes particles and therefore impair the isolation and especially the characterization of the EVs. Subsequently, EV-depleted FCS is routinely used, where particles are usually removed by ultracentrifugation. Alternatively, FCS-free, chemically-defined media such as CD293 medium can be used. Here, we compared CD293 medium with EV-depleted medium regarding EV secretion, EV size, and surface marker expression. The use of CD293 medium showed significantly increased particle size (Fig. 3a), concentration (Fig. 3b), and CD9 expression compared to the EV-depleted medium (Fig. 3c). Other EV surface markers, such as CD63, CD81, and CD29, were also increased; however, no significance could be shown (Fig. 3c). This indicates not only the increase of particle secretion in general but also the specific increase of EVs, as enhanced maker expression was detected.

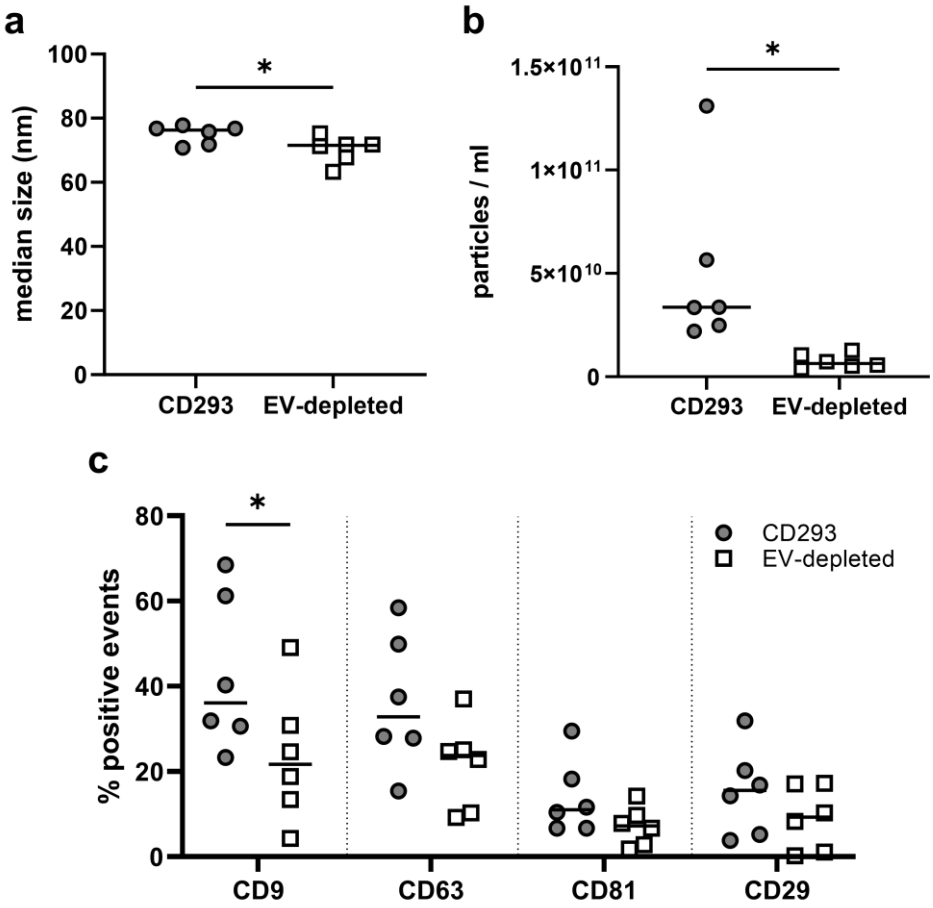

Figure 3: CD293 medium increases particle secretion with enhanced EV markers expression compared to EV-depleted medium.
EVs from OVCAR8 cells were either isolated in the chemically-defined CD293 medium or self-made EV-depleted medium (RPMI + 10 % EV-depleted FCS). **(a)** Median particle size [nm] was measured by nano-flow cytometry and showed a significant increase in particle size for CD293 medium-isolated EVs (*p<0.05, unpaired t-test, two-tailed, n=6). **(b)** Particle concentration was measured by nano-flow cytometry. EVs isolated from CD293 medium show a significant increase in particle secretion (*p<0.05, unpaired t-test, two-tailed, n=6 ±SD). **(c)** A total of $1x10^9$ particles were stained by either CD9-PE, CD63-FITC, CD81-PE, or CD29-FITC antibody, and the percentage of positive events was measured by nano-flow cytometry (*p<0.05, two-way ANOVA with Šidák correction, n=6).

4.2 OVCAR8 p53 knockouts are similar in EV secretion, size, and marker expression compared to the parental cell line

The model cell line in this project is the ovarian cancer cell line OVCAR8, which originated from a 64-year-old female with high-grade serous adenocarcinoma. The cisplatin resistance cell line has several mutations, including in *CTNNB1, ERBB2, KRAS,* and *TP53* (Leroy et al. 2014; Hallas-Potts, Dawson, and Herrington 2019). For *TP53*, a single nucleotide variant (c.376-1G>A) leads to a splice site mutation, subsequently leading to a deletion of seven amino acids at the 5'-site of exon 5 (p.Tyr126_Lys132del)

(Smeby et al. 2019). Although little is known about the exact mutation of OVCAR8, splice site mutations are generally predicted to be loss of function mutations (MacArthur et al. 2012).

To generate *TP53* knockouts, OVCAR8 cells were transfected with two plasmids containing the CRISPR/Cas9 system and guide RNA targeting exons 4 and 9, respectively. Subsequently, single-cell cloning led to three distinct p53KO clones, validated by Western Blot (representative images shown in Figure 4b), named C19, C28 and C39. The morphology of all clones was similar to the parental cell line, as shown by brightfield microscopy (Fig. 4a). By utilizing MTT assays over 168 hours, proliferation was shown to be similar between the parental cells, C19 and C39, while C28 proliferated slightly slower (Fig. 4c).

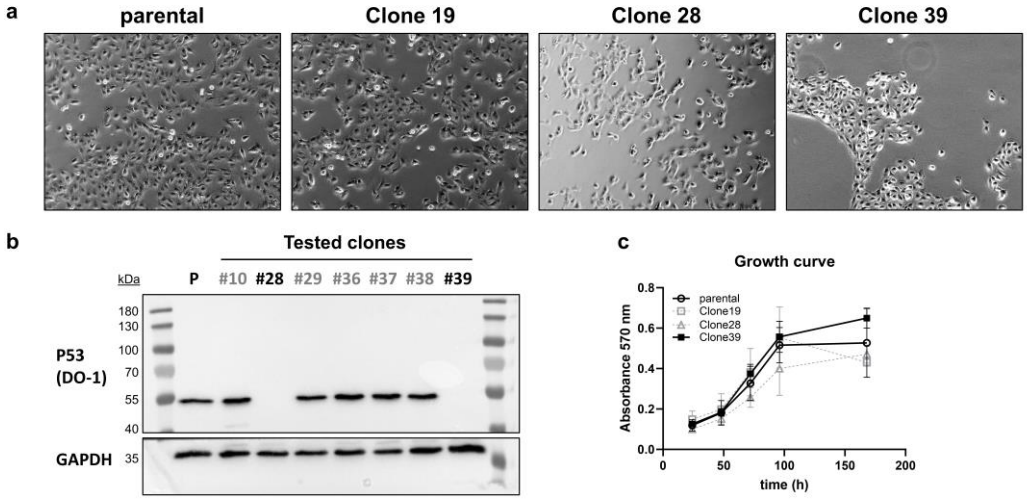

Figure 4: Generation of p53 KO clones from OVCAR8 parental cell line.
(a) Brightfield images of different p53KO clones and the parental. Pictures were taken on a LEICA DM3000 microscope with 10x magnification. **(b)** Representative result of clones tested for p53 expression in Western Blot. GAPDH was detected as a loading control. P = parental **(c)** MTT assay after 48 hours was performed to determine the growth rate. MTT Assays were measured 24, 48, 72, 96, and 168 hours after seeding and absorbance was measured at 570 nm (parental/C19: n=4, C28/C39: n=3 ±SD).

Next, EVs were isolated by differential ultracentrifugation in CD293 medium over 48 hours and characterized by nano-flow cytometry in size, concentration, and marker expression (CD9, CD63, CD81, and CD29). Here, no significant differences could be observed in particle size (nm), concentration (per ml), or surface marker expression (Fig. 5a-c). Due to the similar morphology and growth, OVCAR8 p53KO Clone 39 was picked for all further experiments in this project.

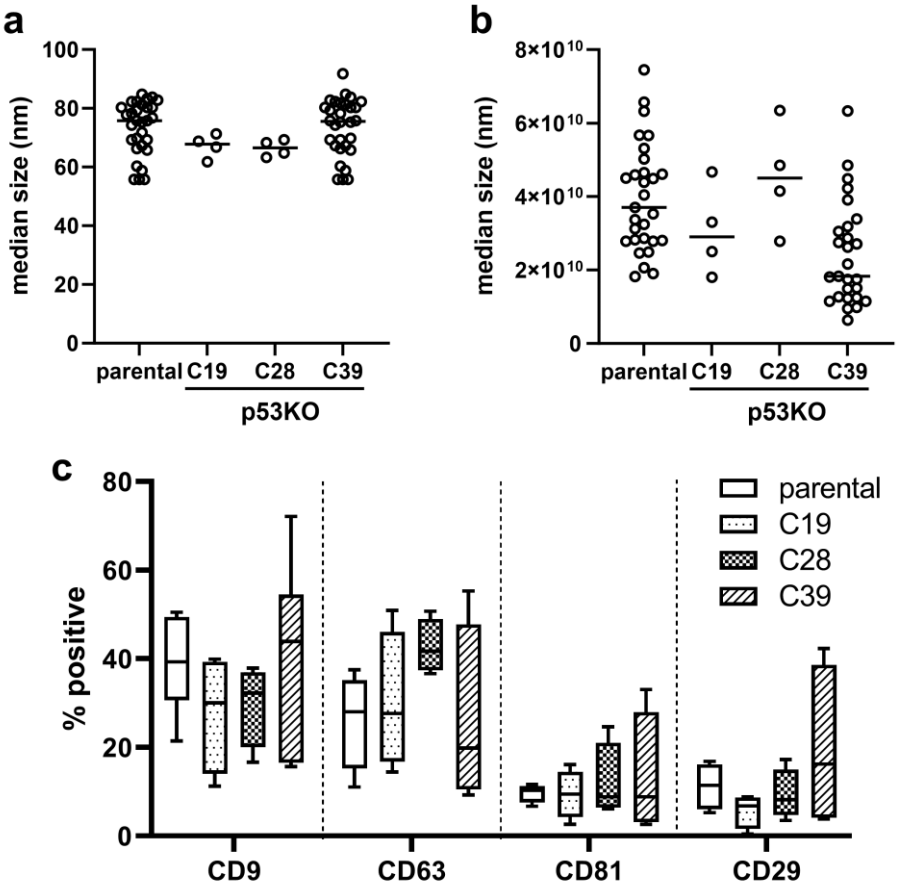

Figure 5: EVs isolated from p53 knockout clones are similar in particle size, concentration, and surface marker expression.
(a) Median particle size [nm] and **(b)** particle concentration per ml were measured by nano-flow cytometry (parental: n=29, C19/C28: n=4, C39 n=27). **(c)** A total of $1x10^9$ particles were stained with CD9-PE, CD63-FITC, CD81-PE, or CD29-FITC antibodies, and the percentage of positive events was measured by nano-flow cytometry (parental: n=6 ±SD, C19/C28: n=3 ±SD, C39 n=6 ±SD).

4.3 Generation and validation of OVCAR8 cells with a defined p53 status

To investigate the role of p53 in EV-mediated communication in ovarian cancer, an OVCAR8 cell line expressing WT or mutp53 (R175H or R273H) was generated by transfecting the KO clone 39 with the GOI in plasmids of the inducible sleeping beauty (SB) system, described in Kowarz et al. (2015) (Kowarz, Löscher, and Marschalek 2015). This system relies on the stable integration of the gene of interest (GOI) in the target cell genome by a “cut and paste” mechanism utilized by a transposase enzyme (Izsvák and Ivics 2004). The SB transposase can cut out the GOI via its flanked inverted repeats and “paste” it into a TA dinucleotide in the recipient DNA sequences. In this thesis, p53KO clone 39 was stably transfected with an inducible SB system, which induced p53 expression by adding doxycycline. This prevents a strong and constant overexpression

of p53, which otherwise could lead to toxic effects (Ishimaru et al. 2004; Chi et al. 2005). The successful transfection was verified by detecting GFP expression via flow cytometric analysis (Fig 6a) and microscopy (Fig. 6b). Protein expression before and after induction by doxycycline was evaluated by Western Blot. WT and both mutp53 cell lines showed p53 expression exclusively after the treatment, demonstrating a working doxycycline-dependent protein induction (Fig. 4c). As expected, p53 expression strongly accumulated in R175H and R273H cells compared to the wild-type cell line. In contrast, the parental cell line only expressed a low amount of the p53 protein, independent of treatment, and KO cells showed no expression (Fig. 6c). In conclusion, distinct OVCAR8 cell lines were generated expressing either p53WT, p53R175H, or p53R273H when induced with doxycycline.

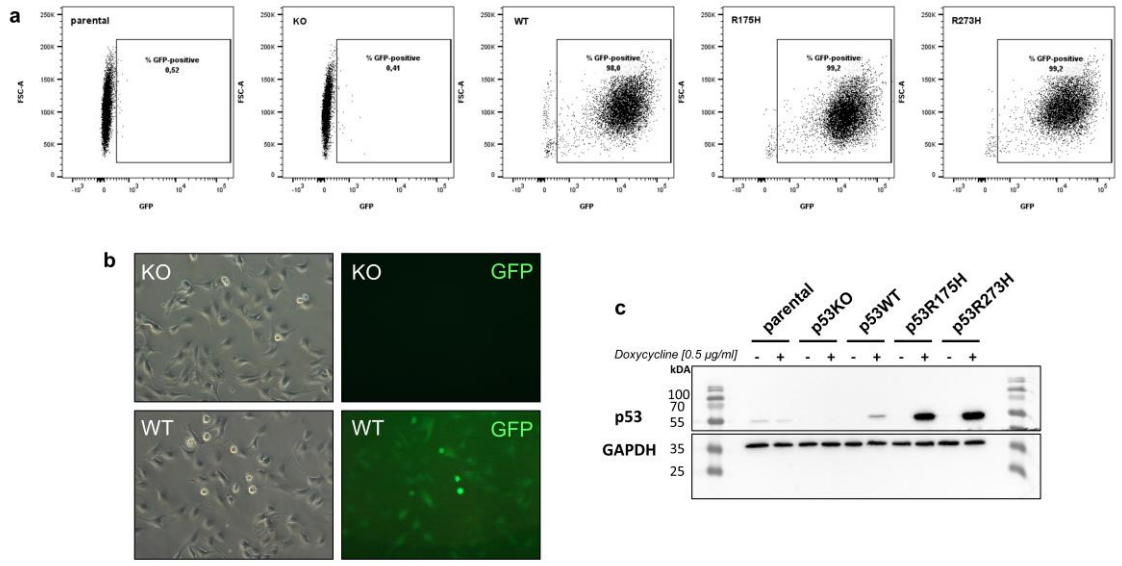

Figure 6: Successful generation of a stable OVCAR8 cell line with doxycycline-inducible p53 expression.
The OVCAR8 p53KO clone 39 was used to generate a cell line expressing either p53WT or a p53 with a hotspot mutation (p53R175H or p53R273H). To obtain stable cells, an inducible Sleeping Beauty system was used (Kowarz, Löscher, and Marschalek 2015). Two plasmids were transfected by lipofectamine, with one containing the gene of interest (e.g., p53WT) and the other containing the transposase SB100X, eventually leading to stable integration of the GOI into the target cells. Antibiotic selection with geneticin (G-418) and subsequent cell sorting by GFP expression with a BD ARIA III flow cytometer (together with Dr. Hartmann Reifer of the FACS Core Facility Marburg) led to cell lines containing a specific p53 variant (WT, R175H or R273H) under a tetracycline-inducible promotor. **(a)** Verification of GFP expression by flow cytometry (FACS CANTO II). **(b)** Representative microscopic pictures validate the GFP expression of the transfected WT cell line compared to the untransfected KO. Images were taken with a LEICA DM3000 microscope with 20x magnification. **(c)** A representative Western Blot showing p53 expression of the generated cell lines after doxycycline induction (0.5 µg/ml) for 24 hours. Cells were lysed, and 15 µg of protein were loaded per lane on a 10 % SDS gel. GAPDH was detected as a loading control.

4.4 p53WT cells show a distinct transcriptomic signature mediated by p53 and potentially NFκB signaling

Next, RNA sequencing was done to investigate the influence of the p53 status in our cell lines, especially regarding EV biogenesis. Therefore, the transcriptomes of doxycycline-treated and untreated cells were sequenced and bioinformatically analyzed. Here, general doxycycline-induced changes (e.g., mitochondrial genes) were excluded from the analysis. After cleaning the data, 19,353 protein-coding genes were detected (Fig. 7a). The data of doxycycline-treated p53WT cells showed an increase in overall detected genes, followed by the mutp53 cell lines, while KO and parental cells did not show notable differences. This indicates an induction of p53-dependent genes.

By utilizing principal component analysis (PCA) with the p53 status and induction as the two variables, induced p53WT cells showed the most considerable discrimination compared to the other groups (Fig. 7b). Blotting transcripts per million (TPM) of *TP53* exon counts revealed strong induction of the gene, especially in the mutants followed by the WT cells (Fig. 7c), which confirms the Western Blot data shown in Fig. 6c. This also reflects the physiological state of p53, since mutant p53 is often stabilized due to lack of degradation by the ubiquitin-proteasome system and therefore overexpressed compared to its WT state (Jiajian Wang et al. 2023).

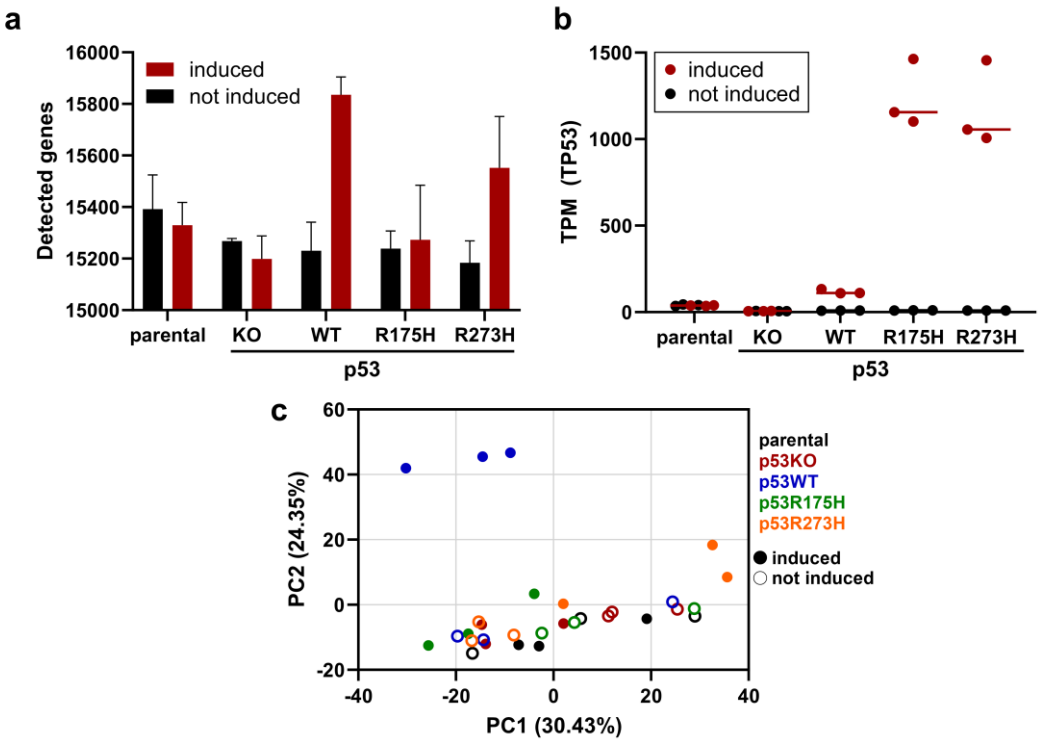

Figure 7: Transcriptomic data shows a distinct genotype of p53WT cells.
All cell lines were incubated (+/- 0.5 µg/ml doxycycline) for 24 hours before RNA was isolated, and two µg was sent for RNA sequencing (n=3). Sequencing data was aligned with STAR (2.7.10a) against the ENSEMBL of homo sapiens and quantified by Python scripts. The list was filtered for protein-coding and lncRNA and normalized on transcripts per million (TPM). **(a)** The bar graph shows the influence of doxycycline on the detected genes in the RNA sequencing data (n=3 ±SD). **(b)** The dot blot displays the p53 gene copy (TPM) after induction (n=3). **(c)** Principal component analysis (PCA). Different colors indicate a distinct p53 status, and the filled or empty shape represents a doxycycline-treated (induced) or untreated (not induced) status, respectively.

Heatmaps displaying row z-scores of all detected genes confirmed the distinct phenotype of the WT cells compared to all other cell lines (Fig. 8a). In contrast, KO cells and the mutants R175H and R273H did not show significant differences in their transcriptomic phenotype (Fig. 8a). Direct comparison of p53WT and p53KO cells showed upregulation (log_2(FC) > 1 and FDR < 0.05) of 1,906 genes in the former, including *TP53, CDKNA1A, FAS; CAV1, CD82, CXCL1* or *CXCL8*.

Enrichment analysis was done with the web-tool EnrichR and the utilization of several databases, including KEGG (Kyoto Encyclopedia of Genes and Genomes), GO:BP (Gene ontology: Biological Processes), and TRRUST (transcriptional regulatory relationships unraveled by sentence-based text-mining (E. Y. Chen et al. 2013). As expected, the p53 signaling pathway (hsa04115) was most significantly enriched (EnrichR, adj. p-value < 10^{-10}) (Fig. 8c). Additional analysis also showed association to

other signaling pathways involved in apoptosis, survival or proliferation, such as the MAPK (hsa04010), TNF (hsa04668) or NFκB (hsa04064) signaling pathways, which are all known to interact with the p53 pathway (G. S. Wu 2004; T. W. Kim et al. 2023). Besides p53, NFκB (RELA, NFKB1), the zinc finger transcription factor SP1 and STAT3 were found as potential upstream regulators (Fig. 8c). Upregulation of the NFκB pathway was surprising, since p53 and NFκB are often described as antagonistic (Carrà et al. 2020; Webster and Perkins 1999). However, a heatmap displaying normalized z-scores of important NFκB pathways and target genes further strengthens the finding. Here, expression of *NFKB1, RELB, NFKBIA, IKBKB, NFKB2, IL6, IL1B,* or *CXCL8* was increased in WT cells (Fig. 8d).

For the KO cells, 496 genes were found upregulated, mainly associated with the cell cycle (hsa04110), such as *CCNA2, CCNB1, CCNB2,* or *CDK1*. Other upregulated genes included *BRCA1, BRCA2, ITGA4, MYC,* or *TGFB2* (Fig. 8b). Here, upstream regulators were mainly from the E2F transcription factor family (E2F1, E2F3, E2F4), which are known to have critical functions in cell cycle regulation (Fig. 8c) (Johnson and Schneider-Broussard 1998). Since this project mainly revolves around the effects of p53 in EV-mediated communication, genes related to EV biogenesis and cargo loading were investigated. Many genes were found upregulated in p53WT cells, such as *CHMP4A, TSG101, PDCD6IP, SDC1, SDC4,* or *CD82* (Fig. 8e). Although p53 was previously described to play a role in EV biogenesis, upregulation of all these markers was not shown (Yu, Harris, and Levine 2006; Bebelman et al. 2020). Interestingly, two of the most defined EV surface markers, the tetraspanins CD9 and CD63, were downregulated in the WT cells (Fig. 8e) (van Niel, D'Angelo, and Raposo 2018). Validation of the transcriptomic data was done by RT-qPCR of selected targets and confirmed significant upregulation (One Way ANOVA with Tukey's test) of *TP53, IL1A* and *IL1B* ($p<0.0001$) as well as downregulation of *TGFB2* ($p<0.001$), *BRCA2* ($p<0.0001$) and *CD9* ($p<0.001$) in the p53WT compared to KO cells (Fig. 8f).

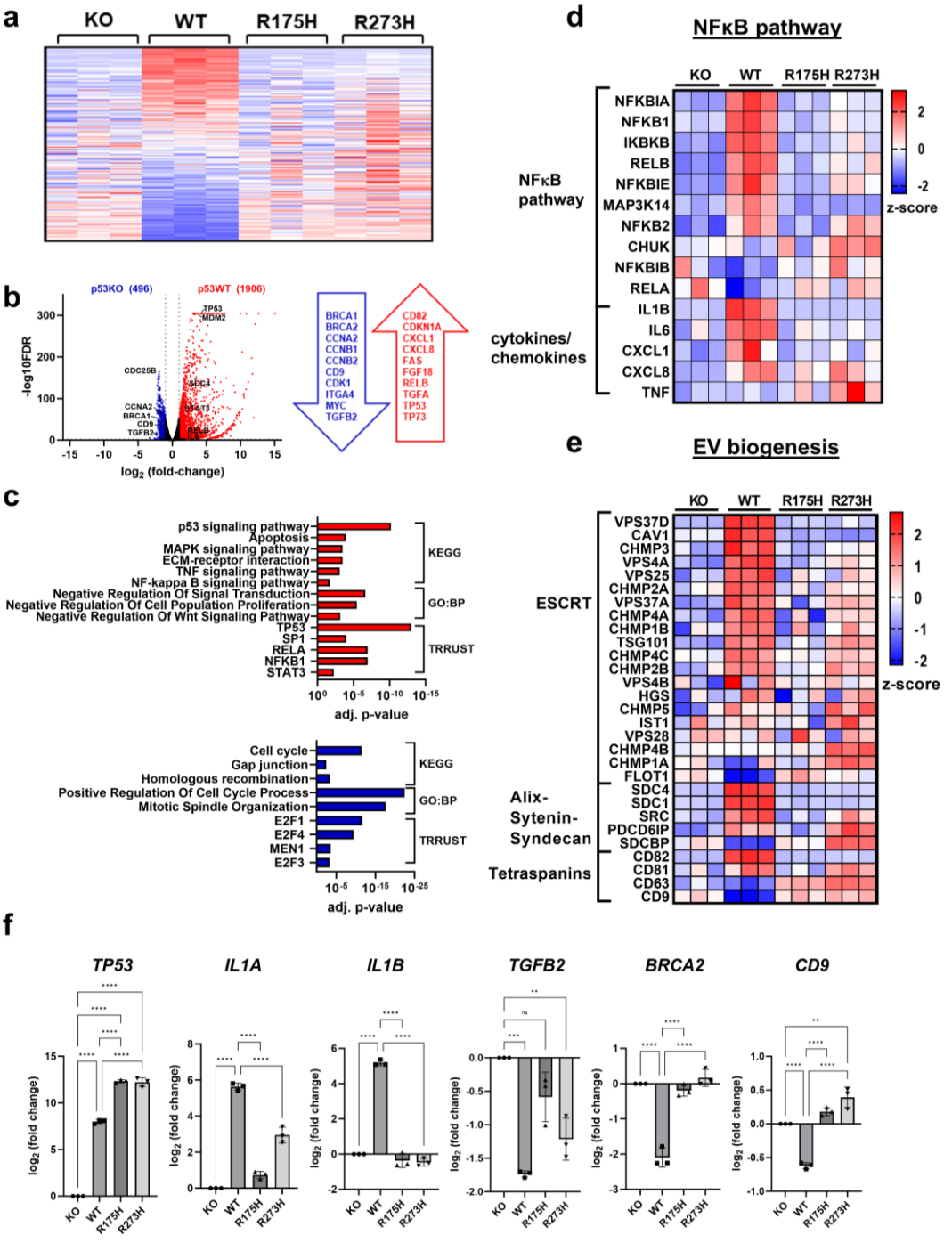

Figure 8: Transcriptomic data reveal a specific phenotype for wild-type cells predominantly driven by p53 and NFκB.
All cell lines were incubated (+/- 0.5 µg/ml doxycycline) for 24 hours before RNA was isolated, and 2 µg were sent for RNA sequencing (n=3). Sequencing data was aligned with STAR (2.7.10a) against Ensembl of homo sapiens (v106) and quantified by Python scripts. The list was filtered for protein-coding and lncRNA and normalized on transcripts per million (TPM). **(a)** Heatmap displaying row z-scores of all detected genes. Sorted after most upregulated genes in the p53WT group. The color indicates a positive (red) or negative (blue) z-score with the color intensity correlating with the value. **(b)** Volcano plot shows differentially expressed genes between WT and KO cells. A Log_2(FC) > and FDR < 0.05 were used as a threshold and colored according to direction. Insignificant genes are represented by black dots **(c)** Enrichment analysis was done via the web-based EnrichR software. Here, significant and interesting pathways are displayed for several databases, including the KEGG, GO:BP, and TRRUST database was used. Significance and p-

values are computed using the Fisher exact test and adjusted using the Benjamini-Hochberg method. **(d)** Heatmap displaying row z-scores of selected NFκB-related genes. Genes were clustered for either NFκB pathway or cytokines/chemokines and sorted for the highest values in the p53WT group. **(e)** Heatmap displaying row z-scores of selected genes related to EV-biogenesis, clustered for the ESCRT, ALIX-syntenin-syndecan, or tetraspanin-related genes. **(f)** RT-qPCR of selected targets was done to validate the transcriptomic data. Significance was calculated by One-Way ANOVA with Tukey's test (****p<0.0001, ***p<0.001, **p<0.01, n=3 ±SD).

Mutp53 cells displayed a similar transcriptomic genotype to the KO cells; however, some expression is detected in between the expression of KO and WT cells (e.g., EV biogenesis genes, Fig. 8e). Both mutants are considered p53 GOF mutations, which combines the loss of the original p53 function with new unique activities (Freed-Pastor and Prives 2012). While R175H is a conformational mutant, the R273H mutant is described as a DNA contact mutant, leading to impairment of binding to target DNA. However, alternate gene expression profiles are described (Freed-Pastor and Prives 2012; Mantovani, Collavin, and Del Sal 2019). Here, some genes were specifically upregulated when compared to both KO and WT cells, especially from the R273H mutant (Fig. 9). This included *SERPINA5, SERPINB9, SEMA4G, TNF, MMP12, TLR5* or *PDGFD*. Moreover, *ITGA5* was found unregulated in the R273H mutant, however, slightly below the set threshold of $log_2(FC) > 1$. For the R175H mutant, only Ret Finger Protein Like 2 (RFPL2) was found to be significantly upregulated. Notably, the expression of *HSP70 (HSPA1A, HSPA1B)* was increased as well (not significant, logFC < 1) (Fig. 9).

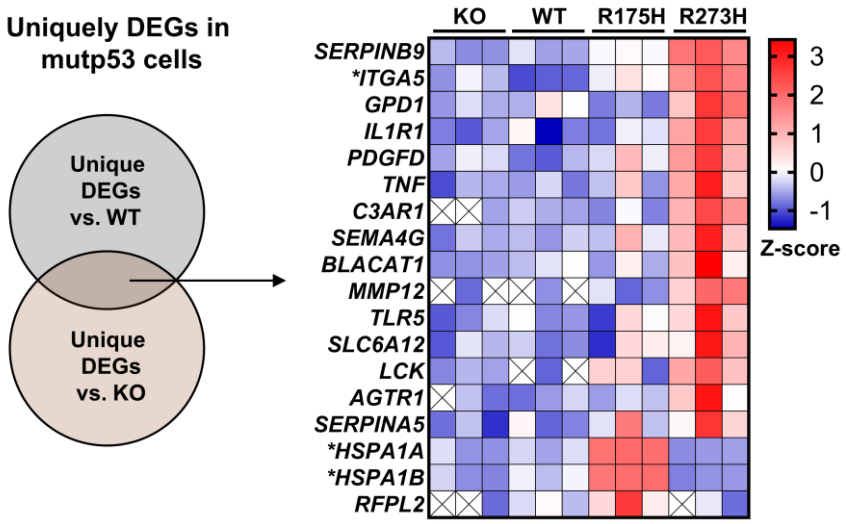

Figure 9: Uniquely expressed genes in p53-mutant compared to KO and WT cells.
Heatmap focuses on differential gene expression for mutp53 (R175H or R273H) cells compared to the KO or WT group. A $Log_2(FC) > 1$ and FDR < 0.05 was used as a threshold (n=3). *Genes were enriched but not significantly ($Log_2(FC) > 0.8$; < 1)

To exclude the possibility that the transcriptomic data was just an artifact of the inducible SB system used in this project, constitutive p53-expressing cells were used to validate selected targets. Therefore, OVCAR8 p53KO Clone 39 was transiently transfected with p53 (WT or mutant) under the constitutive elongation factor-1 alpha (EF-1α) promotor. EF-1α is a commonly used constitutive promotor, described as efficient or even more efficient in specific settings than the CMV promotor (Teschendorf et al. 2002). After transfection, RNA was isolated, transcribed, and used for RT-qPCR (Fig. 10a). The results were compared to cells containing the stably transfected, inducible p53 and similar expression between systems of all targets was observed (Fig. 10b). While *TP53, CDKN1A, CXCL1,* and *CXCL8* were increased in WT vs KO cells, *TGFB1* was found to be decreased (Fig. 10a,b).

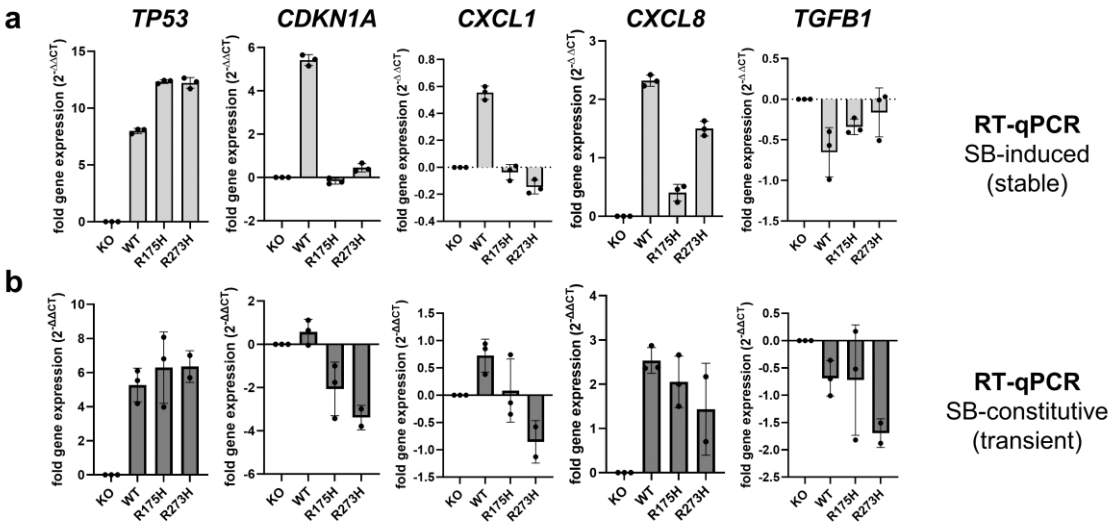

Figure 10: RT-qPCR shows similar results for inducible and constitutive p53-expressing cell lines. (a,b) SYBR Green-based RT-qPCR was done for selected genes (TP53, CDKN1A, CXCL1, CXCL8, and TGFB1) for p53 cell lines under an inducible (a) or constitutive promotor (b). Gene expression was normalized to two housekeeping genes (ΔCT) followed by normalization to the KO sample (ΔΔCT) (n=3 ±SD).

Next, the secretome of the different cell lines was analyzed by Olink to investigate how the distinct phenotype of the cell lines transfers to secreted factors. Olink Explore is a high-throughput discovery platform that combines PEA and NGS to explore the expression of proteins, here in the conditioned media (Wen Zhong et al. 2021). Similar to the transcriptomic data, p53WT cells displayed the most distinct phenotype compared to all other groups. In contrast, KO and mutp53 cells shared many similarities (Fig. 11a). Closer comparisons revealed over 600 unique proteins secreted by WT cells compared to KO, followed by the R273H mutant with 43 and only 3 in the R175H mutant (Fig. 11b).

For WT cells, many p53 or NFκB related genes were found to be abundant including *CDKN1A, BAX, CASP3*, *FAS, BAG6, IL1A, IL1B, and CSF1.* Secreted p53 was found in WT and both mutants. In general, both WT and mutant p53 cells showed an inflammatory phenotype, with the secretion of *IL6, CXCL1, CXCL8,* and *TGFA,* with more robust expression in WT cells (Fig. 11b). Pathway analysis also showed consistency with the transcriptomic data with enrichment of the p53, TNF, MAPK and NFκB signaling pathways (Fig. 11c). The secreted factors were also mainly regulated by the same transcription factors, including p53, SP1, NFκB1, and RelA.

In contrast, VEGFA/B, TGFB1/2, FGF19, and TIMP2 among others, were increased in the supernatant of KO cells, which resulted to enrichment of cytokine-cytokine receptor interaction (hsa04060), PI3K-Akt (hsa04151), MAPK (hsa04010) and Ras signaling (hsa04014). Besides, SP1 and SP2, PPARD, WT1, and SMAD3 were found as potential upstream regulators (Fig. 11c). In line with the transcriptomic data, the secretome of p53 mutants were similar to the KO cells with some expression related to WT phenotype. For example, inflammatory proteins, such as CXCL1, IL6, or CXCL8 were found increased in the CM of mutp53 cells compared to KO, however less abundant than in the WT secretome (Fig. 11b). The p53R273H mutant also showed a specific increase in the secretion of proteins, including IL1R1, MMP7, TNFRSF9, TNFRSF11A, COL9A1, CCL22, CD274, CD55 or LIF (Fig.11d). Together with the R175H mutant, COL4A1, MICA/MICB, CCL5, IL18, CXCL5, IL11, and MMP12 were also more abundantly expressed (Fig. 11d).

In conclusion, OVCAR8 cells expressing WTp53 showed the most distinct phenotype compared to mutp53 or p53KO cells, characterized by an active p53 expression and upregulated NFκB pathway genes. This phenotype was further represented by the secretion of inflammatory cytokines, including IL1α, IL1β, IL6, CXCL1, and CXCL8.

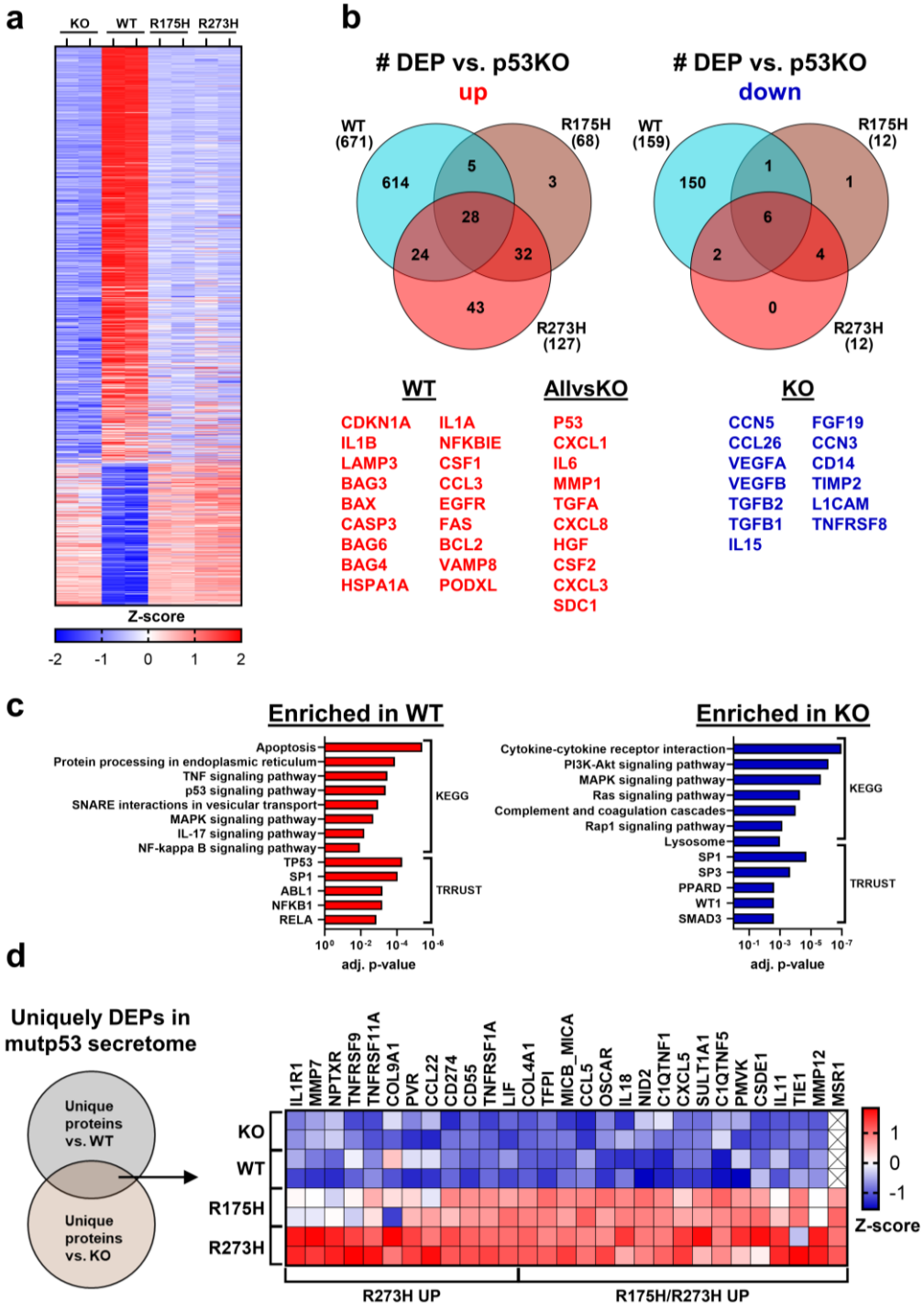

Figure 11: Secretome data of conditioned medium reveal a distinct phenotype of p53WT cells. CM was collected and sent for Olink explore analysis one day after induction with doxycycline. The combination of PEA technology with NGS allowed the parallel analysis of almost 3,000 proteins in the supernatant. The resulting counts were processed to normal protein expression (NPX), which was used for all further analysis. Differences in NPX values between groups were calculated, and only values greater than one were considered (n=2). **(a)** Heatmap displaying row z-scores of NPX data. Sorted for highest z-scores in the p53WT group **(b)** Venn diagram representing differentially expressed proteins in the secretome of p53WT, p53R175H, or p53R273H cells compared to p53KO cells. **(c)** Bar diagrams depicting enrichment analysis, done with the web-based EnrichR software utilizing the KEGG and TRRUST (upstream regulator) databases. Significance and p-values are computed using the Fisher exact test and adjusted using the Benjamini-Hochberg method. **(d)** Heatmap displays row z-scores of differential increased proteins in the secretome of mutp53 cells compared to WT and KO cells.

4.5 EVs from WT cells show specific cargo loading and are enriched in p53

After characterization of the cells, the focus was shifted towards EVs, and changes in the composition related to the p53 status of the cells were investigated. Isolation of EVs was done by differential ultracentrifugation (dUC), which relies on several centrifugation steps to purify the cell supernatant with a subsequent concentration by ultracentrifugation (Théry et al. 2018). In our laboratory, the established protocol involved incubating the cells in FCS-free CD293 medium for 48 hours after induction with doxycycline before collecting the supernatant. Since cell death was observed by microscopy in p53WT cells (data not shown), an MTT assay was done to check for cell viability for various doxycycline concentrations over 48 hours. Results indicated low viability in p53WT cells even with the lowest concentration of doxycycline (0.2 µg/ml) (Fig. 12a).

Therefore, a new protocol had to be established, and different concentrations over time were tested. Cells were treated for either 6, 12, or 24 hours with 0.5 or 1 µg/ml of doxycycline, and apoptosis and necrosis were investigated by an annexinV/PI assay. As expected, cell death in p53WT cells increased with concentration and time. However, 0.5 µg/ml doxycycline over 24 hours still yielded 80 % viable cells (Fig. 12b,c). This was acceptable for this project since apoptosis was expected due to an active p53 function. Notably, apoptosis and necrosis could not be detected in p53KO or mutp53 cells, confirming altered p53 activity in these cells (Appendix Figure S1). Furthermore, Western Blot analysis confirmed strong p53 expression in p53WT cells after treatment of 24 hours with 24 hours of recovery in fresh medium (Fig. 12d). Finally, the new EV isolation protocol was established with 24 hours of induction in 0.5 µg/ml doxycycline followed by one day in CD293 before collection. As described, EVs were isolated by differential ultracentrifugation.

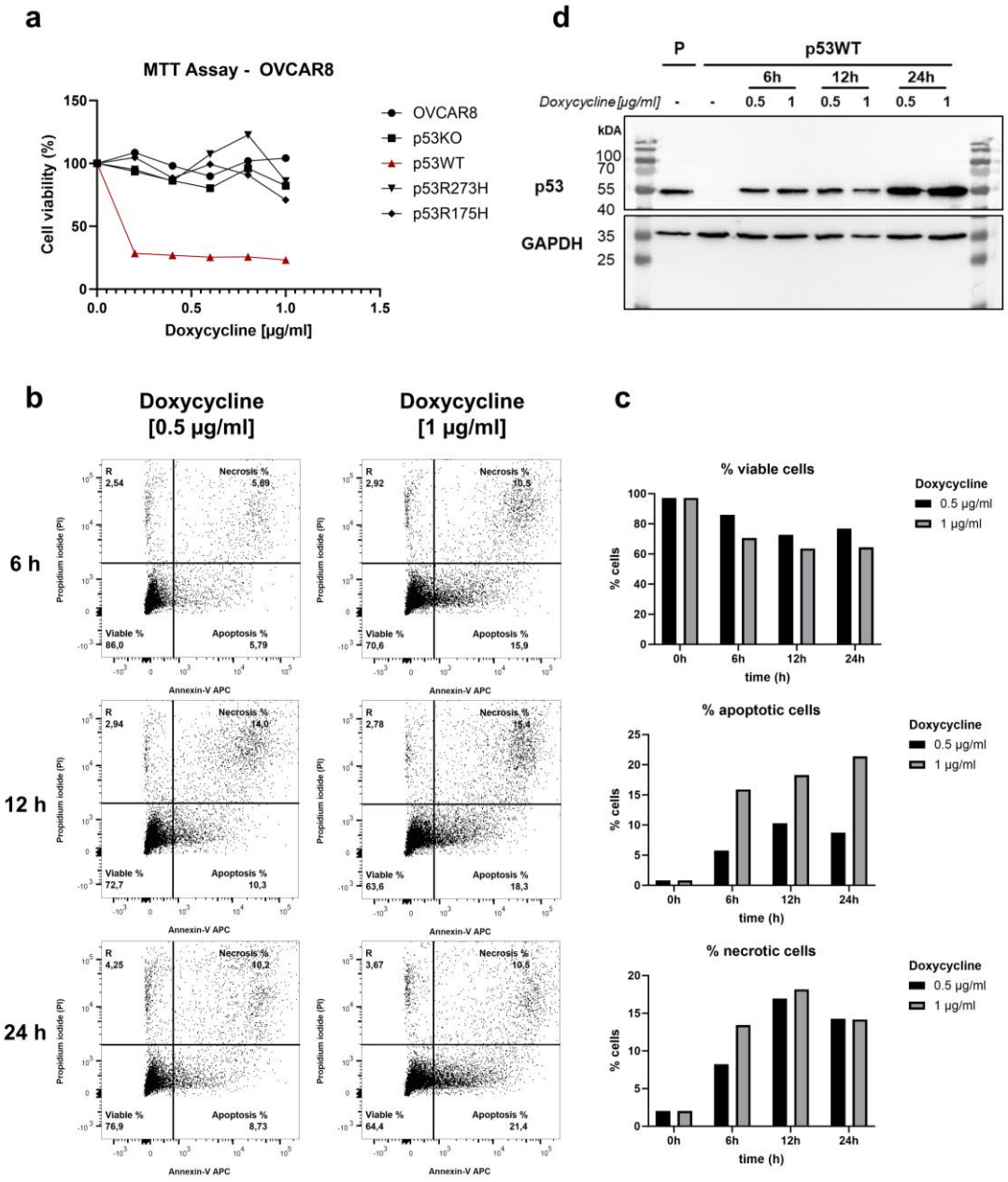

Figure 12: A doxycycline concentration of 0.5 µg/ml for 24 hours is sufficient to induce strong expression of p53WT while maintaining high cell viability.
Cell viability (a, b, c) and p53 expression (d) were measured after induction with different concentrations of doxycycline over time to set up an induction protocol for EV isolation. **(a)** MTT cell viability assay of different OVCAR8 cells was done after treatment with several doxycycline concentrations (0, 0.2, 0.4, 0.6, 0.8, and 1 µg/ml) for 48 hours. The percentage of cell viability was calculated by comparing the 462 nm absorbance from 0 vs. 48 hours. **(b)** AnnexinV/PI assay was performed with p53WT cells 48 hours after induction with 0.5 or 1 µg/ml (6, 12, or 24 hours), and samples were measured at the flow cytometer FACS Canto II. **(c)** Graphical evaluation of annexin assay displaying % of viable, apoptotic, or necrotic cells **(d)** Western Blot of p53WT cells for p53 and GAPDH was done after doxycycline treatment (0.5 or 1 µg/ml) for 6, 12, or 24 hours. Parental OVCAR8 cells (P) were used as a control.

Various methods were used to characterize EVs isolated from the different cell lines, including electron microscopy, nanoflow cytometry, Western Blot, proteomics, and Olink.

Transmission electron microscopy (TEM) was done on a ZEISS EM900 by fixation of $5x10^8$ particles to a copper grid. The pictures revealed round particles with a specific "cup shape," which is described to be typical for EVs and is the result of the fixation and dehydration process prior to the measurement (Fig. 13) (Nieuwland et al. 2022). This shows that EVs were successfully isolated. Differences in size or shape between the groups could not be observed. A moderate background was seen in the pictures, indicating co-isolation of other particles. This, however, was expected since dUC is described as a balanced method of EV purity and yield (Clos-Sansalvador et al. 2022). Other methods, which increase purity, often lack output yield and vice versa.

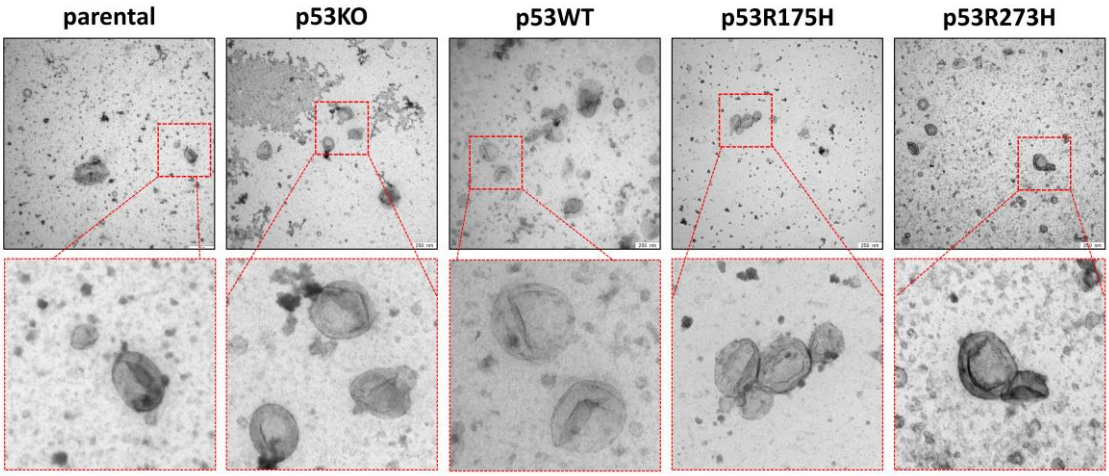

Figure 13: Electron microscopy images display the typical cup shape of EVs in all samples.
$5x10^8$ particles were fixed with 4 % PFA for each sample and placed on a Formvar/carbon-coated 200 mesh copper electron microscopy grid. Images were taken with a ZEISS EM900 at 80 kV by Dr. Frederick Helmprobst from the electron microscopy core facility in Marburg (Scale: 250 nm).

Next, EVs were characterized by proteomic analysis to investigate their cargo and potentially reveal interesting candidates. EVs were isolated from cells by dUC (+/- induction), and $5x10^8$ particles were sent for mass spectrometry. A total of 5,803 proteins were detected, which subsequently were compared to TOP100 EV proteins provided by vesiclepedia and exocarta (Fig. 14a). Both sites are manually curated databases cataloging molecular data (e.g., proteins, lipids or nucleic acid), with vesiclepedia collecting data of various EV populations and exocarta specifically providing exosomal data (Keerthikumar et al. 2016; Pathan et al. 2019).

Almost all of the Top100 proteins could be detected in this EV set, further validating the successful isolation of EVs (Fig. 14a). Interestingly, by blotting the z-score of these proteins in a heatmap and comparing the different cell lines, p53WT cells showed a generally lower expression (Fig. 14b). This is particular interesting since many genes

related to EV biogenesis were upregulated in the transcriptomic data of WT cells, such as *PDCD6IP* (ALIX) or *TSG101*. Coherent to the transcriptomic data, tetraspanins CD9 and CD63, routinely described as common EV markers, are less abundant in WT EVs. (Fig. 14c). In contrast, some proteins seemed to be enriched explicitly in WT EVs, including HSPA5, FASN, FLOT1, CD81, or CD82, which altogether could indicate secretion of different EV subtypes in the different cell lines (Fig. 14c).

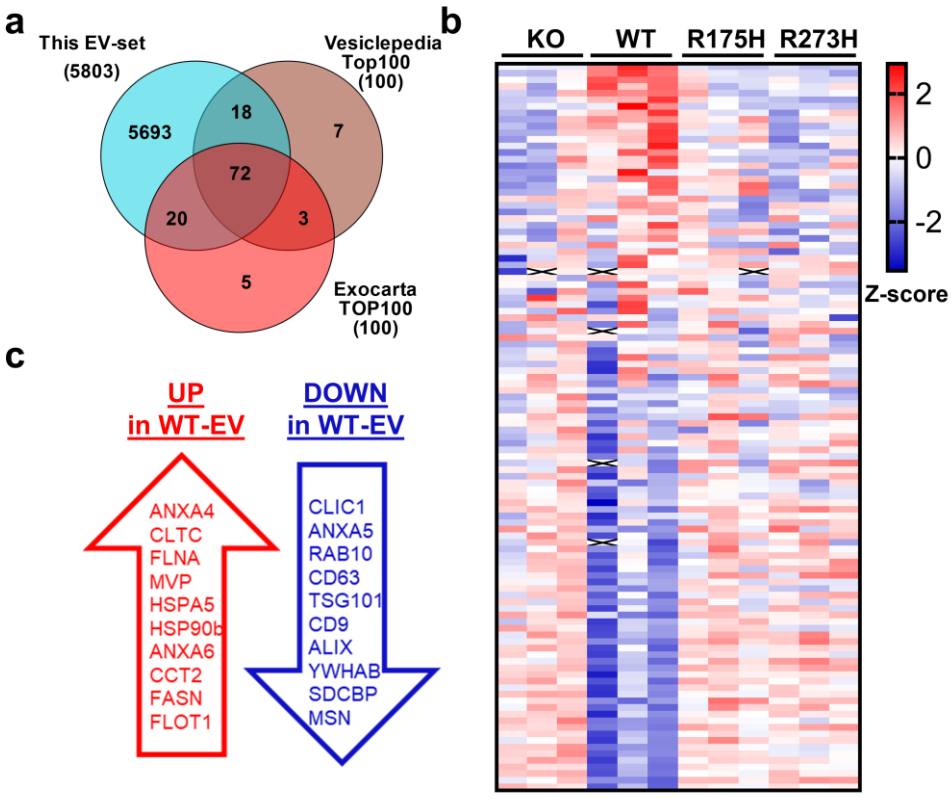

Figure 14: Most common EV-proteins are less abundant in p53WT cells.
A total of 5x10^8 particles isolated by dUC from induced/noninduced cells after 24 hours in CD293 medium were sent for proteomic analysis at the Institute of Translational Proteomics (Marburg University). Peptides were cross-referenced with the UniProt-SwissProt canonical database before normalization by label-free quantification (LFQ). Imputation of the data was done to account for missing values, and statistical differences between groups were calculated by Limma-moderated t-test. Only proteins with a median of at least four peptides in one group were considered for analysis (n=3, FDR < 0.05, logFC > 1) **(a)** Venn diagram shows detected proteins in this EV set (5,803 proteins) compared to the TOP100 EV proteins from the two vesicle databases, Vesiclepedia and Exocarta. **(b)** Heatmap displays the row z-score of the 110 proteins shared between this EV-set and the TOP100 proteins of the vesiclepedia and exocarta database. Proteins were sorted for the highest values in the p53WT group. **(c)** List of selected differentially expressed proteins in the EVs isolated from p53WT cells.

By plotting all detected proteins in a heatmap a specific phenotype for WT EVs could be detected (Fig. 15a). In contrast, KO and both mutants were similar in their protein expression (Fig. 15a). Direct comparison of enriched proteins in WT and KO EVs revealed p53 as a major protein detected in the WT (Fig. 15b). Together with the

secretome analysis of the cell lines (see Fig. 11b), this confirmed direct loading of p53 itself in the EVs. Moreover, BAG6, CAV1, CD82, FAS, PODXL or TNFRSF10B were also detected in the WT EVs as well as proteins associated to the proteasome (hsa03050) or RNA processing (GO:0006396) (e.g., PSMD6, PSMD7, HRNNPR, SF3A3, ADAR) (Fig. 15b,c). Again, detected proteins were mainly regulated by p53 itself.

In EVs isolated by p53KO cells, proteins enriched in the regulation of actin cytoskeleton (hsa04810, e.g., ITGA4, FN1, EGFR, ITGB8), focal adhesion (hsa04510, e.g., LAMA5, LAMB1, COL1A1) and proteoglycans in cancer (mmu05205, e.g., CD63, TGFB1, WNTB5, SDC2, ERBB3) were detected (Fig. 15c). Furthermore, proteins were associated with the regulation of migration (GO:0016477, e.g., SEMA3C, SEMA3D, SEMA3E, CEMIP) or extracellular vesicles (GO:0140112, e.g., SDCBP, ARRDC1, CD9, TSG101) (Fig. 15c).

As already indicated in the secretome data (Fig. 11d), p53 mutated cells did show many differences in their EV cargo (Fig. 15e). With MRGPRF and CFAP74, only two proteins were found uniquely and significantly enriched in EVs of the R273H mutant when compared to KO and WT EVs (Fig. 15e). Moreover, TSPAN4, TSPAN6 and TSPAN9, SDC4, CCN1, CCN2, EPCAM, ADAM9 and LAMB2 were found enriched compared to the WT but not KO EVs (Fig. 15e).

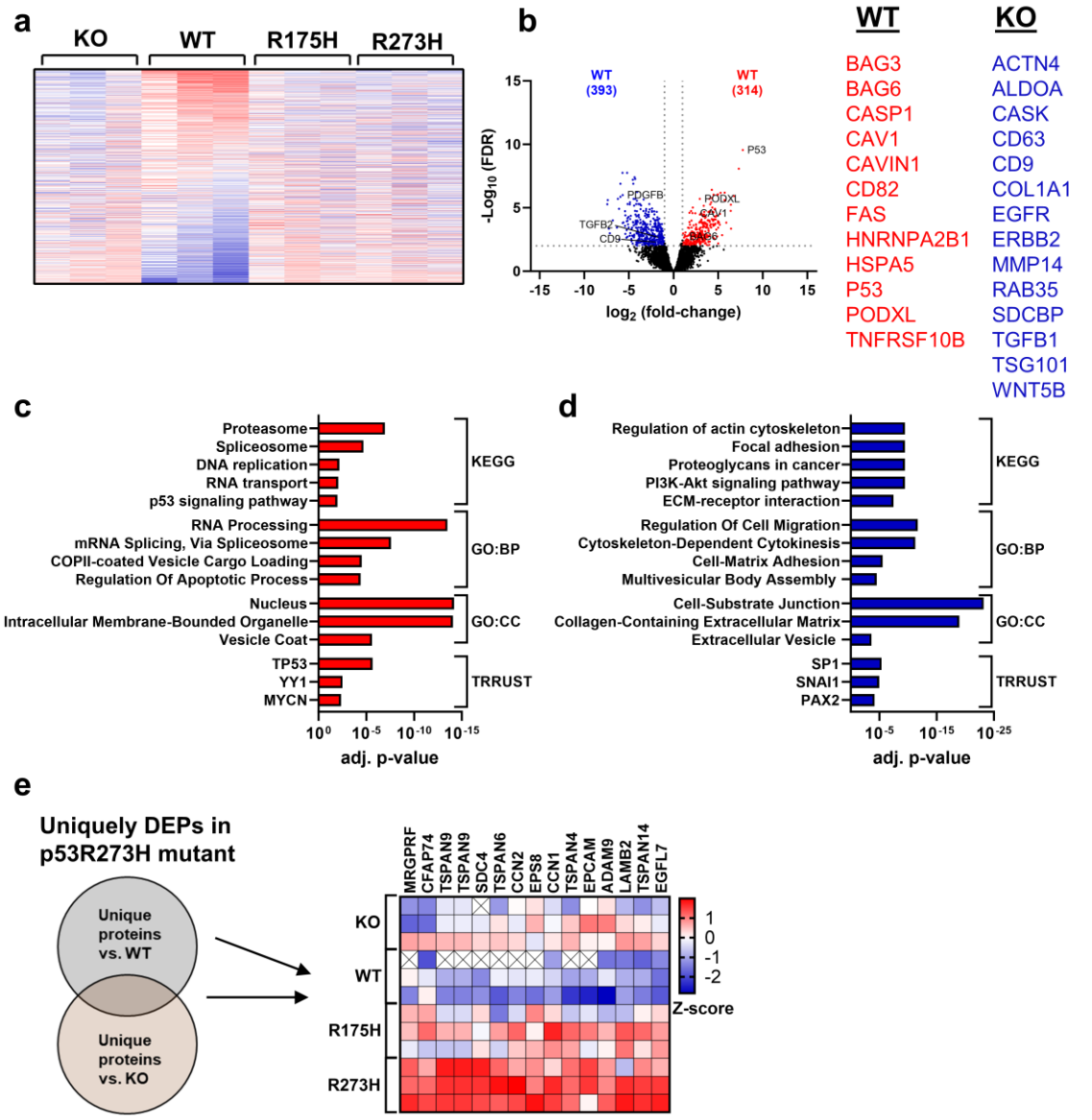

Figure 15: EVs isolated from p53WT cells show distinct cargo loading compared to vesicles from mutant or KO cells.
A total of 5x10^8 particles isolated by dUC from induced/noninduced cells after 24 hours in CD293 medium were sent for proteomic analysis at the Institute of Translational Proteomics (Marburg University). Peptides were cross-referenced with the UniProt-SwissProt canonical database before normalization by label-free quantification (LFQ). Imputation of the data was done to account for missing values, and statistical differences between groups were calculated by Limma-moderated t-test. Only proteins with a median of at least four peptides in one group were considered for analysis (n=3, FDR < 0.05, $\log_2$(FC) > 1) **(a)** Heatmap displays row-z-scores of all 5,803 proteins found in this EV-set. Expression was sorted for the highest values in the p53WT group. **(b)** Volcano-plot showing DEPs in EVs of p53WT compared to p53KO cells (-$\log_{10}$(FDR) > 2, $\log_2$(FC) > 1). (c,d) Gene ontology (BP and CC – cellular component), KEGG pathway, and TRRUST enrichment analysis display selected upregulated pathways, processes, and transcription factors enriched in the proteins of p53 WT **(c)** or p53KO **(d)** EVs. **(e)** Heatmap displays uniquely differential expressed proteins (DEP) in the mutp53 EVs compared to p53KO and p53WT.

In addition to mass spectrometry, EVs from KO and WT cells were further analyzed by Olink. NPX was compared between the samples, and targets with a difference in protein abundance of NPX > 1 were considered. Consistent with the proteomics data, WT EVs

were enriched in proteins connected to the p53 signaling pathway (hsa04115) or apoptosis (hsa04210, e.g., P53, BAX, FAS) (Fig.16 a,b). Moreover, association with NFκB activation (GO:0038061, e.g., TNFRSD10B, CHI3L1) could be detected, which is in line with the transcriptomic data. Altogether, this indicates the interplay of the p53 and NFκB pathways in p53WT cells, leading to the secretion of EVs containing proteins related to both pathways.

KO EVs were associated with proteoglycans in cancer, ECM-receptor interaction (e.g., ITGB1, ITGB5, SDC4, FN1, COL1A1), MAPK signaling (e.g., PDGFRB, NOTCH2, LIF), PI3K-Akt signaling (e.g., LAMB1, EGFR, ERBB3) and regulation of cell migration (e.g. SEMA7A, SEMA3G; PDGFA, CXCL16, VEGFA) (Fig. 16a,b).

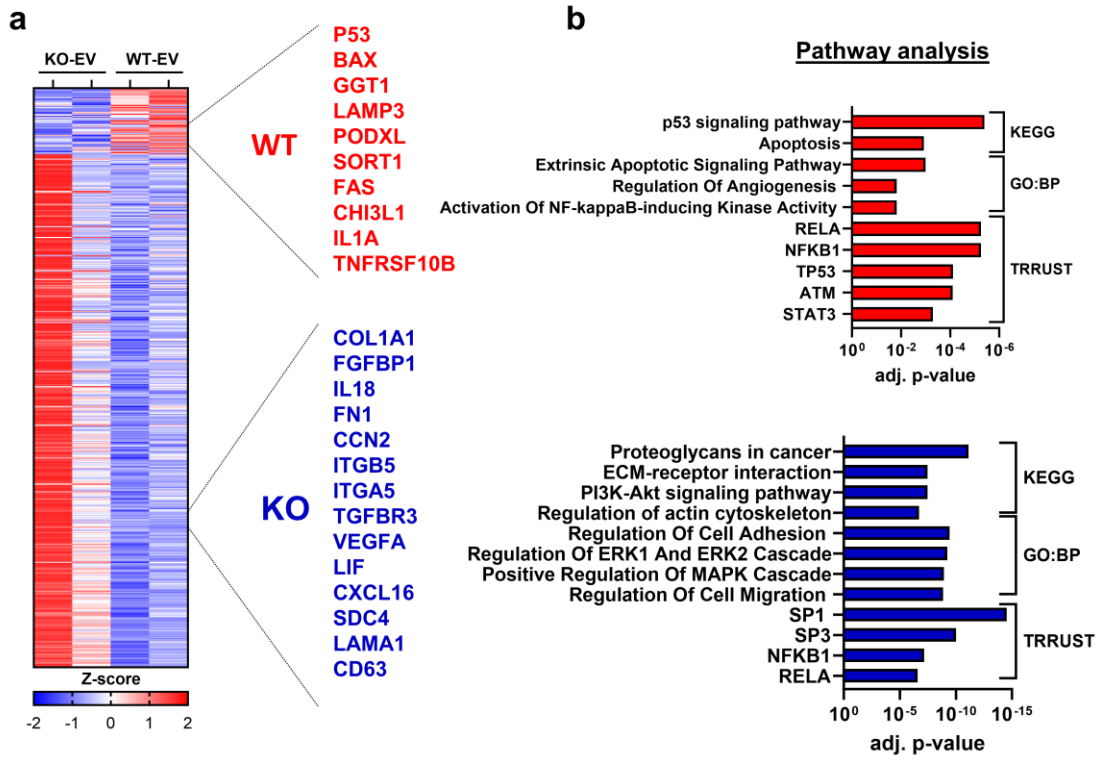

Figure 16: Olink of EVs shows substantial differences in EV cargo between KO and WT EVs. EVs were isolated as described before and sent for Olink explore analysis by the Institute of Translational Proteomics. The combination of PEA technology with NGS allowed the parallel analysis of almost 3,000 proteins. The resulting counts were processed to NPX and used to calculate differences between groups. A difference of at least NPX > 1, which implies a doubling of protein concentration, was considered. **(a)** Heatmap displays the z-score of DEP found in EVs of p53KO or p53WT cells. Each row represents a protein, and each column a sample. **(b)** Enrichment analysis of proteins in EVs from KO (Blue) or WT (red) cells by utilizing the KEGG, GO:BP, and TRRUST databases.

To compare transcriptomic data of the cell lines with proteomic data of EVs, specifically for the comparison between p53WT and KO group, a VENN diagram was generated intersecting all 13,751 expressed genes with the 5,803 detected proteins (Fig. 17a). This

resulted in 5,297 targets, which were further plotted in a scatter plot with the x-axis representing the log_2 ratio of proteins and y-axis the log_2 ratio of transcripts, to investigate a potential correlation (Fig. 17b). The plot was separated into nine quadrants, by a threshold of -1 and 1 on both axes, which is shown by the dotted lines. In general, the data showed a slightly positive correlation with $r = 0.1407$, suggesting that gene expression does not correlate to EV protein in most cases (Pearson correlation, Fig. 17b). While 3,040 targets in quadrant 5 showed no differences in mRNA or protein levels, the 275 and 99 proteins in quadrants 2 and 8, respectively, showed differential expression on mRNA but not on protein level. On the other hand, 807 proteins in quadrant 4 and 742 in quadrant 6 demonstrated significant differences in their abundance in EVs but not in mRNA expression levels, suggesting other factors than the sole gene expression are required to determine protein secretion via EVs. Ninety-eight proteins were significantly negatively correlated (Pearson $r = -0.54$, $p<0.0001$), with 83 in quadrant 1 and 15 in quadrant 9. A significant positive correlation between RNA and protein level with Pearson $r = 0.73$ ($p<0.0001$) was shown for targets in quadrants 3 and 7, with 160 and 77 proteins, respectively (Fig. 17b).

The positively correlated proteins were then further analyzed by pathway analysis via the EnrichR website (E. Y. Chen et al. 2013). This resulted in the enrichment of the p53 signaling pathway (hsa04115) together with negative regulation of cellular processes (GO:0048523), positive regulation of apoptotic signaling pathway (GO:0043065) and negative regulation of epithelial cell proliferation (GO:0050680) for targets of the quadrant 3 (respective to upregulation in WT cells/EVs) (Fig. 17c). Moreover, TRRUST analysis confirmed p53 as primary upstream regulator, followed by EGR1 and p63 (Han et al. 2015). In contrast, the protein in quadrant 7 (= Up in KO cells/EVs) showed enrichment in the cell cycle and its regulation, with potential upstream regulators of the E2F family (E2F1, E2F4, E2F3) (Fig. 17c).

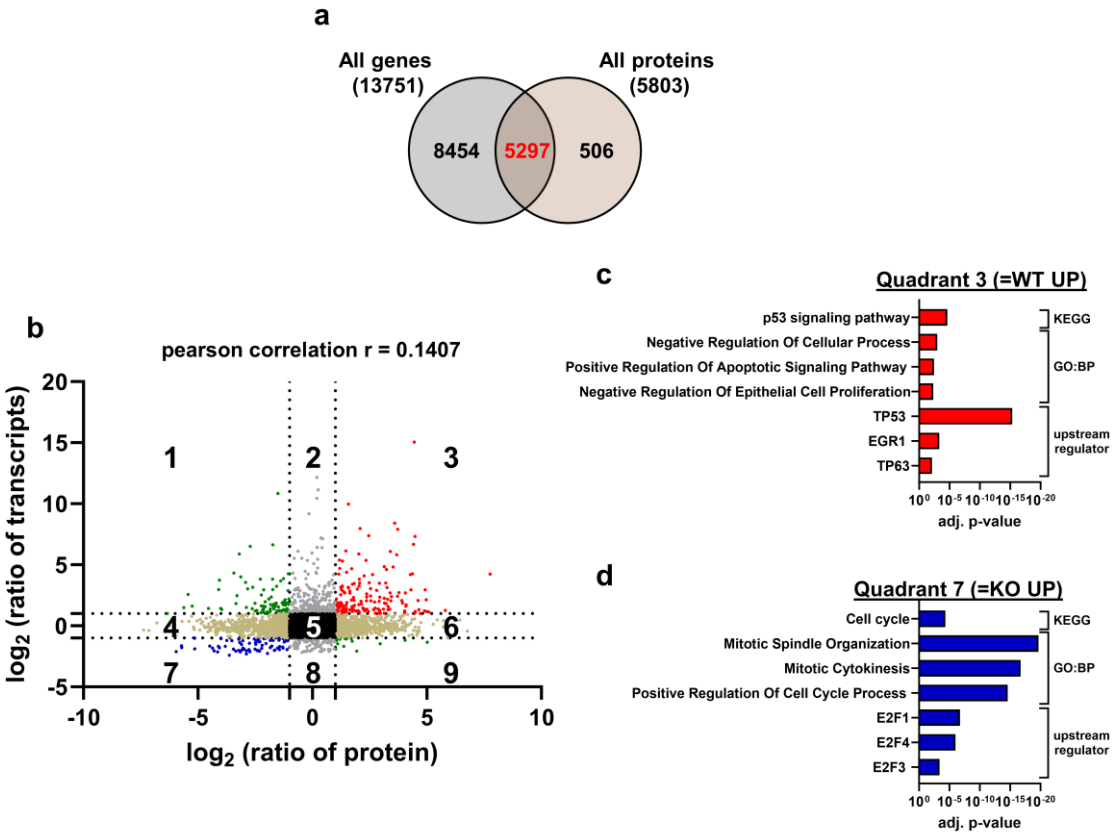

Figure 17: Correlation of transcriptomic and proteomic data confirms p53 or loss of p53 as the primary driver for the cell genotype and associated EVs.
The comparison was focused on comparing the p53 WT and KO groups. **(a)** Venn diagram shows 5,297 targets detected in both the transcriptomic of cells and proteomic data of EVs. **(b)** A scatter plot, divided into nine quadrants, displays the log_2 ratio of proteins and the log_2 ratio of transcripts. Quadrants 3 and 7 display factors with combined increase or decrease in RNA and protein levels. Pearson R correlation was computed by the GraphPad (V10) software (Pearson r = 0.73, ****p<0.0001). Quadrant 1 and 9 displayed factors which are either upregulated in RNA and decreased on protein level or vice versa (Pearson r = -0.58, ****p<0.0001). **(c)** Enrichment analysis of the 160 proteins of quadrant 3 (= upregulated in p53WT) with the EnrichR software and the KEGG, Go:BP, and TRRUST database. **(d)** Enrichment analysis of the 77 proteins in quadrant 7 (= upregulated in p53KO) with EnrichR software and the KEGG, Go:BP, and TRRUST database.

Next, EVs were also characterized by their size and concentration via nano-flow cytometry. Here, p53WT cells showed a significantly increased secretion of EVs compared to all other cell lines (Fig. 18a). This could be due to the enhanced expression of many EV-biogenesis related genes, observed in the transcriptomic data of p53WT cells (Fig. 8e) of However, particle size did not differ between the groups (Fig. 18b). Corresponding to the proteomic analysis, CD9 was found significantly downregulated on vesicles from WT cells compared to KO (Fig. 18c). Western Blot analysis of EV and cell lysate revealed enrichment of the EV marker ALIX in the EV lysates, while HSP70 was found in both (Fig. 18d).

Interestingly, while the mutants showed a higher p53 expression in the cell lysate, which is in agreement with the transcriptomic data, p53 is enriched in the WT EVs (Fig. 18d). Densitometric analysis comparing p53 expression in EVs vs. cells, WT show a significant enrichment of the protein in the EVs (One Way ANOVA with Tukey's test) (Fig. 18e). The expression of the chaperone BAG6, which is known to play a role in acetylation of p53 and subsequent direction of anti-tumor cargo loading of EVs, was also enriched in WT EVs which was shown by Western Blot (Fig. 18f) (Schuldner et al. 2019). Altogether, WTp53 seems to be preferably loaded into EVs of OVCAR8 cells, which calls into question whether the tumor suppressor protein could directly affect recipient cells.

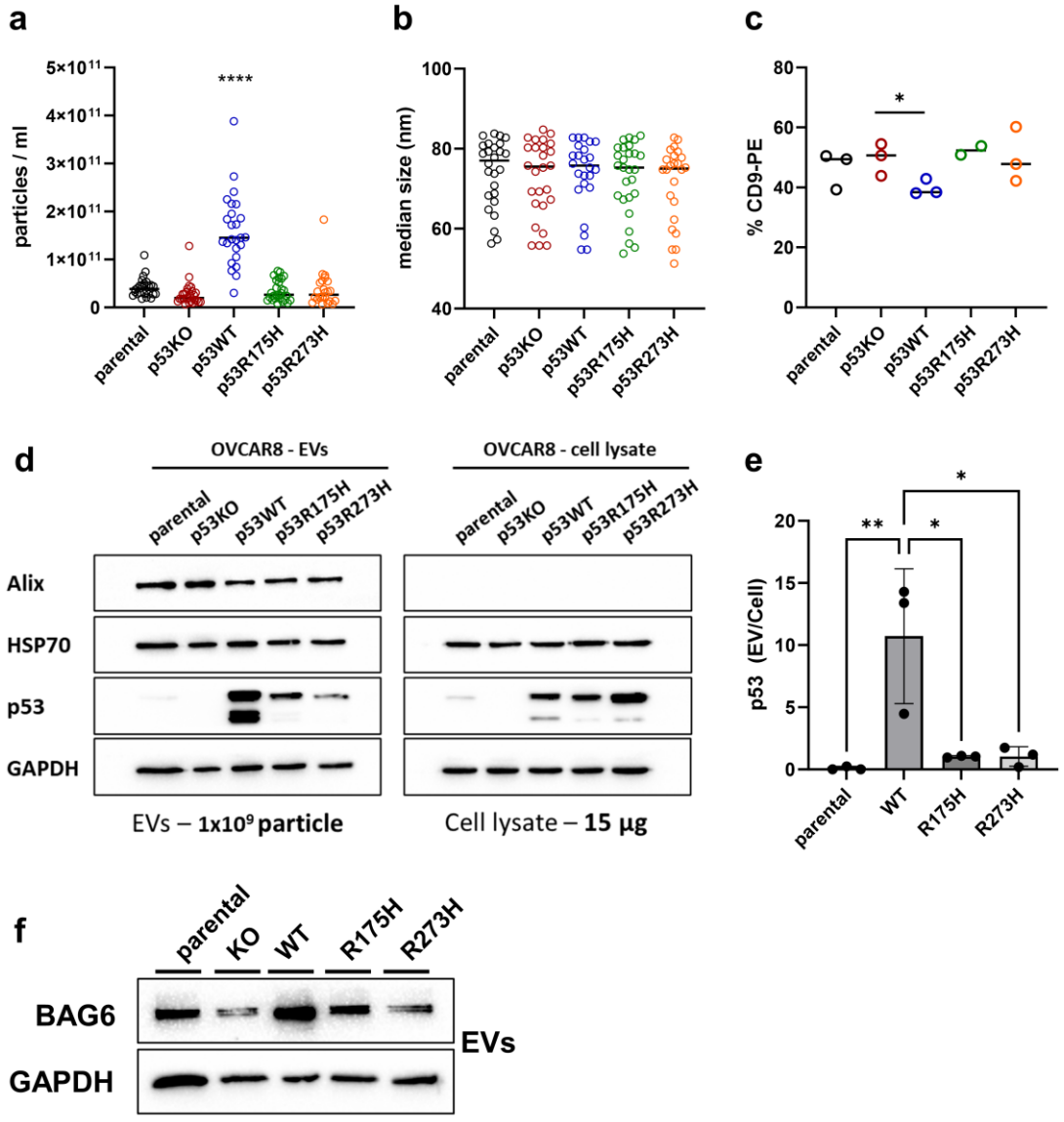

Figure 18: P53WT cells secrete more EVs with a lower CD9 expression and enrichment of p53 and BAG6.

As described earlier, EVs were isolated, and size, concentration, and surface marker expression were measured by nano-flow cytometry. **(a)** Particle concentration released by OVCAR8 cells with different p53 status (parental: n=29, KO: n=29, WT: n=28, R175H: n=30, R273H: n=28, One-Way Anova with Tukey's test, ****p<0.0001). **(b)** Median size of particles released by OVCAR8 cells with different p53 (parental: n=29, KO: n=29, WT: n=28, R175H: n=30, R273H: n=28). **(c)** CD9 expression on the EVs was analyzed using a CD9-PE antibody and measuring positive events by nano-flow cytometry (all n=3, except R175H n=2; two-tailed unpaired t-test, *p<0.05). **(d)** Western Blot was done with EVs (1x109 particles) and cell lysate (15 µg) with antibodies against ALIX, HSP70, p53, and GAPDH. Secondary antibodies were linked to HRP, and detection was done by the ChemiDoc MP Imaging System. **(e)** The figure shows the densitometric analysis of 3 independent blots. Here, band intensity was first normalized by the respective GAPDH band, and then the ratio of EV/Cell was blotted (One-Way ANOVA with Tukey's test, *p<0.05, **p<0.01, n=3 ±SD). **(f)** Western Blot of BAG6 in p53WT EVs. Five micrograms of EV lysate were loaded. Anti-BAG6 (3E4, 1:1,000) and anti-GAPDH (1:10,000) antibodies were used and subsequently detected with HRP-secondary antibodies on the ChemiDoc MP Imaging System (n=1).

4.6 Transfer and uptake of p53-containing EVs and rescue of WT-phenotype in KO cells

In order to mediate any functional effects, EVs need to be taken up by recipient cells, which were initially investigated in cancer cells. Here, p53KO cells were treated with EVs from p53WT cells for 6 hours, and subsequent immunofluorescent staining of p53 was done. Results showed cytoplasmic staining of p53 in treated knockout cells, which was not detectable in untreated cells (Fig. 19). This suggests the successful transfer and uptake of p53-containing EVs by the recipient cells.

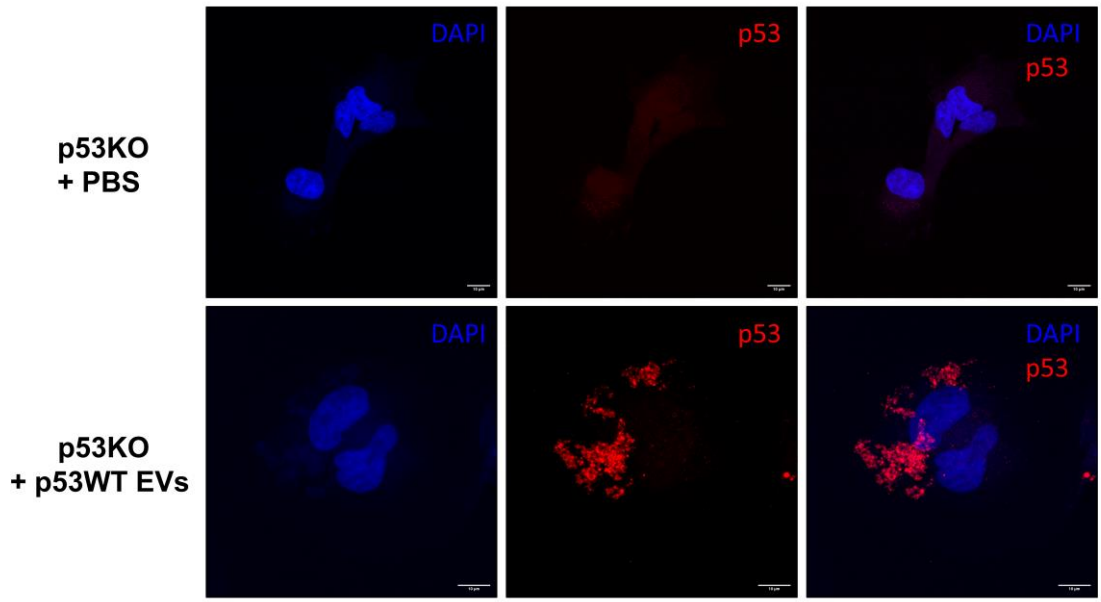

Figure 19: Immunofluorescence staining shows the transfer and uptake of WTp53 via EVs to p53KO cells.
KO cells were treated either with p53WT EVs or PBS for 6 hours. Afterward, cells were fixed in 4 % PFA and permeabilized in 0.5 % Triton-X100 before staining with p53 (DO-1, 1:400) and AlexaFluor-633 (1:500). Images were taken with a LEICA Stellaris microscope together with Prof. Dr. Ralf Jacob (scale: 10 µm).

Next, we contemplated if the uptake of EVs translates into any functional effect and if the distinct phenotype of p53WT cells could be rescued in KO cells. Therefore, p53KO cells

were treated with secretome (CM) or EVs from WT cells, and selected targets were tested in RT-qPCR. The results showed that the WT-CM was able to rescue the specific inflammatory phenotype of WT cells, including expression of *CXCL8* and *IL6*, as well as downregulation of *TGFB2 (*Fig. 20a). Notably, expression of the direct p53 target *CDKN1A* could not be rescued indicating no p53 effects via its direct targets. Knockout cells treated with EVs showed a similar rescue with increased *CXCL8, IL6, CXCL1,* and *RELB* (Fig. 20b). However, *TGFB2* downregulation was not observed after EV treatment meaning that EVs and secretome can have distinct functions on the recipient cells.

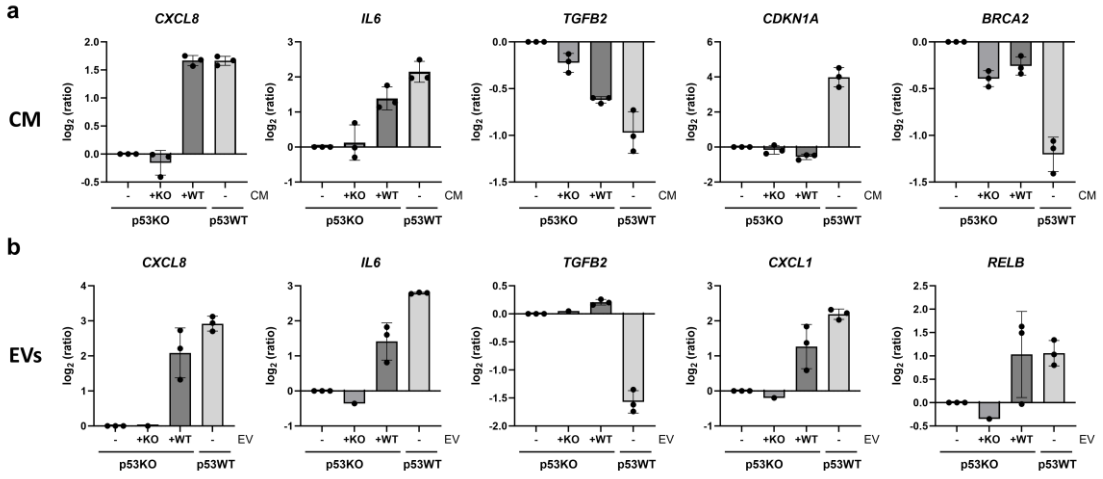

Figure 20: The inflammatory phenotype of OVCAR8 p53WT cells can be partly rescued in knockout cells by treatment with CM or EVs from p53WT cells.
To generate either CM or EVs, cells were induced by 0.5 µg/ml doxycycline for 24 hours, and medium was changed to CD293 for another 24 hours. EVs were isolated by dUC, while CM was collected after the 2,000 xg centrifugation step. For the experiment, 50,000 p53KO cells were treated with either CM or EVs. P53WT cells were used as a positive control, and all cells were treated with 0.5 µg/ml doxycycline. Several genes were tested, for CM (CDKN1A, BRCA2), EVs (CXCL1, RELB) or both (CXCL8, IL6, TGFB2). **(a)** Here, 250 µl of CM was used for treatment (n=3 ±SD). **(b)** The EV treatment was done with either 25 µl of KO or WT-EVs (n=3 ±SD, KO: n=1).

In ovarian cancer, fibroblasts play a critical role in the TME and, hence, in the progression of the disease (M. Zhang et al. 2022). By intercellular communication, tumor cells can shape surrounding fibroblasts to a pro-tumorigenic CAF phenotype. Here, we investigated the transfer and uptake of EVs by fibroblast (HDFn) (Mulcahy, Pink, and Carter 2014). To monitor EV transfer in a co-culture setting, a new OVCAR8 cell line was generated expressing p53 linked to GFP. Since p53 was previously shown to be loaded into EVs (Fig. 18d), this allowed microscopic tracking of the EV transfer. Throughout one hour, EVs were tracked via live cell imaging, demonstrating the merge of EVs with the membrane of fibroblast cells (Fig. 21a). Moreover, figure 21b shows EVs that generate protrusions at the fibroblast membrane. Here, the GFP intensity of the EV decreased over time, indicating the release of its contents into the recipient cell.

In summary, uptake of WTp53 via EVs could be shown in cancer cells, which subsequently at least partially rescued the specific genotype of WT cells in the knockout cell line. In addition, the transfer of p53 between cancer cells and fibroblasts was also demonstrated.

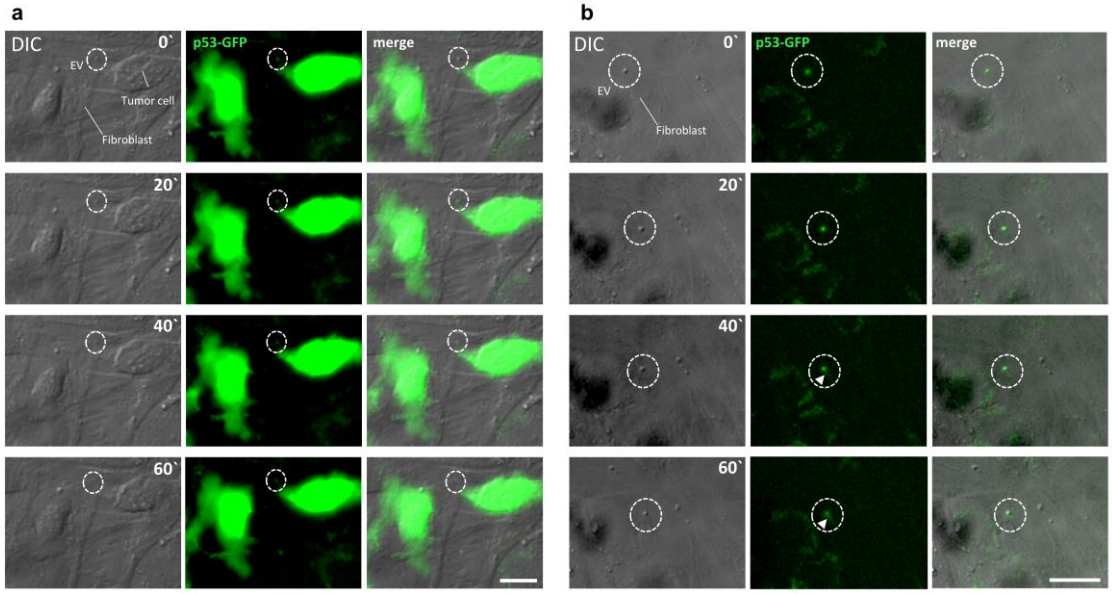

Figure 21: Co-culture of HDFn and OVCAR8 p53-GFP cells demonstrate transfer and uptake of EVs containing p53.
HDFn cells were seeded together with OVCAR8 p53-GFP cells in a 3:1 ratio. Videos were taken with a LEICA DMI8. Here, pictures at different time points (0, 20, 40, 60 min) for differential interference contrast (DIC) and GFP are shown. **(a)** The merged picture shows EVs containing p53-GFP released from tumor cells fusing with the fibroblast membrane. **(b)** The merged image shows tumor-released EVs generating protrusions over time at the membrane of the fibroblast (white arrow) while the fluorescence of the EV decreases. The experiment was done in cooperation with the group of Prof. Dr. Ralf Jacob.

4.7 WT EVs induce an inflammatory phenotype in HDFn cells, which is associated with NFκB and STAT3 activity

HDFn cells were treated with EVs to investigate specific changes in the phenotype. Transcriptomic analysis was done of cells treated by EVs for 48 hours. In total, 19,366 protein-coding and 5,147 lncRNA-coding genes were detected. The general treatment with EV resulted in many changes in gene expression, as displayed in a heatmap depicting row z-scores of all genes. Here, PBS-treated fibroblasts show the most distinct phenotype compared to all other groups (Fig. 22a). This indicates strong activation and potential differentiation by EV treatment, independent of the p53 status. VENN diagrams of differentially expressed genes compared to the KO were done to show differences between the EV-treated groups. This revealed 99 uniquely up and 124 downregulated genes in the WT-EV-treated fibroblasts (Fig. 22b). Notably, cells treated with EVs from

mutp53 cells (R175H/R273H) did not show a specific phenotype compared to the KO cells (Fig. 22b). Subsequently, the main focus was put on the comparison of WT and KO-treated HDFn cells (Fig. 22c). An inflammatory phenotype was observed for WT-EV-treated fibroblasts, with an upregulation of *CXCL1, CXCL8, CXCL6* or *IL6* (Fig. 22c). Pathway analysis demonstrated enrichment in cytokine and chemokine-mediated pathways, including the IL-17 (hsa04657, e.g. CSF3, MMP1, TNFAIP3), TNF (hsa04668, e.g. EDN1, CXCL3, CXCL2) and NFκB signaling pathway (hsa04064, e.g. NFKBIA, RELB, ICAM1) (Fig. 22d). Upstream regulators were found to be associated to NFκB (NFKB1, RELA, JUN) as well as SP1, STAT1 and STAT3 (Fig.22d).

In contrast, KO-EV-treated fibroblasts revealed a different phenotype, with enrichment of ECM organization (GO:0030198, e.g. *VIT, POSTN, COL15A1, COMP*), proteoglycans in cancer (mmu05205, e.g. *FN1, TIMP3, IGF2*) or association to the WNT signaling pathway (hsa04310, e.g. *WNT11, CCN4, WNT16, WNT2, DKK2*) (Fig. 22d). Interestingly, a specific phenotype of HDFn cells treated with EVs from either R175H or R273H mutant could not be observed meaning that in this study EVs from mutp53 cells do not exert any GOF activity in fibroblasts.

To validate the RNA-sequencing data, selected targets of treated fibroblasts were tested in RT-qPCR (Fig. 22e). Here, the inflammatory phenotype of WT-EV-treated HDFn could be confirmed by significant upregulation of *CXCL1, CXCL8* and *IL6* (One-Way ANOVA, Fig. 22e). Moreover, expression of some myofibroblast markers did not change (*αSMA/ACTA2, COL1A1*) or are downregulated (*MMP11*) (Fig. 22e).

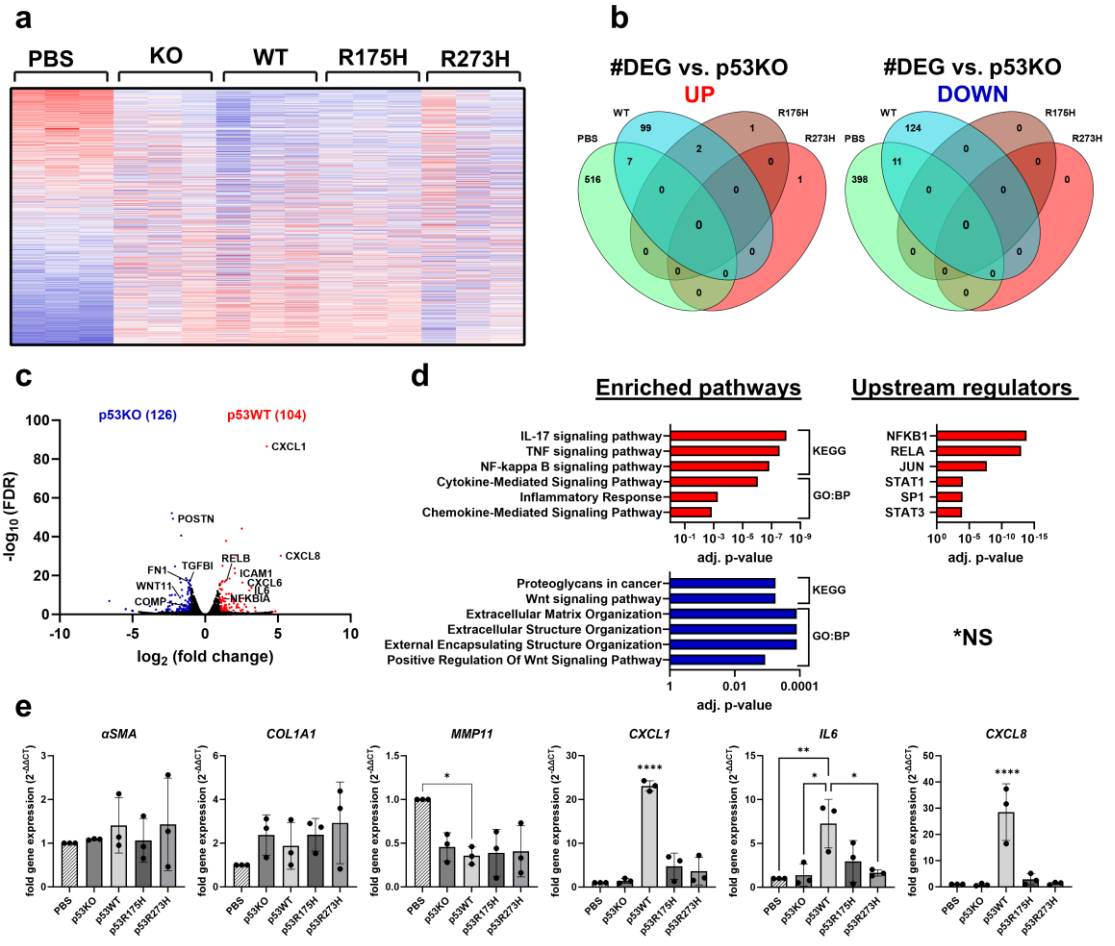

Figure 22: EVs from OVCAR8 p53WT cells induce an inflammatory genotype in HDFn cells. HDFn cells were treated with 5x10^9 particles/ml for 48 hours before RNA was isolated and sent for RNA sequencing (n=3). **(a)** Heatmap displaying row z-scores of all detected genes of untreated (PBS) and EV-treated fibroblasts. Z-scores are sorted for highest values in the untreated (PBS) group **(b)** The Venn diagram represents DEG of fibroblasts treated with PBS or EVs from p53WT, R175H or R273H cells compared to p53KO cells. **(c)** Enrichment analysis was done via the web-based EnrichR software. Significant and interesting pathways are displayed for several databases, including KEGG, GO:BP, and TRRUST. Significance and p-values are computed using the Fisher exact test and adjusted using the Benjamini-Hochberg method. **(d)** SYBR Green-based RT-qPCR was done for selected targets with RNA from untreated or EV-treated fibroblasts. Significance was tested by One-Way ANOVA with Tukey's test (*p<0.05, **p<0.01, ***p<0.001 and ****p<0.0001, n=3 ±SD).

Next, the secretome of treated fibroblasts was analyzed by Olink explore. As done for transcriptomics, HDFn cells were treated for 48 hours with EVs. However, to avoid contamination with remaining EVs, the medium was changed, and cells were incubated another 48 hours in fresh medium before the supernatant was collected, centrifuged, and sent for Olink analysis. The Z-score of NPX was plotted on the heatmap (Fig. 23a), and the most differential detected proteins (NPX of KO-WT) were listed in a bar diagram (Fig. 23b). Heatmap showed that more differential proteins were found in the secretome of KO-treated HDFn cells compared to the WT (Fig. 20a). Specifically, the most abundant proteins in the WT group were C3, CINP, CXCL6 (NPX (KO-WT) > 1), LAMP3, CXCL8,

MAVS (NPX > 0.5), ICAM1, CCL8, P53, LIF and IL6 (NPX > 0.25) (Fig. 20b). Together with the pathway analysis, similarities could be seen in the transcriptomic data with enrichment of cytokine-related pathways, such as IL17 or TNF signaling pathways. Moreover, cellular senescence (hsa04218) was enriched (Fig. 20c). This indicates the potential induction of a senescence-induced secretory phenotype (SASP) by the WT EVs, which is characterized by secretion of proinflammatory factors, such as CXCL8, CXCL1 or IL6 (Coppé et al. 2010). SASP is mainly mediated by NFκB, which was found to be the major upstream regulator in this secretome data for WT-EV-treated fibroblasts. In addition, STAT3 was found to be a potential upstream regulator and is also described to be involved in SASP (Yasuda et al. 2021) (Fig. 23c).

In contrast, differentially abundant proteins in the secretome of KO-EV-treated fibroblasts were associated to cell adhesion molecules (hsa04514, e.g., CD274, VCAN, ITGB2), PI3K-Akt signaling (hsa04151, e.g., BDFN, LAMA1, EGF), ECM organization (GO:0030198, COMP, COL15A1, TGFB1, MMP8, MMP10) and the positive regulation of cell motility (GO:2000147, TGFB1, EGF, CCL24) (Fig. 23c).

Addionally, further secretome analysis was done utilizing a cytokine array (Fig. 23d,e). This time, cells were only treated for one day with EVs and subsequently incubated for 24 hours in fresh medium before collection of the CM. Pictures were taken of the blots, and pixel density for each dot was calculated by ImageJ. WT EV-treated fibroblasts showed increased secretion of CXCL1, CXCL5, CXCL8, CCL2, and IL6 compared to untreated, KO-, and R273H-treated fibroblasts (Fig. 23d,e). This aligns with the transcriptomic and Olink data for treated fibroblasts, further indicating a potential SASP.

For the KO EV-treated group, PTX3 and DKK1 were found more abundantly secreted, while CXCL12, Thrombospondin-1, and Resistin were found most robust in the R273H-EV-treated fibroblasts.

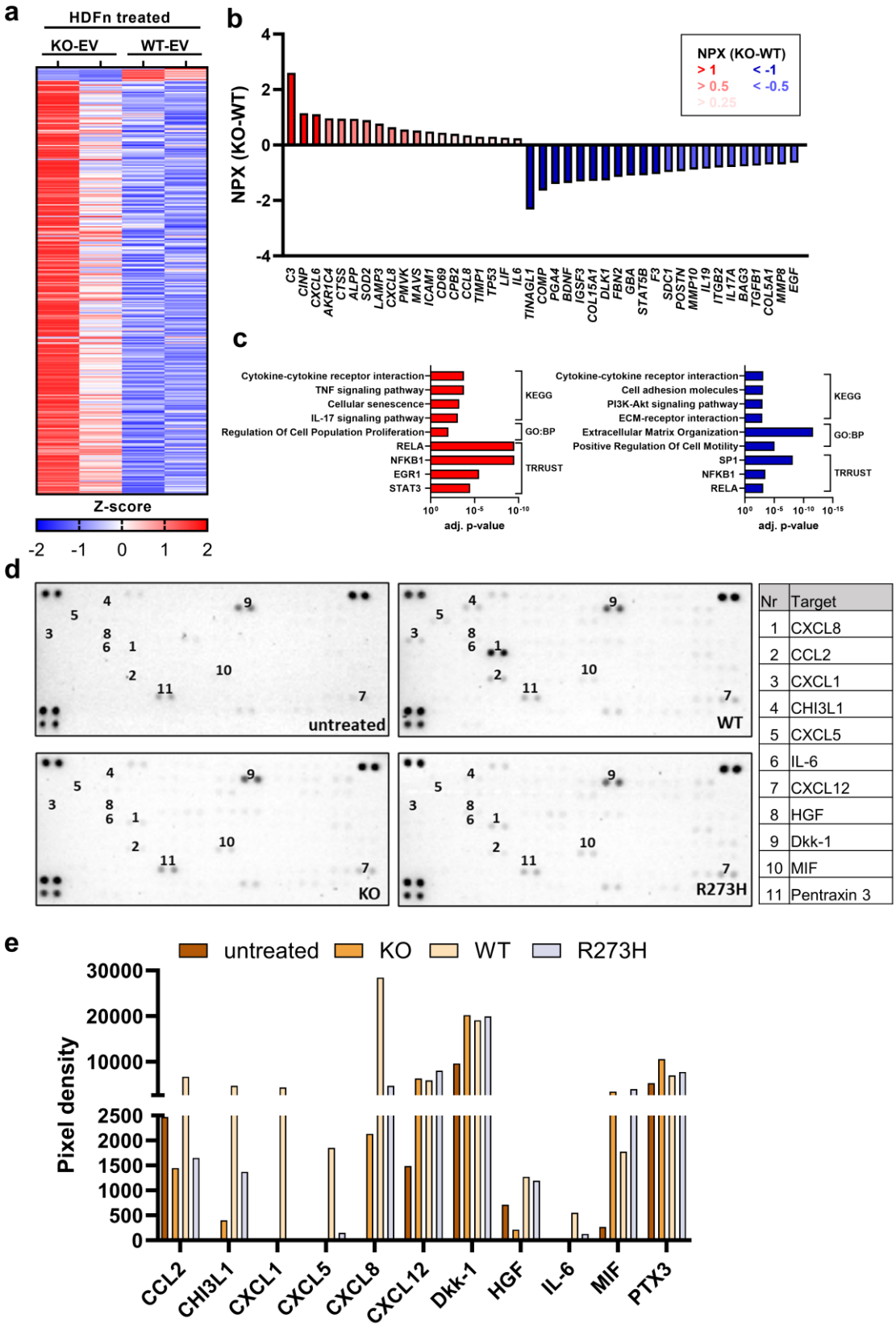

Figure 23: Secretome analysis by Olink and cytokine array confirms inflammatory phenotype of p53WT EV treated fibroblasts.

(a,b,c) HDFn cells were treated for 48 hours with EVs before incubating another 48 hours with fresh medium. CM was collected and sent for Olink analysis by the Institute of Translational Proteomics. The resulting counts were processed to NPX and used to calculate differences between groups. A difference of at least NPX > 1, which implies a doubling of protein concentration, was considered. **(a)** Heatmap displaying row z-scores of NPX values from KO or WT EV-treated HDFn. **(b)** Differences in NPX values (KO-WT) were plotted on a bar graph. Red bars represent DEPs in the secretome of WT EV-treated fibroblasts and blue bars show upregulation in KO EV-treated fibroblasts. Intensity correlates with the NPX value (dark: NPX > 1, medium: NPX > 0.5; light: NPX > 0.25). **(c)** Enrichment analysis was done via the web-based EnrichR software. Significant and interesting pathways are displayed for several databases, including KEGG, GO:BP, and TRRUST. Significance and p-values are computed using the Fisher exact test and adjusted using the Benjamini-Hochberg method. Enrichment of pathway/processes and transcription factors of proteins in WT or KO-EV-treated fibroblasts are displayed in red or blue, respectively. **(d)** CM was collected and used with the Proteome Profiler Human XL Cytokine Array Kit (R&D System). Images of the cytokine arrays done with CM of untreated, KO, WT, or R273H EV-treated fibroblast cells were taken using the Chemidoc MP imaging system. Pixel density was calculated with ImageJ and compared between the groups. **(e)** The bar graph displays the pixel density of selected targets, showing differences between the groups.

Since NFκB pathway and target genes were upregulated in WT-EV-treated fibroblasts, activation of the pathway was further studied. NFκB is a vital protein complex regulating DNA transcription, cell survival, and many inflammatory cytokines (Taniguchi and Karin 2018). In unstimulated cells, NFκB dimers, consisting of two of five proteins of the protein family (NFKB1, NFKB2, RELA, RELB, c-REL), are bound and inhibited by IκB proteins (e.g., IκBα). Upon stimulation, IκB kinases (IKK) phosphorylate IκB proteins, leading to liberation and subsequent translocation of the dimer complex into the nucleus. In the nucleus, NFκB (e.g., RELA/p65) is specifically phosphorylated, which attracts different interaction partners and leads to a specific response (Taniguchi and Karin 2018).

Here, fibroblasts were treated for 6 or 24 hours with WT EVs and subsequently stained by an anti-p65 antibody (Fig. 24b). The percentage of nuclear NFκB (p65) was calculated for a total of 50 nuclei, plotted and statistically analyzed by One-Way ANOVA with Tukey's test (Fig. 24b). This revealed significant translocation of p65 into the nucleus 6 and 24 hours after treatment, indicating activation of NFκB by EVs isolated from WT cells ($p<0.0001$) (Fig. 24b). Differences between 6 and 24 hours could not be observed (ns, $p>0.05$).

Moreover, a Western Blot was done to further study the activation by protein phosphorylation of p65 or IκBα and subsequent translocation to the nucleus. Protein lysates of treated fibroblasts were fractionated into cytoplasmic and nuclear fractions before immunoblotting with total or phosphorylated p65 (Ser536) or IκBα (Ser32) antibodies was done. Results demonstrated phosphorylation and translocation of p65 into the nucleus after treatment with WT EVs (n=3, Fig. 24c,d), confirming NFκB activation seen in other experiments (Immunofluorescence, OMICS). In addition, phosphorylation of IκBα was observed in the cytoplasm, which is necessary for the release and subsequent translocation of p65/NFκB complexes.

In contrast, KO EV treated fibroblasts did not show activation and translocation of p65 compared to the untreated control (Fig. 24e). This indicates specific activation of NFκB by EVs isolated from OVCAR8 p53WT expressing cells.

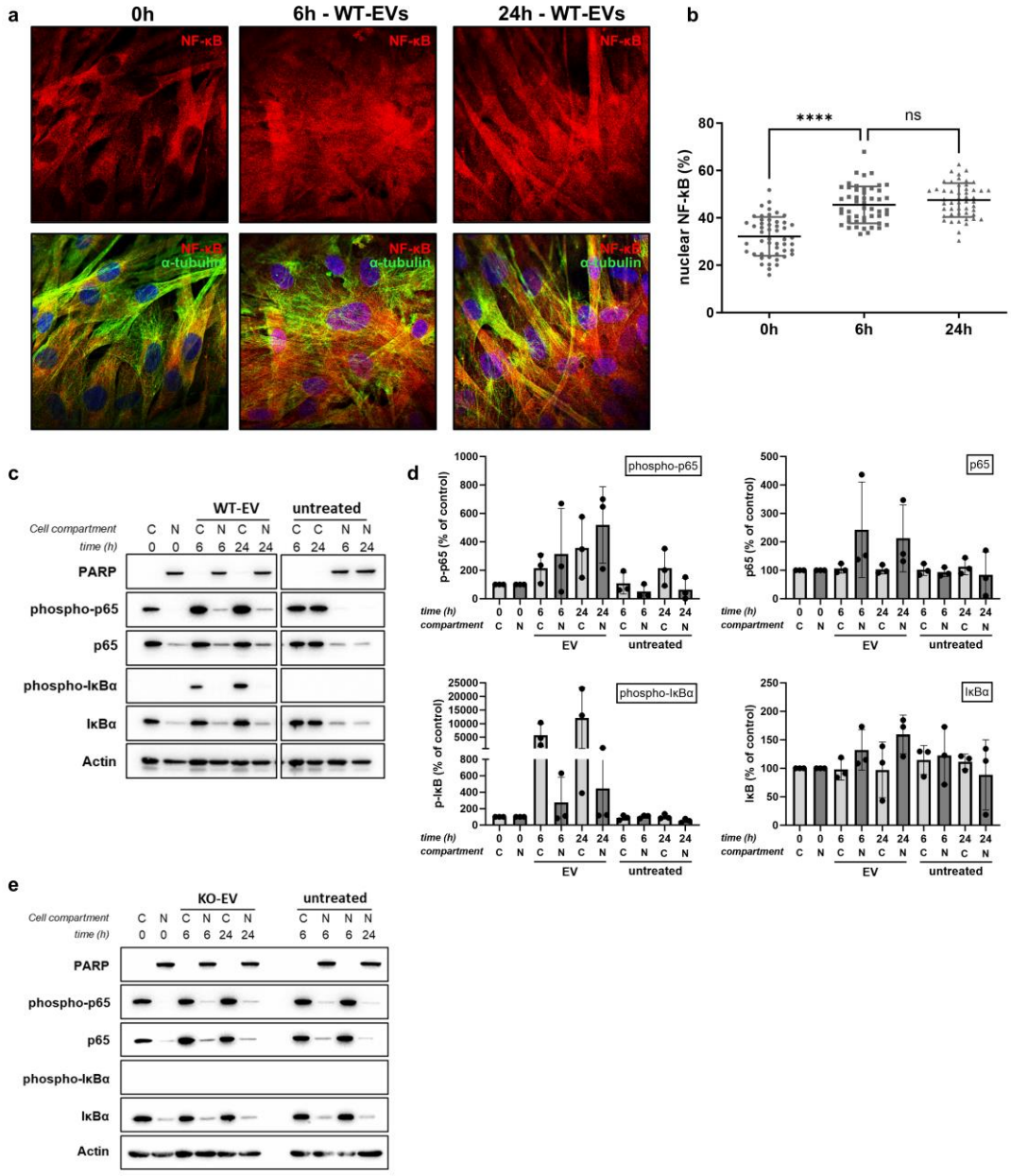

Figure 24: NFκB-p65 is phosphorylated and translocated in the nucleus in HDFn cells after treatment with EVs from p53WT cell.
(a,b) HDFn cells were treated with ~2x10^9 EVs isolated from p53WT cells for 6 or 24 hours. After each time point, cells were fixed with 4 % PFA and permeabilized with 0.1 % TritonX-100. NF-κB p65 (mouse, 1:100) and α-tubulin (rabbit, 1:100) were stained. As secondary antibodies, anti-mouse AlexaFluor555 and anti-rabbit AlexaFluor647 were used (1:200). The nucleus was stained with Hoechst 33342 (1:200). **(a)** Images taken on LEICA Stellaris by the group of Prof. Dr. Ralf Jacob. NFκB/p65 (red), α-tubulin (green), and the nucleus (blue) are stained. **(b)** Nuclear NFκB in % was calculated by measuring AF555 in the nucleus compared to the cytoplasm after 0, 6, or 24 hours. Significancy was calculated by One-Way ANOVA with Tukey's test (****p<0,0001, n=50 ±SD). This experiment was done together with the group of Prof. Dr. Ralf

Jacob. **(c-e)** HDFn cells (700,000) were treated with 100 µl of EVs (WT or KO) for 6 or 24 hours. Subsequently, cells were lysed and fractionalized with the nuclear and cytoplasm extraction kit (Thermo Scientific). Fifteen µg of protein were loaded and analyzed via Western Blot. Primary antibodies against phospho-p65, phospho-IκBα, p65, IκBα, PARP (all 1:1,000), and β-Actin (1:2,500) were used. Secondary antibodies were linked to HRP, and detection was done on a ChemiDOC MP imaging system (n=3 ±SD). **(c)** Representative Western Blot of protein lysates of HDFn cells treated with WT EVs for 0, 6, or 24 hours. **(d)** Densitometric analysis of three independent western Blots (n=3 ±SD). **(e)** Western Blot of HDFn cells treated with EVs from p53KO cells (n=1). N = Nucleus, C = cytoplasmic fraction

Besides NFκB, STAT3 was one of the upstream regulators found in the transcriptomic and Olink data of WT-EV-treated fibroblasts (Fig. 22 and Fig. 23) as well as in the transcriptomic data of the OVCAR8 p53WT expressing cells (Fig. 8). STAT3 and NFκB are also described to work together since both are known to regulated inflammatory factors (Fan, Mao, and Yang 2013). To investigate whether STAT3 is activated in either the OVCAR8 cells lines or in the EV-treated fibroblasts, Western Blot analysis was conducted.

First, OVCAR8 p53KO and p53WT cells were either induced by doxycycline or not and tested for total and phospho-STAT3 (Tyr705) in Western Blot. WT cells showed a significant decrease of phosphorylation of STAT3 after induction ($p=0.0005$) and compared to p53KO cells ($p=0.0002$, One-Way ANOVA with Tukey's test, n=3). This was expected since p53WT is described to inhibit STAT3 phosphorylation (Jiayuh Lin et al. 2002). Total STAT3 levels remained the same, indicating inhibition of STAT3 activity in these cells. For p53KO cells, STAT3 phosphorylation did not change (Fig. 25a).

Second, HDFn cells were treated with either WT or KO EVs, and total- and phospho-STAT3 was detected via immunoblot. The treatment with WT EV led to a significant increase of phosphorylated STAT3 compared to untreated ($p=0.0006$), and KO EV treated cells ($p=0.0020$, One-Way ANOVA with Tukey's test, n=3). Here STAT3 is explicitly activated in fibroblasts by treatment with WT EVs (Fig. 25b). Together with the activation of NFκB, STAT3 could be responsible for the inflammatory phenotype of fibroblasts treated with EVs from WTp53 expressing OVCAR8 cells.

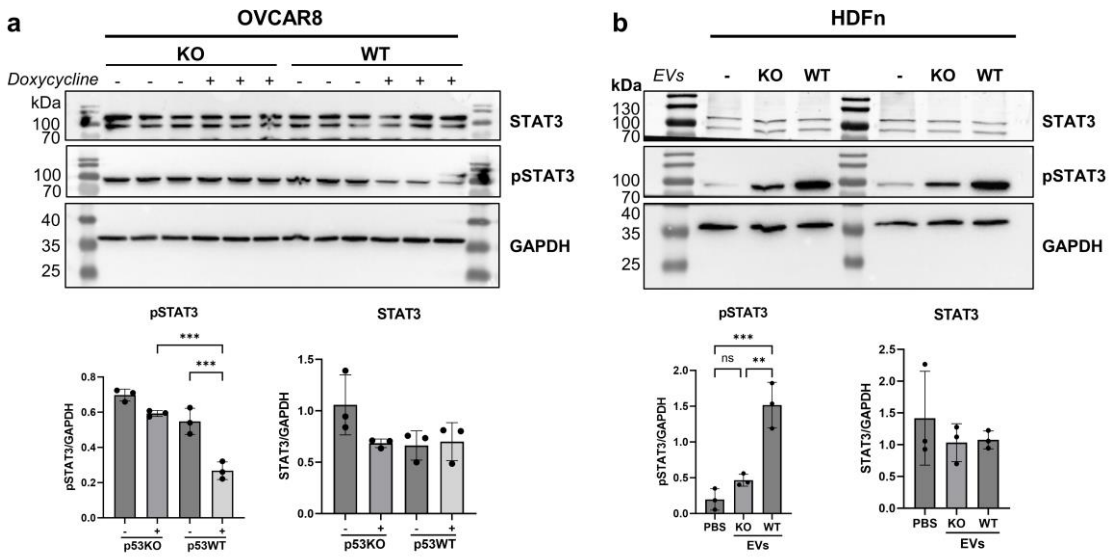

Figure 25: STAT3 phosphorylation is reduced in OVCAR8 p53WT expressing cells and increased in HDFn cells treated with EVs from p53WT.
(a) OVCAR8 p53WT and KO cells were treated with 0.5 µg/ml doxycycline for 24 hours. Cells were lysed, and 15 µg loaded onto 10 % SDS-PAGE. Primary antibodies against pSTAT3, STAT3 (1:1,000), and GAPDH (1:10,000) were used. Detection was done on a ChemiDOC MP imaging system. Densitometric analysis was done, and significance was determined by One-Way ANOVA with Tukey test ($p<0.001$, n=3 ±SD). **(b)** HDFn cells (100,000) were treated with 35 µl of EVs for 24 hours. Cells were lysed, and 15 µg loaded onto 10 % SDS-PAGE. Primary antibodies against pSTAT3, STAT3 (1:1,000), and GAPDH (1:10,000) were used. Detection was done on a ChemiDOC MP imaging system. Densitometric analysis was done, and significance was determined by One-Way ANOVA with Tukey's test (**$p<0.01$, ***$p<0.001$, n=3 ±SD)

4.8 Summary of main findings

The present study underlined a role of p53 in the biogenesis of EVs in ovarian cancer cells and their function on fibroblast. Using many different techniques, ranging from the genetic engineering of p53 cell lines with CRISPR/Cas9 to EV biological techniques (e.g., dUC, nano-flow cytometry, electron microscopy), molecular biological methods (e.g., Western Blot, RT-qPCR, immunofluorescence) and omics technologies (Transcriptomics, Proteomics, Olink), I found that:

I OVCAR8 cells expressing WTp53 show a distinct inflammatory genotype, potentially mediated by the interplay of p53 and NFκB.

II Many EV biogenesis genes are upregulated in p53WT cells (e.g., ESCRT machinery)

III p53WT cells possess distinct cargo in their EVs

IV WTp53 is predominantly loaded into EVs compared to mutp53

V p53WT cells secrete significantly more EVs

VI EVs containing WTp53 can be taken up by p53KO cells and at least partly rescue the p53WT genotype.

VII EVs containing p53 from OVCAR8 cells can be transferred to fibroblast

VIII OVCAR8-derived p53WT EVs induce an inflammatory phenotype in fibroblasts, characterized by upregulation and secretion of many cytokines and chemokines, including CXCL1, CXCL8, and IL6

IX The inflammatory phenotype is potentially mediated by NFκB and STAT3 activity.

X OVCAR8-derived p53KO EVs induce phenotype in fibroblast associated with ECM remodeling.

XI OVCAR8-derived mutp53 EVs do not exert GOF effects on fibroblast. The phenotype mainly reflects the p53KO-induced phenotype with some expression between KO and WT.

Some of the main findings are schematically displayed in Figure 26.

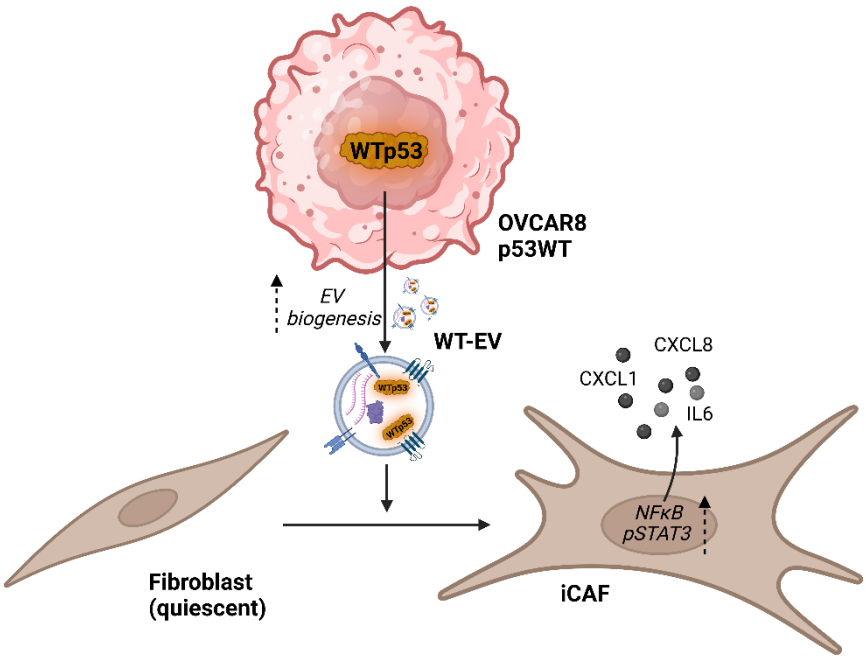

Figure 26: Schematic representation of the induction of an iCAF phenotype by EVs isolated from OVCAR8 p53WT cells.
Created with Biorender.com

5. Discussion

This work has provided further insight into the role of the p53 status on EV formation and the EV-mediated communication of ovarian cancer cells and fibroblasts. The following section will discuss the results, state the limitations of the work, and offer recommendations for further research.

5.1 EV secretion is affected by cell culture conditions

The isolation process of vesicles is a critical step while working with EVs. Although research in recent years has led to major advances in this area, the unique isolation of specific EV subtypes remains difficult (Théry et al. 2018). Typical isolation methods involve the separation of vesicles after size, density, or surface marker expression. Besides the technique, culture conditions can also be critical, including cell culture medium or the oxygen content during cultivation. For instance, standard growth medium often contains FCS, which has large numbers of particles and, therefore, interferes with the isolation and characterization of the isolated vesicles. To avoid this, particles in the FCS are often removed before use by ultracentrifugation. However, the complete depletion of particles remains difficult (Théry et al. 2018; Clos-Sansalvador et al. 2022).

Here, we compared EV-depleted medium with the chemically-defined and serum-free CD293 medium, which resulted in significantly enhanced secretion of particles for the latter (Fig. 3a). This is most likely due to increased cellular stress in the serum-free condition. Li et al. (2015) described similar findings, with increased particle secretion in neuroblastoma cells with serum-free OptiMem compared to EV-depleted medium (Jinghuan Li et al. 2015). Moreover, they also found upregulation of EV biogenesis-related genes, including *ARF6*, which further supports an enhanced secretion (Jinghuan Li et al. 2015)). Interestingly, a recent study from the same research group demonstrated a specific influence of the ceramide-dependent EV biogenesis pathway in the serum-free medium and not in EV-depleted medium (Bost et al. 2022). In contrast, a study in endothelial cells showed no significant differences in EV secretion under different cellular stressors, including hypoxia, TNFα treatment, or high glucose concentration (de Jong et al. 2012). However, serum-free medium was not tested. Interestingly, recently published research showed enhanced EV production in head and neck squamous cell carcinoma (HNSCC) cells under hypoxic conditions. Here, HIF1α was demonstrated to directly downregulate ATP6V1A, which is critical for the homeostasis of lysosomes and, therefore, led to decreased lysosomal degradation and subsequent increase in vesicle

secretion (Xiaoning Wang et al. 2023). In this project, we could not confirm an increase in particle concentration under hypoxic conditions (Appendix Figure S2), suggesting that different stressors can affect EV secretion depending on the cell type. In this work, we also demonstrated an increase in particle size (Fig. 3b) and surface marker expression (Fig. 3c, e.g., CD9 – significant, CD63, CD81, CD29 – not significant) in CD293 medium, suggesting more robust isolation of a specific EV subtype characterized by a higher tetraspanin content. Differences in EV cargo between serum-free and EV-depleted medium were also demonstrated in the literature, e.g., an increase in stress-regulated factors like macrophage migration inhibitory factor (MIF), epoxide hydrolase 1 (EPHX1) or the exonuclease MYG1 (Jinghuan Li et al. 2015). Other stressors, including hypoxia, were also described to alter the EV proteome or miRNA levels (de Jong et al. 2012; Xiaoning Wang et al. 2023). As concluded by Bost et al. (2021), serum-free medium could enhance EV secretion and influence its contents by combining physical, molecular, and transcriptional effects (Bost et al. 2022).

5.2 Model cell line OVCAR8 – comparison with p53KO cells

High-grade serous ovarian carcinoma (HGSOC), the most common and lethal ovarian malignancy, often originates in the epithelium of the fallopian tube. Hallmarks of HGSOC are the mutation in the tumor suppressor gene *TP53* (~96 % of all cases) as well as the strong intercellular communication within the TME (Worzfeld et al. 2017; Bell et al. 2011). Since EVs play an essential part in this communication, investigating the role of p53 in HGSOC TME communication is highly interesting. Here, OVCAR8 was used as a model cell line in this project. The cell line was initially mentioned in 1988 by T.C Hamilton at the Fox Chase Cancer Center of the National Cancer Institute in Philadelphia and was isolated from a 64-year-old female with progressive adenocarcinoma after high-dose of carboplatin treatment (800 mg/m^2) (Schilder et al. 1990). It contains a homozygous p53 single nucleotide mutation from guanine to adenosine at position 376 (c.376-1G>A) that potentially leads to a splice acceptor mutation and loss of seven amino acids at the 5'-site of exon 5 (p.Tyr126_Lys132del) (Leroy et al. 2014; Smeby et al. 2019). Moreover, heterozygote mutations of KRAS (c.362C>A; p.Pro121His), ERBB2 (c.2327G>T; p.Gly776Val) and CTNNB1 (c.77A>G; p.Gln26Arg) are described as well. Although p53 mutation is often seen in HGSOC, mutations in KRAS, ERBB2, or CTNNB1 are usually associated with non-serous or low-serous ovarian carcinomas (Matulonis et al. 2016). Therefore, some studies claim OVCAR8 is not a bona fide HGSOC cell line (Hallas-Potts, Dawson, and Herrington 2019; Domcke et al. 2013). The KRAS^{P121H} in OVCAR8

is a rare mutation with unknown significance; however, Sun et al. (2017) described a similar activation status of the RAS/MAPK pathway compared to more common KRAS mutations (Domcke et al. 2013; C. Sun et al. 2017; Singer et al. 2003). Mutations in ERBB2 are also described to be involved in the activation of the RAS/MAPK pathway (Anglesio et al. 2008). In this project, OVCAR8 p53KO clones were successfully generated by targeting exons 4 and 9 via CRISPR/Cas9 (Fig. 4). A total of three knockout clones were compared together with the parental cell line; however, no significant differences could be observed in proliferation or morphology (Fig. 4a-c). In general, the p53 protein expression was deficient compared to the generated p53WT or other mutp53 cell lines (Fig. 6c, Fig. 7b). Moreover, EV secretion, size, and surface marker expression were similar compared to the p53KO cells (Fig. 5a-c). This indicates no specific function of the mutp53 in OVCAR8 parental cells, which aligns with the literature, where splice site mutations are generally considered a loss of function (MacArthur et al. 2012).

5.3 Influence of p53 on the transcriptomic phenotype of OVCAR8 cells: novel insights in p53-NFκB crosstalk

The generation of cell lines with a defined p53 status was done by utilizing the inducible sleeping beauty system described in Kowarz et al. (2015) (Kowarz, Löscher, and Marschalek 2015). This enabled the successful generation of cells expressing p53WT, p53R175H, or p53R273H under a doxycycline-inducible promotor (Fig. 6a-c, Fig. 7b). In an RNA sequencing analysis, OVCAR8 p53WT cells showed the most distinct genotype compared to KO or mutant p53 expressing cells lines (Fig. 7a-c, Fig. 8a). This was expected since p53 is a transcription factor with hundreds of direct and thousands of indirect targets (Foroutan 2023; Fischer 2017). Almost all direct p53 targets, described in Fisher et al. (2017), were found upregulated in p53WT cells, including *CDKN1A, CD82, BBC3, MDM2, CASP3 or TP73* (Appendix Table S1, Fig. 8b) (Fischer 2017). Moreover, the p53 signaling pathway was significantly enriched in these cells (Fig. 8c). Generally, p53 is a tumor suppressor protein with roles in cell cycle arrest, DNA damage repair, or apoptosis. Here, growth arrest is mainly mediated by upregulation of the cyclin-dependent kinase inhibitor 1A (CDKN1A or p21), the growth and DNA damage protein GADD45 (*GADD45A*) or 14-3-3σ (SNF) (Foroutan 2023). In the literature, downregulation of CDKN1A was shown to promote cisplatin resistance or cancer cell survival and was associated with worse patient survival in ovarian cancer (H.-J. Kim et al. 2019; Jin Wang and Liu 2021; Schmider et al. 2000). More specific functions of p53

and its involvement in cancer are described in many reviews (Hernández Borrero and El-Deiry 2021; Feroz and Sheikh 2020; Hassin et al. 2022).

In contrast, p53KO cells showed enrichment in cell cycle-related genes (e.g., *CCNB1, CCNB2, CCNA1, CDK1*), mainly regulated by transcription factors of the E2F family (Fig. 8c). This indicates increased proliferation due to reduced cell cycle control by p21, which is downregulated in p53KO cells. Moreover, an increase in BRCA1, BRCA2, and TGFB2 compared to the p53WT cell was observed (Fig. 8c). BRCA1 is also a tumor suppressor, preferably active in the repair of double-strand breaks. It was shown to be transcriptionally downregulated by p53 before cell cycle arrest (Arizti et al. 2000). Similarly, p53 can also repress BRCA2 expression (K. Wu, Jiang, and Couch 2003). In summary, the genotype we see in p53KO cells resembles mainly the loss of p53WT expression.

Aside from the p53 pathway, gene expression in the WT cells was further associated with the NFκB signaling pathway (e.g., *RELB, NFKB2, NFKB1, NFKBIA, CXCL1, CXCL8*) (Fig. 8c,e). This is especially interesting since p53 and NFκB are often described to have antagonistic roles, with p53 managing cell cycle arrest as well as apoptosis and NFκB regulating the proliferation and survival of cells (Carrà et al. 2020; Webster and Perkins 1999). Many inhibiting interactions are described for both pathways; for example, WTp53 overexpression was shown to inhibit nuclear translocation of NFκB by increasing cytoplasmic IκBα and subsequently leading to apoptosis in colon cancer cells (Shao et al. 2000). Furthermore, p65 (RELA) and p53 were shown to suppress each other by competing for the transcriptional coactivators CBP or p300 (Webster and Perkins 1999; Ravi et al. 1998). A study by Ikeda et al. (2000) showed that p53 and RELA could interact directly by their dimerization/tetramerization domains, leading to mutual antagonism (Ikeda et al. 2000). Moreover, IKKβ was found to directly upregulate MDM2, the most common negative regulator of p53 (Tergaonkar et al. 2002). Interestingly, MDM2 was also shown to bind and inhibit p65 (Heyne et al. 2013). Therefore, p53 and NFκB can both be regulated by a negative feedback loop via MDM2.

In contrast, p53 and NFκB can also have agonistic functions, which were described to be important in apoptosis, autophagy, or regulation of proinflammatory genes (Ryan et al. 2000; Lowe et al. 2014). For instance, in human macrophages, activation of both pathways induced cytokine expression, especially IL6, leading to neutrophil migration (Lowe et al. 2014). Moreover, Ryan et al. (2000) demonstrated that NFκB activation is essential for p53- but not TNFα-induced apoptosis (Ryan et al. 2000). Here, induction of

p53 by doxycycline led to the expression of the NFκB proteins p65 and p50, which was also dependent on MAP-kinase MEK1 and the mitogen-activated ribosomal S6 kinase ($p90^{rsk1}$, *RPS6KA1*) of the RAF/MAPK pathway. The latter can phosphorylate IκBα at Ser32, releasing NFκB from the complex and leading to its translocation and activation (Ryan et al. 2000; Schouten et al. 1997). IκBα was also shown to bind to the proline-rich domain of p53, retaining it in the cytoplasm. Therefore, degradation by phosphorylation could activate both pathways (Chang 2002). In this thesis, *RPS6K1A* was increased in p53WT and, to a lesser extent, in p53R273H cells compared to p53KO, parental, or p53R175H cells (Appendix

Table **S3**). Together with the generally active RAF/MAPK pathway in OVCAR8 cells ($KRAS^{P121H}$ mutation (C. Sun et al. 2017)), activation of NFκB via p53 could be a vital driver of the apoptotic (e.g., *FAS, CASP3, BBC3*) and inflammatory genotype (e.g., *CXCL1, CXCL8, IL1B*) seen in p53 WT cells. Interestingly, the p53R273H mutant seems to retain some of the NFκB pathway expression demonstrated in WT cells (Fig. 8e). One explanation could be the slightly increased expression of *MEK1* or *RPS6K1A* in these cells (Appendix

Table **S3**). Moreover, in lung cancer cells, both p53R175H and p53R273H showed transactivation of NFκB2 (Scian et al. 2005). However, another study indicated that this transactivation by mutp53 occurs only after TNFα stimulus (Weisz et al. 2007). That could explain why, in this study, increased NFκB activity in mutant cells was not observed (Fig. 6e).

In general, mutp53 cells can influence gene expression differently (Pavlakis and Stiewe 2020). For instance, co-aggregation with the p53 family members p63 and p73 and other transcription factors (e.g., SP1, E2F1) were shown, which demonstrated to alter their activity (Pavlakis and Stiewe 2020). Surprisingly, no unique differences could be observed in the transcriptome of p53R175H mutant cells compared to KO and WT cells (Fig. 8e). Only members of the HSP70 family (*HSPA1A, HSPA1B, HSPA1L, HSPA8*) were increased, however not significantly ($log_2(FC) < 1$, Fig. 9, Appendix

Table **S3**). Interestingly, in pancreas cancer cells, the R175H mutant and not R273H showed specific upregulation of all mentioned genes with subsequent nuclear translocation of HSP70 (Polireddy et al. 2019). By stabilizing the heat shock protein, MDM2-dependent degradation of p53R175H was reduced, and clonogenic growth of the cells was increased (Polireddy et al. 2019; Wiech et al. 2012). However, a recent study showed that enhanced HSP70 concentrations by the anti-cancer agent Triptolide led to

increased MDM2-dependent degradation of the mutant p53 protein, indicating a possible dose-dependent effect of the chaperone (Zhou et al. 2022). Transcriptomic analysis of the p53R273H cells demonstrated some uniquely expressed genes, with some related to the pro-tumorigenic impacts, including *PDGFD, ITGA5, IL1R1,* or *TNF* (Fig. 9). In ovarian cancer patients, the platelet-derived growth factor-D (PDGFD) was associated with invasion and lymph node metastasis. Here, *in vitro* assays showed increased invasion of SKOV-3 cells, potentially due to increased MMP2 and MMP9 expression (Y. Wang et al. 2011). Moreover, high PDGFD levels were correlated to worse disease-free and overall survival in epithelial ovarian cancer (C. Yang et al. 2019). TNFα and IL1R1 expression were also associated with ovarian cancer, especially in HGSOC (Gupta et al. 2016; Schauer et al. 2013). Lau and colleagues (2017) showed that increased TNFα expressed by ovarian cancer cells led to enhanced TGFα secretion from stromal fibroblasts, eventually promoting peritoneal metastasis (Lau et al. 2017). The integrin ITG5A was also observed to be uniquely upregulated in p53R273H cells and was shown to be significantly upregulated in HGSOC patients (Fig. 9) (T. Zhu et al. 2020). Specifically, aggressive tumor cells from the ascites in HGSOC were characterized by high ITGA5 expression (Gao et al. 2019). This expression led to their recruitment by CAFs to form heterotypic spheroids, named metastatic units. These aggregates supported tumor cell survival and promoted peritoneal invasion (Gao et al. 2019). By inhibiting ITGA5 expression with the microRNA miR-92a or miR-17, ovarian cancer cells showed reduced adhesion, invasion, and proliferation (Ohyagi-Hara et al. 2013; Gong et al. 2016). Altogether, the uniquely upregulated genes in the R273H mutant of p53 are generally associated with ovarian cancer progression and worse survival.

5.4 p53 but not the hotspot mutations affect EV-biogenesis-related genes

The secretion of proteins, either directly or shuttled by EVs, was described as part of the p53 response to stress (Komarova et al. 1998; Yu, Harris, and Levine 2006). The biogenesis of EVs is regulated by several pathways, with the endosomal sorting complexes required for transport (ESCRT) machinery acting as a key player (van Niel, D'Angelo, and Raposo 2018; Teng and Fussenegger 2021). In this study, we showed augmented expression of many genes related to EV biogenesis in the OVCAR8 p53WT cells (Fig. 8f, e.g., *TSG101, VPS37, CHMP2, CHMP4, PDCD6IP, SDC1, SDC4, RAB27B*). This indicates direct or indirect functions of WTp53 in regulating EV biogenesis. For instance, CHMP4C, a protein of the ESCRT-III complex, was shown to

be directly induced by p53, increasing EV secretion (Yu, Riley, and Levine 2009). It is crucial in both the canonical and non-canonical ESCRT-dependent pathways and mediates the scission of intraluminal vesicles (ILV) into the lumen of multivesicular bodies (MVB) (Teng and Fussenegger 2021; Wollert and Hurley 2010; Teis, Saksena, and Emr 2008). Other ESCRT-related genes that were upregulated in p53WT cells (e.g., TSG101, CHMP2, VPS37) have not yet been described to be regulated by p53. However, indirect regulation by stress-induced pathways could be one possibility. TSG101 plays a role in the recruitment of ESCRT-I to ESCRT-0 on endosomal membranes and is responsible for its invagination (Lu et al. 2003; Wollert and Hurley 2010). Moreover, TSG101 contains a ubiquitin-binding domain and is believed to enhance the sorting of ubiquitinated proteins into the vesicles (Pornillos 2002; Bilodeau et al. 2003). Caveolin 1 (CAV1), another protein of the endosomal compartment, was also found to be upregulated in p53WT cells (Fig. 8f). A study from Yu and colleagues (2009) showed that CAV1 is directly regulated by p53 and that its expression clears proteins from the plasma membrane, such as EGFR (Yu, Riley, and Levine 2009; Feng et al. 2010),. Furthermore, a study from our group in 2019 demonstrated how p53 could alter cargo sorting of EVs (Schuldner et al. 2019). Through acetylation of p53 by the BAG6/CBP/p300 complex, Schuldner and colleagues could show recruitment of the ESCRT system, eventually leading to the secretion of anti-tumorigenic EVs (Schuldner et al. 2019). PDCD6IP (ALIX) is also essential in EV-mediated biogenesis and cargo sorting. Together with the ESCRT-III subunit, it regulates the sorting of tetraspanins into late endosomes (Baietti et al. 2012; Larios et al. 2020).

EVs' most commonly expressed tetraspanins are CD9, CD63, CD81, CD82, and CD151 (Andreu and Yanez-Mo 2014). Both, CD9 and CD82 were uniquely differentially expressed in p53WT cells in this project (Fig. 8f). The latter can be directly induced by p53 or NFκB, which are both active in these cells (Mashimo et al. 1998; Shinohara et al. 2001). CD82 can form complexes with different integrins and inhibit their adhesion with ECM molecules (e.g., laminin or fibronectin), impairing cell invasion (Jun Li et al. 2020). Moreover, its expression was found to be negatively correlated with the malignancy of tumors, including ovarian cancer (J. Zhu et al. 2017; Yan et al. 2021). In contrast, CD9 was strongly downregulated in p53WT cells; however, no direct link between p53 and CD9 expression is known (Fig. 8f). A recent study linked CD9 expression to hypoxia, with HIF1α as a direct activator of the CD9 promotor (Rouger-Gaudichon et al. 2022). Interestingly, HIF1α was upregulated in the OVCAR8 p53WT cells (Appendix

Table **S3**), suggesting a different mechanism involved in downregulating the tetraspanin in OVCAR8 cells. In 2020, Xing et al. discovered that the knockdown of CD9 promoted p53-dependent apoptosis (C. Xing et al. 2020). Therefore, some could speculate that stress-induced and p53-dependent apoptotic pathways could downregulate CD9. In general, the functions of CD9 are multifaceted, with described anti-and pro-tumorigenic roles in ovarian cancer (Gonzalez et al. 2021; Hwang et al. 2012). For instance, a recent study showed that NK cells could acquire CD9 from ovarian cancer cells via trogocytosis, eventually leading to suppressed cytokine expression and release (Gonzalez et al. 2021). Therefore, higher CD9 concentration in p53KO or mutp53 cells could guide an immune escape.

Besides proteins, RNA is also described as a common cargo in EVs (van Niel, D'Angelo, and Raposo 2018). Here, we could show that many genes involved in RNA sorting to EVs are specifically downregulated in p53WT cells, including *SYNCRIP, HNRNPA2B1, YBX1,* or *SSB* (Appendix Table **S2**). HNRNPA2B1, a protein involved in transcriptional regulation and mRNA location, was shown to recognize a specific motif on RNA and sort it into exosomes (Villarroya-Beltri et al. 2013). In 2008, Prahl et al. showed that Wig1, a direct target of p53, can block hnRNPA2B1, leading to growth arrest (Prahl et al. 2008). Furthermore, the knockdown of hnRNPA2B1 in NSCLC inhibited the proliferation and survival of cells by activating p53 and p21 through ERK/HDM2-dependent inhibition (M. K. Kim et al. 2021). SYNCRIP, another vital protein in RNA sorting to EVs, was shown to be involved in regulating p53 transcription (D.-Y. Kim et al. 2013). Downregulation of these proteins could indicate altered RNA sorting into the EVs, suggesting distinct cargos depending on the p53 status.

Overall, p53 can directly or indirectly regulate many genes involved in EV biogenesis or cargo loading in the OVCAR8 cell line, indicating altered EV production and secretion. This further suggests that p53 status plays a role in the secretion of certain EV subtypes with specific cargos.

5.5 OVCAR8 p53WT secretome resembles a SASP-like phenotype

The secretion of proteins involved in intercellular communication is one hallmark of p53 tumor suppressor functions (Komarova et al. 1998; Yu, Harris, and Levine 2006). One specific phenotype of p53WT cells can be the SASP (Pavlakis and Stiewe 2020). SASP is mediated by the cooperation of p53 and NFκB pathway, which both were enriched in OVCAR8 p53WT cells compared to the knockout cell line (Fig. 8c, Fig. 10c) (Chien et al.

2011; Rovillain et al. 2011). It is characterized by the secretion of inflammatory cytokines and chemokines, such as CXCL1, CXCL8, IL6, IL1A, or IL1B, all of which were found secreted by p53WT cells in this study (Fig. 10b) (Takasugi et al. 2023). Cellular senescence is generally described as permanent cell-cycle arrest mediated by the cyclin-dependent kinase inhibitors p15, p16, or p21 and downregulation of proliferation marker KI67 and Lamin B1 (Takasugi et al. 2023; Freund et al. 2012). Similar regulation of these genes was seen in the transcriptomic data of the WT cell line (Fig. 8b, some not shown). Senescence and SASP can be induced by oncogenes, such as mutated KRAS, which could also be the case in OVCAR8 (Collado et al. 2005). Due to the reintroduction of WTp53 in these cells, together with another stressor (here, doxycycline), senescence could be triggered. Moreover, DNA-damage response, mediated by p53, can induce NFκB, the master-regulator of the SASP (Rodier et al. 2009; Chien et al. 2011). DNA damage leads to the activation of a protein complex consisting of STING, IFI16, TRAF6, and p53, which in turn induces NFκB (Dunphy et al. 2018). Furthermore, COX2 (*PTGS2*), upregulated by p53, contributes to SASP by mediating the biosynthesis of prostaglandins (Wiley et al. 2021). Downstream products of COX-2 can then activate RAS to further reinforce the SASP via p53 (Wiley et al. 2021). In this study, *PTGS2* was found to be uniquely upregulated in the transcriptomic data of p53WT cells, strengthening the idea of p53-induced SASP in these cells (Appendix

Table **S3**). SASP is associated with pro- and anti-tumorigenic functions, potentially dependent on the p53 status (Takasugi et al. 2023; Acosta et al. 2013). For instance, p53 was shown to negatively regulate enhanced SASP by inhibiting p38MAPK activity, another NFκB activator (Freund, Patil, and Campisi 2011). The enhanced inflammatory state is associated with malignant effects, indicating a regulative function of p53 towards an anti-tumorigenic SASP (Coppé et al. 2008). In general, SASP was shown to have autocrine and paracrine effects, possibly leading to the senescence of neighboring tumor cells (Acosta et al. 2013). Moreover, components of SASP could recruit immune cells, leading to the clearance of senescent tumor cells (Xue et al. 2007; Kang et al. 2011). Interestingly, the p53WT phenotype could be partially rescued in p53KO cells by treatment with conditioned medium from WT cells (Fig. 20a). Predominantly, the expression of SASP-related factors, such as IL6, CXCL1 and CXCL8 was rescued, potentially indicating the paracrine transfer of the SASP phenotype (Fig. 20a).

Secretome data from p53KO cells revealed increased secretion of TGFβ1, TGFβ2, VEGFA, VEGFB, FGF19, or TIMP2, potentially indicating a pro-tumorigenic secretome

(Fig. 10b) (Kenny et al. 2014; Hu and Cong 2015). While TGFβ was initially known as a tumor suppressor by activating apoptosis in pre-malignant cells, it has also been shown to induce an immune-suppressive TME that can promote metastasis in cancer cells (J.-C. Cheng, Auersperg, and Leung 2012; Batlle and Massagué 2019). In ovarian cancer, TGFβ1 secretion induces fibronectin secretion via RAC1/SMAD-dependent signaling in mesothelial cells, promoting colonization and metastasis of cancer cells (Kenny et al. 2014). Moreover, SMAD3-dependent downregulation of E-cadherin and simultaneous upregulation of N-cadherin promotes cancer invasion by triggering epithelial to mesenchymal transition (EMT) (J.-C. Cheng, Auersperg, and Leung 2012). In general, TGFβ1 levels were elevated in ovarian cancer patients (Kumari et al. 2021). Another secreted factor in p53KO cells was the vascular endothelial growth factor VEGF, which is a crucial mediator of angiogenesis and was shown to be primarily expressed and secreted in ovarian cancer (Hazelton, Nicosia, and Nicosia 1999; Santin et al. 1999). Regulation of VEGF expression and secretion is complex and can involve many factors. For instance, ERBB2/HER2, which is mutated in OVCAR8 cells, is known to induce VEGF expression. In contrast, p53 was reported to downregulate VEGF expression either by p21/RB-dependent pathway or directly with the E2F1 transcription factor (Farhang Ghahremani et al. 2013; Qin et al. 2006). Therefore, p53KO cells could lack this regulatory mechanism, resulting in increased secretion in these cells (Fig. 10b). In ovarian cancer, VEGF mediates early angiogenesis by upregulating angiopoietin-2 in endothelial cells, which subsequently remodels the vasculature (L. Zhang et al. 2003; Nakanishi et al. 1997). The fibroblast growth factor 19, FGF19, is another pro-tumorigenic protein found in the secretome of p53KO cells (Fig. 10b). It correlates to a worse prognosis in ovarian cancer by activating AKT/MAPK signaling through the fibroblast growth receptor 4 (Hu and Cong 2015; Y. Liu et al. 2020). A recent study further demonstrated that MAPK activation by FGF19 also promotes chemoresistance [265]. In summary, the lack of p53 resulted in the secretion of factors promoting ovarian cancer progression.

It is reported that mutp53 regulates many secreted proteins, which are generally related to tumor progression (Pavlakis and Stiewe 2020). However, here, we only detected a few differential secreted proteins, mainly from the p53R273H cells (Fig. 10d). Although surprising, this is consistent with our transcriptomic data (Fig. 9). Cells expressing p53R273H revealed some genetic variation compared to p53KO cells. In contrast, p53R175H cells were almost identical (Fig. 9). Secretome analysis revealed the release of matrix metalloproteases, MMP7 and MMP12, in p53R273H or both mutant cell lines,

respectively (Fig. 10d). Secretion of MMPs is associated with ovarian cancer progression by promotion of EMT, metastasis, and angiogenesis (Carey et al. 2021). Expression of MMP7 was shown to be enriched in ovarian cancer compared to healthy cells and associated with tumor invasion (F.-Q. Wang et al. 2005). Other factors secreted by mutp53 cells were MICA and MICB (Fig. 10d). Both are stress-induced ligands of the activating NK cell receptor NKG2D. Surface expression of the ligands results in activation of cytolytic responses by NK and T cells, subsequently leading to tumor cell killing. However, tumor cells can shed MICA/B from the surface into the TME by proteolytic cleavage mediated by the isomerase ERp5 and multiple metalloproteases (S. Xing and Ferrari de Andrade 2020). Primarily, this leads to immune escape of the tumor cells. In addition, soluble MICA/B (sMICA/B) can also bind to NKG2D, promoting receptor endocytosis and further impairing immune cell activation (Groh et al. 2002). Therefore, sMICA/B was correlated with poor overall survival in cancer, including ovarian cancer (Zhao et al. 2017). No connection between p53 status and shedding of MICA/B has been reported yet, but here, we show enhanced secretion of both by mutp53 OVCAR8 cells (Fig. 10d). Other tumor-promoting factors were also secreted in mutp53 cells, including LIF, CD274, or CXCL5 (Fig. 10d). Both mutp53 and p53KO cells demonstrated a potentially tumor-promoting secretome, clarifying the important tumor-suppressive function of wildtype p53 on secreted factors (Yu, Harris, and Levine 2006).

5.6 p53 regulates specific cargo loading in EVs from OVCAR8 cells

Although initially designated as “garbage bags” of the cell, many recent studies confirmed EVs are essential mediators in communication with other cells (van Niel, D’Angelo, and Raposo 2018). Furthermore, the general influence of p53 on EV secretion, size, or cargo loading was already shown in some studies; however, much is still unknown (Yu, Harris, and Levine 2006; Schuldner et al. 2019; Pavlakis, Neumann, and Stiewe 2020). Here, we indicated that p53 could regulate EV biogenesis in OVCAR8 cells by influencing the expression of essential pathway genes (Fig. 8f, also see section 5.4). This is further supported by the significant increase in particle secretion in p53WT compared to p53KO or mutp53 cells (Fig. 18a). Besides the direct or indirect upregulation of EV biogenesis genes by p53, stress, and apoptosis could also be a factor (Y. Huang et al. 2023; Chiaradia et al. 2021). For instance, in adipocytes, cellular stress was shown to increase exosome secretion in a p53-dependent manner (Y. Huang et al. 2023). Moreover, apoptosis can increase the secretion of several subtypes of EVs, including ApoExo, which are formed by the fusion of lysosomes, multivesicular bodies,

and autophagosomes (Gregory and Rimmer 2023; Beillevaire et al. 2022). The subsequent release of small ApoExo (30-100 nm) was shown to be mediated by Caspase-3, a direct target of p53 (Dieudé et al. 2015; Beillevaire et al. 2022). Moreover, ApoExo contain components of the proteasome, which was shown to play a role in the immunogenicity of the vesicles (Dieudé et al. 2015; Beillevaire et al. 2022). In this project, some apoptosis could be detected in OVCAR8 p53WT cells, suggesting that small ApoExo could be an exclusive EV subtype in these cells (Fig. 12a-c). This is also supported by the cargo of the isolated WT EVs containing proteins associated with the proteasome, such as PSMC2, PSMD1, or PSMD6 (Fig. 15b; Appendix Figure S3). Other apoptosis-related vesicles (e.g., apoptotic bodies) should not be present due to their large size and subsequent removal by dUC in the isolation process (Szatanek et al. 2015). ApoExo were described to lack classical exosome markers CD9 and CD63, which could further explain the decrease in expression seen on p53WT-released EVs (Fig. 14c, Fig. 15b, Fig. 16a, Fig. 18c) (Beillevaire et al. 2022; Brodeur et al. 2023). Functionally, ApoExo can induce a proinflammatory response in recipient cells, potentially mediated by NFκB (Dieudé et al. 2015; Brodeur et al. 2023; Migneault et al. 2020).

Interestingly, many TOP100 proteins found in EVs, as presented by different databases (vesiclepedia or exocarta), were less abundant in vesicles from OVCAR8 p53WT cells (Fig. 14b,c). However, the Top100 proteins do not obligatorily represent specific EV markers and merely show the most detected proteins in EVs in the collected studies (Pathan et al. 2019). Unexpectedly, some of these proteins (e.g., ALIX, TSG101) were previously demonstrated to be highly expressed on the transcriptomic level (Fig. 8f). On the other hand, factors related to RNA binding and sorting (e.g., HNRNPA2B1, HNRNPA1), were found more often in EVs of WT cells and were less expressed in their respective donor cells (Fig. 15b, Appendix Table S2). Similar findings were presented by Grady et al. (2022), where mRNA and lncRNA transcription negatively correlated with their secretion by EVs (O'Grady et al. 2022). They proposed that EV secretion could contribute to controlling intracellular RNA levels, besides transcriptional and post-transcriptional regulation (O'Grady et al. 2022). Therefore, we can further speculate that a similar process could be valid for protein levels. Paradoxically, this leads back to the beginning of EV research with vesicles as "garbage bags" of the cell (Vidal 2019).

Further results of proteomic data revealed specific phenotypes for p53WT-expressing and non-expressing cells, while p53KO and mutp53-released EVs did not discriminate much from each other (Fig. 15a-e). This is coherent with our RNA sequencing and

secretome data from the cell lines (Fig. 15a,b; Fig. 8a; Fig. 11b). Besides p53, other proteins were found enriched in p53WT EVs, including BAG3, BAG6, FAS, CAV1, CD82, PODXL, or TNFRSF10B (Fig. 15b, Fig. 16a, Fig. 18f). Interestingly, as described in section 5.4, BAG6 is a critical mediator of EV biogenesis by acetylation of p53 together with CBP/p300 and recruitment of the ESCRT system, eventually leading to production of anti-tumorigenic vesicles (Schuldner et al. 2019). Moreover, exosomal BAG6 was shown to be essential for NK cell recruitment in chronic lymphatic leukemia by binding to the NKp30 receptor (Reiners et al. 2013; Simhadri et al. 2008). In contrast, soluble BAG6 inhibited the activation of the immune cells. They postulated that a p53-dependent biogenesis pathway results in BAG6-enriched EVs, which can recruit NK cells for tumor cell killing (Reiners et al. 2013). With BAG3, another factor of the BAG (Bcl2-associated athanogene) family was enriched in p53WT EVs. In pancreatic cancer, it was found in soluble and exosomal fractions and can bind to Interferon-induced transmembrane protein 2 (IFTM2) on macrophages (Rosati et al. 2015). This induced a pro-tumorigenic cytokine release, resulting in tumor growth. However, to our knowledge, no separate analysis of soluble and EV-associated BAG3 was done. Moreover, all used pancreatic cancer cell lines were p53 mutated (Rosati et al. 2015). Therefore, exosomal BAG3 released by p53WT cells does not have to be compulsorily pro-tumorigenic, and more research has to be done. Other enriched proteins of p53WT EVs were described either as pro- or antitumorigenic. For instance, PODXL was shown to be lower expressed in mutp53 EVs, resulting in increased migration of tumor cells and fibroblast (Novo et al. 2018). In contrast, CD82 and CAV1, both labeled as tumor suppressor proteins, were associated with tumor progression in exosomal form in some cancers (Xiaodan Wang et al. 2019).

EVs from p53KO cells showed enrichment in proteins involved in ECM receptor interaction, focal adhesion, proteoglycans in cancer, and cell migration (Fig. 15a-d, Fig. 16a,b). Proteoglycans or molecules interacting with ECM are critical mediators of cancer progression, especially regarding metastasis through communication with the TME (Yuan et al. 2023). In OC, peritoneal metastasis is believed to occur by direct contact of tumor cells with mesothelial cells (Mei et al. 2023, 203; Hoshino et al. 2015). Crucial mediators of this connection are integrins, with some found abundant in p53KO EVs (e.g., ITGA5, ITGB5, ITGB1 ITGA4) (Fig. 15a-d, Fig. 16a,b). In 2020, Li and colleagues demonstrated that exosomal ITGA5, in complex with ITGB1 and asparaginyl endopeptidase (AEP), was able to stimulate the proliferation and migration of human peritoneal mesothelial cells (HPMC) (X. Li et al. 2020). Moreover, exosomal ITGA5 was

uniquely found in aggressive ovarian cancer cells, which further associates it with migration and invasion (Sharma et al. 2018). Notably, more proteins related to tumor migration or angiogenesis were found differential loaded into p53KO EVs, including CD63, PDGFA, VEGF, TGFB, or EGFR (S. Ma et al. 2021; Mazumdar et al. 2020; S. Wu et al. 2021; Jouida et al. 2021) (Fig. 15a-d, Fig. 16a,b). For instance, VEGF is packaged into small EVs by CD63, subsequently promoting angiogenesis and ovarian cancer progression (S. Ma et al. 2021). Moreover, packaged VEGF was shown to be resistant to anti-VEGF therapy, clarifying the importance of EVs in this scenario (MA et al., 2021). Angiogenesis could be further promoted by exosomal EGFR, which can induce VEGF expression after uptake from vascular endothelial cells (VECs) (Jouida et al. 2021). In NSCLC cells, transfer of EGFR via EVs mediated therapy resistance to osimertinib (S. Wu et al. 2021). TGFβ-containing EVs were also demonstrated to reprogram lung fibroblasts to enhance tumor metastasis (Mazdumar et al., 2020).

As mentioned, EVs from mutp53-expressing cells did not differ vastly from p53KO cells (Fig. 15a). However, a few differentially expressed proteins were found, specifically in the R273H mutant (e.g., EPCAM, TSPAN4, TSPAN6, TSPAN9) (Fig. 15e). EPCAM was previously shown to be secreted via EVs in malignant ascites of ovarian cancer patients (Runz et al. 2007). Together with CD45, EPCAM was shown to induce PI3K/AKT signaling, leading to a more aggressive and drug-resistant phenotype in ovarian cancer (Akhter et al. 2018). Interestingly, p53 was shown to regulate the expression of EPCAM (Motohara et al. 2011; Sankpal et al. 2009). This regulation could be impaired in mutp53 cells, somehow leading to increased vesicular secretion of the protein.

Although EVs from mutp53 and p53 cells showed a larger abundance of pro-tumorigenic factors compared to EVs from p53WT cells, proteins described with anti-tumorigenic functions (e.g., SEMA3A, SEMA3E, TSPAN6) could also be found (Fig. 15a-d) (Neufeld et al. 2016). Vice versa, EVs from p53WT cells also contained factors associated with pro-tumorigenic functions (e.g., CAV1) (Fig. 15a-d) (Felicetti et al. 2009). However, many proteins are only described in the cells and not specifically in extracellular vesicles. Similar to the functional differences in cellular and soluble MICA/B (see section 5.5), many proteins could have specific functions in EVs. In conclusion, a different p53 status in OVCAR8 cells resulted in a particular cargo loading in their respective extracellular vesicles.

5.7 WTp53 is predominantly loaded into EVs and transferred to OVCAR8 cells and fibroblasts

One of the most distinctive results in the proteomic data was the direct association of p53 (WT and mutp53) to the vesicles (Fig. 15b, Fig. 16a, Fig. 18d,e). Notably, we could demonstrate that WTp53 was preferential loaded into EVs compared to mutp53 (Fig.18 d,e). This was unexpected since previous research showed preferential loading of mutp53 into small vesicles (S. Ma et al. 2021). They demonstrated that mutp53 and not WTp53 is packaged into EVs through interaction with the heat-shock protein HSP90. These vesicles induced a CAF phenotype in fibroblasts, promoting a pro-tumorigenic microenvironment (S. Ma et al. 2021). However, the general transfer of WTp53 in vesicles to p53-negative cells was also reported (Burdakov et al. 2018). Specific mechanisms of how WTp53 is loaded into EVs are not described. Generally, several proteins can sort ubiquitinated proteins into EVs, including HRS, TSG101, or ALIX, via their ubiquitin-binding domain (Baietti et al. 2012; Sundquist et al. 2004; Bilodeau et al. 2002; 2003). Since MDM2 ubiquitinates p53 before degradation, we could speculate that this mechanism is at least partly responsible.

Besides protein loading, we could also demonstrate the transfer of vesicular-WTp53 to p53KO cells (Fig. 19). Moreover, these EVs were able to partly rescue the specific phenotype of p53WT cells in the knockout cell line (Fig. 20b). Although the expression of p53-specific targets could not be rescued (e.g., CDKN1A, Fig. 20b), the question is raised if p53 elicits an active function by its transfer to recipient cells. To date, the packaging and transfer of p53 via EVs have not been extensively studied, and therefore we can only speculate why WTp53 is preferentially loaded into vesicles in our cells. One option could be that ApoExo favorably transfers p53 since it is a central apoptosis regulator and, therefore, essential for the biogenesis of this EV subtype (Aubrey et al. 2018). This could further indicate a potential tumor suppressive role by transferring WTp53 to recipient cells. Another explanation could be simply a regulatory mechanism to remove excessive p53. Due to the inducible system used in this project, cells are suddenly flooded with p53WT, which could potentially lead to secretion as a protective or regulatory mechanism.

Generally, EV uptake is a complex process, and many different ways are described (Mulcahy, Pink, and Carter 2014). For instance, several ways of endocytosis, phagocytosis, or micropinocytosis are described. Moreover, simple fusion and release of the content in the recipient cells were also shown. EV uptake is an energy-dependent

process that, on the one hand, can be fast (~15 min) but, on the other hand, also slow and inefficient (Bonsergent et al. 2021; Feng et al. 2010; Escrevente et al. 2011). For the latter, Bonsergent et al. (2021) demonstrated that only 1 % of EVs were taken up spontaneously after one hour (Bonsergent et al. 2021). While some studies showed cell-specific uptake of EVs, others demonstrated unspecific uptake by many cells (Mulcahy, Pink, and Carter 2014; Svensson et al. 2013). Since many factors and routes can be involved, EV uptake is potentially possible in all cells. However, specific receptor and protein combinations on the EV or cell surface will enhance the uptake, making it also a targeted and specific process (Mulcahy, Pink, and Carter 2014). In this study, we demonstrated the intake of WTp53-containing EVs into the cytoplasm of a knockout cell line after six hours (Fig. 19). The exact kinetics or if the EVs potentially reached other compartments after time was not shown in this experiment and would be interesting for future studies. Another experiment demonstrated that p53-GFP-containing EVs were taken up by fibroblasts (Fig.21a,b). Interestingly, here, two potential routes could be observed. While figure 21a indicated the fusion and uptake of EVs by fibroblasts, figure 21b showed the merging of a vesicle with the fibroblasts membrane, subsequently forming protrusions and releasing its contents, including p53-GFP, into the cytoplasm of the recipient cell.

5.8 p53 status drives the EV-mediated education of fibroblast in association with NFκB and STAT3

CAFs are an essential part of the TME in ovarian cancer, where they promote angiogenesis, migration, metastasis, immunosuppression, or drug resistance. However, anti-tumorigenic roles are also described (M. Zhang et al. 2022). Here, treatment of HDFn cells with EVs from p53WT cells resulted in an acute inflammatory phenotype, primarily represented by the upregulation and secretion of CXCL1, CXCL8, and IL6 (Fig. 22b; Fig. 23b-e). This was surprising since an inflammatory CAF (iCAF) phenotype was generally associated with eliciting pro-tumorigenic functions (Biffi and Tuveson 2020; Fang et al. 2022; M. Zhang et al. 2022). Especially the mentioned factors (CXCL1, CXCL8, and IL6) are all described with pro-tumorigenic functions (Browning et al. 2018; G.-Y. Park et al. 2021). For instance, the secretion of IL6 by iCAFs was shown to induce JAK/STAT signaling in OC cells, promoting tumor proliferation, metastasis, and chemoresistance (Browning et al. 2018). The latter could be mediated by inhibiting the p53-dependent apoptosis pathway (Cheteh et al. 2020). Moreover, IL6-dependent STAT3 activation was also shown to recruit dendritic cells (DCs) and transdifferentiate

them into regulatory DCs, subsequently promoting tumor immune evasion (J. -t Cheng et al. 2016). In contrast, IL6 was shown to be able to prime and recruit $CD8^+$ cytotoxic T-cells, potentially leading to tumor cell killing (Fisher et al. 2011). Furthermore, Lin et al. (2012) demonstrated another anti-tumor effect of IL6 by inhibiting regulatory T cells and, therefore, enhancing the proliferation and cytotoxic effects of killer cells (G. Lin et al. 2012). CXCL1 was one of the most upregulated and secreted chemokines in the WT-EV-treated fibroblasts (Fig. 22b; Fig. 23b). Similar to IL6, CXCL1 was found to promote OC partially by activating p38 MAP kinase through CXCR2 (G.-Y. Park et al. 2021). Interestingly, OC cells expressing p53WT show more CXCL1-induced proliferation than mutp53 or p53KO cells (Ignacio et al. 2018). CXCL8 is another factor that confers its activity via the CXCR2 or CXCR1 receptor, which is associated with metastasis and poor prognosis in OC (Fu et al. 2023). Both CXCL1 and CXCL8 are essential for the recruitment and migration of neutrophils, the central mediator of the primary innate immune response (M. Yang et al. 2020; L. Wu, Saxena, and Singh 2020). In cancer, the recruitment of neutrophils is often described to support tumor progression by promoting immunosuppression, ECM remodeling, or angiogenesis (L. Wu, Saxena, and Singh 2020). Specifically, in OC, CXCL8 was shown to recruit tumor-associated neutrophils (TANs, N2), which impaired $CD8^+$ T cell cytotoxicity partly by Jagged2 (JAG2). This subsequently led to enhanced tumor growth and migration (M. Yang et al. 2020). In a renal carcinoma model, however, CXCL8 was shown to recruit neutrophils for tumor cell killing (López-Lago et al. 2013). Neutrophils have been shown to kill tumor cells directly *in vitro* and *in vivo* (Albanesi et al. 2013; E. F. Zhu et al. 2015). This could be due to the release of cytotoxic reactive oxygen species (ROS) or cancer cell detachment from the basement membrane by MMP9 (Granot et al. 2011; Mahiddine et al., n.d.). Granot and colleagues (2011) demonstrated that G-CSF (CSF3) and CCL2 are essential for the recruitment of the tumor entrained neutrophils (TEN, N1), which inhibited metastatic seeding of the lung. Furthermore, the cytotoxicity of antitumor N1 neutrophils was blocked by secreted TGFβ (Granot et al. 2011). Here, we could show that CCL2 and G-CSF were upregulated/secreted by WT-EV-treated fibroblasts (Fig. 22e; Fig. 23d,e). Together with lower expression and secretion of TGFβ in the OVCAR8 WTp53 cells, some could speculate that by communication with fibroblast, N1-neutrophils could be recruited for tumor cell killing (Fig. 8b; Fig. 11b). In contrast, OVCAR8 cells harboring p53KO could block the cytotoxicity of the neutrophils by secretion of TGFβ also in association with EVs (Fig. 8b; Fig. 11b; Fig. 15b).

The inflammatory phenotype of p53WT EV-treated fibroblasts was shown to be mediated or at least associated with NFκB activity (Fig. 22d; Fig. 23c; Fig. 24a-d). Here, phosphorylation and nuclear translocation of p65 could be observed 6 and 24 hours after p53WT but not p53KO EV treatment (Fig. 24a-d). Activation of NFκB is described as a key pathway of iCAFs (Biffi and Tuveson 2020; Biffi et al. 2019). In 2019, Biffi and colleagues showed that IL1 induced NFκB-dependent secretion of IL6, which activated the JAK/STAT pathway in an autocrine manner. JAK/STAT pathway and especially STAT3 activation was shown to be necessary for the continuous inflammatory phenotype of fibroblasts (Biffi et al. 2019). Interestingly, in this study, we could verify increased STAT3 phosphorylation in fibroblasts after treatment with p53WT EVs (Fig. 25b). Since we also found IL1 upregulated in p53WT cells and also enriched in their secretome and EVs, this could be a potential mechanism of the observed inflammatory phenotype in HDFn cells (Fig. 8f; Fig. 11b; Fig. 16a).

It was further shown that TGFβ antagonizes the formation of the JAK/STAT-mediated iCAF population. By phosphorylation and activation of SMAD2 and SMAD3, TGFβ induced a more myCAF-like phenotype (Biffi et al. 2019). In this study, secretome and EVs from p53KO cells were enriched in TGFβ, explaining the loss of inflammatory phenotype in the treated cells (Fig. 11b; Fig. 15b; Fig. 16a). TGFβ was shown to activate CAFs and enhance EGF secretion, which we also observed in the secretome of p53KO-treated HDFn cells (Fig. 21b) (Gao et al. 2019). EGF secretion can, in turn, upregulate ITGA5 expression in OC cells, which can recruit CAFs to form pro-metastatic spheroids (Gao et al. 2019). In general, fibroblasts treated with EVs from p53KO cells showed enrichment in ECM organization, proteoglycans in cancer, or WNT signaling pathway (Fig. 22d). Remodeling the ECM is one hallmark of CAFs (Biffi and Tuveson 2020). Here, POSTN (periostin) and ECM proteins were unregulated and secreted by KO EV-treated fibroblasts (Fig. 22c; Fig. 23b). In OC, POSTN expression was shown to be highly enriched in HGSC stromal fibroblasts and correlated to reduced overall survival (Yue et al. 2021). Moreover, binding to integrins on ovarian cancer cells POSTN can induce EMT via the PI3K-Akt pathway and subsequently promote migration and metastasis of the tumor. Yue and colleagues further showed that activation and secretion of POSTN is dependent on tumor-derived TGFβ, which could indicate a similar mechanism in our p53KO-EV-treated fibroblasts (Fig. 11b; Fig. 15b; Fig. 16a) (Yue et al. 2021). A recent study by Huang et al. further confirmed the crucial role of secreted POSTN in ovarian cancer migration, invasion, and chemoresistance. They further postulated its role in aggressive ovarian cancer behavior by promoting cancer cells (Z. Huang et al. 2023).

Another ECM factor, the cartilage oligomeric matrix protein COMP, was also found upregulated and secreted by KO EV-treated fibroblasts (Fig. 22c, Fig. 23b). It was shown that secreted COMP could promote proliferation and EMT in colon cancer by activating PI3K/Akt pathway or interaction with transgelin (TAGLN) respectively (T.-T. Liu et al. 2018; Weilong Zhong et al. 2020). A recent study further implicated a specific role in the TME by enhancing tumor infiltration of pro-tumorigenic M2 macrophages (H. Ma et al. 2022). Besides colon carcinoma, COMP was associated with other cancer types, including OC, and was proposed as a potential biomarker (Guo et al. 2023). Other upregulated or secreted factors related to ECM remodeling, such as VCAN, ITGB2, or MMP10, are also described to promote pro-tumorigenic effects in OC (Yeung et al. 2013b; C. Li et al. 2023). Therefore, in our study, KO EV-treated fibroblasts upregulate and secrete many proteins related to ECM remodeling and organization, which could promote cancer progression.

Unfortunately, no functional validation of the secretome of EV-treated fibroblasts on tumor cells has been done yet. This will be the main focus of future studies.

5.9 Novel tumor suppressor function of p53? - indications and potential therapeutic interventions

Mutation of p53 plays a pivotal role in the progression of many cancer types, including OC (Mantovani, Collavin, and Del Sal 2019; Matulonis et al. 2016). Notably, CAFs commonly do not harbor p53 mutations (Hosein et al. 2010). However, p53 function was shown to be suppressed or altered by cancer cells to induce a pro-tumorigenic phenotype (Arandkar et al. 2018; Inoue et al. 2021; Jair Bar, Moskovits, and Oren 2010). This education of fibroblasts was shown to be at least partially dependent on the p53 status of the cancer cell (Inoue et al. 2021; Vennin et al. 2019). Specifically, altered p53 in fibroblasts was shown to induce expression of POSTN or MMP10, which in our study was lower expressed and secreted in p53WT EV-treated cells (Fig. 22c; Fig. 23b) (Arandkar et al. 2018). This could indicate that p53 status in OVCAR8 cells plays a role in the education of CAF related to their p53 functionality. Moreover, a recent study demonstrated that mutp53 can be transferred by EVs, which induces a tumor-promoting CAF phenotype (S. Ma et al. 2021). In our research, we were able to show a preferential loading of WTp53 into EVs (Fig. 18d,e). Although direct p53 targets were not upregulated in fibroblasts (e.g., CDKN1A, see appendix Table S4), it is still interesting to speculate if

WTp53 could have a direct tumor-suppressing effect on the fibroblast phenotype, for instance, by inhibiting the pro-tumorigenic education of the p53 functions in CAFs.

Education of the tumor microenvironment by p53 could also be an interesting therapy area. For instance, EVs isolated from ovarian p53WT cells could potentially be used to treat OC by re-educating the TME. In general, EVs and exosomes, in particular, are gaining more and more interest as a prospect for cancer treatment. Currently, there are several ways EVs could be utilized in cancer therapy, including as biomarkers, drug delivery systems, vaccines, or by inhibiting the secretion of tumor-promoting EVs (S. B. Kim 2022). One of the major advantages of EVs is their low immunogenicity. For instance, Hadla and colleagues demonstrated that exosomal-delivered doxycycline was less toxic and, therefore, increased the therapeutic index of the drug in an OC model (Hadla et al. 2016). It was further shown that EVs can efficiently cross biological barriers and migrate to target tissues without blood supply (S. B. Kim 2022; H. Chen et al. 2021). Compared to liposomes or other nanosized carriers, EVs showed superior stability and pharmacokinetics. However, stability and half-life are also considered drawbacks of the vesicles (S. B. Kim 2022; H. Chen et al. 2021). Another major drawback is the low extraction yield since isolation methods are often inefficient and cost-intensive (Akuma, Okagu, and Udenigwe 2019). In summary, EVs have many excellent characteristics and can be modified to enhance their stability and functionality, making them a promising therapeutic option in the future.

5.10 Concluding remarks and future perspective

In summary, our findings underscore the influence of p53 status on the biogenesis and cargo loading of EVs in OVCAR8 cells. Notably, cells with wildtype p53 exhibited a SASP-like phenotype and released EVs enriched in p53, BAG6, and other potentially anti-tumorigenic factors. Intriguingly, crucial differences between p53 knockout and mutp53 cells or their respective EVs were not apparent. EVs derived from p53WT cells induced an inflammatory phenotype in fibroblasts, potentially relying on NFκB and STAT3 signaling, whereas p53KO EV-treated fibroblasts were primarily associated with extracellular matrix (ECM) remodeling.

Our proposed hypothesis suggests that p53 may exert a tumor suppressor function either directly through its transportation to recipient fibroblasts or by shaping the EV phenotype. However, a comprehensive functional assessment of the secretome of treated fibroblasts remains outstanding and is planned for future experiments. Presently,

migration and invasion assays are in the pipeline for tumor cells treated with conditioned media (CM) from EV-treated fibroblasts. Furthermore, transcriptomic analysis of CM-treated tumor cells could provide additional insights into the functional effects. To further verify the involvement of NFκB and STAT3 in the induction of the iCAF phenotype in WT-EV-treated fibroblast, inhibitors of the respective targets could be utilized. Moreover, potentially involved pathways in the phenotype of KO-EV-treated fibroblasts, such as the TGFβ/SMAD axis, could be studied.

One limitation of this study is the exclusive use of OVCAR8 cells. Consequently, future investigations should prioritize exploring other cell lines, ideally focusing on primary cells to broaden the scope of our understanding. Additionally, examining other facets within this thesis, such as the potential effects of EV-transported WTp53 or the discrimination between exosomes of healthy cells and ApoExos, presents an avenue for further exploration and elucidation.

References

Abrahams, Vikki M., Shawn L. Straszewski, Marijke Kamsteeg, Bozena Hanczaruk, Peter E. Schwartz, Thomas J. Rutherford, and Gil Mor. 2003. “Epithelial Ovarian Cancer Cells Secrete Functional Fas Ligand.” *Cancer Research* 63 (17): 5573–81.

Acosta, Juan Carlos, Ana Banito, Torsten Wuestefeld, Athena Georgilis, Peggy Janich, Jennifer P. Morton, Dimitris Athineos, et al. 2013. “A Complex Secretory Program Orchestrated by the Inflammasome Controls Paracrine Senescence.” *Nature Cell Biology* 15 (8): 978–90. https://doi.org/10.1038/ncb2784.

Addadi, Yoseph, Neta Moskovits, Dorit Granot, Guillermina Lozano, Yaron Carmi, Ron N. Apte, Michal Neeman, and Moshe Oren. 2010. “P53 Status in Stromal Fibroblasts Modulates Tumor Growth in an SDF1-Dependent Manner.” *Cancer Research* 70 (23): 9650–58. https://doi.org/10.1158/0008-5472.CAN-10-1146.

Akhter, Md Zahid, Surender K. Sharawat, Vikash Kumar, Veena Kochat, Zaffar Equbal, Mallika Ramakrishnan, Umesh Kumar, Sandeep Mathur, Lalit Kumar, and Asok Mukhopadhyay. 2018. “Aggressive Serous Epithelial Ovarian Cancer Is Potentially Propagated by EpCAM+CD45+ Phenotype.” *Oncogene* 37 (16): 2089–2103. https://doi.org/10.1038/s41388-017-0106-y.

Akuma, Precious, Ogadimma D. Okagu, and Chibuike C. Udenigwe. 2019. “Naturally Occurring Exosome Vesicles as Potential Delivery Vehicle for Bioactive Compounds.” *Frontiers in Sustainable Food Systems* 3. https://www.frontiersin.org/articles/10.3389/fsufs.2019.00023.

Albacete-Albacete, Lucas, Inmaculada Navarro-Lérida, Juan Antonio López, Inés Martín-Padura, Alma M. Astudillo, Alessia Ferrarini, Michael Van-Der-Heyden, et al. 2020. “ECM Deposition Is Driven by Caveolin-1–Dependent Regulation of Exosomal Biogenesis and Cargo Sorting.” *The Journal of Cell Biology* 219 (11): e202006178. https://doi.org/10.1083/jcb.202006178.

Albanesi, Marcello, David A. Mancardi, Friederike Jönsson, Bruno Iannascoli, Laurence Fiette, James P. Di Santo, Clifford A. Lowell, and Pierre Bruhns. 2013. “Neutrophils Mediate Antibody-Induced Antitumor Effects in Mice.” *Blood* 122 (18): 3160–64. https://doi.org/10.1182/blood-2013-04-497446.

Andreu, Zoraida, and Maria Yanez-Mo. 2014. “Tetraspanins in Extracellular Vesicle Formation and Function.” *Frontiers in Immunology* 5 (September). https://doi.org/10.3389/fimmu.2014.00442.

Anglesio, Michael S., Jeremy M. Arnold, Joshy George, Anna V. Tinker, Richard Tothill, Nic Waddell, Lisa Simms, et al. 2008. “Mutation of ERBB2 Provides a Novel Alternative Mechanism for the Ubiquitous Activation of RAS-MAPK in Ovarian Serous Low Malignant Potential Tumors.” *Molecular Cancer Research* 6 (11): 1678–90. https://doi.org/10.1158/1541-7786.MCR-08-0193.

Arandkar, Sharathchandra, Noa Furth, Yair Elisha, Nishanth Belugali Nataraj, Heiko van der Kuip, Yosef Yarden, Walter Aulitzky, Igor Ulitsky, Benjamin Geiger, and Moshe Oren. 2018. “Altered P53 Functionality in Cancer-Associated Fibroblasts Contributes to Their Cancer-Supporting Features.” *Proceedings of the National Academy of Sciences* 115 (25): 6410–15. https://doi.org/10.1073/pnas.1719076115.

Arizti, Paz, Li Fang, Iha Park, Yuxin Yin, Ellen Solomon, Toru Ouchi, Stuart A. Aaronson, and Sam W. Lee. 2000. “Tumor Suppressor P53 Is Required To Modulate BRCA1 Expression.” *Molecular and Cellular Biology* 20 (20): 7450–59.

Asare-Werehene, Meshach, Laudine Communal, Euridice Carmona, Youngjin Han, Yong Sang Song, Dylan Burger, Anne-Marie Mes-Masson, and Benjamin K. Tsang. 2020. “Plasma Gelsolin Inhibits CD8+ T-Cell Function and Regulates

Glutathione Production to Confer Chemoresistance in Ovarian Cancer." *Cancer Research* 80 (18): 3959–71. https://doi.org/10.1158/0008-5472.CAN-20-0788.

Au Yeung, Chi Lam, Ngai-Na Co, Tetsushi Tsuruga, Tsz-Lun Yeung, Suet-Ying Kwan, Cecilia S. Leung, Yong Li, et al. 2016. "Exosomal Transfer of Stroma-Derived miR21 Confers Paclitaxel Resistance in Ovarian Cancer Cells through Targeting APAF1." *Nature Communications* 7 (1): 11150. https://doi.org/10.1038/ncomms11150.

Aubrey, Brandon J., Gemma L. Kelly, Ana Janic, Marco J. Herold, and Andreas Strasser. 2018. "How Does P53 Induce Apoptosis and How Does This Relate to P53-Mediated Tumour Suppression?" *Cell Death & Differentiation* 25 (1): 104–13. https://doi.org/10.1038/cdd.2017.169.

Babst, Markus, David J. Katzmann, William B. Snyder, Beverly Wendland, and Scott D. Emr. 2002. "Endosome-Associated Complex, ESCRT-II, Recruits Transport Machinery for Protein Sorting at the Multivesicular Body." *Developmental Cell* 3 (2): 283–89. https://doi.org/10.1016/S1534-5807(02)00219-8.

Baietti, Maria Francesca, Zhe Zhang, Eva Mortier, Aurélie Melchior, Gisèle Degeest, Annelies Geeraerts, Ylva Ivarsson, et al. 2012. "Syndecan–Syntenin–ALIX Regulates the Biogenesis of Exosomes." *Nature Cell Biology* 14 (7): 677–85. https://doi.org/10.1038/ncb2502.

Baker, S. J., E. R. Fearon, J. M. Nigro, S. R. Hamilton, A. C. Preisinger, J. M. Jessup, P. vanTuinen, et al. 1989. "Chromosome 17 Deletions and P53 Gene Mutations in Colorectal Carcinomas." *Science (New York, N.Y.)* 244 (4901): 217–21. https://doi.org/10.1126/science.2649981.

Bar, J, R Feniger-Barish, N Lukashchuk, H Shaham, N Moskovits, N Goldfinger, D Simansky, et al. 2009. "Cancer Cells Suppress P53 in Adjacent Fibroblasts." *Oncogene* 28 (6): 933–36. https://doi.org/10.1038/onc.2008.445.

Bar, Jair, Neta Moskovits, and Moshe Oren. 2010. "Involvement of Stromal P53 in Tumor-Stroma Interactions." *Seminars in Cell & Developmental Biology* 21 (1): 47–54. https://doi.org/10.1016/j.semcdb.2009.11.006.

Batlle, Eduard, and Joan Massagué. 2019. "Transforming Growth Factor-β Signaling in Immunity and Cancer." *Immunity* 50 (4): 924–40. https://doi.org/10.1016/j.immuni.2019.03.024.

Bebelman, Maarten P., Eline Janssen, D. Michiel Pegtel, and Caitrin Crudden. 2020. "The Forces Driving Cancer Extracellular Vesicle Secretion." *Neoplasia (New York, N.Y.)* 23 (1): 149–57. https://doi.org/10.1016/j.neo.2020.11.011.

Beillevaire, Déborah, Francis Migneault, Julie Turgeon, Diane Gingras, Annie Karakeussian Rimbaud, Geneviève Marcoux, Crysta Spino, et al. 2022. "Autolysosomes and Caspase-3 Control the Biogenesis and Release of Immunogenic Apoptotic Exosomes." *Cell Death & Disease* 13 (2): 145. https://doi.org/10.1038/s41419-022-04591-5.

Bell, D., A. Berchuck, M. Birrer, J. Chien, D. W. Cramer, F. Dao, R. Dhir, et al. 2011. "Integrated Genomic Analyses of Ovarian Carcinoma." *Nature* 474 (7353): 609–15. https://doi.org/10.1038/nature10166.

Biffi, Giulia, Tobiloba E. Oni, Benjamin Spielman, Yuan Hao, Ela Elyada, Youngkyu Park, Jonathan Preall, and David A. Tuveson. 2019. "IL1-Induced JAK/STAT Signaling Is Antagonized by TGFβ to Shape CAF Heterogeneity in Pancreatic Ductal Adenocarcinoma." *Cancer Discovery* 9 (2): 282–301. https://doi.org/10.1158/2159-8290.CD-18-0710.

Biffi, Giulia, and David A. Tuveson. 2020. "Diversity and Biology of Cancer-Associated Fibroblasts." *Physiological Reviews* 101 (1): 147–76. https://doi.org/10.1152/physrev.00048.2019.

Bilodeau, Patricia S., Jennifer L. Urbanowski, Stanley C. Winistorfer, and Robert C. Piper. 2002. "The Vps27p Hse1p Complex Binds Ubiquitin and Mediates

Endosomal Protein Sorting." *Nature Cell Biology* 4 (7): 534–39. https://doi.org/10.1038/ncb815.

Bilodeau, Patricia S., Stanley C. Winistorfer, William R. Kearney, Andrew D. Robertson, and Robert C. Piper. 2003. "Vps27-Hse1 and ESCRT-I Complexes Cooperate to Increase Efficiency of Sorting Ubiquitinated Proteins at the Endosome." *The Journal of Cell Biology* 163 (2): 237–43. https://doi.org/10.1083/jcb.200305007.

Bonsergent, Emeline, Eleonora Grisard, Julian Buchrieser, Olivier Schwartz, Clotilde Théry, and Grégory Lavieu. 2021. "Quantitative Characterization of Extracellular Vesicle Uptake and Content Delivery within Mammalian Cells." *Nature Communications* 12 (1): 1864. https://doi.org/10.1038/s41467-021-22126-y.

Bost, Jeremy P., Osama Saher, Daniel Hagey, Doste R. Mamand, Xiuming Liang, Wenyi Zheng, Giulia Corso, et al. 2022. "Growth Media Conditions Influence the Secretion Route and Release Levels of Engineered Extracellular Vesicles." *Advanced Healthcare Materials* 11 (5): 2101658. https://doi.org/10.1002/adhm.202101658.

Bougherara, Houcine, Audrey Mansuet-Lupo, Marco Alifano, Charlotte Ngô, Diane Damotte, Marie-Aude Le Frère-Belda, Emmanuel Donnadieu, and Elisa Peranzoni. 2015. "Real-Time Imaging of Resident T Cells in Human Lung and Ovarian Carcinomas Reveals How Different Tumor Microenvironments Control T Lymphocyte Migration." *Frontiers in Immunology* 6: 500. https://doi.org/10.3389/fimmu.2015.00500.

Bowtell, David D., Steffen Böhm, Ahmed A. Ahmed, Paul-Joseph Aspuria, Robert C. Bast, Valerie Beral, Jonathan S. Berek, et al. 2015. "Rethinking Ovarian Cancer II: Reducing Mortality from High-Grade Serous Ovarian Cancer." *Nature Reviews. Cancer* 15 (11): 668–79. https://doi.org/10.1038/nrc4019.

Brodeur, Alexandre, Francis Migneault, Maude Lanoie, Déborah Beillevaire, Julie Turgeon, Annie Karakeussian-Rimbaud, Nicolas Thibodeau, Éric Boilard, Mélanie Dieudé, and Marie-Josée Hébert. 2023. "Apoptotic Exosome-like Vesicles Transfer Specific and Functional mRNAs to Endothelial Cells by Phosphatidylserine-Dependent Macropinocytosis." *Cell Death & Disease* 14 (7): 1–15. https://doi.org/10.1038/s41419-023-05991-x.

Browning, Landon, Megha R Patel, Eli Bring Horvath, Ken Tawara, and Cheryl L Jorcyk. 2018. "IL-6 and Ovarian Cancer: Inflammatory Cytokines in Promotion of Metastasis." *Cancer Management and Research* 10 (December): 6685–93. https://doi.org/10.2147/CMAR.S179189.

Burdakov, V. S., R. A. Kovalev, R. A. Pantina, E. Yu. Varfolomeeva, E. M. Makarov, and M. V. Filatov. 2018. "Exosomes Transfer P53 between Cells and Can Suppress Growth and Proliferation of P53-Negative Cells." *Cell and Tissue Biology* 12 (1): 20–26. https://doi.org/10.1134/S1990519X18010030.

C, Raiborg, Bache Kg, Gillooly Dj, Madshus Ih, Stang E, and Stenmark H. 2002. "Hrs Sorts Ubiquitinated Proteins into Clathrin-Coated Microdomains of Early Endosomes." *Nature Cell Biology* 4 (5). https://doi.org/10.1038/ncb791.

Cai, Jing, Huijuan Tang, Linjuan Xu, Xiaoyi Wang, Chun Yang, Shasha Ruan, Jianfeng Guo, Sha Hu, and Zehua Wang. 2012. "Fibroblasts in Omentum Activated by Tumor Cells Promote Ovarian Cancer Growth, Adhesion and Invasiveness." *Carcinogenesis* 33 (1): 20–29. https://doi.org/10.1093/carcin/bgr230.

Carey, Preston, Ethan Low, Elizabeth Harper, and M. Sharon Stack. 2021. "Metalloproteinases in Ovarian Cancer." *International Journal of Molecular Sciences* 22 (7): 3403. https://doi.org/10.3390/ijms22073403.

Carrà, Giovanna, Marcello Francesco Lingua, Beatrice Maffeo, Riccardo Taulli, and Alessandro Morotti. 2020. "P53 vs NF-κB: The Role of Nuclear Factor-Kappa B in the Regulation of P53 Activity and Vice Versa." *Cellular and Molecular Life Sciences* 77 (22): 4449–58. https://doi.org/10.1007/s00018-020-03524-9.

Chang, Nan-Shan. 2002. “The Non-Ankyrin C Terminus of IκBα Physically Interacts with P53 in Vivo and Dissociates in Response to Apoptotic Stress, Hypoxia, DNA Damage, and Transforming Growth Factor-B1-Mediated Growth Suppression.” *Journal of Biological Chemistry* 277 (12): 10323–31. https://doi.org/10.1074/jbc.M106607200.

Chen, Edward Y., Christopher M. Tan, Yan Kou, Qiaonan Duan, Zichen Wang, Gabriela Vaz Meirelles, Neil R. Clark, and Avi Ma’ayan. 2013. “Enrichr: Interactive and Collaborative HTML5 Gene List Enrichment Analysis Tool.” *BMC Bioinformatics* 14 (April): 128. https://doi.org/10.1186/1471-2105-14-128.

Chen, Huizhi, Liyan Wang, Xinling Zeng, Herbert Schwarz, Himansu Sekhar Nanda, Xinsheng Peng, and Yubin Zhou. 2021. “Exosomes, a New Star for Targeted Delivery.” *Frontiers in Cell and Developmental Biology* 9 (October): 751079. https://doi.org/10.3389/fcell.2021.751079.

Cheng, J.-t, Y.-n Deng, H.-m Yi, G.-y Wang, B.-s Fu, W.-j Chen, W. Liu, Y. Tai, Y.-w Peng, and Q. Zhang. 2016. “Hepatic Carcinoma-Associated Fibroblasts Induce IDO-Producing Regulatory Dendritic Cells through IL-6-Mediated STAT3 Activation.” *Oncogenesis* 5 (2): e198–e198. https://doi.org/10.1038/oncsis.2016.7.

Cheng, Jung-Chien, Nelly Auersperg, and Peter C. K. Leung. 2012. “TGF-Beta Induces Serous Borderline Ovarian Tumor Cell Invasion by Activating EMT but Triggers Apoptosis in Low-Grade Serous Ovarian Carcinoma Cells.” Edited by Rakesh K. Srivastava. *PLoS ONE* 7 (8): e42436. https://doi.org/10.1371/journal.pone.0042436.

Cheteh, Emarndeena H., Victoria Sarne, Sophia Ceder, Julie Bianchi, Martin Augsten, Helene Rundqvist, Lars Egevad, Arne Östman, and Klas G. Wiman. 2020. “Interleukin-6 Derived from Cancer-Associated Fibroblasts Attenuates the P53 Response to Doxorubicin in Prostate Cancer Cells.” *Cell Death Discovery* 6 (1): 1–14. https://doi.org/10.1038/s41420-020-0272-5.

Chi, Tian-Yi, George G Chen, Lok-Kee Ho, and Paul BS Lai. 2005. “Establishment of a Doxycycline-Regulated Cell Line with Inducible, Doubly-Stable Expression of the Wild-Type P53 Gene from P53-Deleted Hepatocellular Carcinoma Cells.” *Cancer Cell International* 5 (August): 27. https://doi.org/10.1186/1475-2867-5-27.

Chiaradia, Elisabetta, Brunella Tancini, Carla Emiliani, Federica Delo, Roberto Maria Pellegrino, Alessia Tognoloni, Lorena Urbanelli, and Sandra Buratta. 2021. “Extracellular Vesicles under Oxidative Stress Conditions: Biological Properties and Physiological Roles.” *Cells* 10 (7): 1763. https://doi.org/10.3390/cells10071763.

Chien, Yuchen, Claudio Scuoppo, Xiaowo Wang, Xueping Fang, Brian Balgley, Jessica E. Bolden, Prem Premsrirut, et al. 2011. “Control of the Senescence-Associated Secretory Phenotype by NF-κB Promotes Senescence and Enhances Chemosensitivity.” *Genes & Development* 25 (20): 2125–36. https://doi.org/10.1101/gad.17276711.

Cho, Jung Ah, Ho Park, Eun Hye Lim, Kye Hyun Kim, Joong Sub Choi, Jung Hoon Lee, Jae Wook Shin, and Kyo Won Lee. 2011. “Exosomes from Ovarian Cancer Cells Induce Adipose Tissue-Derived Mesenchymal Stem Cells to Acquire the Physical and Functional Characteristics of Tumor-Supporting Myofibroblasts.” *Gynecologic Oncology* 123 (2): 379–86. https://doi.org/10.1016/j.ygyno.2011.08.005.

Clos-Sansalvador, Marta, Marta Monguió-Tortajada, Santiago Roura, Marcella Franquesa, and Francesc E. Borràs. 2022. “Commonly Used Methods for Extracellular Vesicles’ Enrichment: Implications in Downstream Analyses and Use.” *European Journal of Cell Biology* 101 (3): 151227. https://doi.org/10.1016/j.ejcb.2022.151227.

Collado, Manuel, Jesús Gil, Alejo Efeyan, Carmen Guerra, Alberto J. Schuhmacher, Marta Barradas, Alberto Benguría, et al. 2005. “Senescence in Premalignant Tumours.” *Nature* 436 (7051): 642–642. https://doi.org/10.1038/436642a.

Cooks, Tomer, Ioannis S. Pateras, Lisa M. Jenkins, Keval M. Patel, Ana I. Robles, James Morris, Tim Forshew, Ettore Appella, Vassilis G. Gorgoulis, and Curtis C. Harris. 2018. “Mutant P53 Cancers Reprogram Macrophages to Tumor Supporting Macrophages via Exosomal miR-1246.” *Nature Communications* 9 (1): 771. https://doi.org/10.1038/s41467-018-03224-w.

Coppé, Jean-Philippe, Pierre-Yves Desprez, Ana Krtolica, and Judith Campisi. 2010. “The Senescence-Associated Secretory Phenotype: The Dark Side of Tumor Suppression.” *Annual Review of Pathology* 5: 99–118. https://doi.org/10.1146/annurev-pathol-121808-102144.

Coppé, Jean-Philippe, Christopher K Patil, Francis Rodier, Yu Sun, Denise P Muñoz, Joshua Goldstein, Peter S Nelson, Pierre-Yves Desprez, and Judith Campisi. 2008. “Senescence-Associated Secretory Phenotypes Reveal Cell-Nonautonomous Functions of Oncogenic RAS and the P53 Tumor Suppressor.” Edited by Julian Downward. *PLoS Biology* 6 (12): e301. https://doi.org/10.1371/journal.pbio.0060301.

Dieudé, Mélanie, Christina Bell, Julie Turgeon, Deborah Beillevaire, Luc Pomerleau, Bing Yang, Katia Hamelin, et al. 2015. “The 20S Proteasome Core, Active within Apoptotic Exosome-like Vesicles, Induces Autoantibody Production and Accelerates Rejection.” *Science Translational Medicine* 7 (318): 318ra200-318ra200. https://doi.org/10.1126/scitranslmed.aac9816.

Domcke, Silvia, Rileen Sinha, Douglas A. Levine, Chris Sander, and Nikolaus Schultz. 2013. “Evaluating Cell Lines as Tumour Models by Comparison of Genomic Profiles.” *Nature Communications* 4 (1): 2126. https://doi.org/10.1038/ncomms3126.

Dores, Michael R., Buxin Chen, Huilan Lin, Unice J.K. Soh, May M. Paing, William A. Montagne, Timo Meerloo, and JoAnn Trejo. 2012. “ALIX Binds a YPX3L Motif of the GPCR PAR1 and Mediates Ubiquitin-Independent ESCRT-III/MVB Sorting.” *The Journal of Cell Biology* 197 (3): 407–19. https://doi.org/10.1083/jcb.201110031.

Doyle, Laura M., and Michael Zhuo Wang. 2019. “Overview of Extracellular Vesicles, Their Origin, Composition, Purpose, and Methods for Exosome Isolation and Analysis.” *Cells* 8 (7): 727. https://doi.org/10.3390/cells8070727.

Dunphy, Gillian, Sinéad M. Flannery, Jessica F. Almine, Dympna J. Connolly, Christina Paulus, Kasper L. Jønsson, Martin R. Jakobsen, Michael M. Nevels, Andrew G. Bowie, and Leonie Unterholzner. 2018. “Non-Canonical Activation of the DNA Sensing Adaptor STING by ATM and IFI16 Mediates NF-κB Signaling after Nuclear DNA Damage.” *Molecular Cell* 71 (5): 745-760.e5. https://doi.org/10.1016/j.molcel.2018.07.034.

Dvorak, H. F. 1986. “Tumors: Wounds That Do Not Heal. Similarities between Tumor Stroma Generation and Wound Healing.” *The New England Journal of Medicine* 315 (26): 1650–59. https://doi.org/10.1056/NEJM198612253152606.

Escrevente, Cristina, Sascha Keller, Peter Altevogt, and Júlia Costa. 2011. “Interaction and Uptake of Exosomes by Ovarian Cancer Cells.” *BMC Cancer* 11 (March): 108. https://doi.org/10.1186/1471-2407-11-108.

Fan, Yihui, Renfang Mao, and Jianhua Yang. 2013. “NF-κB and STAT3 Signaling Pathways Collaboratively Link Inflammation to Cancer.” *Protein & Cell* 4 (3): 176. https://doi.org/10.1007/s13238-013-2084-3.

Fang, Zengli, Qingcai Meng, Jin Xu, Wei Wang, Bo Zhang, Jiang Liu, Chen Liang, et al. 2022. “Signaling Pathways in Cancer-associated Fibroblasts: Recent Advances

and Future Perspectives." *Cancer Communications* 43 (1): 3–41. https://doi.org/10.1002/cac2.12392.

Farhang Ghahremani, M, S Goossens, D Nittner, X Bisteau, S Bartunkova, A Zwolinska, P Hulpiau, et al. 2013. "P53 Promotes VEGF Expression and Angiogenesis in the Absence of an Intact P21-Rb Pathway." *Cell Death and Differentiation* 20 (7): 888–97. https://doi.org/10.1038/cdd.2013.12.

Felicetti, Federica, Isabella Parolini, Lisabianca Bottero, Katia Fecchi, Maria Cristina Errico, Carla Raggi, Mauro Biffoni, et al. 2009. "Caveolin-1 Tumor-Promoting Role in Human Melanoma." *International Journal of Cancer. Journal International Du Cancer* 125 (7): 1514–22. https://doi.org/10.1002/ijc.24451.

Feng, Du, Wen-Long Zhao, Yun-Ying Ye, Xiao-Chen Bai, Rui-Qin Liu, Lei-Fu Chang, Qiang Zhou, and Sen-Fang Sui. 2010. "Cellular Internalization of Exosomes Occurs through Phagocytosis." *Traffic (Copenhagen, Denmark)* 11 (5): 675–87. https://doi.org/10.1111/j.1600-0854.2010.01041.x.

Feroz, Wasim, and Arwah Mohammad Ali Sheikh. 2020. "Exploring the Multiple Roles of Guardian of the Genome: P53." *Egyptian Journal of Medical Human Genetics* 21 (1): 49. https://doi.org/10.1186/s43042-020-00089-x.

Fischer, M. 2017. "Census and Evaluation of P53 Target Genes." *Oncogene* 36 (28): 3943–56. https://doi.org/10.1038/onc.2016.502.

Fisher, Daniel T., Qing Chen, Joseph J. Skitzki, Jason B. Muhitch, Lei Zhou, Michelle M. Appenheimer, Trupti D. Vardam, et al. 2011. "IL-6 Trans-Signaling Licenses Mouse and Human Tumor Microvascular Gateways for Trafficking of Cytotoxic T Cells." *The Journal of Clinical Investigation* 121 (10): 3846–59. https://doi.org/10.1172/JCI44952.

Foroutan, Behzad. 2023. "A Narrative Review of the TP53 and Its Product the P53 Protein." *OBM Genetics* 7 (3): 1–71. https://doi.org/10.21926/obm.genet.2302185.

Freed-Pastor, William A., and Carol Prives. 2012. "Mutant P53: One Name, Many Proteins." *Genes & Development* 26 (12): 1268–86. https://doi.org/10.1101/gad.190678.112.

Freund, Adam, Remi-Martin Laberge, Marco Demaria, and Judith Campisi. 2012. "Lamin B1 Loss Is a Senescence-Associated Biomarker." Edited by Thomas M. Magin. *Molecular Biology of the Cell* 23 (11): 2066–75. https://doi.org/10.1091/mbc.e11-10-0884.

Freund, Adam, Christopher K. Patil, and Judith Campisi. 2011. "p38MAPK Is a Novel DNA Damage Response-Independent Regulator of the Senescence-Associated Secretory Phenotype." *The EMBO Journal* 30 (8): 1536–48. https://doi.org/10.1038/emboj.2011.69.

Fu, Xuanrong, Qimeng Wang, Hang Du, and Huifang Hao. 2023. "CXCL8 and the Peritoneal Metastasis of Ovarian and Gastric Cancer." *Frontiers in Immunology* 14 (June): 1159061. https://doi.org/10.3389/fimmu.2023.1159061.

Gao, Qinglei, Zongyuan Yang, Sen Xu, Xiaoting Li, Xin Yang, Ping Jin, Yi Liu, et al. 2019. "Heterotypic CAF-Tumor Spheroids Promote Early Peritoneal Metastasis of Ovarian Cancer." *Journal of Experimental Medicine* 216 (3): 688–703. https://doi.org/10.1084/jem.20180765.

Ghasemi, Mahshid, Tyron Turnbull, Sonia Sebastian, and Ivan Kempson. 2021. "The MTT Assay: Utility, Limitations, Pitfalls, and Interpretation in Bulk and Single-Cell Analysis." *International Journal of Molecular Sciences* 22 (23): 12827. https://doi.org/10.3390/ijms222312827.

Gill, David J., Hsiangling Teo, Ji Sun, Olga Perisic, Dmitry B. Veprintsev, Scott D. Emr, and Roger L. Williams. 2007. "Structural Insight into the ESCRT-I/-II Link and Its Role in MVB Trafficking." *The EMBO Journal* 26 (2): 600–612. https://doi.org/10.1038/sj.emboj.7601501.

Giusti, Ilaria, Marianna Di Francesco, Sandra D' Ascenzo, Maria Grazia Palmerini, Guido Macchiarelli, Gaspare Carta, and Vincenza Dolo. 2018. "Ovarian Cancer-Derived Extracellular Vesicles Affect Normal Human Fibroblast Behavior." *Cancer Biology & Therapy*, March, 1–44. https://doi.org/10.1080/15384047.2018.1451286.

Givel, Anne-Marie, Yann Kieffer, Alix Scholer-Dahirel, Philemon Sirven, Melissa Cardon, Floriane Pelon, Ilaria Magagna, et al. 2018. "miR200-Regulated CXCL12β Promotes Fibroblast Heterogeneity and Immunosuppression in Ovarian Cancers." *Nature Communications* 9. https://doi.org/10.1038/s41467-018-03348-z.

Gobbo, Jessica, Guillaume Marcion, Marine Cordonnier, Alexandre M. M. Dias, Nicolas Pernet, Arlette Hammann, Sarah Richaud, et al. 2016. "Restoring Anticancer Immune Response by Targeting Tumor-Derived Exosomes With a HSP70 Peptide Aptamer." *Journal of the National Cancer Institute* 108 (3). https://doi.org/10.1093/jnci/djv330.

Göhler, Thomas, Stefan Jäger, Gabriele Warnecke, Hideyo Yasuda, Ella Kim, and Wolfgang Deppert. 2005. "Mutant P53 Proteins Bind DNA in a DNA Structure-Selective Mode." *Nucleic Acids Research* 33 (3): 1087–1100. https://doi.org/10.1093/nar/gki252.

Gong, Cheng, Zongyuan Yang, Fenghua Wu, Lintao Han, Yi Liu, and Wei Gong. 2016. "miR-17 Inhibits Ovarian Cancer Cell Peritoneal Metastasis by Targeting ITGA5 and ITGB1." *Oncology Reports* 36 (4): 2177–83. https://doi.org/10.3892/or.2016.4985.

Gonzalez, Veronica D., Ying-Wen Huang, Antonio Delgado-Gonzalez, Shih-Yu Chen, Kenyi Donoso, Karen Sachs, Andrew J. Gentles, et al. 2021. "High-Grade Serous Ovarian Tumor Cells Modulate NK Cell Function to Create an Immune-Tolerant Microenvironment." *Cell Reports* 36 (9): 109632. https://doi.org/10.1016/j.celrep.2021.109632.

Granot, Zvi, Erik Henke, Elizabeth A. Comen, Tari A. King, Larry Norton, and Robert Benezra. 2011. "Tumor Entrained Neutrophils Inhibit Seeding in the Premetastatic Lung." *Cancer Cell* 20 (3): 300–314. https://doi.org/10.1016/j.ccr.2011.08.012.

Gregory, Christopher D., and Ian Dransfield. 2018. "Apoptotic Tumor Cell-Derived Extracellular Vesicles as Important Regulators of the Onco-Regenerative Niche." *Frontiers in Immunology* 9 (May): 1111. https://doi.org/10.3389/fimmu.2018.01111.

Gregory, Christopher D, and Michael P Rimmer. 2023. "Extracellular Vesicles Arising from Apoptosis: Forms, Functions, and Applications." *The Journal of Pathology* 260 (5): 592–608. https://doi.org/10.1002/path.6138.

Groh, Veronika, Jennifer Wu, Cassian Yee, and Thomas Spies. 2002. "Tumour-Derived Soluble MIC Ligands Impair Expression of NKG2D and T-Cell Activation." *Nature* 419 (6908): 734–38. https://doi.org/10.1038/nature01112.

Guo, Bingjie, Yajing Wang, Wenyu Liu, and Sailong Zhang. 2023. "Cartilage Oligomeric Matrix Protein Acts as a Molecular Biomarker in Multiple Cancer Types." *Clinical & Translational Oncology: Official Publication of the Federation of Spanish Oncology Societies and of the National Cancer Institute of Mexico* 25 (2): 535–54. https://doi.org/10.1007/s12094-022-02968-8.

Gupta, Mamta, Ana Babic, Andrew H. Beck, and Kathryn Terry. 2016. "TNF-α Expression, Risk Factors, and Inflammatory Exposures in Ovarian Cancer: Evidence for an Inflammatory Pathway of Ovarian Carcinogenesis?" *Human Pathology* 54 (August): 82–91. https://doi.org/10.1016/j.humpath.2016.03.006.

Hadla, Mohamad, Stefano Palazzolo, Giuseppe Corona, Isabella Caligiuri, Vincenzo Canzonieri, Giuseppe Toffoli, and Flavio Rizzolio. 2016. "Exosomes Increase the Therapeutic Index of Doxorubicin in Breast and Ovarian Cancer Mouse Models."

Nanomedicine (London, England) 11 (18): 2431–41. https://doi.org/10.2217/nnm-2016-0154.

Hainaut, Pierre, and Gerd P. Pfeifer. 2016. “Somatic TP53 Mutations in the Era of Genome Sequencing.” *Cold Spring Harbor Perspectives in Medicine* 6 (11): a026179. https://doi.org/10.1101/cshperspect.a026179.

Hallas-Potts, Amelia, John C. Dawson, and C. Simon Herrington. 2019. “Ovarian Cancer Cell Lines Derived from Non-Serous Carcinomas Migrate and Invade More Aggressively than Those Derived from High-Grade Serous Carcinomas.” *Scientific Reports* 9 (1): 5515. https://doi.org/10.1038/s41598-019-41941-4.

Han, Heonjong, Hongseok Shim, Donghyun Shin, Jung Eun Shim, Yunhee Ko, Junha Shin, Hanhae Kim, et al. 2015. “TRRUST: A Reference Database of Human Transcriptional Regulatory Interactions.” *Scientific Reports* 5 (1): 11432. https://doi.org/10.1038/srep11432.

Hassin, Ori, Nishanth Belugali Nataraj, Michal Shreberk-Shaked, Yael Aylon, Rona Yaeger, Giulia Fontemaggi, Saptaparna Mukherjee, et al. 2022. “Different Hotspot P53 Mutants Exert Distinct Phenotypes and Predict Outcome of Colorectal Cancer Patients.” *Nature Communications* 13 (May): 2800. https://doi.org/10.1038/s41467-022-30481-7.

Hayashi, Yoshito, Masahiko Tsujii, Takahiro Kodama, Tomofumi Akasaka, Jumpei Kondo, Hayato Hikita, Takuya Inoue, et al. 2016. “P53 Functional Deficiency in Human Colon Cancer Cells Promotes Fibroblast-Mediated Angiogenesis and Tumor Growth.” *Carcinogenesis* 37 (10): 972–84. https://doi.org/10.1093/carcin/bgw085.

Hazelton, D., R. F. Nicosia, and S. V. Nicosia. 1999. “Vascular Endothelial Growth Factor Levels in Ovarian Cyst Fluid Correlate with Malignancy.” *Clinical Cancer Research: An Official Journal of the American Association for Cancer Research* 5 (4): 823–29.

He, Chuanshi, Linlin Wang, Ling Li, and Guiquan Zhu. 2021. “Extracellular Vesicle-Orchestrated Crosstalk between Cancer-Associated Fibroblasts and Tumors.” *Translational Oncology* 14 (12): 101231. https://doi.org/10.1016/j.tranon.2021.101231.

Hernández Borrero, Liz J., and Wafik S. El-Deiry. 2021. “Tumor Suppressor P53: Biology, Signaling Pathways, and Therapeutic Targeting.” *Biochimica et Biophysica Acta (BBA) - Reviews on Cancer* 1876 (1): 188556. https://doi.org/10.1016/j.bbcan.2021.188556.

Heyne, Kristina, Christine Winter, Fabian Gerten, Christina Schmidt, and Klaus Roemer. 2013. “A Novel Mechanism of Crosstalk between the P53 and NFκB Pathways: MDM2 Binds and Inhibits p65RelA.” *Cell Cycle* 12 (15): 2479–92. https://doi.org/10.4161/cc.25495.

Horbay, Rostyslav, Ali Hamraghani, Leonardo Ermini, Sophie Holcik, Shawn T. Beug, and Behzad Yeganeh. 2022. “Role of Ceramides and Lysosomes in Extracellular Vesicle Biogenesis, Cargo Sorting and Release.” *International Journal of Molecular Sciences* 23 (23): 15317. https://doi.org/10.3390/ijms232315317.

Hornburg, Milena, Mélanie Desbois, Shan Lu, Yinghui Guan, Amy A. Lo, Susan Kaufman, Ashley Elrod, et al. 2021. “Single-Cell Dissection of Cellular Components and Interactions Shaping the Tumor Immune Phenotypes in Ovarian Cancer.” *Cancer Cell* 39 (7): 928-944.e6. https://doi.org/10.1016/j.ccell.2021.04.004.

Hosein, Abdel Nasser, Min Wu, Suzanna L. Arcand, Sylvie Lavallée, Josée Hébert, Patricia N. Tonin, and Mark Basik. 2010. “Breast Carcinoma-Associated Fibroblasts Rarely Contain P53 Mutations or Chromosomal Aberrations.” *Cancer Research* 70 (14): 5770–77. https://doi.org/10.1158/0008-5472.CAN-10-0673.

Hoshino, Ayuko, Bruno Costa-Silva, Tang-Long Shen, Goncalo Rodrigues, Ayako Hashimoto, Milica Tesic Mark, Henrik Molina, et al. 2015. “Tumour Exosome Integrins Determine Organotropic Metastasis.” *Nature* 527 (7578): 329–35. https://doi.org/10.1038/nature15756.

Hu, Lingling, and Lanxiang Cong. 2015. “Fibroblast Growth Factor 19 Is Correlated with an Unfavorable Prognosis and Promotes Progression by Activating Fibroblast Growth Factor Receptor 4 in Advanced-Stage Serous Ovarian Cancer.” *Oncology Reports* 34 (5): 2683–91. https://doi.org/10.3892/or.2015.4212.

Huang, Weijun, LaTonya J. Hickson, Alfonso Eirin, James L. Kirkland, and Lilach O. Lerman. 2022. “Cellular Senescence: The Good, the Bad and the Unknown.” *Nature Reviews Nephrology* 18 (10): 611–27. https://doi.org/10.1038/s41581-022-00601-z.

Huang, Yimao, Ann V. Hertzel, Shayla R. Fish, Catherine L. Halley, Ellie K. Bohm, Hector Martell Martinez, Cameron C. Durfee, et al. 2023. “TP53/P53 Facilitates Stress-Induced Exosome and Protein Secretion by Adipocytes.” *Diabetes* 72 (11): 1560–73. https://doi.org/10.2337/db22-1027.

Huang, Zhiqing, Olivia Byrd, Sarah Tan, Katrina Hu, Bailey Knight, Gaomong Lo, Lila Taylor, Yuan Wu, Andrew Berchuck, and Susan K. Murphy. 2023. “Periostin Facilitates Ovarian Cancer Recurrence by Enhancing Cancer Stemness.” *Scientific Reports* 13 (1): 21382. https://doi.org/10.1038/s41598-023-48485-8.

Hwang, Jae Ryoung, Kiwon Jo, Yoonna Lee, Byung-Jun Sung, Young Woo Park, and Je-Ho Lee. 2012. “Upregulation of CD9 in Ovarian Cancer Is Related to the Induction of TNF-α Gene Expression and Constitutive NF-κB Activation.” *Carcinogenesis* 33 (1): 77–83. https://doi.org/10.1093/carcin/bgr257.

Ignacio, Rosa Mistica C., Eun-Sook Lee, Andrew J. Wilson, Alicia Beeghly-Fadiel, Margaret M. Whalen, and Deok-Soo Son. 2018. “Chemokine Network and Overall Survival in TP53 Wild-Type and Mutant Ovarian Cancer.” *Immune Network* 18 (4). https://doi.org/10.4110/in.2018.18.e29.

Ikeda, Akiko, Xiangao Sun, Yan Li, Yong-kang Zhang, Richard Eckner, Takahiro S. Doi, Toshitada Takahashi, Yuichi Obata, Katsuji Yoshioka, and Ken-ichi Yamamoto. 2000. “P300/CBP-Dependent and -Independent Transcriptional Interference between NF-κB RelA and P53.” *Biochemical and Biophysical Research Communications* 272 (2): 375–79. https://doi.org/10.1006/bbrc.2000.2786.

Inoue, Takanori, Yoshito Hayashi, Yoshiki Tsujii, Shunsuke Yoshii, Akihiko Sakatani, Keiichi Kimura, Ryotaro Uema, et al. 2021. “Suppression of Autophagy Promotes Fibroblast Activation in P53-Deficient Colorectal Cancer Cells.” *Scientific Reports* 11 (1): 19524. https://doi.org/10.1038/s41598-021-98865-1.

Ishimaru, Daniella, Luis M. T. R. Lima, Lenize F. Maia, Priscila M. Lopez, Ana P. Ano Bom, Ana P. Valente, and Jerson L. Silva. 2004. “Reversible Aggregation Plays a Crucial Role on the Folding Landscape of P53 Core Domain.” *Biophysical Journal* 87 (4): 2691–2700. https://doi.org/10.1529/biophysj.104.044685.

Izsvák, Zsuzsanna, and Zoltán Ivics. 2004. “Sleeping Beauty Transposition: Biology and Applications for Molecular Therapy.” *Molecular Therapy* 9 (2): 147–56. https://doi.org/10.1016/j.ymthe.2003.11.009.

Jahn, Reinhard, and Richard H. Scheller. 2006. “SNAREs — Engines for Membrane Fusion.” *Nature Reviews Molecular Cell Biology* 7 (9): 631–43. https://doi.org/10.1038/nrm2002.

Johnson, D. G., and R. Schneider-Broussard. 1998. “Role of E2F in Cell Cycle Control and Cancer.” *Frontiers in Bioscience: A Journal and Virtual Library* 3 (April): d447-448. https://doi.org/10.2741/a291.

Jong, Olivier G. de, Marianne C. Verhaar, Yong Chen, Pieter Vader, Hendrik Gremmels, George Posthuma, Raymond M. Schiffelers, Marjan Gucek, and Bas W.M. van Balkom. 2012. “Cellular Stress Conditions Are Reflected in the Protein and RNA

Content of Endothelial Cell-Derived Exosomes." *Journal of Extracellular Vesicles* 1 (1): 18396. https://doi.org/10.3402/jev.v1i0.18396.

Joshi, Bhagyashree S., Marit A. de Beer, Ben N. G. Giepmans, and Inge S. Zuhorn. 2020. "Endocytosis of Extracellular Vesicles and Release of Their Cargo from Endosomes." *ACS Nano* 14 (4): 4444. https://doi.org/10.1021/acsnano.9b10033.

Jouida, Amina, Cormac McCarthy, Aurelie Fabre, and Michael P. Keane. 2021. "Exosomes: A New Perspective in EGFR-Mutated Lung Cancer." *Cancer Metastasis Reviews* 40 (2): 589–601. https://doi.org/10.1007/s10555-021-09962-6.

Ju, Qiang, Lina Zhao, Jiajia Gao, Lanping Zhou, Yang Xu, Yulin Sun, and Xiaohang Zhao. 2019. "Mutant P53 Increases Exosome-Mediated Transfer of miR-21-3p and miR-769-3p to Promote Pulmonary Metastasis." *Chinese Journal of Cancer Research* 31 (3): 533–46. https://doi.org/10.21147/j.issn.1000-9604.2019.03.15.

Kalluri, Raghu. n.d. "The Biology and Function of Exosomes in Cancer." *The Journal of Clinical Investigation* 126 (4): 1208–15. https://doi.org/10.1172/JCI81135.

Kalluri, Raghu, and Valerie S. LeBleu. 2020. "The Biology, Function, and Biomedical Applications of Exosomes." *Science* 367 (6478). https://doi.org/10.1126/science.aau6977.

Kang, Tae-Won, Tetyana Yevsa, Norman Woller, Lisa Hoenicke, Torsten Wuestefeld, Daniel Dauch, Anja Hohmeyer, et al. 2011. "Senescence Surveillance of Pre-Malignant Hepatocytes Limits Liver Cancer Development." *Nature* 479 (7374): 547–51. https://doi.org/10.1038/nature10599.

Keerthikumar, Shivakumar, David Chisanga, Dinuka Ariyaratne, Haidar Al Saffar, Sushma Anand, Kening Zhao, Monisha Samuel, et al. 2016. "ExoCarta: A Web-Based Compendium of Exosomal Cargo." *Journal of Molecular Biology* 428 (4): 688–92. https://doi.org/10.1016/j.jmb.2015.09.019.

Kelleher, Raymond J., Sathy Balu-Iyer, Jenni Loyall, Anthony J. Sacca, Gautam N. Shenoy, Peng Peng, Vandana Iyer, et al. 2015. "Extracellular Vesicles Present in Human Ovarian Tumor Microenvironments Induce a Phosphatidylserine-Dependent Arrest in the T-Cell Signaling Cascade." *Cancer Immunology Research* 3 (11): 1269–78. https://doi.org/10.1158/2326-6066.CIR-15-0086.

Kenny, Hilary A., Chun-Yi Chiang, Erin A. White, Elizabeth M. Schryver, Mohammed Habis, Iris L. Romero, Andras Ladanyi, et al. 2014. "Mesothelial Cells Promote Early Ovarian Cancer Metastasis through Fibronectin Secretion." *The Journal of Clinical Investigation* 124 (10): 4614–28. https://doi.org/10.1172/JCI74778.

Kieffer, Yann, Hocine R. Hocine, Géraldine Gentric, Floriane Pelon, Charles Bernard, Brigitte Bourachot, Sonia Lameiras, et al. 2020. "Single-Cell Analysis Reveals Fibroblast Clusters Linked to Immunotherapy Resistance in Cancer." *Cancer Discovery* 10 (9): 1330–51. https://doi.org/10.1158/2159-8290.CD-19-1384.

Kim, D.-Y., W. Kim, K.-H. Lee, S.-H. Kim, H.-R. Lee, H.-J. Kim, Y. Jung, J.-H. Choi, and K.-T. Kim. 2013. "hnRNP Q Regulates Translation of P53 in Normal and Stress Conditions." *Cell Death and Differentiation* 20 (2): 226–34. https://doi.org/10.1038/cdd.2012.109.

Kim, E., and W. Deppert. 2007. "Interactions of Mutant P53 with DNA: Guilt by Association." *Oncogene* 26 (15): 2185–90. https://doi.org/10.1038/sj.onc.1210312.

Kim, Hyun-Jung, Hye Jin Kim, Mi-Kyung Kim, Moon Kyoung Bae, Hye Youn Sung, Jung-Hyuck Ahn, Yun Hwan Kim, Seung Cheol Kim, and Woong Ju. 2019. "SPSB1 Enhances Ovarian Cancer Cell Survival by Destabilizing P21." *Biochemical and Biophysical Research Communications* 510 (3): 364–69. https://doi.org/10.1016/j.bbrc.2019.01.088.

Kim, Michael P., and Guillermina Lozano. 2018. "Mutant P53 Partners in Crime." *Cell Death and Differentiation* 25 (1): 161–68. https://doi.org/10.1038/cdd.2017.185.

Kim, Min Kyu, Mun Ju Choi, Hyun Min Lee, Hong Seo Choi, Young-Kwon Park, and Chun Jeih Ryu. 2021. “Heterogeneous Nuclear Ribonucleoprotein A2/B1 Regulates the ERK and P53/HDM2 Signaling Pathways to Promote the Survival, Proliferation and Migration of Non-small Cell Lung Cancer Cells.” *Oncology Reports* 46 (2): 1–10. https://doi.org/10.3892/or.2021.8104.

Kim, Sang Bum. 2022. “Function and Therapeutic Development of Exosomes for Cancer Therapy.” *Archives of Pharmacal Research* 45 (5): 295–308. https://doi.org/10.1007/s12272-022-01387-1.

Kim, Tae Wan, So Yeon Koo, Markus Riessland, Hyunwoo Cho, Fayzan Chaudhry, Benjamin Kolisnyk, Marco Vincenzo Russo, et al. 2023. “TNF-NFkB-P53 Axis Restricts in Vivo Survival of hPSC-Derived Dopamine Neuron.” bioRxiv. https://doi.org/10.1101/2023.03.29.534819.

Komarova, Elena A, Luda Diatchenko, Oskar W Rokhlin, Jason E Hill, Zhaohui J Wang, Vadim I Krivokrysenko, Elena Feinstein, and Andrei V Gudkov. 1998. “Stress-Induced Secretion of Growth Inhibitors: A Novel Tumor Suppressor Function of P53.” *Oncogene* 17 (9): 1089–96. https://doi.org/10.1038/sj.onc.1202303.

Kortlever, Roderik M., Paul J. Higgins, and René Bernards. 2006. “Plasminogen Activator Inhibitor-1 Is a Critical Downstream Target of P53 in the Induction of Replicative Senescence.” *Nature Cell Biology* 8 (8): 877–84. https://doi.org/10.1038/ncb1448.

Kowarz, Eric, Denise Löscher, and Rolf Marschalek. 2015. “Optimized Sleeping Beauty Transposons Rapidly Generate Stable Transgenic Cell Lines.” *Biotechnology Journal* 10 (4): 647–53. https://doi.org/10.1002/biot.201400821.

Kress, M., E. May, R. Cassingena, and P. May. 1979. “Simian Virus 40-Transformed Cells Express New Species of Proteins Precipitable by Anti-Simian Virus 40 Tumor Serum.” *Journal of Virology* 31 (2): 472–83. https://doi.org/10.1128/JVI.31.2.472-483.1979.

Kumari, Asha, Zainab Shonibare, Mehri Monavarian, Rebecca C. Arend, Nam Y. Lee, Gareth J. Inman, and Karthikeyan Mythreye. 2021. “TGFβ Signaling Networks in Ovarian Cancer Progression and Plasticity.” *Clinical & Experimental Metastasis* 38 (2): 139–61. https://doi.org/10.1007/s10585-021-10077-z.

Labidi-Galy, S. Intidhar, Eniko Papp, Dorothy Hallberg, Noushin Niknafs, Vilmos Adleff, Michael Noe, Rohit Bhattacharya, et al. 2017. “High Grade Serous Ovarian Carcinomas Originate in the Fallopian Tube.” *Nature Communications* 8 (1): 1093. https://doi.org/10.1038/s41467-017-00962-1.

Ladanyi, Andras, Abir Mukherjee, Hilary A. Kenny, Alyssa Johnson, Anirban K. Mitra, Sinju Sundaresan, Kristin M. Nieman, et al. 2018. “Adipocyte-Induced CD36 Expression Drives Ovarian Cancer Progression and Metastasis.” *Oncogene* 37 (17): 2285–2301. https://doi.org/10.1038/s41388-017-0093-z.

Larios, Jorge, Vincent Mercier, Aurélien Roux, and Jean Gruenberg. 2020. “ALIX- and ESCRT-III–Dependent Sorting of Tetraspanins to Exosomes.” *Journal of Cell Biology* 219 (3). https://doi.org/10.1083/jcb.201904113.

Lau, T.-S., L. K.-Y. Chan, E. C.-H. Wong, C. W.-C. Hui, K. Sneddon, T.-H. Cheung, S.-F. Yim, et al. 2017. “A Loop of Cancer-Stroma-Cancer Interaction Promotes Peritoneal Metastasis of Ovarian Cancer via TNFα-TGFα-EGFR.” *Oncogene* 36 (25): 3576–87. https://doi.org/10.1038/onc.2016.509.

Lee, Amy H., Deepraj Ghosh, Nhat Quach, Devin Schroeder, and Michelle R. Dawson. 2020. “Ovarian Cancer Exosomes Trigger Differential Biophysical Response in Tumor-Derived Fibroblasts.” *Scientific Reports* 10 (1): 8686. https://doi.org/10.1038/s41598-020-65628-3.

Leroy, Bernard, Luc Girard, Antoinette Hollestelle, John D. Minna, Adi F. Gazdar, and Thierry Soussi. 2014. “Analysis of TP53 Mutation Status in Human Cancer Cell

Lines: A Reassessment." *Human Mutation* 35 (6): 756–65. https://doi.org/10.1002/humu.22556.

Li, Chanyuan, Ting Deng, Junya Cao, Yun Zhou, Xiaolin Luo, Yanling Feng, He Huang, and Jihong Liu. 2023. "Identifying ITGB2 as a Potential Prognostic Biomarker in Ovarian Cancer." *Diagnostics* 13 (6). https://doi.org/10.3390/diagnostics13061169.

Li, Jinghuan, Yi Lee, Henrik J. Johansson, Imre Mäger, Pieter Vader, Joel Z. Nordin, Oscar P. B. Wiklander, Janne Lehtiö, Matthew J. A. Wood, and Samir EL Andaloussi. 2015. "Serum-Free Culture Alters the Quantity and Protein Composition of Neuroblastoma-Derived Extracellular Vesicles." *Journal of Extracellular Vesicles* 4. https://doi.org/10.3402/jev.v4.26883.

Li, Jun, Jiawen Xu, Luhan Li, Alessandro Ianni, Poonam Kumari, Shuo Liu, Peiqing Sun, et al. 2020. "MGAT3-Mediated Glycosylation of Tetraspanin CD82 at Asparagine 157 Suppresses Ovarian Cancer Metastasis by Inhibiting the Integrin Signaling Pathway." *Theranostics* 10 (14): 6467–82. https://doi.org/10.7150/thno.43865.

Li, Xiaoduan, Meiling Tang, Qinyi Zhu, Xinjing Wang, Yingying Lin, and Xipeng Wang. 2020. "The Exosomal Integrin A5β1/AEP Complex Derived from Epithelial Ovarian Cancer Cells Promotes Peritoneal Metastasis through Regulating Mesothelial Cell Proliferation and Migration." *Cellular Oncology* 43 (2): 263–77. https://doi.org/10.1007/s13402-019-00486-4.

Lin, Guohe, Jin Wang, Xiangming Lao, Jun Wang, Lian Li, Shuhong Li, Jinye Zhang, et al. 2012. "Interleukin-6 Inhibits Regulatory T Cells and Improves the Proliferation and Cytotoxic Activity of Cytokine-Induced Killer Cells." *Journal of Immunotherapy (Hagerstown, Md.: 1997)* 35 (4): 337–43. https://doi.org/10.1097/CJI.0b013e318255ada3.

Lin, J., J. Chen, B. Elenbaas, and A. J. Levine. 1994. "Several Hydrophobic Amino Acids in the P53 Amino-Terminal Domain Are Required for Transcriptional Activation, Binding to Mdm-2 and the Adenovirus 5 E1B 55-kD Protein." *Genes & Development* 8 (10): 1235–46. https://doi.org/10.1101/gad.8.10.1235.

Lin, Jiayuh, Huaijing Tang, Xiaohong Jin, Guiyue Jia, and Jer-Tsong Hsieh. 2002. "P53 Regulates Stat3 Phosphorylation and DNA Binding Activity in Human Prostate Cancer Cells Expressing Constitutively Active Stat3." *Oncogene* 21 (19): 3082–88. https://doi.org/10.1038/sj.onc.1205426.

Liu, Qing, Biao Yu, Yingbin Tian, Juhua Dan, Ying Luo, and Xiaoming Wu. 2020. "P53 Mutant p53N236S Regulates Cancer-Associated Fibroblasts Properties Through Stat3 Pathway." *OncoTargets and Therapy* 13: 1355–63. https://doi.org/10.2147/OTT.S229065.

Liu, Ting-Ting, Xi-Sheng Liu, Meng Zhang, Xue-Ni Liu, Fu-Xiang Zhu, Fang-Ming Zhu, Si-Wen Ouyang, et al. 2018. "Cartilage Oligomeric Matrix Protein Is a Prognostic Factor and Biomarker of Colon Cancer and Promotes Cell Proliferation by Activating the Akt Pathway." *Journal of Cancer Research and Clinical Oncology* 144 (6): 1049–63. https://doi.org/10.1007/s00432-018-2626-4.

Liu, Yanan, Meng Cao, Yuepiao Cai, Xiaokun Li, Chengguang Zhao, and Ri Cui. 2020. "Dissecting the Role of the FGF19-FGFR4 Signaling Pathway in Cancer Development and Progression." *Frontiers in Cell and Developmental Biology* 8 (February): 95. https://doi.org/10.3389/fcell.2020.00095.

Lopes-Paciencia, Stéphane, Emmanuelle Saint-Germain, Marie-Camille Rowell, Ana Fernández Ruiz, Paloma Kalegari, and Gerardo Ferbeyre. 2019. "The Senescence-Associated Secretory Phenotype and Its Regulation." *Cytokine* 117 (May): 15–22. https://doi.org/10.1016/j.cyto.2019.01.013.

López-Lago, M. A., S. Posner, V. J. Thodima, A. M. Molina, R. J. Motzer, and R. S. K. Chaganti. 2013. "Neutrophil Chemokines Secreted by Tumor Cells Mount a Lung

Antimetastatic Response during Renal Cell Carcinoma Progression." *Oncogene* 32 (14): 1752–60. https://doi.org/10.1038/onc.2012.201.

Lowe, Julie M., Daniel Menendez, Pierre R. Bushel, Maria Shatz, Erin L. Kirk, Melissa A. Troester, Stavros Garantziotis, Michael B. Fessler, and Michael A. Resnick. 2014. "P53 and NF-κB Coregulate Proinflammatory Gene Responses in Human Macrophages." *Cancer Research* 74 (8): 2182–92. https://doi.org/10.1158/0008-5472.CAN-13-1070.

Lu, Quan, Lila Weiqiao Hope, Michael Brasch, Christoph Reinhard, and Stanley N. Cohen. 2003. "TSG101 Interaction with HRS Mediates Endosomal Trafficking and Receptor Down-Regulation." *Proceedings of the National Academy of Sciences* 100 (13): 7626–31. https://doi.org/10.1073/pnas.0932599100.

Lukashchuk, Natalia, and Karen H. Vousden. 2007. "Ubiquitination and Degradation of Mutant P53." *Molecular and Cellular Biology* 27 (23): 8284–95. https://doi.org/10.1128/MCB.00050-07.

M, Cerezo-Magaña, Christianson Hc, van Kuppevelt Th, Forsberg-Nilsson K, and Belting M. 2021. "Hypoxic Induction of Exosome Uptake through Proteoglycan-Dependent Endocytosis Fuels the Lipid Droplet Phenotype in Glioma." *Molecular Cancer Research : MCR* 19 (3). https://doi.org/10.1158/1541-7786.MCR-20-0560.

Ma, He, Qingqing Qiu, Dan Tan, Qiaofeng Chen, Yaping Liu, Bing Chen, and Mingliang Wang. 2022. "The Cancer-Associated Fibroblasts-Related Gene COMP Is a Novel Predictor for Prognosis and Immunotherapy Efficacy and Is Correlated with M2 Macrophage Infiltration in Colon Cancer." *Biomolecules* 13 (1): 62. https://doi.org/10.3390/biom13010062.

Ma, Shaolin, Michael H. McGuire, Lingegowda S. Mangala, Sanghoon Lee, Elaine Stur, Wen Hu, Emine Bayraktar, et al. 2021. "Gain-of-Function P53 Protein Transferred via Small Extracellular Vesicles Promotes Conversion of Fibroblasts to a Cancer-Associated Phenotype." *Cell Reports* 34 (6): 108726. https://doi.org/10.1016/j.celrep.2021.108726.

MacArthur, Daniel G., Suganthi Balasubramanian, Adam Frankish, Ni Huang, James Morris, Klaudia Walter, Luke Jostins, et al. 2012. "A Systematic Survey of Loss-of-Function Variants in Human Protein-Coding Genes." *Science (New York, N.Y.)* 335 (6070): 823–28. https://doi.org/10.1126/science.1215040.

Mahiddine, Karim, Adam Blaisdell, Stephany Ma, Amandine Créquer-Grandhomme, Clifford A. Lowell, and Adrian Erlebacher. n.d. "Relief of Tumor Hypoxia Unleashes the Tumoricidal Potential of Neutrophils." *The Journal of Clinical Investigation* 130 (1): 389–403. https://doi.org/10.1172/JCI130952.

Mantovani, Fiamma, Licio Collavin, and Giannino Del Sal. 2019. "Mutant P53 as a Guardian of the Cancer Cell." *Cell Death & Differentiation* 26 (2): 199–212. https://doi.org/10.1038/s41418-018-0246-9.

Mashimo, Tomoyuki, Misako Watabe, Shigeru Hirota, Sadahiro Hosobe, Kunio Miura, Peter J. Tegtmeyer, Carrie W. Rinker-Shaeffer, and Kounosuke Watabe. 1998. "The Expression of the KAI1 Gene, a Tumor Metastasis Suppressor, Is Directly Activated by P53." *Proceedings of the National Academy of Sciences* 95 (19): 11307–11. https://doi.org/10.1073/pnas.95.19.11307.

Matulonis, Ursula A., Anil K. Sood, Lesley Fallowfield, Brooke E. Howitt, Jalid Sehouli, and Beth Y. Karlan. 2016. "Ovarian Cancer." *Nature Reviews Disease Primers* 2 (1): 16061. https://doi.org/10.1038/nrdp.2016.61.

Mazumdar, Alekhya, Joaquin Urdinez, Aleksandar Boro, Jessica Migliavacca, Matthias J. E. Arlt, Roman Muff, Bruno Fuchs, Jess Gerrit Snedeker, and Ana Gvozdenovic. 2020. "Osteosarcoma-Derived Extracellular Vesicles Induce Lung Fibroblast Reprogramming." *International Journal of Molecular Sciences* 21 (15): 5451. https://doi.org/10.3390/ijms21155451.

Mei, Shuangshuang, Xing Chen, Kai Wang, and Yuxin Chen. 2023. “Tumor Microenvironment in Ovarian Cancer Peritoneal Metastasis.” *Cancer Cell International* 23 (1): 11. https://doi.org/10.1186/s12935-023-02854-5.

Migneault, Francis, Mélanie Dieudé, Julie Turgeon, Déborah Beillevaire, Marie-Pierre Hardy, Alexandre Brodeur, Nicolas Thibodeau, Claude Perreault, and Marie-Josée Hébert. 2020. “Apoptotic Exosome-like Vesicles Regulate Endothelial Gene Expression, Inflammatory Signaling, and Function through the NF-κB Signaling Pathway.” *Scientific Reports* 10 (1): 12562. https://doi.org/10.1038/s41598-020-69548-0.

Mijit, Mahmut, Valentina Caracciolo, Antonio Melillo, Fernanda Amicarelli, and Antonio Giordano. 2020. “Role of P53 in the Regulation of Cellular Senescence.” *Biomolecules* 10 (3): 420. https://doi.org/10.3390/biom10030420.

Millimaggi, Danilo, Marianna Mari, Sandra D’Ascenzo, Eleonora Carosa, Emmanuele Angelo Jannini, Stanley Zucker, Gaspare Carta, Antonio Pavan, and Vincenza Dolo. 2007. “Tumor Vesicle-Associated CD147 Modulates the Angiogenic Capability of Endothelial Cells.” *Neoplasia (New York, N.Y.)* 9 (4): 349–57.

Motohara, Takeshi, Sachiko Masuko, Takatsugu Ishimoto, Toshifumi Yae, Nobuyuki Onishi, Teruyuki Muraguchi, Atsushi Hirao, et al. 2011. “Transient Depletion of P53 Followed by Transduction of C-Myc and K-Ras Converts Ovarian Stem-like Cells into Tumor-Initiating Cells.” *Carcinogenesis* 32 (11): 1597–1606. https://doi.org/10.1093/carcin/bgr183.

Muhl, Lars, Guillem Genové, Stefanos Leptidis, Jianping Liu, Liqun He, Giuseppe Mocci, Ying Sun, et al. 2020. “Single-Cell Analysis Uncovers Fibroblast Heterogeneity and Criteria for Fibroblast and Mural Cell Identification and Discrimination.” *Nature Communications* 11 (August): 3953. https://doi.org/10.1038/s41467-020-17740-1.

Mulcahy, Laura Ann, Ryan Charles Pink, and David Raul Francisco Carter. 2014. “Routes and Mechanisms of Extracellular Vesicle Uptake.” *Journal of Extracellular Vesicles* 3 (August): 10.3402/jev.v3.24641. https://doi.org/10.3402/jev.v3.24641.

Muller, Patricia A. J., Patrick T. Caswell, Brendan Doyle, Marcin P. Iwanicki, Ee H. Tan, Saadia Karim, Natalia Lukashchuk, et al. 2009. “Mutant P53 Drives Invasion by Promoting Integrin Recycling.” *Cell* 139 (7): 1327–41. https://doi.org/10.1016/j.cell.2009.11.026.

Nakamura, Koji, Kenjiro Sawada, Yasuto Kinose, Akihiko Yoshimura, Aska Toda, Erika Nakatsuka, Kae Hashimoto, et al. 2017. “Exosomes Promote Ovarian Cancer Cell Invasion through Transfer of CD44 to Peritoneal Mesothelial Cells.” *Molecular Cancer Research: MCR* 15 (1): 78–92. https://doi.org/10.1158/1541-7786.MCR-16-0191.

Nakanishi, Y., J. Kodama, M. Yoshinouchi, K. Tokumo, S. Kamimura, H. Okuda, and T. Kudo. 1997. “The Expression of Vascular Endothelial Growth Factor and Transforming Growth Factor-Beta Associates with Angiogenesis in Epithelial Ovarian Cancer.” *International Journal of Gynecological Pathology: Official Journal of the International Society of Gynecological Pathologists* 16 (3): 256–62. https://doi.org/10.1097/00004347-199707000-00011.

Nakase, Ikuhiko, Natsumi Ueno, Mie Matsuzawa, Kosuke Noguchi, Mami Hirano, Mika Omura, Tomoya Takenaka, et al. 2021. “Environmental pH Stress Influences Cellular Secretion and Uptake of Extracellular Vesicles.” *FEBS Open Bio* 11 (3): 753–67. https://doi.org/10.1002/2211-5463.13107.

Neufeld, Gera, Yelena Mumblat, Tatyana Smolkin, Shira Toledano, Inbal Nir-Zvi, Keren Ziv, and Ofra Kessler. 2016. “The Role of the Semaphorins in Cancer.” *Cell Adhesion & Migration* 10 (6): 652–74. https://doi.org/10.1080/19336918.2016.1197478.

Niel, Guillaume van, Stéphanie Charrin, Sabrina Simoes, Maryse Romao, Leila Rochin, Paul Saftig, Michael S. Marks, Eric Rubinstein, and Graça Raposo. 2011. “The Tetraspanin CD63 Regulates ESCRT-Independent and Dependent Endosomal Sorting during Melanogenesis.” *Developmental Cell* 21 (4): 708–21. https://doi.org/10.1016/j.devcel.2011.08.019.

Niel, Guillaume van, Gisela D’Angelo, and Graça Raposo. 2018. “Shedding Light on the Cell Biology of Extracellular Vesicles.” *Nature Reviews Molecular Cell Biology* 19 (4): 213–28. https://doi.org/10.1038/nrm.2017.125.

Nieman, Kristin M., Hilary A. Kenny, Carla V. Penicka, Andras Ladanyi, Rebecca Buell-Gutbrod, Marion R. Zillhardt, Iris L. Romero, et al. 2011. “Adipocytes Promote Ovarian Cancer Metastasis and Provide Energy for Rapid Tumor Growth.” *Nature Medicine* 17 (11): 1498–1503. https://doi.org/10.1038/nm.2492.

Nieuwland, Rienk, Pia R. -M. Siljander, Juan M. Falcón-Pérez, and Kenneth W. Witwer. 2022. “Reproducibility of Extracellular Vesicle Research.” *European Journal of Cell Biology* 101 (3): 151226. https://doi.org/10.1016/j.ejcb.2022.151226.

Novo, David, Nikki Heath, Louise Mitchell, Giuseppina Caligiuri, Amanda MacFarlane, Dide Reijmer, Laura Charlton, et al. 2018. “Mutant P53s Generate Pro-Invasive Niches by Influencing Exosome Podocalyxin Levels.” *Nature Communications* 9 (November). https://doi.org/10.1038/s41467-018-07339-y.

Nunes, Mariana, and Sara Ricardo. 2022. “Chemoresistance in Ovarian Cancer: The Role of Malignant Ascites.” In *Ovarian Cancer*, edited by Shashikant Lele. Brisbane (AU): Exon Publications. http://www.ncbi.nlm.nih.gov/books/NBK585987/.

O’Brien, Killian, Stefano Ughetto, Shadi Mahjoum, Anil V. Nair, and Xandra O. Breakefield. 2022. “Uptake, Functionality, and Re-Release of Extracellular Vesicle-Encapsulated Cargo.” *Cell Reports* 39 (2): 110651. https://doi.org/10.1016/j.celrep.2022.110651.

O’Grady, Tina, Makon-Sébastien Njock, Michelle Lion, Jonathan Bruyr, Emeline Mariavelle, Bartimée Galvan, Amandine Boeckx, Ingrid Struman, and Franck Dequiedt. 2022. “Sorting and Packaging of RNA into Extracellular Vesicles Shape Intracellular Transcript Levels.” *BMC Biology* 20 (1): 72. https://doi.org/10.1186/s12915-022-01277-4.

Ohyagi-Hara, Chifumi, Kenjiro Sawada, Shoji Kamiura, Yasuhiko Tomita, Aki Isobe, Kae Hashimoto, Yasuto Kinose, et al. 2013. “miR-92a Inhibits Peritoneal Dissemination of Ovarian Cancer Cells by Inhibiting Integrin A5 Expression.” *The American Journal of Pathology* 182 (5): 1876–89. https://doi.org/10.1016/j.ajpath.2013.01.039.

Pachane, Bianca Cruz, Ana Carolina Caetano Nunes, Thais Regiani Cataldi, Kelli Cristina Micocci, Bianca Caruso Moreira, Carlos Alberto Labate, Heloisa Sobreiro Selistre-de-Araujo, and Wanessa Fernanda Altei. 2022. “Small Extracellular Vesicles from Hypoxic Triple-Negative Breast Cancer Cells Induce Oxygen-Dependent Cell Invasion.” *International Journal of Molecular Sciences* 23 (20): 12646. https://doi.org/10.3390/ijms232012646.

Park, Geun-Young, Harsh B. Pathak, Andrew K. Godwin, and Youngjoo Kwon. 2021. “Epithelial-Stromal Communication via CXCL1-CXCR2 Interaction Stimulates Growth of Ovarian Cancer Cells through P38 Activation.” *Cellular Oncology* 44 (1): 77–92. https://doi.org/10.1007/s13402-020-00554-0.

Park, Soo Jeong, Jeong Mi Kim, Jihyo Kim, Jaehark Hur, Sun Park, Kyongmin Kim, Ho-Joon Shin, and Yong-Joon Chwae. 2018. “Molecular Mechanisms of Biogenesis of Apoptotic Exosome-like Vesicles and Their Roles as Damage-Associated Molecular Patterns.” *Proceedings of the National Academy of Sciences* 115 (50): E11721–30. https://doi.org/10.1073/pnas.1811432115.

Parolini, Isabella, Cristina Federici, Carla Raggi, Luana Lugini, Simonetta Palleschi, Angelo De Milito, Carolina Coscia, et al. 2009. “Microenvironmental pH Is a Key Factor for Exosome Traffic in Tumor Cells.” *The Journal of Biological Chemistry* 284 (49): 34211–22. https://doi.org/10.1074/jbc.M109.041152.

Pathan, Mohashin, Pamali Fonseka, Sai V Chitti, Taeyoung Kang, Rahul Sanwlani, Jan Van Deun, An Hendrix, and Suresh Mathivanan. 2019. “Vesiclepedia 2019: A Compendium of RNA, Proteins, Lipids and Metabolites in Extracellular Vesicles.” *Nucleic Acids Research* 47 (D1): D516–19. https://doi.org/10.1093/nar/gky1029.

Pavlakis, Evangelos, Michelle Neumann, and Thorsten Stiewe. 2020. “Extracellular Vesicles: Messengers of P53 in Tumor–Stroma Communication and Cancer Metastasis.” *International Journal of Molecular Sciences* 21 (24). https://doi.org/10.3390/ijms21249648.

Pavlakis, Evangelos, and Thorsten Stiewe. 2020. “P53’s Extended Reach: The Mutant P53 Secretome.” *Biomolecules* 10 (2): 307. https://doi.org/10.3390/biom10020307.

Pedro, María Ángeles de, Esther López, Francisco Manuel González-Nuño, María Pulido, Verónica Álvarez, Ana María Marchena, Christian Preußer, et al. 2023. “Menstrual Blood-Derived Mesenchymal Stromal Cells: Impact of Preconditioning on the Cargo of Extracellular Vesicles as Potential Therapeutics.” *Stem Cell Research & Therapy* 14 (1): 187. https://doi.org/10.1186/s13287-023-03413-5.

Peng, Y., L. Chen, C. Li, W. Lu, and J. Chen. 2001. “Inhibition of MDM2 by Hsp90 Contributes to Mutant P53 Stabilization.” *The Journal of Biological Chemistry* 276 (44): 40583–90. https://doi.org/10.1074/jbc.M102817200.

Peng, Zhiwei, Zhiwei Tong, Zihao Ren, Manping Ye, and Kongwang Hu. 2023. “Cancer-Associated Fibroblasts and Its Derived Exosomes: A New Perspective for Reshaping the Tumor Microenvironment.” *Molecular Medicine* 29 (1): 66. https://doi.org/10.1186/s10020-023-00665-y.

Pfaffl, M. W. 2001. “A New Mathematical Model for Relative Quantification in Real-Time RT-PCR.” *Nucleic Acids Research* 29 (9): e45. https://doi.org/10.1093/nar/29.9.e45.

Pink, Ryan Charles, Priya Samuel, Davide Massa, Daniel Paul Caley, Susan Ann Brooks, and David Raul Francisco Carter. 2015. “The Passenger Strand, miR-21-3p, Plays a Role in Mediating Cisplatin Resistance in Ovarian Cancer Cells.” *Gynecologic Oncology* 137 (1): 143–51. https://doi.org/10.1016/j.ygyno.2014.12.042.

Plikus, Maksim V., Xiaojie Wang, Sarthak Sinha, Elvira Forte, Sean M. Thompson, Erica L. Herzog, Ryan R. Driskell, Nadia Rosenthal, Jeff Biernaskie, and Valerie Horsley. 2021. “Fibroblasts: Origins, Definitions, and Functions in Health and Disease.” *Cell* 184 (15): 3852–72. https://doi.org/10.1016/j.cell.2021.06.024.

Pogge von Strandmann, Elke, Silke Reinartz, Uwe Wager, and Rolf Müller. 2017. “Tumor–Host Cell Interactions in Ovarian Cancer: Pathways to Therapy Failure.” *Trends in Cancer* 3 (2): 137–48. https://doi.org/10.1016/j.trecan.2016.12.005.

Polireddy, Kishore, Kanchan Singh, Melissa Pruski, Neal C. Jones, Naveen V. Manisundaram, Pavani Ponnela, Michel Ouellette, et al. 2019. “Mutant p53R175H Promotes Cancer Initiation in the Pancreas by Stabilizing HSP70.” *Cancer Letters* 453 (July): 122–30. https://doi.org/10.1016/j.canlet.2019.03.047.

Poon, Ivan K. H., Michael A. F. Parkes, Lanzhou Jiang, Georgia K. Atkin-Smith, Rochelle Tixeira, Christopher D. Gregory, Dilara C. Ozkocak, et al. 2019. “Moving beyond Size and Phosphatidylserine Exposure: Evidence for a Diversity of Apoptotic Cell-Derived Extracellular Vesicles in Vitro.” *Journal of Extracellular Vesicles* 8 (1): 1608786. https://doi.org/10.1080/20013078.2019.1608786.

Pornillos, O. 2002. “Structure and Functional Interactions of the Tsg101 UEV Domain.” *The EMBO Journal* 21 (10): 2397–2406. https://doi.org/10.1093/emboj/21.10.2397.

Prahl, Magdalena, Anna Vilborg, Carina Palmberg, Hans Jörnvall, Charlotte Asker, and Klas G. Wiman. 2008. “The P53 Target Protein Wig-1 Binds hnRNP A2/B1 and RNA Helicase A via RNA.” *FEBS Letters* 582 (15): 2173–77. https://doi.org/10.1016/j.febslet.2008.04.065.

Procopio, Maria-Giuseppina, Csaba Laszlo, Dania Al Labban, Dong Eun Kim, Pino Bordignon, Seung-Hee Jo, Sandro Goruppi, et al. 2015. “Combined CSL and P53 Downregulation Promotes Cancer-Associated Fibroblast Activation.” *Nature Cell Biology* 17 (9): 1193–1204. https://doi.org/10.1038/ncb3228.

Punzón-Jiménez, Paula, Victor Lago, Santiago Domingo, Carlos Simón, and Aymara Mas. 2022. “Molecular Management of High-Grade Serous Ovarian Carcinoma.” *International Journal of Molecular Sciences* 23 (22): 13777. https://doi.org/10.3390/ijms232213777.

Qin, Gangjian, Raj Kishore, Christine M. Dolan, Marcy Silver, Andrea Wecker, Corinne N. Luedemann, Tina Thorne, et al. 2006. “Cell Cycle Regulator E2F1 Modulates Angiogenesis via P53-Dependent Transcriptional Control of VEGF.” *Proceedings of the National Academy of Sciences of the United States of America* 103 (29): 11015–20. https://doi.org/10.1073/pnas.0509533103.

Raiborg, C., B. Bremnes, A. Mehlum, D. J. Gillooly, A. D’Arrigo, E. Stang, and H. Stenmark. 2001. “FYVE and Coiled-Coil Domains Determine the Specific Localisation of Hrs to Early Endosomes.” *Journal of Cell Science* 114 (Pt 12): 2255–63. https://doi.org/10.1242/jcs.114.12.2255.

Ravi, R., B. Mookerjee, Y. van Hensbergen, G. C. Bedi, A. Giordano, W. S. El-Deiry, E. J. Fuchs, and A. Bedi. 1998. “P53-Mediated Repression of Nuclear Factor-kappaB RelA via the Transcriptional Integrator P300.” *Cancer Research* 58 (20): 4531–36.

Reiners, Katrin S., Daniela Topolar, Alexander Henke, Venkateswara R. Simhadri, Jörg Kessler, Maike Sauer, Martina Bessler, et al. 2013. “Soluble Ligands for NK Cell Receptors Promote Evasion of Chronic Lymphocytic Leukemia Cells from NK Cell Anti-Tumor Activity.” *Blood* 121 (18): 3658–65. https://doi.org/10.1182/blood-2013-01-476606.

Ribovski, Lais, Bhagyashree S. Joshi, Jie Gao, and Inge S. Zuhorn. 2023. “Breaking Free: Endocytosis and Endosomal Escape of Extracellular Vesicles.” *Extracellular Vesicles and Circulating Nucleic Acids* 4 (2): 283–305. https://doi.org/10.20517/evcna.2023.26.

Rickard, Brittany P., Christina Conrad, Aaron J. Sorrin, Mustafa Kemal Ruhi, Jocelyn C. Reader, Stephanie A. Huang, Walfre Franco, et al. 2021. “Malignant Ascites in Ovarian Cancer: Cellular, Acellular, and Biophysical Determinants of Molecular Characteristics and Therapy Response.” *Cancers* 13 (17): 4318. https://doi.org/10.3390/cancers13174318.

Ringuette Goulet, Cassandra, Geneviève Bernard, Sarah Tremblay, Stéphane Chabaud, Stéphane Bolduc, and Frédéric Pouliot. 2018. “Exosomes Induce Fibroblast Differentiation into Cancer-Associated Fibroblasts through TGFβ Signaling.” *Molecular Cancer Research* 16 (7): 1196–1204. https://doi.org/10.1158/1541-7786.MCR-17-0784.

Rodier, Francis, Jean-Philippe Coppé, Christopher K. Patil, Wieteke A. M. Hoeijmakers, Denise P. Muñoz, Saba R. Raza, Adam Freund, Eric Campeau, Albert R. Davalos, and Judith Campisi. 2009. “Persistent DNA Damage Signalling Triggers Senescence-Associated Inflammatory Cytokine Secretion.” *Nature Cell Biology* 11 (8): 973–79. https://doi.org/10.1038/ncb1909.

Rodier, Francis, Denise P. Muñoz, Robert Teachenor, Victoria Chu, Oanh Le, Dipa Bhaumik, Jean-Philippe Coppé, et al. 2011. “DNA-SCARS: Distinct Nuclear Structures That Sustain Damage-Induced Senescence Growth Arrest and Inflammatory Cytokine Secretion.” *Journal of Cell Science* 124 (1): 68–81. https://doi.org/10.1242/jcs.071340.

Rosati, Alessandra, Anna Basile, Raffaella D’Auria, Morena d’Avenia, Margot De Marco, Antonia Falco, Michelina Festa, et al. 2015. “BAG3 Promotes Pancreatic Ductal Adenocarcinoma Growth by Activating Stromal Macrophages.” *Nature Communications* 6 (1): 8695. https://doi.org/10.1038/ncomms9695.

Rouger-Gaudichon, Jérémie, Elie Cousin, Hélène Jakobczyk, Lydie Debaize, Anne-Gaëlle Rio, Anne Forestier, Marie-Pierre Arnaud, et al. 2022. “Hypoxia Regulates CD9 Expression and Dissemination of B Lymphoblasts.” *Leukemia Research* 123 (December): 106964. https://doi.org/10.1016/j.leukres.2022.106964.

Rovillain, E, L Mansfield, C Caetano, M Alvarez-Fernandez, O L Caballero, R H Medema, H Hummerich, and P S Jat. 2011. “Activation of Nuclear Factor-Kappa B Signalling Promotes Cellular Senescence.” *Oncogene* 30 (20): 2356–66. https://doi.org/10.1038/onc.2010.611.

Runz, Steffen, Sascha Keller, Christian Rupp, Alexander Stoeck, Yasmin Issa, Dominique Koensgen, Alexander Mustea, Jalid Sehouli, Glen Kristiansen, and Peter Altevogt. 2007. “Malignant Ascites-Derived Exosomes of Ovarian Carcinoma Patients Contain CD24 and EpCAM.” *Gynecologic Oncology* 107 (3): 563–71. https://doi.org/10.1016/j.ygyno.2007.08.064.

Ryan, Kevin M., Mary K. Ernst, Nancy R. Rice, and Karen H. Vousden. 2000. “Role of NF-κB in P53-Mediated Programmed Cell Death.” *Nature* 404 (6780): 892–97. https://doi.org/10.1038/35009130.

Sahai, Erik, Igor Astsaturov, Edna Cukierman, David G. DeNardo, Mikala Egeblad, Ronald M. Evans, Douglas Fearon, et al. 2020. “A Framework for Advancing Our Understanding of Cancer-Associated Fibroblasts.” *Nature Reviews Cancer* 20 (3): 174–86. https://doi.org/10.1038/s41568-019-0238-1.

Saison-Ridinger, Maya, Kathleen E. DelGiorno, Tejia Zhang, Annabelle Kraus, Randall French, Dawn Jaquish, Crystal Tsui, et al. 2017. “Reprogramming Pancreatic Stellate Cells via P53 Activation: A Putative Target for Pancreatic Cancer Therapy.” *PloS One* 12 (12): e0189051. https://doi.org/10.1371/journal.pone.0189051.

Samuel, Priya, Laura Ann Mulcahy, Fiona Furlong, Helen O. McCarthy, Susan Ann Brooks, Muller Fabbri, Ryan Charles Pink, and David Raul Francisco Carter. 2018. “Cisplatin Induces the Release of Extracellular Vesicles from Ovarian Cancer Cells That Can Induce Invasiveness and Drug Resistance in Bystander Cells.” *Philosophical Transactions of the Royal Society B: Biological Sciences* 373 (1737): 20170065. https://doi.org/10.1098/rstb.2017.0065.

Sankpal, Narendra V., Michael W. Willman, Timothy P. Fleming, John D. Mayfield, and William E. Gillanders. 2009. “Transcriptional Repression of Epithelial Cell Adhesion Molecule Contributes to P53 Control of Breast Cancer Invasion.” *Cancer Research* 69 (3): 753–57. https://doi.org/10.1158/0008-5472.CAN-08-2708.

Santangelo, Laura, Giorgio Giurato, Carla Cicchini, Claudia Montaldo, Carmine Mancone, Roberta Tarallo, Cecilia Battistelli, Tonino Alonzi, Alessandro Weisz, and Marco Tripodi. 2016. “The RNA-Binding Protein SYNCRIP Is a Component of the Hepatocyte Exosomal Machinery Controlling MicroRNA Sorting.” *Cell Reports* 17 (3): 799–808. https://doi.org/10.1016/j.celrep.2016.09.031.

Santavanond, Jascinta P., Stephanie F. Rutter, Georgia K. Atkin-Smith, and Ivan K. H. Poon. 2021. “Apoptotic Bodies: Mechanism of Formation, Isolation and

Functional Relevance." *Sub-Cellular Biochemistry* 97: 61–88. https://doi.org/10.1007/978-3-030-67171-6_4.

Santin, A. D., P. L. Hermonat, A. Ravaggi, M. J. Cannon, S. Pecorelli, and G. P. Parham. 1999. "Secretion of Vascular Endothelial Growth Factor in Ovarian Cancer." *European Journal of Gynaecological Oncology* 20 (3): 177–81.

Schauer, Isaiah Gregory, Jing Zhang, Zhen Xing, Xiaoqing Guo, Imelda Mercado-Uribe, Anil K Sood, Peng Huang, and Jinsong Liu. 2013. "Interleukin-1β Promotes Ovarian Tumorigenesis through a P53/NF-κB-Mediated Inflammatory Response in Stromal Fibroblasts." *Neoplasia (New York, N.Y.)* 15 (4): 409–20.

Schilder, R. J., L. Hall, A. Monks, L. M. Handel, A. J. Fornace Jr., R. F. Ozols, A. T. Fojo, and T. C. Hamilton. 1990. "Metallothionein Gene Expression and Resistance to Cisplatin in Human Ovarian Cancer." *International Journal of Cancer* 45 (3): 416–22. https://doi.org/10.1002/ijc.2910450306.

Schmid, Jens O., Meng Dong, Silke Haubeiss, Godehard Friedel, Sabine Bode, Andreas Grabner, German Ott, et al. 2012. "Cancer Cells Cue the P53 Response of Cancer-Associated Fibroblasts to Cisplatin." *Cancer Research* 72 (22): 5824–32. https://doi.org/10.1158/0008-5472.CAN-12-1201.

Schmider, Annette, Conway Gee, Wolfgang Friedmann, Jason J. Lukas, Michael F. Press, Werner Lichtenegger, and Angela Reles. 2000. "P21 (WAF1/CIP1) Protein Expression Is Associated with Prolonged Survival but Not with P53 Expression in Epithelial Ovarian Carcinoma." *Gynecologic Oncology* 77 (2): 237–42. https://doi.org/10.1006/gyno.2000.5748.

Schouten, G. J., A. C. Vertegaal, S. T. Whiteside, A. Israël, M. Toebes, J. C. Dorsman, A. J. van der Eb, and A. Zantema. 1997. "IkappaB Alpha Is a Target for the Mitogen-Activated 90 kDa Ribosomal S6 Kinase." *The EMBO Journal* 16 (11): 3133–44. https://doi.org/10.1093/emboj/16.11.3133.

Schuldner, Maximiliane, Bastian Dörsam, Olga Shatnyeva, Katrin S. Reiners, Andriy Kubarenko, Hinrich P. Hansen, Florian Finkernagel, et al. 2019. "Exosome-Dependent Immune Surveillance at the Metastatic Niche Requires BAG6 and CBP/P300-Dependent Acetylation of P53." *Theranostics* 9 (21): 6047–62. https://doi.org/10.7150/thno.36378.

Scian, Mariano J., Katherine E. R. Stagliano, Michelle A. E. Anderson, Sajida Hassan, Melissa Bowman, Mike F. Miles, Swati Palit Deb, and Sumitra Deb. 2005. "Tumor-Derived P53 Mutants Induce NF-κB2 Gene Expression." *Molecular and Cellular Biology* 25 (22): 10097–110. https://doi.org/10.1128/MCB.25.22.10097-10110.2005.

Shamseddine, A. A., C. J. Clarke, B. Carroll, M. V. Airola, S. Mohammed, A. Rella, L. M. Obeid, and Y. A. Hannun. 2015. "P53-Dependent Upregulation of Neutral Sphingomyelinase-2: Role in Doxorubicin-Induced Growth Arrest." *Cell Death & Disease* 6 (10): e1947. https://doi.org/10.1038/cddis.2015.268.

Shao, Jianghua, Toshiyoshi Fujiwara, Yoshihiko Kadowaki, Takuya Fukazawa, Toshihiko Waku, Takahiro Itoshima, Tomoki Yamatsuji, Masahiko Nishizaki, Jack A Roth, and Noriaki Tanaka. 2000. "Overexpression of the Wild-Type P53 Gene Inhibits NF-κB Activity and Synergizes with Aspirin to Induce Apoptosis in Human Colon Cancer Cells." *Oncogene* 19 (6): 726–36. https://doi.org/10.1038/sj.onc.1203383.

Sharma, Shayna, Mona Alharbi, Miharu Kobayashi, Andrew Lai, Dominic Guanzon, Felipe Zuñiga, Valeska Ormazabal, et al. 2018. "Proteomic Analysis of Exosomes Reveals an Association between Cell Invasiveness and Exosomal Bioactivity on Endothelial and Mesenchymal Cell Migration in Vitro." *Clinical Science* 132 (18): 2029–44. https://doi.org/10.1042/CS20180425.

Shimoda, Masayuki, Simona Principe, Hartland W. Jackson, Valbona Luga, Hui Fang, Sam D. Molyneux, Yang W. Shao, et al. 2014. "Loss of the Timp Gene Family Is

Sufficient for the Acquisition of the CAF-like Cell State." *Nature Cell Biology* 16 (9): 889–901. https://doi.org/10.1038/ncb3021.

Shinohara, Tsutomu, Toyokazu Miki, Naoki Nishimura, Hiroshi Nokihara, Hirofumi Hamada, Naofumi Mukaida, and Saburo Sone. 2001. "Nuclear Factor-κB-Dependent Expression of Metastasis Suppressor KAI1/CD82 Gene in Lung Cancer Cell Lines Expressing Mutant P531." *Cancer Research* 61 (2): 673–78.

Simhadri, Venkateswara Rao, Katrin S. Reiners, Hinrich P. Hansen, Daniela Topolar, Vijaya Lakshmi Simhadri, Klaus Nohroudi, Thomas A. Kufer, Andreas Engert, and Elke Pogge von Strandmann. 2008. "Dendritic Cells Release HLA-B-Associated Transcript-3 Positive Exosomes to Regulate Natural Killer Function." *PloS One* 3 (10): e3377. https://doi.org/10.1371/journal.pone.0003377.

Singer, Gad, Robert Oldt, Yoram Cohen, Brant G. Wang, David Sidransky, Robert J. Kurman, and Ie-Ming Shih. 2003. "Mutations in BRAF and KRAS Characterize the Development of Low-Grade Ovarian Serous Carcinoma." *Journal of the National Cancer Institute* 95 (6): 484–86. https://doi.org/10.1093/jnci/95.6.484.

Sirois, I., M.-A. Raymond, N. Brassard, J.-F. Cailhier, M. Fedjaev, K. Hamelin, I. Londono, M. Bendayan, A. V. Pshezhetsky, and M.-J. Hébert. 2011. "Caspase-3-Dependent Export of TCTP: A Novel Pathway for Antiapoptotic Intercellular Communication." *Cell Death and Differentiation* 18 (3): 549–62. https://doi.org/10.1038/cdd.2010.126.

Slagsvold, Thomas, Rein Aasland, Satoshi Hirano, Kristi G. Bache, Camilla Raiborg, Daniel Trambaiolo, Soichi Wakatsuki, and Harald Stenmark. 2005. "Eap45 in Mammalian ESCRT-II Binds Ubiquitin via a Phosphoinositide-Interacting GLUE Domain*♦." *Journal of Biological Chemistry* 280 (20): 19600–606. https://doi.org/10.1074/jbc.M501510200.

Smeby, Jørgen, Anita Sveen, Ina A. Eilertsen, Stine A. Danielsen, Andreas M. Hoff, Peter W. Eide, Bjarne Johannessen, et al. 2019. "Transcriptional and Functional Consequences of TP53 Splice Mutations in Colorectal Cancer." *Oncogenesis* 8 (6): 35. https://doi.org/10.1038/s41389-019-0141-3.

Stenmark, Harald. 2009. "Rab GTPases as Coordinators of Vesicle Traffic." *Nature Reviews. Molecular Cell Biology* 10 (8): 513–25. https://doi.org/10.1038/nrm2728.

Strandmann, Elke Pogge von, and Rolf Müller. 2016. "Shipping Drug Resistance: Extracellular Vesicles in Ovarian Cancer." *Trends in Molecular Medicine* 22 (9): 741–43. https://doi.org/10.1016/j.molmed.2016.07.006.

Sun, Chaoyang, Yong Fang, Jun Yin, Jian Chen, Zhenlin Ju, Dong Zhang, Xiaohua Chen, et al. 2017. "Rational Combination Therapy with PARP and MEK Inhibitors Capitalizes on Therapeutic Liabilities in RAS Mutant Cancers." *Science Translational Medicine* 9 (392). https://doi.org/10.1126/scitranslmed.aal5148.

Sun, Yulin, Weiwei Zheng, Zhengguang Guo, Qiang Ju, Lin Zhu, Jiajia Gao, Lanping Zhou, et al. 2016. "A Novel TP53 Pathway Influences the HGS -Mediated Exosome Formation in Colorectal Cancer." *Scientific Reports* 6 (1): 28083. https://doi.org/10.1038/srep28083.

Sundquist, Wesley I., Heidi L. Schubert, Brian N. Kelly, Gina C. Hill, James M. Holton, and Christopher P. Hill. 2004. "Ubiquitin Recognition by the Human TSG101 Protein." *Molecular Cell* 13 (6): 783–89. https://doi.org/10.1016/S1097-2765(04)00129-7.

Svensson, Katrin J., Helena C. Christianson, Anders Wittrup, Erika Bourseau-Guilmain, Eva Lindqvist, Lena M. Svensson, Matthias Mörgelin, and Mattias Belting. 2013. "Exosome Uptake Depends on ERK1/2-Heat Shock Protein 27 Signaling and Lipid Raft-Mediated Endocytosis Negatively Regulated by Caveolin-1." *The Journal of Biological Chemistry* 288 (24): 17713–24. https://doi.org/10.1074/jbc.M112.445403.

Szatanek, Rafal, Jarek Baran, Maciej Siedlar, and Monika Baj-Krzyworzeka. 2015. “Isolation of Extracellular Vesicles: Determining the Correct Approach (Review).” *International Journal of Molecular Medicine* 36 (1): 11. https://doi.org/10.3892/ijmm.2015.2194.

Szulc-Kielbik, Izabela, Michal Kielbik, Marek Nowak, and Magdalena Klink. 2021. “The Implication of IL-6 in the Invasiveness and Chemoresistance of Ovarian Cancer Cells. Systematic Review of Its Potential Role as a Biomarker in Ovarian Cancer Patients.” *Biochimica et Biophysica Acta (BBA) - Reviews on Cancer* 1876 (2): 188639. https://doi.org/10.1016/j.bbcan.2021.188639.

Takasugi, Masaki, Yuya Yoshida, Eiji Hara, and Naoko Ohtani. 2023. “The Role of Cellular Senescence and SASP in Tumour Microenvironment.” *The FEBS Journal* 290 (5): 1348–61. https://doi.org/10.1111/febs.16381.

Taniguchi, Koji, and Michael Karin. 2018. “NF-κB, Inflammation, Immunity and Cancer: Coming of Age.” *Nature Reviews Immunology* 18 (5): 309–24. https://doi.org/10.1038/nri.2017.142.

Teis, David, Suraj Saksena, and Scott D. Emr. 2008. “Ordered Assembly of the ESCRT-III Complex on Endosomes Is Required to Sequester Cargo during MVB Formation.” *Developmental Cell* 15 (4): 578–89. https://doi.org/10.1016/j.devcel.2008.08.013.

Teng, Fei, and Martin Fussenegger. 2021. “Shedding Light on Extracellular Vesicle Biogenesis and Bioengineering.” *Advanced Science* 8 (1): 2003505. https://doi.org/10.1002/advs.202003505.

Teo, Hsiangling, Olga Perisic, Beatriz González, and Roger L. Williams. 2004. “ESCRT-II, an Endosome-Associated Complex Required for Protein Sorting: Crystal Structure and Interactions with ESCRT-III and Membranes.” *Developmental Cell* 7 (4): 559–69. https://doi.org/10.1016/j.devcel.2004.09.003.

Tergaonkar, Vinay, Matthew Pando, Omid Vafa, Geoffrey Wahl, and Inder Verma. 2002. “P53 Stabilization Is Decreased upon NF□B Activation: A Role for NF□B in Acquisition of Resistance to Chemotherapy.” *CANCER CELL*.

Teschendorf, Christian, Kenneth H. Warrington, Dietmar W. Siemann, and Nicholas Muzyczka. 2002. “Comparison of the EF-1 Alpha and the CMV Promoter for Engineering Stable Tumor Cell Lines Using Recombinant Adeno-Associated Virus.” *Anticancer Research* 22 (6A): 3325–30.

Théry, Clotilde, Kenneth W. Witwer, Elena Aikawa, Maria Jose Alcaraz, Johnathon D. Anderson, Ramaroson Andriantsitohaina, Anna Antoniou, et al. 2018. “Minimal Information for Studies of Extracellular Vesicles 2018 (MISEV2018): A Position Statement of the International Society for Extracellular Vesicles and Update of the MISEV2014 Guidelines.” *Journal of Extracellular Vesicles* 7 (1): 1535750. https://doi.org/10.1080/20013078.2018.1535750.

Tian, Wanjia, Ningjing Lei, Junying Zhou, Mengyu Chen, Ruixia Guo, Bo Qin, Yong Li, and Lei Chang. 2022. “Extracellular Vesicles in Ovarian Cancer Chemoresistance, Metastasis, and Immune Evasion.” *Cell Death & Disease* 13 (1): 1–12. https://doi.org/10.1038/s41419-022-04510-8.

Tian, Ye, Ling Ma, Manfei Gong, Guoqiang Su, Shaobin Zhu, Wenqiang Zhang, Shuo Wang, et al. 2018. “Protein Profiling and Sizing of Extracellular Vesicles from Colorectal Cancer Patients via Flow Cytometry.” *ACS Nano* 12 (1): 671–80. https://doi.org/10.1021/acsnano.7b07782.

Trajkovic, Katarina, Chieh Hsu, Salvatore Chiantia, Lawrence Rajendran, Dirk Wenzel, Felix Wieland, Petra Schwille, Britta Brügger, and Mikael Simons. 2008. “Ceramide Triggers Budding of Exosome Vesicles into Multivesicular Endosomes.” *Science (New York, N.Y.)* 319 (5867): 1244–47. https://doi.org/10.1126/science.1153124.

Tricarico, Christopher, James Clancy, and Crislyn D'Souza-Schorey. 2017. "Biology and Biogenesis of Shed Microvesicles." *Small GTPases* 8 (4): 220–32. https://doi.org/10.1080/21541248.2016.1215283.

Van Linthout, Sophie, Kapka Miteva, and Carsten Tschöpe. 2014. "Crosstalk between Fibroblasts and Inflammatory Cells." *Cardiovascular Research* 102 (2): 258–69. https://doi.org/10.1093/cvr/cvu062.

Vennin, Claire, Pauline Mélénec, Romain Rouet, Max Nobis, Aurélie S. Cazet, Kendelle J. Murphy, David Herrmann, et al. 2019. "CAF Hierarchy Driven by Pancreatic Cancer Cell P53-Status Creates a pro-Metastatic and Chemoresistant Environment via Perlecan." *Nature Communications* 10 (1): 3637. https://doi.org/10.1038/s41467-019-10968-6.

Verel-Yilmaz, Yesim, Juan Pablo Fernández, Agnes Schäfer, Sheila Nevermann, Lena Cook, Norman Gercke, Frederik Helmprobst, et al. 2021. "Extracellular Vesicle-Based Detection of Pancreatic Cancer." *Frontiers in Cell and Developmental Biology* 9. https://www.frontiersin.org/articles/10.3389/fcell.2021.697939.

Vidal, Michel. 2019. "Exosomes: Revisiting Their Role as 'Garbage Bags.'" *Traffic* 20 (11): 815–28. https://doi.org/10.1111/tra.12687.

Vietri, Marina, Maja Radulovic, and Harald Stenmark. 2020. "The Many Functions of ESCRTs." *Nature Reviews Molecular Cell Biology* 21 (1): 25–42. https://doi.org/10.1038/s41580-019-0177-4.

Villarroya-Beltri, Carolina, Francesc Baixauli, María Mittelbrunn, Irene Fernández-Delgado, Daniel Torralba, Olga Moreno-Gonzalo, Sara Baldanta, Carlos Enrich, Susana Guerra, and Francisco Sánchez-Madrid. 2016. "ISGylation Controls Exosome Secretion by Promoting Lysosomal Degradation of MVB Proteins." *Nature Communications* 7 (November): 13588. https://doi.org/10.1038/ncomms13588.

Villarroya-Beltri, Carolina, Cristina Gutiérrez-Vázquez, Fátima Sánchez-Cabo, Daniel Pérez-Hernández, Jesús Vázquez, Noa Martin-Cofreces, Dannys Jorge Martinez-Herrera, Alberto Pascual-Montano, María Mittelbrunn, and Francisco Sánchez-Madrid. 2013. "Sumoylated hnRNPA2B1 Controls the Sorting of miRNAs into Exosomes through Binding to Specific Motifs." *Nature Communications* 4: 2980. https://doi.org/10.1038/ncomms3980.

Wang, Feng-Qiang, John So, Scott Reierstad, and David A. Fishman. 2005. "Matrilysin (MMP-7) Promotes Invasion of Ovarian Cancer Cells by Activation of Progelatinase." *International Journal of Cancer* 114 (1): 19–31. https://doi.org/10.1002/ijc.20697.

Wang, Jiajian, Wenjun Liu, Lanqing Zhang, and Jihong Zhang. 2023. "Targeting Mutant P53 Stabilization for Cancer Therapy." *Frontiers in Pharmacology* 14. https://www.frontiersin.org/articles/10.3389/fphar.2023.1215995.

Wang, Jin, and Lingxia Liu. 2021. "MiR-149-3p Promotes the Cisplatin Resistance and EMT in Ovarian Cancer through Downregulating TIMP2 and CDKN1A." *Journal of Ovarian Research* 14 (1): 165. https://doi.org/10.1186/s13048-021-00919-5.

Wang, Shuo, Lihong Li, Shenghao Jin, Weifeng Li, Wei Hang, and Xiaomei Yan. 2017. "Rapid and Quantitative Measurement of Single Quantum Dots in a Sheath Flow Cuvette." *Analytical Chemistry* 89 (18): 9857–63. https://doi.org/10.1021/acs.analchem.7b01885.

Wang, Weimin, Ilona Kryczek, Lubomír Dostál, Heng Lin, Lijun Tan, Lili Zhao, Fujia Lu, et al. 2016. "Effector T Cells Abrogate Stroma-Mediated Chemoresistance in Ovarian Cancer." *Cell* 165 (5): 1092–1105. https://doi.org/10.1016/j.cell.2016.04.009.

Wang, Xiaodan, Weiliang Zhong, Jingya Bu, Yuzhong Li, Ruihua Li, Rong Nie, Chenyang Xiao, Keli Ma, Xiaohua Huang, and Ying Li. 2019. "Exosomal Protein CD82 as a

Diagnostic Biomarker for Precision Medicine for Breast Cancer." *Molecular Carcinogenesis* 58 (5): 674–85. https://doi.org/10.1002/mc.22960.

Wang, Xiaoning, Ruoyi Wu, Peisong Zhai, Zheqi Liu, Ronghui Xia, Zhen Zhang, Xing Qin, et al. 2023. "Hypoxia Promotes EV Secretion by Impairing Lysosomal Homeostasis in HNSCC through Negative Regulation of ATP6V1A by HIF-1α." *Journal of Extracellular Vesicles* 12 (2): e12310. https://doi.org/10.1002/jev2.12310.

Wang, Yuan, Chaoying Hu, Ruofan Dong, Xiaoyan Huang, and Haifeng Qiu. 2011. "Platelet-Derived Growth Factor-D Promotes Ovarian Cancer Invasion by Regulating Matrix Metalloproteinases 2 and 9." *Asian Pacific Journal of Cancer Prevention: APJCP* 12 (12): 3367–70.

Webster, Gill A., and Neil D. Perkins. 1999. "Transcriptional Cross Talk between NF-κB and P53." *Molecular and Cellular Biology* 19 (5): 3485–95. https://doi.org/10.1128/MCB.19.5.3485.

Wei, Denghui, Weixiang Zhan, Ying Gao, Liyan Huang, Run Gong, Wen Wang, Ruhua Zhang, Yuanzhong Wu, Song Gao, and Tiebang Kang. 2021. "RAB31 Marks and Controls an ESCRT-Independent Exosome Pathway." *Cell Research* 31 (2): 157–77. https://doi.org/10.1038/s41422-020-00409-1.

Weisz, Lilach, Alexander Damalas, Michalis Liontos, Panagiotis Karakaidos, Giulia Fontemaggi, Revital Maor-Aloni, Marina Kalis, et al. 2007. "Mutant P53 Enhances Nuclear Factor κB Activation by Tumor Necrosis Factor α in Cancer Cells." *Cancer Research* 67 (6): 2396–2401. https://doi.org/10.1158/0008-5472.CAN-06-2425.

Wiech, Milena, Maciej B. Olszewski, Zuzanna Tracz-Gaszewska, Bartosz Wawrzynow, Maciej Zylicz, and Alicja Zylicz. 2012. "Molecular Mechanism of Mutant P53 Stabilization: The Role of HSP70 and MDM2." Edited by Peter Csermely. *PLoS ONE* 7 (12): e51426. https://doi.org/10.1371/journal.pone.0051426.

Wiley, Christopher D., Rishi Sharma, Sonnet S. Davis, Jose Alberto Lopez-Dominguez, Kylie P. Mitchell, Samantha Wiley, Fatouma Alimirah, et al. 2021. "Oxylipin Biosynthesis Reinforces Cellular Senescence and Allows Detection of Senolysis." *Cell Metabolism* 33 (6): 1124-1136.e5. https://doi.org/10.1016/j.cmet.2021.03.008.

Willis, Amy, Eun Joo Jung, Therese Wakefield, and Xinbin Chen. 2004. "Mutant P53 Exerts a Dominant Negative Effect by Preventing Wild-Type P53 from Binding to the Promoter of Its Target Genes." *Oncogene* 23 (13): 2330–38. https://doi.org/10.1038/sj.onc.1207396.

Wollert, Thomas, and James H. Hurley. 2010. "Molecular Mechanism of Multivesicular Body Biogenesis by ESCRT Complexes." *Nature* 464 (7290): 864–69. https://doi.org/10.1038/nature08849.

Wong, Daniel Senh, and Daniel G. Jay. 2016. "Emerging Roles of Extracellular Hsp90 in Cancer." *Advances in Cancer Research* 129: 141–63. https://doi.org/10.1016/bs.acr.2016.01.001.

Worzfeld, Thomas, Elke Pogge von Strandmann, Magdalena Huber, Till Adhikary, Uwe Wagner, Silke Reinartz, and Rolf Müller. 2017. "The Unique Molecular and Cellular Microenvironment of Ovarian Cancer." *Frontiers in Oncology* 7. https://doi.org/10.3389/fonc.2017.00024.

Wu, Gen Sheng. 2004. "The Functional Interactions between the P53 and MAPK Signaling Pathways." *Cancer Biology & Therapy* 3 (2): 156–61. https://doi.org/10.4161/cbt.3.2.614.

Wu, Kangjian, Shi-Wen Jiang, and Fergus J. Couch. 2003. "P53 Mediates Repression of the BRCA2 Promoter and Down-Regulation of BRCA2 mRNA and Protein Levels in Response to DNA Damage." *The Journal of Biological Chemistry* 278 (18): 15652–60. https://doi.org/10.1074/jbc.M211297200.

Wu, Lingyun, Sugandha Saxena, and Rakesh K. Singh. 2020. “Neutrophils in the Tumor Microenvironment.” *Advances in Experimental Medicine and Biology* 1224: 1–20. https://doi.org/10.1007/978-3-030-35723-8_1.

Wu, Shaocong, Min Luo, Kenneth K. W. To, Jianye Zhang, Chaoyue Su, Hong Zhang, Sainan An, Fang Wang, Da Chen, and Liwu Fu. 2021. “Intercellular Transfer of Exosomal Wild Type EGFR Triggers Osimertinib Resistance in Non-Small Cell Lung Cancer.” *Molecular Cancer* 20 (1): 17. https://doi.org/10.1186/s12943-021-01307-9.

Xing, Chongyun, Wanling Xu, Yifen Shi, Bin Zhou, Dijiong Wu, Bin Liang, Yuhong Zhou, Shenmeng Gao, and Jianhua Feng. 2020. “CD9 Knockdown Suppresses Cell Proliferation, Adhesion, Migration and Invasion, While Promoting Apoptosis and the Efficacy of Chemotherapeutic Drugs and Imatinib in Ph+ ALL SUP-B15 Cells.” *Molecular Medicine Reports*, July. https://doi.org/10.3892/mmr.2020.11350.

Xing, Samantha, and Lucas Ferrari de Andrade. 2020. “NKG2D and MICA/B Shedding: A ‘tag Game’ between NK Cells and Malignant Cells.” *Clinical & Translational Immunology* 9 (12): e1230. https://doi.org/10.1002/cti2.1230.

Xue, Wen, Lars Zender, Cornelius Miething, Ross A. Dickins, Eva Hernando, Valery Krizhanovsky, Carlos Cordon-Cardo, and Scott W. Lowe. 2007. “Senescence and Tumour Clearance Is Triggered by P53 Restoration in Murine Liver Carcinomas.” *Nature* 445 (7128): 656–60. https://doi.org/10.1038/nature05529.

Yan, Wei, Jinny Huang, Qian Zhang, and Jian Zhang. 2021. “Role of Metastasis Suppressor KAI1/CD82 in Different Cancers.” *Journal of Oncology* 2021 (July): 9924473. https://doi.org/10.1155/2021/9924473.

Yang, Chunyan, Mengjun Zhang, Yuqing Cai, Zhiwei Rong, Ce Wang, Zhenyi Xu, Huan Xu, Wei Song, Yan Hou, and Ge Lou. 2019. “Platelet-derived Growth factor-D Expression Mediates the Effect of Differentiated Degree on Prognosis in Epithelial Ovarian Cancer.” *Journal of Cellular Biochemistry* 120 (5): 6920–25. https://doi.org/10.1002/jcb.27432.

Yang, Hui, Hanze Wang, Junyao Ren, Qi Chen, and Zhijian J. Chen. 2017. “cGAS Is Essential for Cellular Senescence.” *Proceedings of the National Academy of Sciences* 114 (23): E4612–20. https://doi.org/10.1073/pnas.1705499114.

Yang, Moran, Guodong Zhang, Yiying Wang, Mengdi He, Qing Xu, Jiaqi Lu, Haiou Liu, and Congjian Xu. 2020. “Tumour-Associated Neutrophils Orchestrate Intratumoural IL-8-Driven Immune Evasion through Jagged2 Activation in Ovarian Cancer.” *British Journal of Cancer* 123 (9): 1404–16. https://doi.org/10.1038/s41416-020-1026-0.

Yang, Xi, Yida Li, Liqing Zou, and Zhengfei Zhu. 2019. “Role of Exosomes in Crosstalk Between Cancer-Associated Fibroblasts and Cancer Cells.” *Frontiers in Oncology* 9. https://doi.org/10.3389/fonc.2019.00356.

Yasuda, Tadahito, Mayu Koiwa, Atsuko Yonemura, Keisuke Miyake, Ryusho Kariya, Sho Kubota, Takako Yokomizo-Nakano, et al. 2021. “Inflammation-Driven Senescence-Associated Secretory Phenotype in Cancer-Associated Fibroblasts Enhances Peritoneal Dissemination.” *Cell Reports* 34 (8): 108779. https://doi.org/10.1016/j.celrep.2021.108779.

Yeung, Tsz-Lun, Cecilia S. Leung, Kwong-Kwok Wong, Goli Samimi, Melissa S. Thompson, Jinsong Liu, Tarrik M. Zaid, Sue Ghosh, Michael J. Birrer, and Samuel C. Mok. 2013a. “TGF-β Modulates Ovarian Cancer Invasion by Upregulating CAF-Derived Versican in the Tumor Microenvironment.” *Cancer Research* 73 (16): 5016–28. https://doi.org/10.1158/0008-5472.CAN-13-0023.

Yeung. 2013b. “TGF-β Modulates Ovarian Cancer Invasion by Upregulating CAF-Derived Versican in the Tumor Microenvironment.” *Cancer Research* 73 (16): 5016–28. https://doi.org/10.1158/0008-5472.CAN-13-0023.

Yoshii, Shunsuke, Yoshito Hayashi, Hideki Iijima, Takanori Inoue, Keiichi Kimura, Akihiko Sakatani, Kengo Nagai, et al. 2019. “Exosomal microRNAs Derived from Colon Cancer Cells Promote Tumor Progression by Suppressing Fibroblast TP53 Expression.” *Cancer Science* 110 (8): 2396–2407. https://doi.org/10.1111/cas.14084.

Yu, Xin, Sandra L. Harris, and Arnold J. Levine. 2006. “The Regulation of Exosome Secretion: A Novel Function of the P53 Protein.” *Cancer Research* 66 (9): 4795–4801. https://doi.org/10.1158/0008-5472.CAN-05-4579.

Yu, Xin, Todd Riley, and Arnold J. Levine. 2009. “The Regulation of the Endosomal Compartment by P53 the Tumor Suppressor Gene.” *The FEBS Journal* 276 (8): 2201–12. https://doi.org/10.1111/j.1742-4658.2009.06949.x.

Yuan, Zhennan, Yingpu Li, Sifan Zhang, Xueying Wang, He Dou, Xi Yu, Zhiren Zhang, Shanshan Yang, and Min Xiao. 2023. “Extracellular Matrix Remodeling in Tumor Progression and Immune Escape: From Mechanisms to Treatments.” *Molecular Cancer* 22 (1): 48. https://doi.org/10.1186/s12943-023-01744-8.

Yue, Huiran, Wenzhi Li, Ruifang Chen, Jieyu Wang, Xin Lu, and Jun Li. 2021. “Stromal POSTN Induced by TGF-B1 Facilitates the Migration and Invasion of Ovarian Cancer.” *Gynecologic Oncology* 160 (2): 530–38. https://doi.org/10.1016/j.ygyno.2020.11.026.

Zhang, Chunxue, Yuxiang Fei, Hui Wang, Sheng Hu, Chao Liu, Rong Hu, and Qianming Du. 2023. “CAFs Orchestrates Tumor Immune Microenvironment—A New Target in Cancer Therapy?” *Frontiers in Pharmacology* 14 (March): 1113378. https://doi.org/10.3389/fphar.2023.1113378.

Zhang, Lin, Nuo Yang, Jin-Wan Park, Dionyssios Katsaros, Stefano Fracchioli, Gaoyuan Cao, Ann O’Brien-Jenkins, Thomas C. Randall, Stephen C. Rubin, and George Coukos. 2003. “Tumor-Derived Vascular Endothelial Growth Factor up-Regulates Angiopoietin-2 in Host Endothelium and Destabilizes Host Vasculature, Supporting Angiogenesis in Ovarian Cancer.” *Cancer Research* 63 (12): 3403–12.

Zhang, Mo, Zhixian Chen, Yan Wang, Hongbo Zhao, and Yan Du. 2022. “The Role of Cancer-Associated Fibroblasts in Ovarian Cancer.” *Cancers* 14 (11): 2637. https://doi.org/10.3390/cancers14112637.

Zhang, Shaosen, Caihong Wang, Boyuan Ma, Min Xu, Siran Xu, Jie Liu, Yang Tian, Yan Fu, and Yongzhang Luo. 2020. “Mutant P53 Drives Cancer Metastasis via RCP-Mediated Hsp90α Secretion.” *Cell Reports* 32 (1): 107879. https://doi.org/10.1016/j.celrep.2020.107879.

Zhao, Yijing, Naifei Chen, Yu Yu, Lili Zhou, Chao Niu, Yudi Liu, Huimin Tian, Zheng Lv, Fujun Han, and Jiuwei Cui. 2017. “Prognostic Value of MICA/B in Cancers: A Systematic Review and Meta-Analysis.” *Oncotarget* 8 (56): 96384–95. https://doi.org/10.18632/oncotarget.21466.

Zhong, Weilong, Huiqin Hou, Tianyu Liu, Shuai Su, Xiaonan Xi, Yusheng Liao, Runxiang Xie, et al. 2020. “Cartilage Oligomeric Matrix Protein Promotes Epithelial-Mesenchymal Transition by Interacting with Transgelin in Colorectal Cancer.” *Theranostics* 10 (19): 8790–8806. https://doi.org/10.7150/thno.44456.

Zhong, Wen, Fredrik Edfors, Anders Gummesson, Göran Bergström, Linn Fagerberg, and Mathias Uhlén. 2021. “Next Generation Plasma Proteome Profiling to Monitor Health and Disease.” *Nature Communications* 12 (1): 2493. https://doi.org/10.1038/s41467-021-22767-z.

Zhou, Jie, Junwen Luo, Peiwei Li, Yongjia Zhou, Peichao Li, Fang Wang, Carlo Augusto Mallio, et al. 2022. “Triptolide Promotes Degradation of the Unfolded Gain-of-Function Tp53R175H/Y220C Mutant Protein by Initiating Heat Shock Protein 70 Transcription in Non-Small Cell Lung Cancer.” *Translational Lung Cancer Research* 11 (5): 802–16. https://doi.org/10.21037/tlcr-22-312.

Zhu, Eric F., Shuning A. Gai, Cary F. Opel, Byron H. Kwan, Rishi Surana, Martin C. Mihm, Monique J. Kauke, et al. 2015. “Synergistic Innate and Adaptive Immune Response to Combination Immunotherapy with Anti-Tumor Antigen Antibodies and Extended Serum Half-Life IL-2.” *Cancer Cell* 27 (4): 489–501. https://doi.org/10.1016/j.ccell.2015.03.004.

Zhu, Jundong, Chenkui Miao, Shouyong Liu, Ye Tian, Chao Zhang, Chao Liang, Aiming Xu, Qiang Cao, and Zengjun Wang. 2017. “Prognostic Role of CD82/KAI1 in Multiple Human Malignant Neoplasms: A Meta-Analysis of 31 Studies.” *OncoTargets and Therapy* 10 (December): 5805–16. https://doi.org/10.2147/OTT.S150349.

Zhu, Tingting, Ruifang Chen, Jieyu Wang, Huiran Yue, Xin Lu, and Jun Li. 2020. “The Prognostic Value of ITGA and ITGB Superfamily Members in Patients with High Grade Serous Ovarian Cancer.” *Cancer Cell International* 20 (1): 257. https://doi.org/10.1186/s12935-020-01344-2.

Zou, Xianghui, Qian Lei, Xinghong Luo, Jingyao Yin, Shuoling Chen, Chunbo Hao, Liu Shiyu, and Dandan Ma. 2023. “Advances in Biological Functions and Applications of Apoptotic Vesicles.” *Cell Communication and Signaling* 21 (1): 1–24. https://doi.org/10.1186/s12964-023-01251-9.

Appendix

List of figures and tables

Figures

Supplemental figures

Tables

Supplemental Tables

Supplemental material

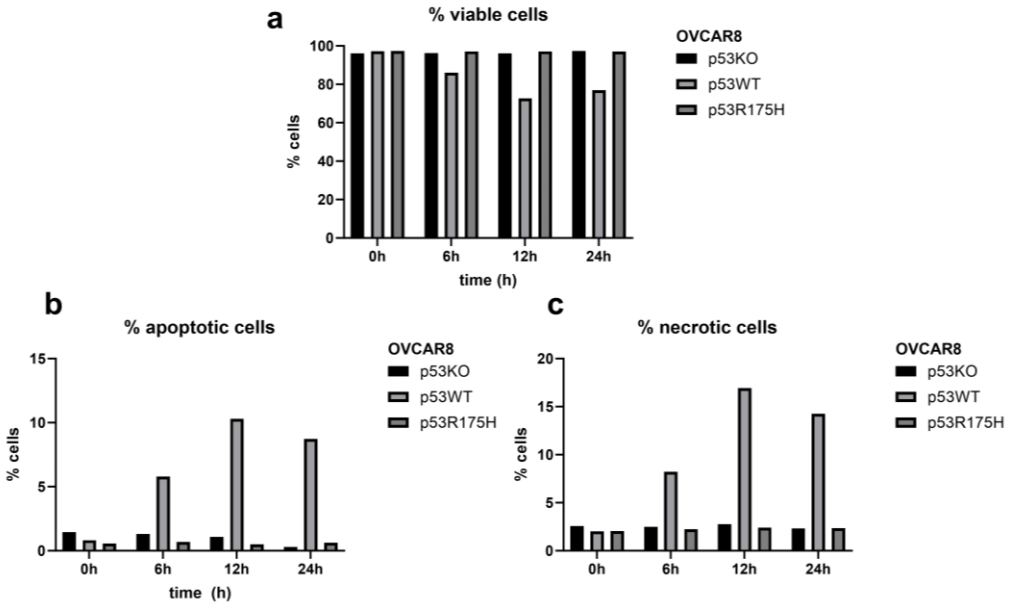

Figure S1: P53WT cells show apoptosis and necrosis after treatment with doxycycline.
(a-c) Cell viability was measured after induction with different concentrations of doxycycline over time to set up an induction protocol for EV isolation. (AnnexinV/PI assay was performed with p53KO, WT, or R175H cells 48 hours after induction with 0.5 or 1 µg/ml (6, 12, or 24 hours), and samples were measured at the flow cytometer FACS Canto II. The result shows % of viable (a), apoptotic (b), or necrotic (c) cells (n=1).

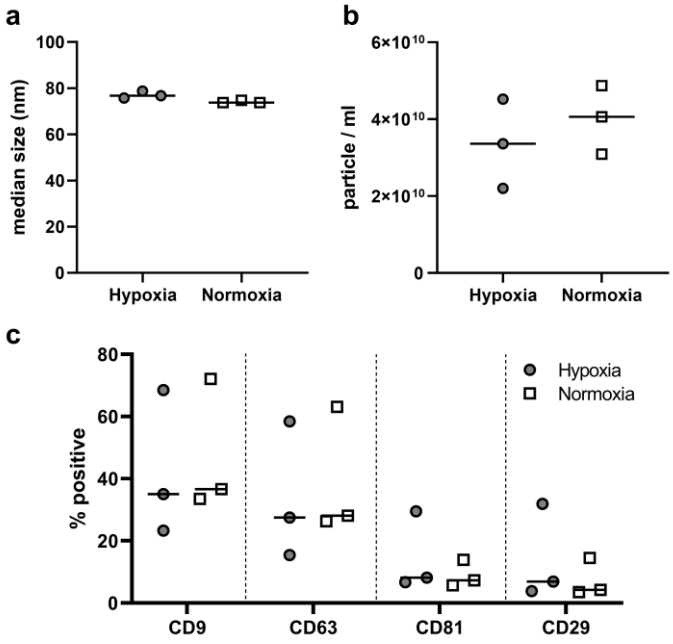

Figure S2: Effects of hypoxic or normoxic conditions on particle size, concentration, and tetraspanin/integrin expression.
EVs from OVCAR8 cells were either isolated in hypoxic or normoxic conditions. **(a)** Median particle size (nm) and **(b)** Particle concentration (particles/ml) was measured by nanoflow cytometry (n=3). **(c)** $1x10^9$ particles were stained by either 200 ng of CD9-PE, CD63-FITC, CD81-PE or CD29-FITC overnight at 4°C. After

centrifuging the samples at 100,000 xg for 2 hours, EVs were resuspended in 0.2 µm filtered PBS, and % of FITC/PE positive particles were measured by nanoflow cytometry (n=3).

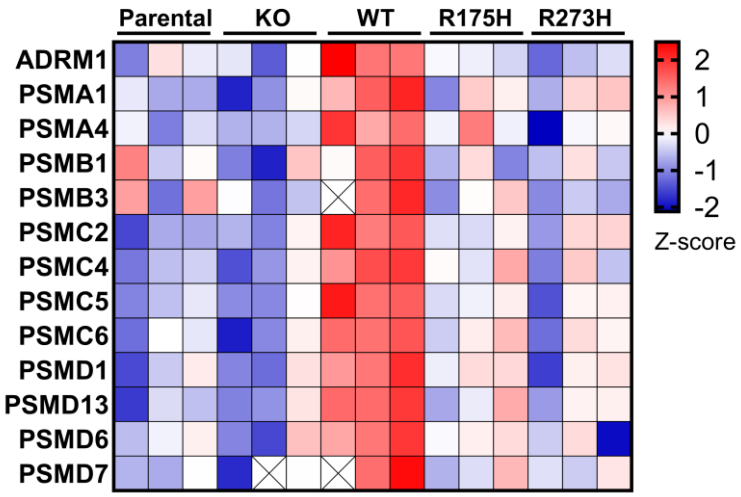

Figure S3: Proteasomal proteins are abundant in EVs from p53WT cells.
Heatmap displays row z-scores of proteins detected in proteomic analysis of EVs from OVCAR8 cells with distinct p53 status.

Table S1: TPM of p53 target genes in the RNA sequencing data of OVCAR8 cells.
The list of target genes is derived from Fisher et al., 2017 and only TOP50 targets were selected. TPM values are shown as the mean of triplicates. P: parental

	#TPM	Induced (+ doxycycline)				
Nr.	**Gene**	**P**	**KO**	**WT**	**R175H**	**R273H**
1	**CDKN1A**	18.2	24.6	987.0	30.7	39.1
2	**RRM2B**	9.2	12.2	123.7	13.1	19.6
3	**MDM2**	18.4	22.7	326.8	21.3	26.5
4	**SUSD6**	4.1	4.6	48.1	5.1	7.8
5	**GDF15**	0.0	0.0	17.1	0.0	0.0
6	**BTG2**	1.5	1.4	82.3	2.0	3.1
7	**DDB2**	7.6	6.6	60.3	7.6	7.9
8	**GADD45A**	86.0	77.1	214.7	79.0	78.9
9	**PLK3**	8.2	6.2	49.9	7.6	8.5
10	**TIGAR**	5.5	4.8	24.4	4.7	5.6
11	**RPS27L**	7.1	6.6	46.4	6.6	7.5
12	**TNFRSF10B**	33.6	32.1	167.2	32.0	45.3
13	**TRIAP1**	53.5	57.4	153.3	58.4	60.4
14	**ZMAT3**	2.7	3.6	22.2	3.7	5.1
15	**BAX**	67.7	70.3	216.1	64.6	72.4
16	**PGF**	0.2	0.1	8.2	0.2	0.2
17	**POLH**	15.3	14.6	43.3	14.8	18.2
18	**PPM1D**	7.6	8.3	25.6	8.4	8.7

19	**SULF2**	0.0	0.0	1.7	0.0	0.0
20	**XPC**	13.9	14.6	50.8	15.4	15.8
21	**AEN**	26.3	25.7	68.1	23.8	23.9
22	**BLOC1S2**	20.2	24.4	75.8	25.0	28.5
23	**FAS**	1.2	1.7	16.1	1.8	1.5
24	**GPR87**	0.0	0.0	10.1	0.0	0.0
25	**NINJ1**	12.2	13.4	121.2	13.9	19.1
26	**PLK2**	550.1	596.0	596.4	507.4	362.3
27	**PSTPIP2**	2.9	3.8	29.3	4.0	4.8
28	**SESN1**	1.1	1.2	18.1	1.7	2.0
29	**TP53I3**	25.2	27.5	376.2	27.6	34.6
30	**TP53INP1**	0.4	0.6	40.2	0.8	2.1
31	**ABCA12**	0.0	0.0	0.9	0.0	0.0
32	**ANKRA2**	5.1	4.5	32.0	5.1	5.0
33	**CCNG1**	144.6	142.8	265.3	145.1	154.7
34	**CYFIP2**	3.2	3.1	80.7	2.7	3.3
35	**DRAM1**	38.1	42.0	136.4	38.2	34.5
36	**FBXO22**	5.8	5.5	23.7	5.8	6.6
37	**ISCU**	41.2	40.9	147.1	43.0	48.7
38	**PHLDA3**	11.6	11.9	93.0	11.6	11.8
39	**SERPINB5**	0.1	0.0	31.7	0.1	0.1
40	**SERTAD1**	21.0	19.6	35.0	17.7	26.0
41	**TRAF4**	28.7	28.6	62.2	28.5	34.6
42	**TRIM22**	0.0	0.0	5.6	0.0	0.0
43	**CES2**	21.2	20.0	193.1	22.0	23.0
44	**CMBL**	0.0	0.0	0.0	0.0	0.0
45	**FBXW7**	2.7	3.5	7.5	3.2	3.8
46	**HSPA4L**	30.8	40.7	98.5	51.0	47.4
47	**KITLG**	5.4	4.0	35.5	4.0	3.9
48	**SLC12A4**	33.8	31.6	87.5	34.1	44.2
49	**ATF3**	2.2	2.2	15.2	3.4	2.5
50	**BBC3**	1.6	2.8	27.1	2.9	2.6

Table S2: TPM values of EV-biogenesis genes from the RNAseq data of the OVCAR8 cell lines.
TPM values are shown as the mean of triplicates.

Group	Gene	Parental	KO	WT	R175H	R273H
ESCRT pathway	**HGS**	46.04	43.55	46.84	44.43	45.63
	STAM	26.46	29.61	28.78	30.07	30.31
	STAM2	6.65	7.50	7.32	7.64	9.10
	TSG101	37.85	39.78	52.83	45.10	50.43
	VPS28	82.18	93.76	92.96	93.70	91.88
	VPS37A	12.05	12.18	17.74	13.39	15.70
	VPS37B	25.70	27.76	31.58	29.89	33.00

	VPS37C	20.41	20.97	20.21	23.40	25.86
	VPS37D	2.65	2.57	15.04	3.29	3.64
	MVB12A	28.56	23.49	24.51	27.23	26.16
	UBAP1	24.85	28.55	22.41	27.27	30.02
	SNF8	81.68	79.77	70.17	79.16	84.51
	VPS25	72.57	75.43	102.84	81.57	84.18
	VPS36	33.55	37.60	31.96	37.43	37.55
	CHMP1A	80.27	82.67	79.31	85.21	90.30
	CHMP1B	39.09	41.09	51.55	44.17	46.53
	CHMP2A	43.58	52.89	64.79	53.87	55.57
	CHMP2B	35.58	42.37	52.94	47.22	50.99
	CHMP3	48.12	51.00	77.25	52.73	57.29
	CHMP4A	30.58	29.49	35.54	30.54	32.60
	CHMP4B	96.46	119.80	120.05	128.75	145.17
	CHMP4C	15.59	31.64	45.06	34.00	37.79
	CHMP5	61.67	61.94	70.69	68.22	75.49
	CHMP6	11.67	14.05	12.38	14.45	15.00
	CHMP7	29.85	29.45	22.73	30.63	32.89
	IST1	45.13	49.09	49.94	48.66	52.25
	VPS4A	55.43	54.78	81.14	60.53	65.99
	VPS4B	18.59	18.83	21.19	19.96	19.95
	VTA1	18.20	19.03	19.44	20.01	20.76
ALIX-Syndecan-Syntenin pathway	**PDCD6IP**	71.41	70.95	85.34	77.20	90.09
	SRC	20.98	22.91	30.25	23.77	26.78
	SDC1	74.18	83.76	196.47	82.16	84.14
	SDC2	67.11	114.88	52.69	97.09	98.72
	SDC3	14.99	11.35	10.51	13.64	15.21
	SDC4	122.44	134.75	522.37	135.70	152.61
	SDCBP	40.45	44.62	29.49	48.39	57.61
	ARF1	498.05	487.41	460.64	485.03	528.61
	PLD2	11.63	10.21	7.65	11.10	12.08
Tetraspanins	**CD9**	58.02	54.48	26.11	59.10	60.23
	CD63	289.87	286.29	269.47	328.44	337.00
	CD81	96.48	105.93	120.34	109.48	119.52
	CD82	2.76	1.66	68.70	3.56	5.19
Flot and CAV	**FLOT1**	281.76	258.63	196.05	267.66	251.86
	FLOT2	49.14	61.90	70.28	66.92	72.19
	CAV1	292.71	309.26	707.03	191.96	158.99
RNA sorting	**SSB**	67.68	70.61	44.66	66.19	71.69
	YBX1	529.34	494.90	366.61	481.13	496.30
	SYNCRIP	185.62	192.68	103.47	162.21	159.44
	HNRNPU	178.20	180.20	122.03	159.80	157.89
	HNRNPA1	601.83	589.40	481.78	536.94	527.79

	HNRNPA2B1	301.50	327.59	217.56	293.95	303.40
RAB GTPase	**RAB27A**	6.66	8.25	9.05	9.67	9.73
	RAB27B	0.59	0.64	1.68	0.68	0.99
	RAB35	70.87	74.69	66.11	73.70	79.01
Heat shock proteins	**HSPD1**	596.51	629.41	402.96	615.93	522.68
	HSPA1A	905.67	916.87	966.77	1399.70	881.30
	HSPA1B	836.07	836.87	936.48	1273.13	807.12
	HSP90AB1	1726.69	1700.01	1291.93	1750.42	1530.36

Table S3: TPM values of selected genes from the RNAseq data of the OVCAR8 cell lines.
TPM values are shown as the mean of triplicates.

Gene	Parental	KO	WT	R175H	R273H
CDKN1A	18.24	24.62	987.01	30.73	39.14
CDKN2A	148.44	148.18	105.88	151.39	145.83
CDKN2B	7.13	8.44	13.54	8.25	12.25
HIF1A	123.67	129.55	32.33	109.93	117.30
HSPA1A	147.23	119.09	62.13	104.22	96.12
HSPA1B	25.45	31.99	41.92	32.67	38.20
HSPA1L	905.67	916.87	966.77	1659.80	881.30
HSPA8	836.07	836.87	936.48	1506.20	807.12
LMNB1	1.42	1.97	1.29	2.65	1.94
MKI67	1271.84	1101.52	897.54	1454.71	1043.71
PTGS2	150.30	140.35	228.82	134.79	163.30
RPS6KA1	0.07	0.05	3.72	0.06	0.03

Table S4: TPM of p53 target genes in the RNA sequencing data of EV-treated fibroblasts.
The list of target genes is derived from Fisher et al., 2017 and only TOP20 targets were selected. TPM values are shown as the mean of triplicates.

Gene	PBS	parental	KO	WT	R175H	R273H
CDKN1A	768.60	657.88	599.08	675.03	567.05	727.20
RRM2B	31.98	25.80	27.09	25.54	24.79	26.04
MDM2	48.95	46.34	44.88	48.15	43.16	44.82
SUSD6	10.67	15.22	14.36	19.28	15.02	14.92
GDF15	87.55	92.40	73.97	97.02	59.04	89.40
BTG2	32.25	17.60	17.06	17.68	16.30	24.25
DDB2	93.86	64.96	70.36	60.26	61.15	70.84
GADD45A	66.49	59.11	55.79	58.07	53.80	55.30
PLK3	41.03	56.63	56.85	53.02	55.75	55.84
TIGAR	6.93	8.05	7.51	8.65	7.73	7.66
RPS27L	51.83	50.62	47.23	50.64	45.22	49.49
TNFRSF10B	109.79	99.03	95.56	97.19	91.98	100.37
TRIAP1	57.04	62.09	63.66	60.74	60.52	61.39
ZMAT3	36.25	27.49	27.05	21.35	24.13	26.03

BAX	204.45	208.54	209.45	248.59	214.35	232.51
PGF	54.19	39.16	43.11	37.18	42.64	48.53
POLH	16.78	13.08	14.25	11.81	13.52	13.48
PPM1D	7.81	6.05	6.45	5.93	5.69	6.91
SULF2	13.50	8.44	7.64	5.83	6.15	9.76
XPC	94.52	83.62	97.69	82.88	93.79	93.37
AEN	45.28	56.99	57.90	67.19	58.96	55.72
BLOC1S2	30.99	31.06	30.51	31.30	30.89	29.87

List of academic teachers

My academic teachers at Ulm University were:

Ayasse, Manfred
Barth, Holger
Ehret, Günther
Hoppe, Jürgen
Jacob, Timo
Johnsonn, Niels
Kirchoff, Frank
Knöll, Bernd
Kühl, Michael
Liss, Birgit
Mader, Wolfgang
Michaelis, Jens
Munch, Jan
Rosenau, Frank
Stenger, Steffen
Tuckermann, Jan
Wirth, Thomas
Wolf, Harald

My academic teachers at Saarland University were:

Becker, Sören
Bernhardt, Ingolf
Boehm, Ulrich
Bruns, Dieter
Cavalie, Adolfo
Diehl, Björn
Engel, Jutta
Ernst, Robert
Faßbender, Klaus
Flockerzi, Veit
Hoth, Markus
Kirchoff, Frank
Lancaster, Roy
Lipp, Peter
Meyer, Markus
Rettig, Jens
Römisch, Karin
Schmitz, Frank
Smola, Sigrun
Tschernig, Thomas
Walter, Jörn

Acknowledgments

An dieser Stelle möchte ich allen Menschen danken, die mich bei der Anfertigung meiner Dissertation unterstützt haben.

Mein besonderer Dank gilt Elke Pogge von Strandmann für die Möglichkeit meine Arbeit in Ihrem Labor durchzuführen. Außerdem bedanke ich mich für die Unterstützung bei der Durchführung der gesamten Arbeit.

Des Weiteren möchte ich mich bei den Initiatoren es Graduiertenkollegs GRK2573/1 bedanken die mir die Möglichkeit gegeben haben ein Teil dieses tollen Programms zu sein. Ebenso bedanke ich mich bei allen beteiligten des Graduiertenkollegs die mich auf meinem Weg mit diversen Kooperationen, Rat, Anregungen und produktiven Gesprächen begleitet haben.

Ich möchte mich weiterhin bei allen Kooperationspartnern und Core Facilities der Phillips-Universität Marburg für die erfolgreiche Zusammenarbeit und Unterstützung bedanken. Ein besonderer Dank geht hierbei an Dr. Florian Finkernagel von der Core Facility Bioinformatik, an Dr. Hartmut Reifer und Dr. Christian Preußer von der FACS Core Facility, an Prof. Dr. Ralf Jacob von dem Institut der Zytobiologie, an Prof. Dr. Graumann, Dr. Witold Szymanski und Dr. Vanessa Beutgen vom Institut für Translationale Proteomik, an Dr. Kathrin Roth von der Core Facility Zelluläre Bildgebung sowie an Dr. Frederik Helmprobst von der Core Facility Elektronenmikroskopie.

Bei dieser Gelegenheit muss ich zudem einen Dank an alle meine Kollegen im Institut für Tumorimmunologie für Ihre Unterstützung und der tollen Arbeitsatmosphäre aussprechen.

Besonderer Dank geht hierbei and Dr. Bilal Alashkar Alhamwe für seine Unterstützung und gnereller Hilfe bezüglich der Arbeit.

Außerdem möchte ich mich gesondert bei Stefanie Maldonado und Katrin Stelter für ihre unterstützenden Arbeiten im Labor bedanken.

Danke außerdem an meinen Bachelorstudenten Max und meiner HIWI Studentin Fenja für ihre tolle Arbeit und die Motivation die sie während ihrern Abreiten zeigten.

Ein spezieller Dank gilt auch Viviane Ponath, für das Korrekturlesen meine Arbeit sowie generelle Hilfe und Unterstützung bei jeglichen Fragen.

Weiterhin möchte ich mich bei allen meinen Freunden bedanken die mich über die Jahre begleitet haben. Ein besonderer Dank geht hierbei an Anna für die tolle Unterstützung und den Rückhalt auch in schweren Zeiten.

Schließlich möchte ich ganz herzlich meinen Eltern und Geschwistern danken für ihre Ermutigungen, Zusprüche und Unterstützung während des Studiums und der Arbeit an dieser Dissertation.

Dankeschön!